Novel Phosphine Oxide Complexes and Inositol Derivatives as Amphitropic Liquid Crystals and Surfactants

I n a u g u r a l – D i s s e r t a t i o n

zur

Erlangung des Doktorgrades

der Mathematisch-Naturwissenschaftlichen Fakultät

der Universität zu Köln

vorgelegt von

Gabriela Cătănoiu

aus Hunedoara (Rumänien)

Köln 2009

"Nothing in life is to be feared, it is only to be understood."

Marie Curie

Familiei mele

ACKNOWLEDGEMENTS

Abstract

Carbohydrates are an attractive class of starting materials for organic syntheses since they are highly functionalized and environmentally sound, in this way promoting a sustainable chemistry. A somewhat exotic, but nevertheless readily available family of carbohydrates allowing a fascinating chemistry are inositols (cyclohexane-1,2,3,4,5,6-hexols). *myo*-Inositol which is the stereoisomer with one axial hydroxyl group, is commercially available at reasonable prices. Inositols have been used previously as hydrophilic head group in amphiphilic liquid crystals, and recently our group involved *myo*-inositol in syntheses of <u>surf</u>ace <u>act</u>ive <u>agents</u> (surfactants). It seems that one unit of *myo*-inositol is not enough to assure a good aqueous solubility for these compounds. To improve the inositol-based amphiphiles in this respect we extended the inositol head group by a triethylene oxide substructure leading to a new class of inositol surfactants.

This thesis describes the synthetic routes to novel inositol amphiphiles as well as their characterization concerning liquid crystalline, solution and surface properties. The supramolecular properties of the new amphiphiles will be related to those of surfactants with comparable structures.

The second topic presented in this work refers to syntheses of new phosphine oxide metal complexes. Phosphine oxide groups can bind various metal cations such as alkaline, alkaline earth, transition and lanthanide metal ions through ion dipolar interactions. This property allows phosphine oxide-based derivatives to be used in various fields of large economical impact. In addition to the synthesis, the liquid crystalline properties of these complexes are investigated and presented.

Kurzzusammenfassung

Aufgrund ihrer hohen Funktionalisierung und ihrer guten Umweltverträglichkeit sind Kohlenhydrate ein attraktiver Ausgangsstoff für die organische Synthese und fördern zudem eine nachhaltige Chemie. Eine etwas exotische, aber dennoch leicht zugängliche Familie der Kohlenhydrate, die eine faszinierende Chemie ermöglicht, sind die Inosite (Cyclohexan-1,2,3,4,5,6-hexole). *myo*-Inosit, also das Stereoisomer mit einer axialen Hydroxylfunktion, ist zu angemessenen Preisen kommerziell erhältlich. Im Vorfeld wurden Inosite bereits als hydrophile Kopfgruppe von amphiphilen Flüssigkristallen eingesetzt und kürzlich wurden in unserer Arbeitsgruppe oberflächenaktive Verbindungen (*engl.: surfactants*) auf der Basis von *myo*-Inosit synthetisiert. Jedoch scheint eine *myo*-Inosit-Einheit nicht auszureichen, um eine gute Wasserlöslichkeit des oberflächenaktiven Moleküls gewährleisten zu können. Um die Löslichkeit der Inosit-basierten Amphiphile zu verbessern, wurde die Inosit-Kopfgruppe um eine Triethylenoxid-Substruktur erweitert und eine neue Klasse der Inosit-Surfactants geschaffen.

Die vorliegende Dissertation beschreibt sowohl den synthetischen Zugang zu neuen Inosit-Amphiphilen, als auch deren Charakterisierung in Bezug auf ihre Flüssigkristallinität und ihrer lösungs- und oberflächenaktiven Eigenschaften. Ihre supramolekularen Eigenschaften werden in Relation zu Amphiphilen mit vergleichbaren Strukturen gesetzt.

Das zweite Themengebiet dieser Arbeit widmet sich der Synthese von neuen Phosphinoxid-Metall-Komplexen. Phosphinoxid-Funktionen können durch ionische Dipolwechselwirkungen an zahlreiche Metall-Kationen binden, darunter Alkali- und Erdalkali-, sowie Übergangsmetall- und auch Lanthanoid-Kationen. Diese Eigenschaft ermöglicht den Einsatz von Phosphinoxid-basierten Verbindungen in diversen Bereichen von hoher ökonomischer Bedeutung. Zusätzlich zu der Synthese werden die flüssigkristallinen Eigenschaften dieser Komplexe untersucht und vorgestellt.

TABLE OF CONTENTS

1. INTRODUCTION

The present work is part of a complex project which was funded by the European Community's Marie Curie Research Training Network "Self-Organisation under Confinement" (SOCON). The SOCON network ran for four years (2005-2008) and it counted thirteen research groups from nine European countries: Ireland (Dublin), Sweden (Stockholm, Lund, Stenungsund), Bulgaria (Sofia), Germany (Cologne, Berlin), Lithuania (Vilnius), Hungary (Budapest), United Kingdom (Oxford, Durham), Denmark (Aarhus), and France (Paris). The focus of the network was on aqueous films, which are either confined between two solid surfaces or by air (foam film) or oil (emulsion film), respectively. Its emphasis was put on complex self-organising systems of environmentally friendly components, such as sugar-based surfactants and polymeric carbohydrate derivatives, but also on the use of traditional surfactants and polymers. The interest in the former class of surfactants and polymers is motivated by the fact that they can be made from renewable materials and that they have favourable properties with respect to applications in various fields. To advance the increased use of more environmentally friendly components, synergistic and antagonistic effects in multicomponent systems have to be understood. In fact, this is one essential element of the joint network research. The wide range of systems which were examined has had in common self-assembly and strong surface activity. The main objective of our research team was to design and synthesize new environmentally friendly compounds from natural building blocks which were further characterized within the network.[1]

One of the models of the multicomponent systems studied in our network dealt with mixtures of the two non-ionic surfactants n-dodecyl-β-D-maltoside (β-$C_{12}G_2$) and n-dodecyl-hexaethylene oxide ($C_{12}E_6$) (Fig. 1.1).

n-dodecyl-β-maltoside (β-$C_{12}G_2$) n-dodecyl-hexaethylene oxide ($C_{12}E_6$)
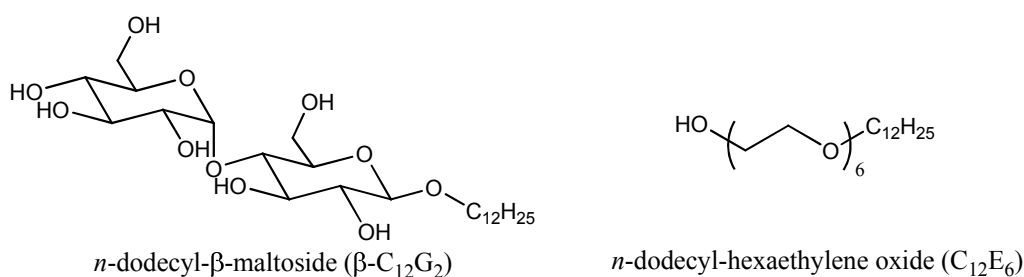
Fig. 1.1. Molecular structures of the surfactants n-dodecyl-β-D-maltoside (β-$C_{12}G_2$) and n-dodecyl-hexaethylene oxide ($C_{12}E_6$)

The reason for studying mixtures of ethylene oxide (C_iE_j) and sugar (C_nG_m) – based surfactants is that they behave quite differently despite of both being non-ionic. To illustrate how differently they behave five examples will be given.

The first example is the adsorption of *n*-dodecyl-hexaethylene oxide ($C_{12}E_6$) and *n*-dodecyl-β-D-maltoside (β-$C_{12}G_2$), respectively, on hydrophilic silica. At first sight, one would not expect a big difference as both surfactants are uncharged, *i.e.*, that the interactions between the silica surface and the non-ionic surfactants cannot differ very much. In fact, quite the opposite was observed. While $C_{12}E_6$ adsorbs strongly on silica, β-$C_{12}G_2$ does not adsorb at all. This is surprising and still not understood.[2,3]

A second prominent difference lays in the temperature-sensitivity of the phase properties: while the phase properties of aqueous solutions of sugar surfactants are not very temperature-sensitive, those of the corresponding ethylene oxide solutions are. The temperature–insensitivity of sugar surfactants in aqueous solution results from the strength of the hydrogen bonds between the hydroxyl groups of the sugar unit and water, which prevents any significant dehydration of the head group in the experimentally relevant temperature range. In contrast to the strong hydrogen bonds between water and sugar units, the hydration water of the corresponding ethylene oxide units is attached only via weak dipole–dipole interactions, which leads to an easy dehydration of the head group.[4]

Thirdly, it is not only the strength of hydration but also the hydration number that is completely different. It was found that under similar conditions and for similar head group sizes (as a rule of thumb, a glucose unit is comparable to three to four ethylene oxide units) the hydration of ethylene oxide-based surfactants is one order of magnitude higher than that of sugar-based surfactants.[5]

Fourthly, the flexibility of the head groups is different. While a maltoside unit behaves like a hard rod, the ethylene oxide units behave more like short polymer chains, which, in turn, means that they are much more flexible.[6]

Last but not least, the surface charge density q_0 of foam films stabilized by sugar surfactants is pH insensitive down to the so-called isoelectric point, while that of ethylene oxide-based surfactants changes linearly with the pH. It is argued that this difference is a consequence of the fact that an ethylene oxide unit is able to "react" to pH-changes by changing either its hydration degree (easy uptake and release of water) or its conformation (high flexibility).[7] As both processes are very unlikely in the case of a sugar unit, the uptake of HO^- ions is given by the total surfactant concentration rather than by the pH, which results in the observed pH insensitivity.

The mentioned differences automatically lead to the question of how mixtures of C_iE_j and C_nG_m surfactants would behave. The answer to this question does not concern only the physical mixtures of the named surfactants[8] but also a "chemical" one, which would be possible by synthesis of a new class of surfactants which contains in the head groups a sugar unit ("half" of the maltoside) together with three units of ethylene oxide ("half" of the hexaethylene oxide) and the dodecyl chain as hydrophobic tail.

The aim of the present work is the synthesis and characterization of this new class of surfactants using as sugar a relatively unknown class of carbohydrates named inositols.

Inositols (cyclohexane-1,2,3,4,5,6-hexols) belong to the group of carbohydrates since they have the same molecular formula $C_6H_{12}O_6$ as conventional hexoses but a different constitution. In a way they present the homocyclic carbon analogue of pyranoses like e.g. glucopyranose, which is why they are sometimes called "C-sugars". The nine possible stereoisomers of inositol are renewable primary natural products which differ only in their relative stereochemical configuration (Fig. 1.2).
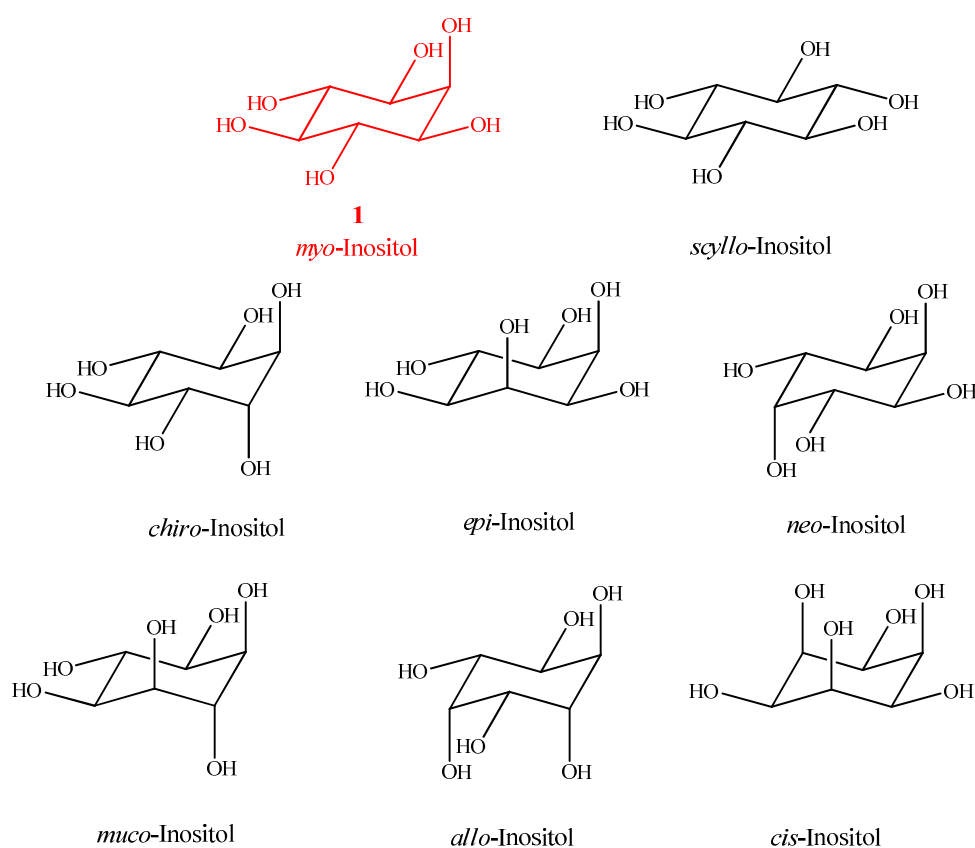
Fig. 1.2. The molecular structures of the inositol stereoisomers. *chiro*-Inositol occurs as both enantiomers, but here only one of them is represented.

Inositol-based surfactants are expected to have properties which are very similar to those of sugar-based ones. The polyol structure of inositol makes it as suitable as conventional sugars to be used as a hydrophilic head group. Compared to the latter, inositol derivatives possess a higher thermal stability, cannot undergo mutarotation or ring opening reaction, not even at low pH-values, because an anomeric center is lacking. Due to their natural occurrence and similarity to conventional sugars, should be as biodegradable as other carbohydrates.

The past decade witnessed a renaissance in the chemistry and biochemistry of inositols, mainly due to the realization of the role played by phosphorylated *myo*-inositol (**1**, Fig. 1.2) derivatives in important biological phenomena such as cellular signal transduction, calcium mobilization, insulin stimulation, exocytosis, cytoskeletal regulation, intracellular trafficking of vesicles, and anchoring of certain proteins to cell membrane.

myo-Inositol (**1**), the major nutritionally active form of inositol, is a cheap and easily accessible compound as it is industrially extracted from wheat pods. It could be found as well in beans, nuts and fruits. It is vital to many biological processes of the body, participating in a diverse range of activities. It is essential for the growth of rodents, but not for most animals, including humans. Humans can produce *myo*-inositol endogenously, from glucose, and, even though *myo*-inositol is sometimes referred to as a vitamin, it is not a vitamin for humans or most animals.

myo-Inositol belongs to the class of cyclitols caring five equatorial and one axial hydroxyl groups. The carbon atom which bears the axial hydroxyl function is always indicated as C_2 while the other carbon atoms of the inositol ring are counted from C_1 to C_6 (Fig. 1.3). *myo*-Inositol does not present optical activity being a *meso* compound since it presents a plane of symmetry through the atoms C_2 and C_5 of the inositol ring.
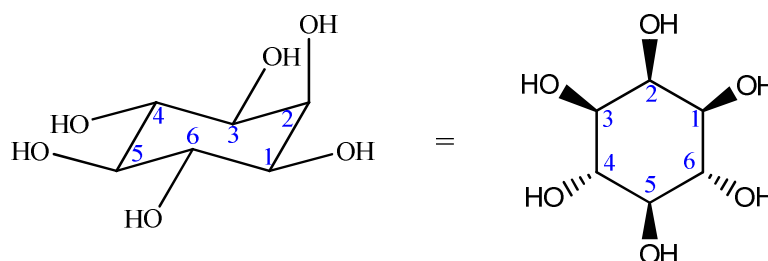
Fig. 1.3. The molecular structure of *myo*-inositol

In the last decade, inositols have been used as hydrophilic head group in amphiphilic molecules. To improve the knowledge on the properties of such inositol-based amphiphiles a

number of new regiochemically defined *myo*-inositol ethers and esters (Fig. 1.4) were previously synthesized and investigated by means of their liquid crystalline mesomorphism as well as their surface activity in aqueous solution.[9-15]
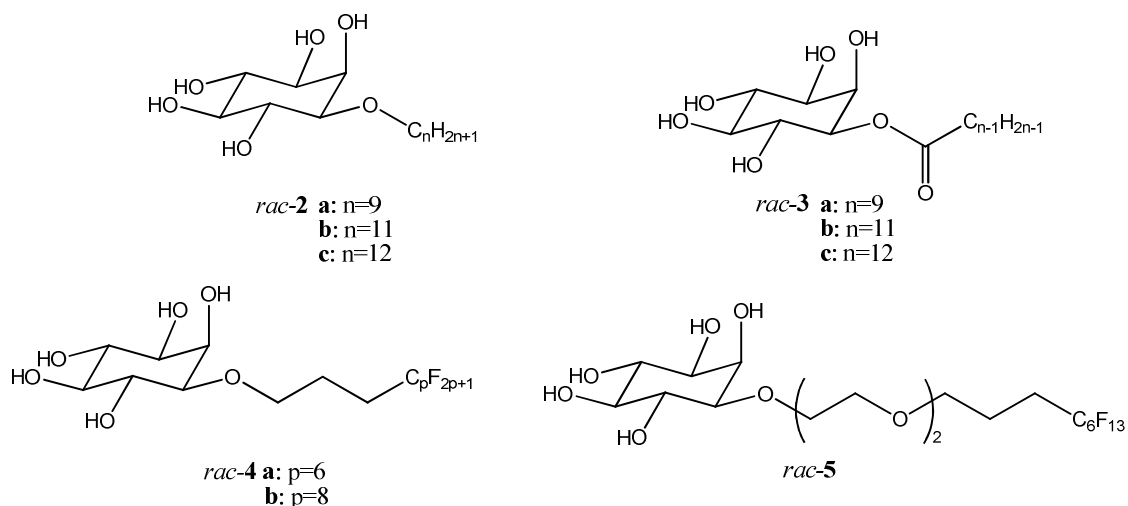
Fig. 1.4. Examples of *myo*-inositol derivatives previously synthesized

The main problem of the above mentioned derivatives regarding the surface activity was their low solubility in aqueous media. In order to improve the inositol amphiphiles with respect of this propriety, a new class of inositol-based derivatives which contain a triethylene oxide unit in their head group was developed. The present work is going to describe the synthesis and characterization of this new class of amphiphiles.

A second project which will be treated in this thesis involves studies regarding the synthesis and characterization of phosphine oxide metal complexes. Phosphine oxide groups can bind various metal cations such as alkaline, alkaline earth, transition and lanthanide metal ions through ion dipolar interactions. This property allows phosphine oxide-based derivatives to be used in various fields of large economical impacts, such as environmental sciences, medical diagnostics, cell biology, etc. Lipophilic phosphine oxides have been used also as extraction agent for precious metals from aqueous solutions. This property raised the question if it would be possible to induce supramolecular order like e.g. thermotropic or lyotropic liquid crystallinity in phosphine oxides metal complexes amphiphiles. The results of respective investigations will be presented.

2. STATE OF KNOWLEDGE

Surfactants (a contraction of the term *surface active agent*) are among the most versatile products of the chemical industry, appearing in such diverse products as motor oils for automobiles, pharmaceuticals, detergents, drilling muds used in prospecting for petroleum, and flotation agents used in benefication of ores. The last decades have seen the extension of surfactant applications to such high-technology areas as electronic printing, magnetic recording, biotechnology, micro-electronics, and viral research.[16]

Over the past thirty years liquid crystals (LCs) have become the quintessential molecular electronic materials of our present day era (Fig. 2.1). The ease with which they can be reoriented in electrical fields has led to the development of a plethora of high technology applications, resulting, for example, in the dominance of the flat-panel displays market. Yet, even though the field of displays may appear mature, there is still considerable interest in the development of 3D-diplays, trans-reflective mode displays which utilise the ability of LCDs for daylight viewing, and colour frame sequential devices which in combination with LEDs could lead to brighter displays.[17]
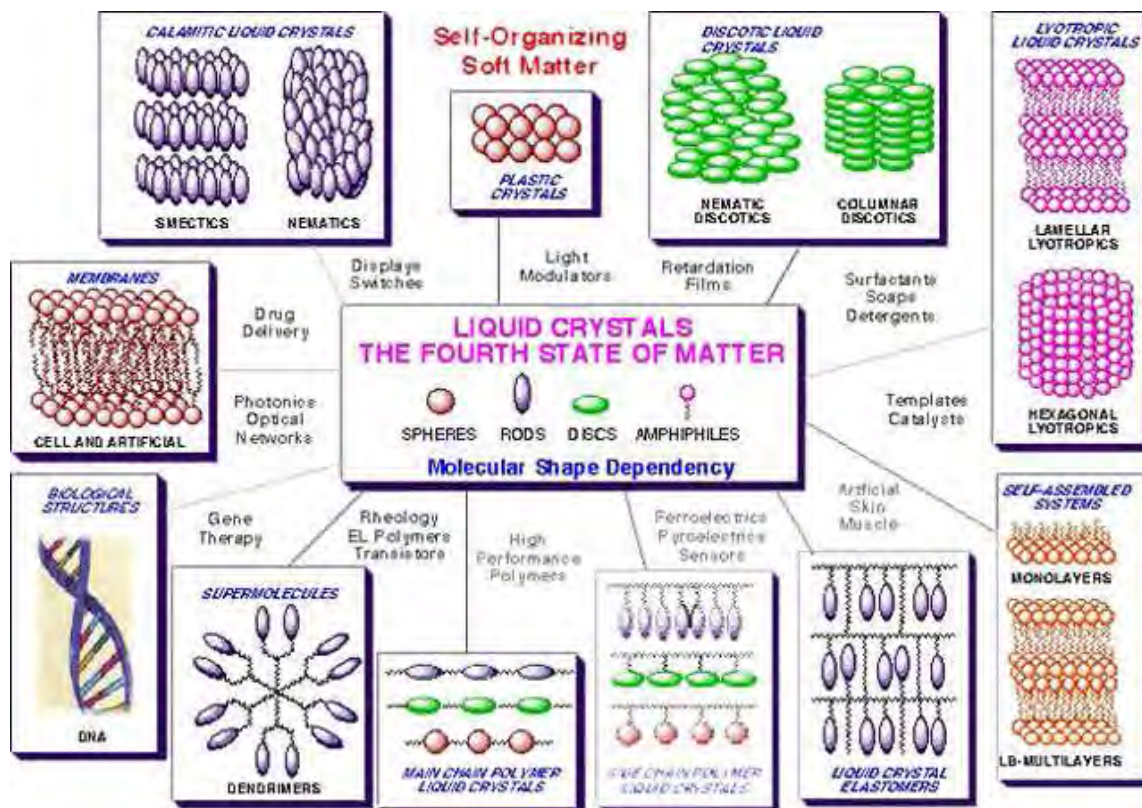
Fig. 2.1. Structural design in, and applications of, liquid crystals. The molecules are shown as molecular materials of defined shape.[17]

2.1. Surfactants

2.1.1. General structural features and behaviour of surfactants

A surface active agent (surfactant) is a substance that, when present at low concentration in a system, has the property of adsorbing onto the surfaces or interfaces of the system and of altering to a marked degree the surface or the interfacial free energies of those surfaces (or interfaces). The term *interface* indicates a boundary between any two immiscible phases; the term *surface* denotes an interface where one phase is a gas, usually air.[16]

The surface tension is a measure of the difference in nature of the two phases meeting at the surface. The greater the dissimilarity in their nature, the greater the surface tension between them. A surfactant is a substance which at low concentrations adsorbs at some or all of the interfaces in the system and significantly changes the amount of work required to expand those interfaces. Surfactants usually act to reduce interfacial free energy rather than to increase it, although there are occasions when they are used to increase it.[16]

Surfactants have a characteristic molecular structure consisting of a structural group that has very little attraction for the solvent, known as a *lyophobic group*, together with a group that has strong attraction for the solvent, called the *lyophilic group*. This is known as an *amphiphilic* structure (Fig. 2.2.).

Lyophilic group ┆ *Lyophobic group*
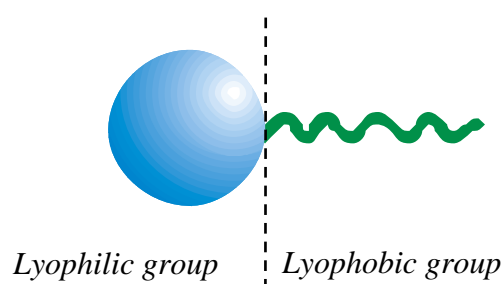
Fig. 2.2. Schematic representation of an amphiphilic structure.

When a molecule with an amphiphilic structure is dissolved in a solvent, the lyophobic group may distort the structure of the solvent, increasing the free energy of the system. When that occurs, the system responds in some fashion in order to minimize the contact between the lyophobic group and the solvent. In case of a surfactant dissolved in aqueous medium, the lyophobic (hydrophobic) group distorts the structure of the water by breaking hydrogen bonds between the water molecules and by structuring the water in the vicinity of the hydrophobic group. As a result of this distortion, some of the surfactant molecules are expelled to the

interfaces of the system, with their hydrophobic groups oriented in such a way that their contact with water molecules is minimized. The surface of the water becomes covered with a single layer of surfactant molecules with their hydrophobic groups oriented predominantly towards the air. Since the air molecules are essentially nonpolar in nature, as are the hydrophobic groups, this decrease in the dissimilarity of the two phases contacting each other at the interface results in a decrease in the surface tension of water. On the other hand, the presence of the lyophilic (hydrophilic) groups prevents the surfactant from being expelled completely from the solvent as a separate phase, since that would require dehydration of the hydrophilic group. The amphiphilic structure of the surfactant therefore causes not only concentration of the surfactant at the surface and reduction of the surface tension of the water, but also orientation of the molecules at the surface with its hydrophilic group in the aqueous phase and its hydrophobic group oriented away from it.[16]

The chemical structures of groups suitable as the lyophobic and lyophilic portions of the surfactant molecule vary with the nature of the solvent and the conditions of use. The hydrophobic group is usually a long-chain hydrocarbon residue, and less often a halogenated or oxygenated hydrocarbon or siloxane chain. The hydrophilic group is an ionic or highly polar group. Depending on the nature of the hydrophilic group, surfactants are classified as:

1. *Anionic* – the surface active portion of the molecules bears a negative charge, for example $RCOO^-Na^+$ (soap), sodium dodecyl sulfate (SDS) (Fig. 2.3).
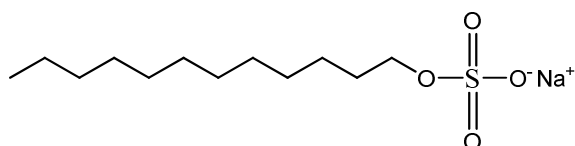
Fig. 2.3. The molecular structure of sodium dodecyl sulfate (SDS).

2. *Cationic* – the surface active portion bears a positive charge, for example $RNH_3^+Cl^-$ (salt of a long-chain amine), cetyl trimethylammonium bromide (CTAB) (Fig. 2.4).
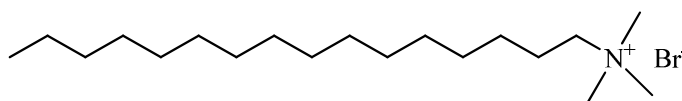
Fig. 2.4. The molecular structure of cetyl trimethylammonium bromide (CTAB).

3. *Zwitterionic* – both positive and negative charges may be present in the surface active portion, for example long-chain amino acid like *N,N*-dimethyl-*N*-dodecylglycine (dodecylbetaine, $C_{12}BET$) (Fig. 2.5).
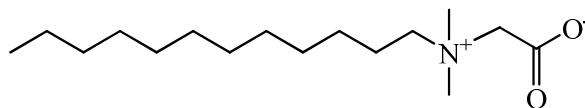
Fig. 2.5. The molecular structure of *N,N*-dimethyl-*N*-dodecylglycine (dodecylbetaine, $C_{12}BET$).

4. *Nonionic* – the surface active portion bears no apparent ionic charge, for example oligo(ethylene) oxides or sugar based surfactants (Fig. 2.6).

n-dodecyl-β-maltoside (β-$C_{12}G_2$)   *n*-dodecyl-hexaethylene oxide ($C_{12}E_6$)
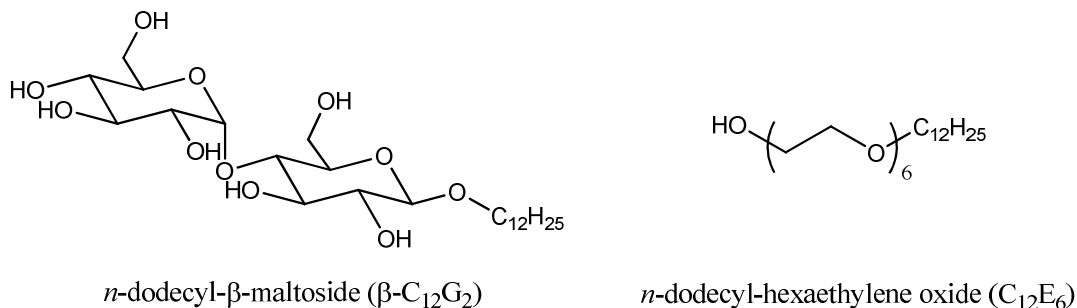
Fig. 2.6. Molecular structures of the surfactants *n*-dodecyl-β-D-maltoside (β-$C_{12}G_2$) and *n*-dodecyl-hexaethylene oxide ($C_{12}E_6$).

2.1.2. Nonionic surfactants

As it was previously mentioned the nonionic surfactants have the surface active portion bearing no apparent ionic charge. There are few advantages and disadvantages of using nonionic surfactants. As advantages could be counted that they are compatible with all other types of surfactants; are generally available as 100% active material free of electrolyte; can be made resistant to hard water, polyvalent metallic cations, electrolyte at high concentrations; are soluble in water and organic solvents, including hydrocarbons. The disadvantages depend on the class of the nonionic surfactants, some of them are poor foamers (which also can be an advantage sometimes) or have no electrical effects (e.g., no strong adsorption onto charged surfaces). Ethylene oxide derivatives show inverse temperature effect on solubility in water, may become insoluble in water on heating, etc.

The present work is dealing with two main classes of nonionic surfactants: the carbohydrate (sugar)-based and the oligo(ethylene) oxide-based surfactants.

Carbohydrate-based surfactants

Natural surfactants are abundant in both plants and animals in small quantities. The cost of the isolation of these compounds led to the development of the cheaper synthetic surfactants, mainly derived from petroleum. The increasing need for products less toxic and highly biodegradable resulted in numerous studies of new sugar-based surfactants, also considered "natural surfactants", as they can occur in nature or may be prepared from natural raw materials.[18] This class of surfactants can be used in several areas, such as food industry (having good functional properties as emulsion stabilization, foaming, etc.), biology (extraction and purification of membranes proteins), molecular recognition in glycobiology or immunology and detergents. Carbohydrate-derived surfactants that are produced and used on an industrial scale are sorbitan esters, sucrose esters, and, which is rather new, fatty acyl glucamides and alkyl polyglucoside.[19]

Sugar-based surfactants possess a carbohydrate hydrophilic part, which can be a mono- or oligosaccharide, and a hydrophobic tail, usually hydrocarbon long-chains. The two moieties can be directly linked via a functional group (ester, ether, hydrazine, amino group, etc.) or separated by a spacer (gemini surfactants).

Alkyl polyglucosides with a worldwide production capacity recently increased to about 60.000 metric tons/year are by far the most important sugar-based surfactant. They are produced by proton-catalyzed acetalation of carbohydrates, preferably of glucose, or by transacetalation of butyl polyglucoside with fatty alcohol.

Strictly speaking, alkyl polyglucosides are not new surfactants but were described as early as 100 years ago by E. Fischer.[20] However, it was not until 1934 that their potential as surface-active agents was appreciated in a patent granted to H. Th. Böhme AG of Chemnitz.[21] They then felt into obscurity for a long time, probably not only because they were difficult to manufacture but also because many other surfactants were already in production. It was not until the first half of the 1980s that this old class of surfactants was unearthed again, against a background of increasing environmental concern.

The intensive use of anomeric alkyl glucosides such as n-octyl β-D-glucoside (β-C_8G_1) and n-dodecyl β-D-maltoside (β-$C_{12}G_2$) (Fig. 2.7) in biology as effective solubilizing agents for

membrane proteins, among other applications, indicated that these surfactants should be very safe.

n-octyl-β-glucoside (β-C$_8$G$_1$)   n-dodecyl-β-maltoside (β-C$_{12}$G$_2$)
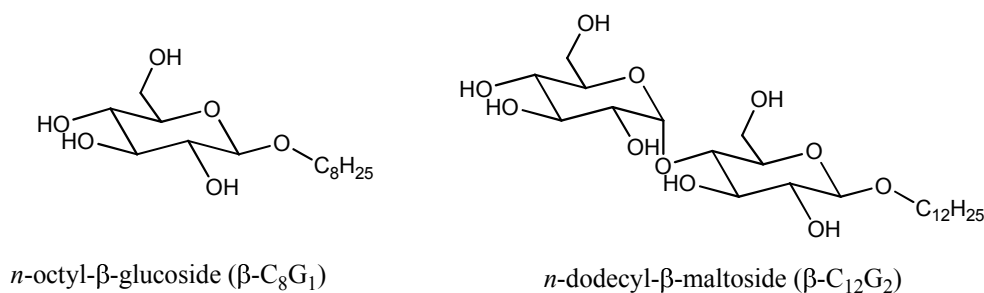
Fig. 2.7. Molecular structures of sugar-based surfactants n-octyl-β-D-glucoside (β-C$_8$G$_1$) and n-dodecyl-β-D-maltoside (β-C$_{12}$G$_2$)

A huge number of application-related patents in particular are based on the special properties of alkyl polyglucosides, including their compatibility and synergetic effects when they are combined with many other surfactants and ingredients of surfactant-based formulation. This, combined with their low environmental impact, as already mentioned, their amazingly economical cost/performance ratio, and finally the high quality standard already achieved, explains the current interest in carbohydrate-based surfactants. Hence, there is a good chance that sugar-based amphiphiles will play a major role alongside the frequently used traditional surfactants.[22,23]

Polyethylene oxide-based surfactants

The most important class of commercially available nonionic surfactants is the polyethylene oxide alcohols derived from reaction of an alcohol with ethylene oxide. These materials are produced in an excess of billions tons a year and are used in such diverse applications as household and institutional laundry, textile scouring, pulp and paper manufacturing, oil field surfactants, agriculture spray adjuvants, and environmental clean-up. The type of alcohol used as the initiator and the length of the polyethylene oxide chain define the application of these versatile commercial products. A primary driving force for the use of these surfactants is their ready biodegradability and overall environmental acceptability. Nevertheless, current and anticipated environmental pressures ensure their continued replacement of other surfactant materials.[23]

Alcohol ethoxylates, like alcohol sulfates and alcohol ethoxysulfates, can be made from either oleochemical or petrochemical alcohols. Consequently, the linearity of the hydrophobe can

vary from highly linear when the alcohol is derived from oleochemical sources and some petrochemical sources to highly branched from other petrochemical sources. Often a blend of several carbon chain length alcohols is used to produce commercial products.

2.1.3. Critical micelle concentration. Surface tension. Surface concentration.

Micelle formation is the property of surfactant that may be as fundamental, and certainly is as important, as their property of being adsorbed at interfaces and consists in ability of surface active solutes of forming colloidal-sized clusters in solution. Micelle formation or micellization is an important phenomenon not only because a number of important interfacial phenomena, such as detergency and solubilization, depend on the existence of the micelles in solution, but also because it affects other interfacial phenomena, such as surface or interfacial tension reduction, that do not directly involve micelles. Micelles have become a subject of great interest to the organic chemist and the biochemist – to the former because of their unusual catalysis of organic reactions and to the latter because of their similarity to the biological membranes and globular proteins.

The shape of the micelle produced in aqueous media is of importance in determining various properties of the surfactant solution, such as viscosity, its capacity to solubilize water-insoluble material, and its cloud point.

At the present time, the major types of micelles appear to be:

a) relatively small, spherical structures (aggregation number < 100);
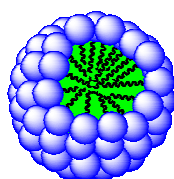
b) elongated cylindrical, rod like micelles with hemispherical ends;
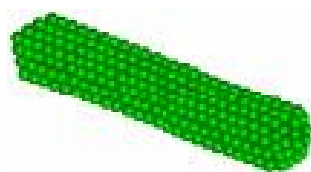
c) large, flat lamellar micelles (dislike extended oblate spheroids);
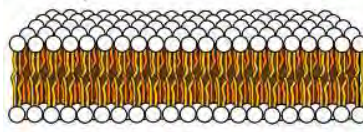
d) vesicles – more or less spherical structures consisting of bilayer lamellar micelles arranged in one or more concentric spheres.
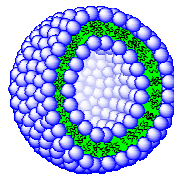
The proportion of molecules present at the surface or as micelles in the bulk of the liquid depends on the concentration of the amphiphile. At low concentrations surfactants will favour arrangement on the surface. As the surface becomes crowded with surfactant more molecules will arrange into micelles. At a specific concentration the surface becomes completely loaded with surfactant and any further additions must arrange as micelles. This concentration is called the **critical micelle concentration** (*cmc*). It follows that measurement of surface tension may be used to determine the *cmc*. A graph of surface tension versus log of concentration of surfactant added will appear as follows (Fig. 2.8):
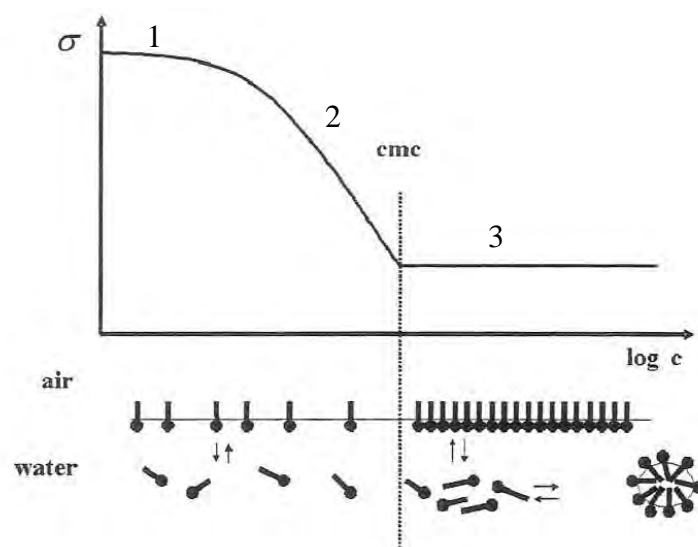
Fig. 2.8. Schematic drawing of the concentration dependence of the surface tension.

In this graph one can identify three phases:

1) At very low concentrations of surfactant only a slight change in surface tension is detected;

2) Additional surfactant decreases the surface tension;

3) Surface becomes fully loaded, no further change in surface tension.

As shown above, the technique to determine the *cmc* by measurement of surface tension σ is simple and straightforward. A graph of surface tension versus log concentration is produced. The *cmc* is found as the point at which two lines intersect: the baseline of minimal surface tension and the slope where surface tension shows linear decline (plateau).

There are different theoretical models to describe surface tension σ versus log concentration curves. The most common is the model derived by Langmuir and Szyszkowski.[24,25] The *Langmuir – Szyszkowski* equation is given by equation (2.1):

$$\sigma = \sigma_0 - \Gamma_\infty RT \ln\left(1 + \frac{a}{c}\right) \qquad (2.1)$$

where σ is the surface tension of the surfactant solution, σ_0 is the surface tension of the solvent, Γ_∞ is the maximum surface concentration (saturation monolayer coverage), R is the gas constant, T is the temperature, c is the surfactant concentration, and a is the concentration at which a surface concentration of $\Gamma_\infty/2$ is reached. The equation (2.1) is only valid if there are no interactions between the adsorbed molecules.

In the present work another model is used to describe the surface tension curves, namely the *Frumkin* model. This model takes into account the attractive interactions between molecules adsorbed at the interface. The equation for the *Frumkin* model is given by equation (2.2):

$$\sigma = \sigma_0 + \Gamma_\infty RT \ln\left(1 - \frac{\Gamma}{\Gamma_\infty}\right) + a'\left(\frac{\Gamma}{\Gamma_\infty}\right)^2 \qquad (2.2)$$

with *a'* being the interaction parameter. According to this model the surface tension increases with increasing interaction between absorbed surfactant molecules because the mobility of the molecules decreases.[26]

The tendency to adsorb at the water/air interface increases with increasing hydrophobic chain length in a homologous series, which means that the concentration needed for some particular adsorption value decreases with increasing chain length. For a homologous series the shape of the curve itself stays the same. The adsorption rises with increasing concentration until the *cmc* when the adsorption value reaches a plateau. The interface concentration reaches its maximum Γ_∞ at this point. Further surfactant addition has no effect on the adsorption density

and thus on the surface tension. The minimal required space per surfactant molecule can be calculated from the Γ_∞ value and is given by the equation (2.3):

$$\Gamma_\infty = \frac{1}{N_A A_{\min}}$$ (2.3)

where N_A is the *Avogadro* constant ($N_A = 6.023 \ 10^{23} \ \text{mol}^{-1}$) and A_{min} is the minimal surface area per surfactant molecule.

2.1.4. The Krafft boundary

Most systems possess many qualitatively different solubility boundaries at different temperatures. If we talk about solubility boundary, we tend to think about the liquid phases. But it is important to remember that other phases may possess solubility boundaries as well. In other words, two liquids, a liquid and a solid or two solids can coexist in a miscibility gap.[27]

The amphiphilic nature of surfactants allows them to form numerous aggregates in aqueous solutions, which, in turn, may result in numerous different phases, depending on the temperature and the composition. Many surfactants are high soluble in liquid water at high temperatures, but separate from the solution as a crystal phase at lower temperatures. The crystal solubility boundary in aqueous surfactant solutions is called the "Krafft boundary" in honour of its discoverer, Prof. Friedrich Krafft (1852-1923). This boundary has a distinctive shape (Fig. 2.9), and terminates at its upper temperature limit at a eutectic discontinuity. This eutectic is called the Krafft discontinuity or Krafft eutectic. The saturating phase at the solubility boundary at temperatures above the Krafft eutectic is usually (but not always) a liquid crystalline phase.
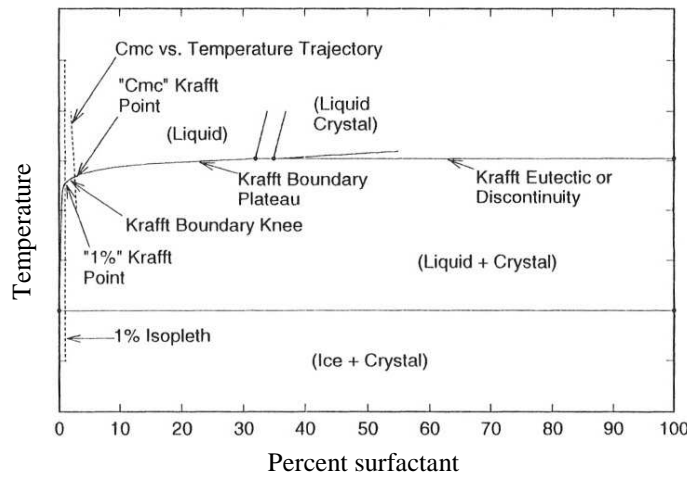
Fig. 2.9. The general form of the Krafft boundary.[28]

Far below the temperature of the Krafft eutectic the solubility of surfactants is small and the crystal solubility boundary is steep, which signifies that a low temperature coefficient of solubility exists. As the temperature is increased a turnover or "knee" develops, and just above this knee a plateau exists. Along the plateau the slope is small and the temperatures coefficient of solubility is very large. The plateau terminates at the Krafft eutectic, at which the crystal solubility boundary intersects that solubility boundary which exists at higher temperatures. The liquid phase at the intersection of these two solubility boundaries is also the most dilute of the three phases that may coexist at the Krafft eutectic. [28]

In a series of studies aiming to explain the shape of the Krafft boundary it was noted that the composition of the boundary at the knee is similar to the critical micelle concentration (*cmc*) of surfactants. The dependence of the *cmc* on temperature, at values above the Krafft boundary, has been determined for a number of soluble alkyl sulfate salt surfactants. The *cmc* versus temperature function has been extrapolated to its intersection with the independently determined Krafft boundary, and the point of intersection (which clearly falls within the knee) has been termed the Krafft point (Fig. 2.9).

The presence of a knee and a plateau in a crystal solubility boundary is *not* unique to aqueous surfactant systems, and the existence of these features does *not* require that micellar phenomena exist within the liquid phase. They are found in the crystal solubility boundary in the phase diagrams of all solute-solvent systems that are useful for purification by recrystallization, and micellization within the liquid phase does not exist in the vast majority of these systems. [28]

2.1.5. Few analytical methods used in surfactants characterization

2.1.5.1. Methods for surface and interfacial measurements

Reduction of the surface and interfacial tension is one of the most commonly measured properties of surfactants in solution. Since it depends directly on the replacement of molecules of solvent at the interface by molecules of surfactant, and therefore on the surface (or interfacial) excess concentration of the surfactant, it is also one of the most fundamental of interfacial phenomena.[16]

Measurements of the surface or interfacial tension of liquid systems is accomplished readily by a number of methods. Some of them are based on dynamic principles and are thus suitable to measure the tension as a function of time. Others are static or quasi-static methods and yield dynamic tensions as well, but also allow reaching the equilibrium state of a liquid interface and hence are able to measure the equilibrium tension. While dynamic methods require theories for data interpretation that take the dynamic character into consideration, the data from static methods can be understood more easily. To overcome this problem Joos developed a theory which reduces the data from dynamic methods to a so-called effective lifetime of the interface, which is equivalent to the time needed at a static interface to reach the same adsorption state.[29] In this way measurement results from all experimental techniques can be directly compared.

The following Table 2.1 gives an overview of methods dedicated to surface tension measurements of liquid interfaces.

Table 2.1. Methods for measuring surface and interfacial tension of liquid interfaces[30]

Method	Suitability for liquid/liquid	Suitability for liquid/gas
Capillary Rise Technique	possible	good
Capillary Wave Damping	possible	possible
Drop Volume Method	good	good
Growing Drops and Bubbles	good	good
Inclined Plate Method	bad	good
Maximum Bubble Pressure Method	possible	good
Oscillating jet	bad	good
Pendent Drop Method	good	good
Plate Tensiometry	bad	good
Ring Tensiometry	bad	good
Sessile Drop Method	possible	possible
Spinning Drop Method	good	possible
Static Drop Method	good	good

In the present work the method used to measure the surface tension is the ring tensiometry after Du Noüy, therefore this method is going to be described more detailed.

Ring tensiometry after du Noüy

The ring tensiometry is the most frequently used technique to measure the surface tension of pure liquids and solutions. As mentioned above the ring tensiometry is difficult to apply to liquid/liquid interfaces, as it is connected with complicated wetting problems. The same is true for the plate tensiometry, so that complementary techniques are required for these interfaces.

In the du Noüy ring method, a thin wire ring is inserted below the interface and held horizontal. Then the ring is pulled up through the interface. The force F measured by a balance goes through a maximum F_{max}.[31] In a first approximation the surface tension σ is given by equation (2.4):

$$\sigma = \frac{F_{max}}{4\pi R} \qquad (2.4)$$

where R is the radius of the ring. Note that for equation (2.4) to hold, the radius of the wire must be much smaller than the radius of the ring and that the solution must wet the wire completely. For this reason a clean platinum wire is usually used. For precise measurements, a correction factor f to the ideal case is required:

$$\sigma = \frac{F_{max}}{4\pi R f} \qquad (2.5)$$

This correction factor f takes in account the ring geometry and the liquid density ρ and usually is included into the software of most tensiometers but can be also determined by using the tables. For this thesis, the values for measured surface tension were calculated using the Harkins and Jordan correction factors which are expressed as a function of R/r and R^3/V, where r is the radius of the wire and V is the volume of the liquid raised above the free surface.

Surface tension measurements for the present work were carried out using a STA-1 tensiometer from *Sinterface* (Fig. 2.10), which has an accuracy of 0.1 mN m^{-1}.
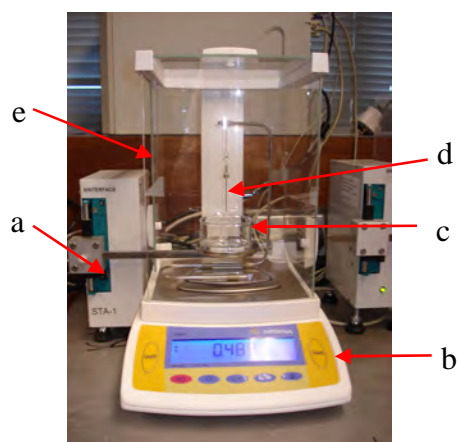
Fig. 2.10. (a) STA-1 tensiometer, (b) Sartorius balance, (c) measurement vessel, (d) platinum ring, (e) Plexiglas box.

The equipment consists of three parts: a computer to control the measurements, a Sartorius balance and the tensiometer itself (Fig. 2.11). Solutions were placed into a glass vessel, and the measurements are done in a closed Plexiglas box to prevent contamination and to maintain the humidified environment.

Fig. 2.11. The surface tension measurements equipment: the computer, the STA-1 tensiometer and the Sartorius balance.

2.1.5.2. Diffusion ordered spectroscopy (DOSY)

Studies of surfactants have constituted a cornerstone in physical chemistry ever since the pioneering work of McBain[32] at the beginning of the twentieth century, and many different experimental methods as well as the theoretical modelling have been employed. Of the experimental methods, nuclear magnetic resonance (NMR) has come to play a pivotal role during the last decades. It is fair to say that no other spectroscopic methods can compete with

NMR regarding versatility, and the technique offers many unique capabilities. It is essentially a nonperturbing method in that it utilises nuclei already present in the investigated molecules or inserted into them by means of isotope labelling as probes.[33]

There are many different aspects of NMR studies of surfactant systems, covering both liquid solution phases and liquid crystalline phases. This subchapter will summarise one of the NMR diffusion methods for surfactants in solution, respectively diffusion ordered spectroscopy (DOSY) using pulsed field-gradient (PFG) NMR spectroscopy.

Over the last decade, pulsed field-gradient (PFG) NMR spectroscopy has become the method of choice for measuring diffusion in solution in both chemical and biological systems. In principle, the diffusion coefficient of a certain molecular species under given conditions (for example, solvent and temperature) depends on its "effective" molecular weight, size and shape. Therefore, it is evident that diffusion can be used to map intermolecular interactions that play an important role in both chemistry and biology in solution and which lie at the heart of molecular recognition, a process which is essential to supramolecular and combinatorial chemistry.[34]

The fact that molecular diffusion can be measured by NMR methods was realised in the early days of NMR spectroscopy.[35] The most practical pulse sequence for measuring diffusion coefficients was introduced by Stejskal and Tanner in 1965[36] long before the advent of 2D NMR spectroscopy which is currently routinely used by chemists worldwide. The last decade has witnessed an explosion in the utilization of gradients in all areas of NMR spectroscopy, ranging from coherence selection in high-resolution NMR spectroscopy to magnetic resonance imaging (MRI). Being a totally non-invasive technique it is particularly suited to studying molecular dynamics and translational diffusion.

Translational diffusion is one of the most important modes of the molecular transport. Self-diffusion is the random translational motion of ensembles of particles (molecules or ions) as a consequence of their thermal energy. In case of self-diffusion, no (net) force acts on the molecular particles and, consequently, no net displacement is observed. It is well known that diffusion is closely related to molecular size, as seen from the Einstein-Smoluchowski equation:

$$D = \frac{k_b T}{f} = \frac{RT}{N_A f} \tag{2.6}$$

where D is the self-diffusion coefficient, k_b is the Boltzmann constant, T is the absolute temperature, f is the so-called hydrodynamic frictional coefficient, N_A is Avogadro's number,

and R is the gas constant. For a sphere in a continuous medium of viscosity η, f is given by the Stokes equation:

$$f = 6\pi\eta R_H \tag{2.7}$$

where R_H is the hydrodynamic radius. Combining equations (2.6) and (2.7) leads to the familiar Stokes-Einstein equation:

$$D = \frac{k_b T}{6\pi\eta R_H} \tag{2.8}$$

The Stokes-Einstein equation (2.8) indicates that, by measuring the self-diffusion coefficient of a given molecular species under controlled conditions, one may obtain information on its effective size or weight and, therefore, on the specific interactions of the species with its molecular environment. Thus the diffusion coefficients are sensitive to structural properties of the observed molecular species such as weight, size and shape, as well as binding phenomena, aggregation and molecular interactions.[34]

Different mobility rates or diffusion coefficients may also be used as the basis for the separation of the spectra of mixtures of compounds in solution, this procedure being referred to as *diffusion ordered spectroscopy* or DOSY. The application of NMR diffusion measurements to the separation of small-molecule mixtures in this way is a relative newcomer to high-resolution NMR and is a developing area that is sure to find increasing use in the research laboratory.

All modern NMR-based diffusion measurements rely on the application of pulsed field gradients to map the physical location of a molecule in solution and have recently been made possible on conventional high-resolution NMR spectrometers through the provision of actively shielded PFG probe heads. Molecular diffusion is then characterized along the direction of the applied field gradient, which is typically along the *z*-axis of conventional gradient probeheads. The basic scheme for the characterization of diffusion is the pulsed field gradient spin-echo (Fig. 2.12).
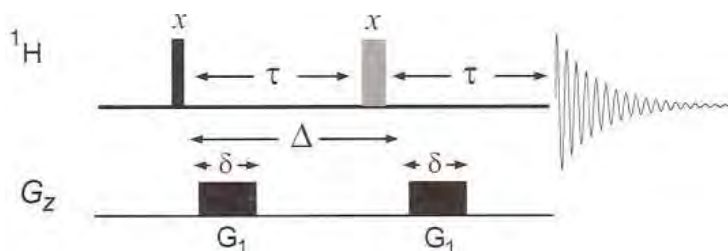
Fig. 2.12. The pulsed field gradient spin-echo sequence (G_z – gradient chanel, τ – evolution time, Δ – diffusion time, δ – gradient length).[37]

In the absence of gradient pulses, this will refocus chemical shift evolution such that the detected signal is attenuated only by transverse relaxation during the 2τ period. When pulsed field gradients are employed, complete refocusing of the signal will only occur when the local field experienced by a spin is identical during the two gradient pulses. Since a field gradient is used, the local field is spatially dependent, meaning this refocusing condition is only met if the spin remains in the same physical location when the two PFGs are applied. If the molecule was to diffuse away from its initial position during the diffusion delay $\varDelta$, the local field experienced during the second PFG would not exactly match that of the first and only partial refocusing of the signal would occur. The detected signal would therefore be attenuated by an amount dictated by how far the molecule moved during the period $\varDelta$, and hence by its diffusion coefficient.[37]

To characterise diffusion rates, it is possible to progressively alter the delay $\varDelta$, the length or the strength of the gradient pulses and to monitor the corresponding signal decay. However, changes made to the overall length of the echo sequence will introduce additional complications arising from increasing relaxation losses, so it is universal practice to increase gradient strength whilst keeping all time periods invariant. Whilst T_2 relaxation losses still occur in this case, they are constant for all experiments and thus do not contribute to the progressive signal attenuation that is monitored (Fig. 2.13).
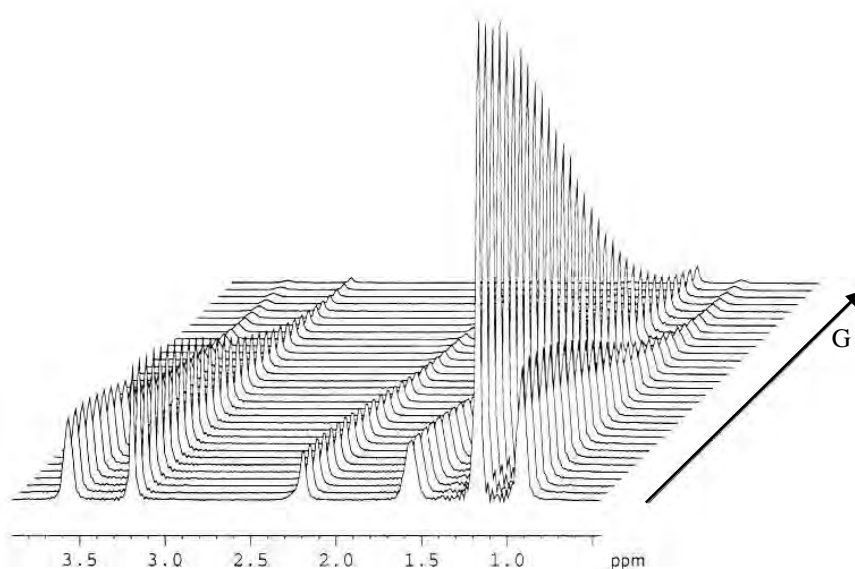
Fig. 2.13. Diffusion proton spectra measured at constant diffusion delay $\varDelta$
and progressively increasing gradient strength G.

The observed signal intensity I, for the basic PFG spin-echo experiment is given by the Stejskal-Tanner equation:

$$I = I_0 \exp\left(\frac{-2\tau}{T_2} - (\gamma \delta G)^2 D\left(\Delta - \frac{\delta}{3}\right)\right)$$
(2.9)

where I_0 is the signal intensity at zero gradient strength, τ is the time between the 90° and 180° pulses, T_2 is the transverse relaxation time, γ is the proton magnetogyric constant, G is the gradient strength, D is the diffusion coefficient, Δ is the diffusion time and δ is the length of the gradient.

In the procedure used in this work, τ was kept constant and thus the T_2 effects are kept constant, which means that there are no variations in the relaxation term that affects the intensity I, and thus only diffusion contributes to the echo-decay. Since the relaxation term $2\tau/T_2$ is constant it can be included in I_0, so that equation (2.9) can be simplified to:

$$I = I_0 \exp\left(-(\gamma \delta G)^2 D\left(\Delta - \frac{\delta}{3}\right)\right)$$
(2.10)

The PFG spin-echo sequence is limited in practice by the afore-mentioned relaxation losses and is nowadays little used for diffusion measurements. Because magnetization is transverse during the diffusion period, these losses are dictated by the transverse (T_2) relaxation rates which themselves increase with molecular size. Since larger molecules (or aggregates) require longer diffusion periods to move significant distances, the use of long Δ delays can lead to unacceptable signal-to-noise degradation. In the stimulated-echo sequence (Fig. 2.14) magnetisation is longitudinal during the diffusion period, by virtue of the second 90° pulse, meaning the sequence is now limited by slower longitudinal (T_1) relaxation rates instead. Following the diffusion period, the magnetization is returned to the transverse plane by the third 90° pulse for refocusing and detection. All recently introduced diffusion sequences are derived from this basic stimulated-echo sequence.[37]
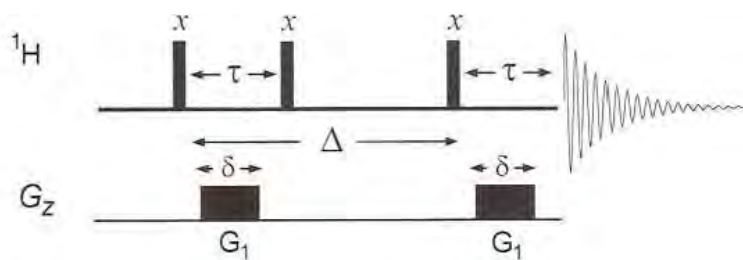
Fig. 2.14. The pulsed field gradient stimulated-echo sequence.[37]

The diffusion experiments presented above can be processed and displayed as a 2D matrix with chemical shifts plotted along one axis and diffusion coefficients plotted along the perpendicular axis (Fig. 2.15).
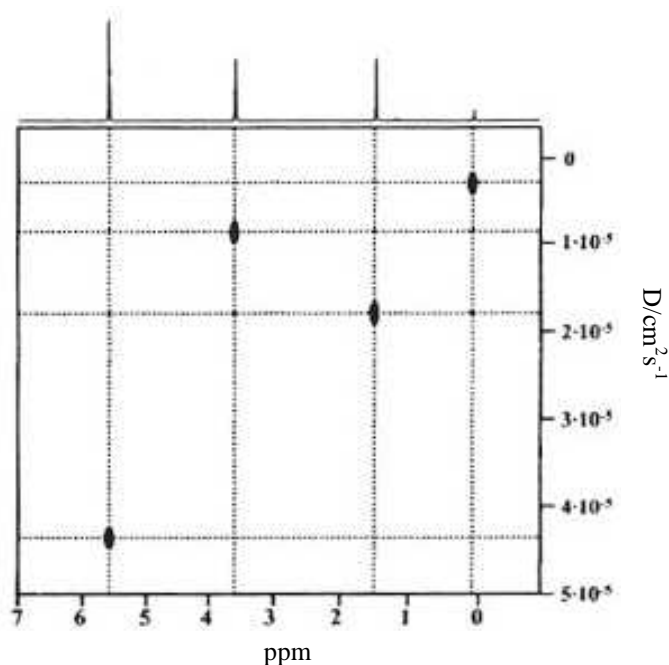
Fig. 2.15. 2D DOSY spectrum showing four different species characterized by four different diffusion coefficients.[34]

One of the applications of DOSY experiments is to separate species spectroscopically (not physically) present in a mixture of compounds. In this sense the use of DOSY is reminiscent of the physical separation of compounds by chromatography. Thus, DOSY is also termed "NMR chromatography". Fig. 2.15 illustrates this concept, each horizontal line represents a distinct diffusion coefficient and, hence, all peaks on the horizontal line correlate with signals in the chemical shifts dimension, and should be attributed to a specific molecular species.

Solvent suppression

Fortunately the majority of solvents used in organic NMR spectroscopy are readily available in the deuterated form. For proton spectroscopy in particular, this allows the chemist to focus on the solute spectrum, undisturbed by the solvent that is present in vast excess. Unfortunately, there are applications like surfactants systems, molecules of biochemical or medicinal interest, which must be studied in water and in order to observe all protons of interest within these systems, protonated water must be employed as the solvent. Whereas H_2O is 110 M in protons, solute concentrations are more typically in the millimolar region and the $10^4 - 10^5$ concentration difference imposes severe experimental difficulties which demand the attenuation of the solvent resonance.[37]

 The goal of the solvent suppression is therefore to reduce the magnitude of the solvent resonance before the NMR signal reaches the receiver. This seemingly simple requirement has generated an enormous research area[38] emphasising the fact this is by no means a trivial exercise. The more widely used approaches can be broadly classified into three areas: a) methods that saturate the water resonance, b) methods that produce zero net excitation of the water resonance and c) methods that destroy the water resonance with pulsed field gradients.

The most effective approach to date to solvent suppression is the destruction of the net solvent magnetization by pulsed field gradients (PFGs), so ensuring nothing of this remains observable immediately prior to acquisition. The method used within the present work is called excitation sculpting and is an improved approach to gradient suppression applying a double PFG spin-echo instead of one (Fig. 2.16).[39] This may be represented $G_1 - S - G_1$ where S represents any selective 180° pulse and the bracketing gradients are identical. The phase profile of the selected resonance(s) is also dictated by the phase proprieties of the selective pulse S, which may not be ideal. Repeating the gradient-echo once again (Fig. 2.16, with a different gradient strength G_2 to avoid accidental refocusing of the previously dephased unwanted magnetisation) exactly cancels any remaining phase errors and the resulting pure-phase excitation profile depends only on the inversion properties of the selective pulse. Experimentally this is an enormous benefit because it makes implementation of the selective sequence straightforward and because the field gradients ensure excellent suppression of the unwanted resonance.
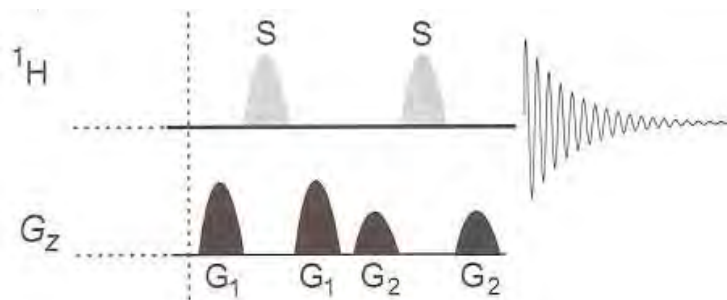
Fig. 2.16. Exitation sculpting (double pulsed field gradient spin-echo) principle.[37]

The resulting excitation profile of the double PFG spin-echo (DPFGSE) is dictated by the cumulative effect of the repeated inversion pulses, resulting in a "chipping away" of magnetisation by the series of gradient-echoes, hence the term *excitation sculpting*.[39,40]

Self-diffusion measurements in dilute micellar solutions

The observed surfactant diffusion coefficient, as obtained from NMR experiment, is an average including contribution from both the monomers and the aggregated surfactant. However it is the contribution from the aggregated surfactant to the observed diffusion coefficient that conveys the information about size and structure of the micelles. Of course, D_{mono} also gives information about size and structure of the single molecule, but this is not the subject of interest for this chapter. The observed diffusion coefficient (D_{obs}) is assumed to be a combination of the diffusion coefficients for aggregated (D_{mic}) and free surfactant monomers (D_{mono}), so that under fast exchange[41,42]:

$$D_{obs} = PD_{mic} + (1 - P)D_{mono} \qquad (2.11)$$

where P is the fraction of micellized surfactant, which is given by:

$$P = \frac{c - cmc}{c} \qquad (2.12)$$

where c is the total surfactant concentration and *cmc* is the critical micelle concentration. D_{mono} can be obtained by measuring the surfactant self-diffusion below *cmc*, where the diffusion coefficient is expected to have a constant value, and can be assumed to be constant

above *cmc*. Once D_{mic} has been determined, it can be compared with theoretical models to predict the size and indicate the structure of the micelles in solution.

As it was mention at the beginning of this subchapter, the hydrodynamic radius R_H can be calculated from the self-diffusion coefficients using the Stokes-Einstein equation (2.8), which describe a spherical particle diffusing in a solvent at infinite dilution:

$$D = \frac{k_b T}{6\pi\eta R_H} \tag{2.8}$$

where k_b is the Boltzmann constant, T is the absolute temperature, η is the viscosity of the solvent and R_H is the hydrodynamic radius including the hydrophobic part, the head group and the hydration water.

The Stokes-Einstein equation (2.8) assumes the absence of intermolecular interaction of the surfactant, i.e. infinite dilution. In the presence of micelles, aggregate obstruction effects must be taken into account. In the case of spherical micelles, a functional form according to the following equation (2.13) is often used:

$$D_{mic} = D_0 \left(1 - k\Phi\right) \tag{2.13}$$

where D_{mic} is the measured micelle diffusion coefficient, D_0 is the micelle diffusion coefficient at infinite dilution, k is a constant and Φ is the volume fraction of micelles. In the case of spherical aggregates, $k \approx 2\text{-}2.5$, depending on the surfactant.

Not only the aggregate self-diffusion, but also the self-diffusion of solvent molecules depends on the shape of aggregates. Different micellar geometries, i.e. spheres, prolates and oblates, give different obstruction effects. This allows the determination of micellar shape through the measurement of solvent diffusion. The relevant theory for this has been worked out by Jönsson et al.[43] In short, the presence of spherical and rod-shaped aggregates give rise to minor obstruction effects, while oblate or disk-shaped particles cause a larger effect.

2.2. Liquid crystals

At a certain moment of life everyone learned that there are three states of matter: solid, liquid and gas. This, however, is not the whole story. There are situations in which more than just three states of matter exist. For now, consider the large class of organic molecules which no not show a single transition from solid to liquid, but rather a series of transitions between the solid and the normal (isotropic) liquid as their temperature is raised. These new phases have mechanical, optical, and structural properties between those of the crystalline solid and the corresponding isotropic liquid. For this reason this phases are referred to as *liquid crystalline* phases, and the materials which form them upon a change in phase are often referred to as *thermotropic liquid crystal*. Another proper name which is used is mesomorphic (or intermediate) phases.[44]

But the temperature is not the only term which may be variable. Another possible way of generating this intermediate state is by addition of solvents in appropriate amount to convenient compounds leading to *lyotropic liquid crystals*. In this type of liquid crystals the concentration range in which the system is liquid crystalline can be compared with the temperature between the melting- and the clearing point of thermotropic liquid crystals.

Chemical compounds which exhibit both kinds of liquid crystal formation are named *amphitropic* (*or amphotropic*) liquid crystals. Such particular compounds show thermotropic liquid crystalline behaviour in their pure state on heating or the formation of lyotropic mesophases on the addition of a further component, mostly of an inorganic or organic solvent in certain amounts.[45]

Almost all novel inositol derivatives which are going to be presented in this work are amphitropic liquid crystals. For this reason the next two chapters will present some features about both the thermotropic and lyotropic liquid crystals.

2.2.1. Thermotropic liquid crystals

As it was mentioned above, the thermotropic liquid crystals exist in dependence of temperature in certain temperature interval. Thermotropic liquid crystals which are stable at temperatures above the melting point of the compound are called *enantiotropic*. In certain cases the liquid crystalline state is only stable at temperatures below the melting point and can be obtained only with decreasing the temperature. Phases of this kind are called *monotropic*.

The structure of the liquid crystalline phases is characterized by the arrangement and conformation of the molecules and the intermolecular interaction. Similar phase structures can be formed by molecules which belong to completely different classes from the chemical stand point. This could be explained by looking at some of the most important phase structures.[44]

The nematic mesophases

The simplest liquid crystalline phase is the nematic phase. There are several types of nematic phases (Fig. 2.17) but all of them can, to a first approximation, simply be described as liquids which have long range orientational order, but lack of positional or bond orientational order. The various types of nematics have slightly different properties based on the details of their molecular structure and chemical behaviour. The two primary types of nematics are uniaxial and biaxial.

The uniaxial is characterized by the following features: a) no positional order, so no bond orientational order; b) orientational order parallel to the director *n*; c) the direction of *n* in space is arbitrary and typically imposed by outside forces such as electric/magnetic fields; d) *n* and –*n* are equivalent; ad e) molecules which form nematics are either achiral or racemic .
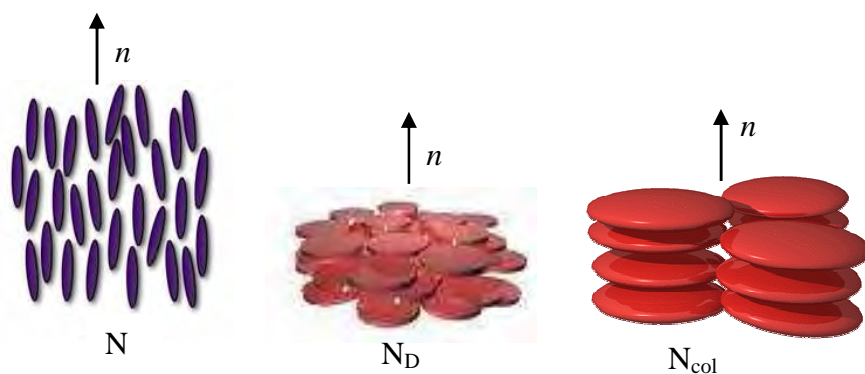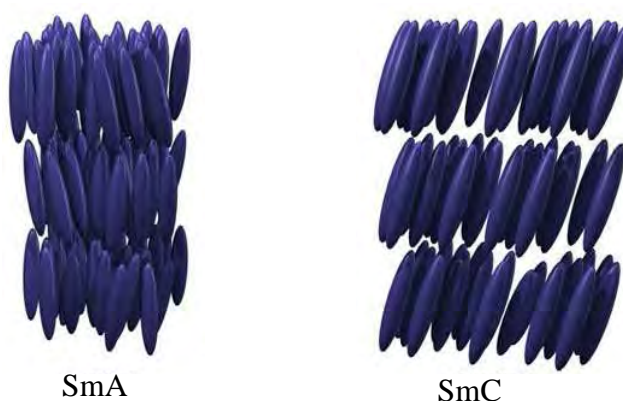

Fig. 2.17. Schematic representation of the most common nematic phases (N = nematic "rod-like" phase, N_D = nematic discotic, N_{col} = nematic columnar).

The biaxial nematic phase is also characterized by the above properties. However this liquid crystalline phase does not posses cylindrical symmetry about *n*. This phase presents two unique directions perpendicular to *n* rendering it biaxial. It should be pointed out that the existence of biaxial phases has been confirmed mostly in lyotropic than in thermotropic liquid crystals.

The smectic mesophases

The name "smectic" was given by G. Friedel to describe certain mesophases that feel slippery like soap when touched, and was originally associated with what is now known as smectic A (SmA) phase. The important feature that distinguishes smectic phases is that they have a layered structure. In fact, positional and bond orientational order have been observed among molecules lying in a smectic phase resulting in over 20 smectic liquid crystalline phases. The most common phase are SmA, SmB, SmC, SmF and SmI.

The simplest is the SmA phase made of achiral and nonpolar molecules and characterized by one-dimensional layered structure on which each layer is essentially a two-dimensional liquid (Fig. 2.18). This phase is uniaxial, the layers are essentially incompressible, and the long axes of molecules within the layer, on the average, are perpendicular to the layers. The SmA phase is characterized by short range positional order and short range bond orientational in the layers.

SmA   SmC

Fig. 2.18. Schematic representation of two smectic phases:
smectic A (SmA) and smectic C (SmC).

The smectic B (or hexatic smectic B) describes a phase which is characterized by a layered structure, just like the SmA phase, *and* long range bond orientational order within the layers. The bond orientational order is the essential property of a hexatic phase. In the SmB phase, the molecules are locally hexagonally packed and the resulting six-fold bond orientational order is maintained for macroscopic distances. The hexatic smectic B phase is a uniaxial phase.

The smectic C (SmC) phase is similar to the SmA phase in that it is a layered structure and each layer may be described as a two dimensional liquid film. However, in this case the molecules are on the average tilted with respect to the normal to the layers, i.e. *n* and the

smectic layer normal are not collinear (Fig. 2.18). Furthermore, the tilt angle, which the molecular long axis makes with the layer normal, is a strong function of temperature. A consequence of the tilting of the molecules is that this phase exhibits biaxial optical and physical properties. There are also chiral versions of the tilted smectic C phases. In these phase the director rotates around the cone generated by the tilt angle as the position along the normal to the layers is varied. These phases with chiral structures are designated by an asterisk to differentiate them from their achiral analogues.

The smectic F (SmF) and smectic I (SmI) phases may be described as tilted analogues of the hexatic smectic B phase. However, with a hexagonal arrangement within smectic planes, the molecules can tilt along two distinct directions with respect to the hexagonal lattice.

The columnar mesophases

Positional order in discotic liquid crystals displays itself by the tendency of the molecules to arrange themselves in columns. This means that in the plane perpendicular to the columns, the molecules tend to arrange themselves in a two-dimensional lattice, either rectangular or hexagonal, as they diffuse throughout the sample. This is called a *columnar phase* (Fig. 2.19). The stacking along the columns is sometimes not regular. In some columnar phases, the molecules are tilted with their short axes not parallel to the column axes. The tilt direction alternates from one column to the next.
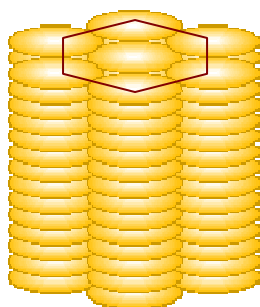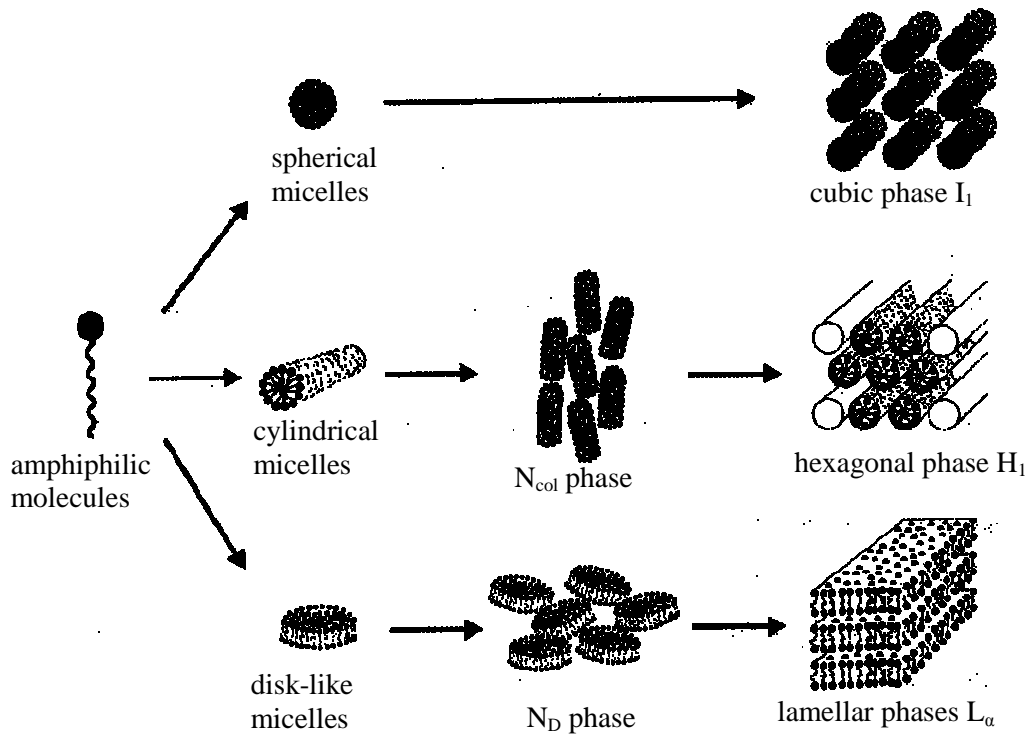

Fig. 2.19. Schematic representation of a hexagonal columnar phase (Col$_h$).

Cubic mesophases

Optically isotropic cubic mesophases are known to occur in some thermotropic systems and more commonly in lyotropic systems. In contrast to the rich information available on lyotropic materials, not much is known about cubic mesophases in thermotropic systems.

2.2.2. Lyotropic liquid crystals

A mesophase formed by dissolving an amphiphilic mesogen in a suitable solvent, under appropiate conditions of concentration, temperature, and pressure is called *lyotropic mesophase*.[46] There are six classes of lytropic liquid crystals: lamellar, hexagonal, cubic, nematic, gel and intermediate phases (Fig. 2.20).

Fig. 2.20. Schematic representation of different types of lyotropic mesophases.[47]

In all of the states except the gel phases, both surfactant and water have a liquid-like molecular mobility that is short-range rotational and translational diffusion on a time scale of 10^{-12} s. They differ in the long-range symmetry of the surfactant aggregates and in the curvature of micelle surface. Except for the phases with flat aggregate surfaces, each class can occur with the polar or the nonpolar regions as the continuous medium, the former being referred to as *normal*, while the latter are *reversed*. Each class of mesophases is usually labelled by a particular letter (Fig. 2.20) with the symbols having subscripts 1 or 2 to distinguish between the *normal* and *reversed* forms.

Lamellar phase (L$_\alpha$)

The most common surfactant mesophase is the lamellar phase (L$_\alpha$), also known as the neat phase from its occurrence during soap manufacture. In this phase, the surfactant molecules are arranged in bilayers frequently extending over large distances (a micron or more) which are

separated by water layers (Fig. 2.21a). This phase is similar to the thermotropic SmA phases. Its major repeating unit, the bilayer, forms the basic structural matrix of biological membranes (Fig. 2.21b). While the lamellar phase does not usually flow under gravity, it has a fairly low viscosity, with the material easily shaken into a container. It is readily identify from its characteristic optical textures. [45]

(a)   (b)
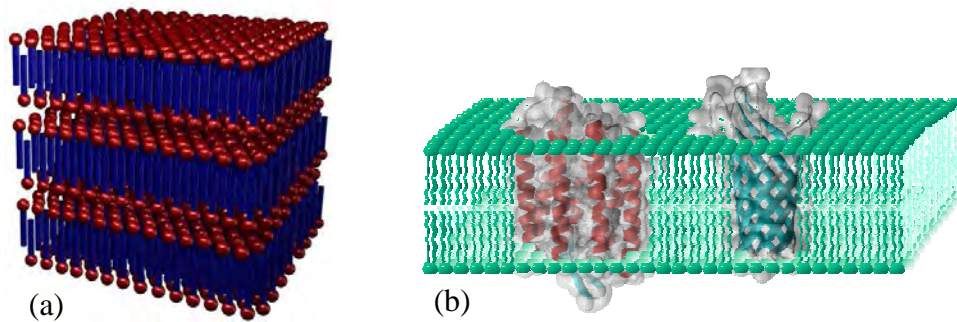
Fig. 2.21. Schematic representation of a) a lamellar phase and
b) a model of biological membranes.

Hexagonal phases (H₁, H₂)

The next most common mesophase type is the hexagonal. There are two distinct classes of hexagonal phase, these being *normal hexagonal* (H_1) also known as the middle phase (again from the soap industry) and a *reversed hexagonal* (H_2) (Fig. 2.22).


H_1 H_2
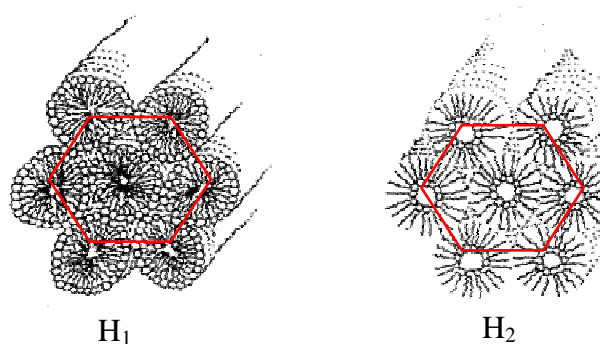
Fig. 2.22. Schematic representation of a normal (H_1) and reversed (H_2) hexagonal phase.

The *normal* phase (H_1) is water-continuous, while the *reversed* (H_2) is alkyl chain-continuous. They consist of indefinitely long circular aggregates packed on hexagonal lattice.[45]

Cubic phases (I, V)

A third category of mesophases formed by surfactants comprises the cubic phases. They are also known as "viscous isotropic". As the name implies, these phases are based around one of three cubic lattices, namely the primitive, face centred and body centred. Therefore, they have no optical texture under polarized light. There are at least four classes of cubic phase, these being the normal and reversed forms of two very different structures. One set of structures (I) is comprised of small globular micelles while the second (V) consists of a 3D micellar network. Within each class several different structures occur.

The simplest cubic phase is that of the I type where the surfactant aggregates are small globular micelles. For the water- continuous I_1 phases, primitive, body centred and face centred lattices have all been proposed. A reversed I_2 structure of globular aggregates packed in a cubic array has been reported recently for some surfactants. Here it appears that the micelles are spherical, but of two different sizes. For reversed micelles the alkyl chain packing constrains no longer limit the micelle diameter, hence the coexistence of two spherical micelles of different size is more plausible than for I_1.
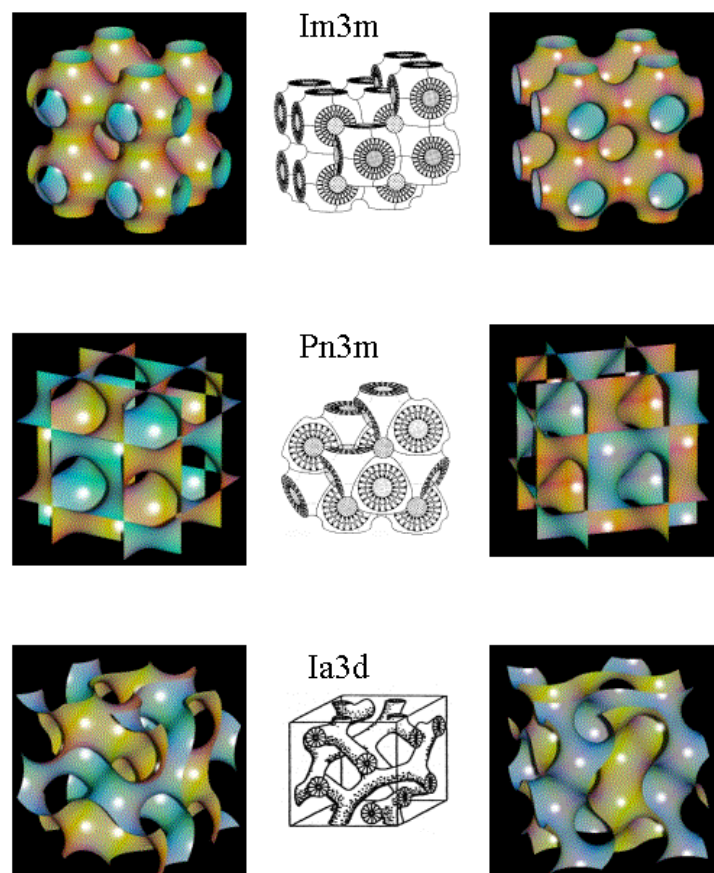
Fig. 2.23. Schematic representation of bicontinuous cubic phases.

The second set of cubic phases has a bicontinuous aggregate structure. Three main space groups Pn3m, Im3m and Ia3d have been reported (Fig. 2.23). The aggregates form a 3D network extending throughout the sample, having curvature towards water (V_1) or towards oil (V_2). These phases are structurally similar to the intermediate phases and although organized around the same cubic lattices as the I phases, have a completely different aggregate structure. The cubic phases are all optically isotropic (as are micellar solutions), but they have very high viscosities hence are easily distinguished from micellar solutions. The two classes of cubic phase, I and V, are distinguished from each other by their location in the phase diagram. I phases occur at the composition between micellar solutions and hexagonal phases, whilst V phases occur between hexagonal and lamellar phases.[45]

Nematic phases (N)

Lyotropic nematic phases are some what less common than the mesophases discussed so far. They occur at the boundary between an isotropic micellar phase (L_1) and the hexagonal phase (H_1) or between L_1 and the lamellar phase (L_α). As their name implies they have a similar long range micellar order to that of molecules in thermotropic nematic phase. They are of low viscosity, possessing long range micellar orientational order but reduced translational order compared to the other lyotropic phases, and like the thermotropic phase can be aligned in a magnetic field. It is possible to identify nematic phases optically because of their characteristic schlieren texture.[45]

Gel phases (L_β)

The gel phase (L_β) closely resembles the lamellar phase in that it is comprised of surfactant layers, but it differs in its very high viscosity. The term "gel" originates from industry where these systems were observed to have a gel-like rheology. There are commonly reported to be three different structures of the gel phase normal, tilted and interdigitated. The first structure, with the bilayer normal to the liquid crystal axis, is the structure most commonly found in dialkyl lipid systems. The second structure, the tilted bilayer, is found in systems where the polar head group is larger than the width of the alkyl chain (monoglyceride systems). The third structure, the interdigitated form, is found with long chain monoalkyl systems (potassium stearate).[45]

Intermediate phases

A number of so-called "intermediate" phases have been identified. They replace V_1 bicontinuous cubic phases for surfactants with longer or more rigid hydrophobic chains. It is likely that they can replace the V_2 phases under some conditions. Unlike the V_1/V_2 phases, intermediate phases are anisotropic in structure, and consequently birefringent. Also they are often much more fluid than the cubic phases. There are three broad types of intermediate phases according with the symmetry: rectangular ribbon structures, layered mesh structures, and the bicontinuous structures which do not have cubic symmetry. Ribbon phases may be regarded as a distorted hexagonal phase. Mesh phases are distorted lamellar phases in which the continuous bilayers are broken by water filled defects which may or may not be correlated from one layer to the next. The bicontinuous phases are distorted cubic structures.[45]

Phase diagrams of binary systems

The best way to illustrate the behaviour of an amphiphilic material in water is to show a phase diagram. The typical phase diagram of a binary system is a graph-like plot of composition (along the abscissa) against temperature (along the ordinate). A general convention established placing water to the left and the surfactant to the right. The term "graph-like" is used advisedly, for the phase diagrams differ importantly from the graphs. The span of compositions is restricted to 0-100%, and the vertical boundaries at these limits have special significance: they are phase diagrams in their own right.

The area within phase diagrams is divided into regions by lines. Some of these are straight lines that are either precisely horizontal or vertical, while others are smooth curves. The latter generally depict the limits of miscibility of the components, and are called *phase boundaries*. A one-phase region always exists to one side of phase boundaries and a two-phase region to the other. The regions are labelled so that both the number of phases present, and their structures, can be read from the diagram.[28]

A phase diagram can present horizontal lines (lines of constant temperature or isotherms) called *isothermal discontinuities*. These reflect the existence of discontinuities in phase behaviour which occur at these temperatures. Vertical lines (lines of constant composition or isopleths) can also exist and are called *isoplethal discontinuities*. Two vertical lines are always found at 0 and 100% compositions which are the unary diagrams of components. In

the diagnosis of phase behaviour, these isopleths (as well as the components themselves) should be treated as phase regions whose span of composition is zero.

Phase diagrams constitute a dense form of information. With a little practice it is easily possible to read phase behaviour at specific coordinates. With further practice progressive changes in phase behaviour along isothermal or isoplethal process trajectories may be readily be perceived. Finally, phase diagrams make it possible to grasp quickly and comprehensive the phase behaviour of a system as a whole. No better way to communicate visually all these kinds of information has been yet devised.

2.2.3. Analytical methods to characterize liquid crystals

The liquid crystalline phase is a distinct phase of matter, but there are many different types of liquid crystalline phases. The various liquid crystalline phases and other mesophases are characterised and then classified according to the molecular ordering that constitutes the phase structure. Not surprisingly, the difference between the many different liquid crystal phases is generally minimal. Such minimal differences in structure mean that the precise classification of liquid crystals often requires the use of several analytical techniques (and a great deal of experience).[48]

The most common analytical techniques used in characterization of liquid crystalline materials are optical polarizing microscopy (PM), differential scanning calorimetry (DSC), X-ray diffraction, and miscibility studies. Other techniques used to identify the structure of liquid crystalline mesophases include neutron scattering studies and nuclear magnetic resonance (NMR) studies.

Optical polarizing microscopy

The most widely used technique of liquid crystal phase identification is optical polarizing microscopy (PM), which reveals that each different liquid crystal phase has a distinct optical texture.

The identification of mesophase trough PM usually involves the magnified view of a thin sample of a mesogenic material sandwiched between a glass microscope slide and a glass coverslip. The microscope slide of material is usually placed on a stage, which can be accurately temperature-controlled, between polarizers which are crossed at 90° to each other. The manner in which the molecules are arranged within the phase can be detected by careful

analysis of the microscopic texture. Since the polarizers in the microscope are crossed at 90° to each other, then with no sample in place light is extinguished and so blackness is seen. Similarly, if an isotropic liquid is analyzed, the polarized light remains unaffected by the sample and so no light passes trough the analyser. However, when an anisotropic, birefringent medium is present (e.g. a liquid crystalline mesophase) light is not extinguished and an optical texture appears that gives information relating to the arrangement of the molecules within the medium. When analyzing mesophases by PM, the texture that is revealed depends upon how the sample is aligned, in addition to being dependent upon the phase structure of the sample. There are two basic forms of alignment for the liquid crystalline compounds, *homeotropic* and *homogeneous* (*planar*). Homeotropic alignment is where the molecules that constitute the phase are oriented such that their long axes (more importantly their optic axes) are normal to the supporting substrate. When the molecules are so oriented polarised lights is unaffected by the material and so light cannot pass trough the analyser. Hence from this vantage point the observer looking trough the microscope will see complete blackness. In homogeneous (planar) alignment the constituent molecules of the liquid crystal phase are oriented parallel to the supporting substrates.

The optical polarizing microscopy enables the identification of the type of liquid crystal and other mesophases from the optical texture that is generated. However, the technique is also essential when evaluating the physical properties of liquid crystals in certain phases and over particular temperature ranges.[48]

Differential scanning calorimetry (DSC)

Differential Scanning Calorimetry (DSC) is a useful tool which complements optical methods in the study of liquid crystal phase transitions. DSC means the measurement of the change of the difference in the heat flow rate to the sample and a reference sample while they are subjected to a control temperature program.[49]

This method has the advantages of high sensitivity for detecting enthalpy changes (as small as ~0.01J/g), very small sample size (up to 10 mg), rapid and convenient operation procedures using commercial instruments with flexible computer software programs.

The basic principle underlying this technique is that, when the sample undergoes a physical transformation such as phase transitions, more or less heat will need to flow to it than the reference to maintain both at the same temperature. Whether more or less heat must flow to the sample depends on whether the process is exothermic or endothermic. For example, as a

solid sample melts to a liquid it will require more heat flowing to the sample to increase its temperature at the same rate as the reference. This is due to the absorption of heat by the sample as it undergoes the endothermic phase transition from solid to liquid. Likewise, as the sample undergoes exothermic processes (such as crystallization) less heat is required to raise the sample temperature. By observing the difference in heat flow between the sample and reference, differential scanning calorimeters are able to measure the amount of heat absorbed or released during such transitions. DSC may also be used to observe more subtle phase changes, such as glass transitions. There are two types of DSC systems in common use, the power compensation DSC and the heat flux DSC.

In power compensation DSC the temperatures of the sample and reference are controlled independently using separate, identical furnaces. The temperature of the sample and reference are made identical by varying the power input to the two furnaces. The energy required to do this is a measure of the enthalpy or heat capacity changes in the sample relative to the reference.

In heat flux DSC a defined exchange of the heat to be measured with the environment takes place via a well-defined heat conduction path with given thermal resistance. The primary measurement signal is a temperature difference which is related to enthalpy change in the sample using calibration experiments. In commercial heat flux differential scanning calorimeters, the heat exchange path is realized in different ways. The most important fundamental types are the disk-type, the turret-type and the cylinder-type measuring systems.
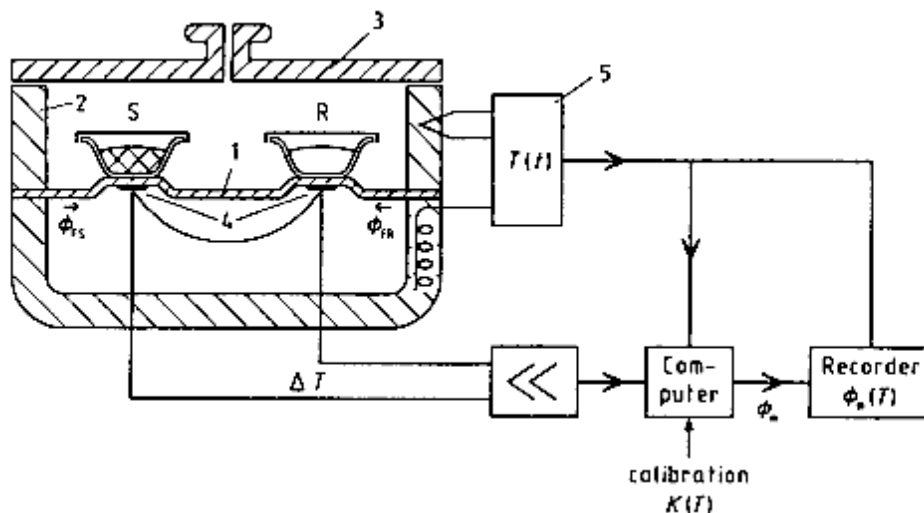
Fig. 2.24. Schematic representation of a heat-flux DSC with disk-type measuring system: 1 – disk, 2 – furnace, 3 – lid, 4 – differential thermocouple(s), 5 – programmer and controller, S – crucible with sample substance, R – crucible with reference sample substance, Φ_{FS} – heat flow rate from furnace to sample crucible, Φ_{FR} - heat flow rate from furnace to reference sample substance, Φ_m – measured heat flow rate, K – calibration factor.

In case of disk-type measuring system the main heat flow from the furnace to the samples passes symmetrically trough a disk of medium thermal conductivity (Fig. 2.24). The samples (or the samples containers) are positioned on this disk symmetrical to the centre. The temperature sensors are integrated in the disk which can be made from metal, quartz glass or ceramic.

The characteristic feature of the turret-type measuring system is that the essential heat flow passes from the bottom of the furnace through the jacket of two thin-walled cylinders to the top of them which serve as sample and reference sample support.

For the case of the cylinder-type measuring system, a block-type cylindrical furnace is provided with two cylindrical cavities, each containing a cylindrical, fixed sample container, which is connected with the furnace or directly with the other container by means of several thermocouples.

The differential scanning calorimetry cannot identify the type of liquid crystal phase, but the level of the enthalpy change does give some information about the degree of molecular ordering within the mesophase.[49]

X-ray diffraction

X-ray diffraction is the most useful technique in investigating the microscopic structure of liquid crystals. This technique will map the positions of the molecules within the phase and hence determine the phase structure and classification to which the particular phase belongs. However, to maximize information, aligned samples are needed.

Miscibility studies

Liquid crystal phases present in novel compounds can be identified and classified by miscibility studies. The material with unknown mesophase is mixed with a known material that possesses mesophases that have been already identified. If a particular mesophase of the unknown material is completely miscible with a known mesophase of the known material, then it can be concluded that the two phases of each compound are identical and belong to the same miscibility group.

3. RESULTS AND DISCUSSION I

The present chapter is divided in two subchapters. The first one offers details concerning the syntheses of a number of new regiochemically defined inositol derivatives, while the second one presents the physical properties with regard to liquid crystalline mesomorphism as well as the solution/surface activity in aqueous solution.
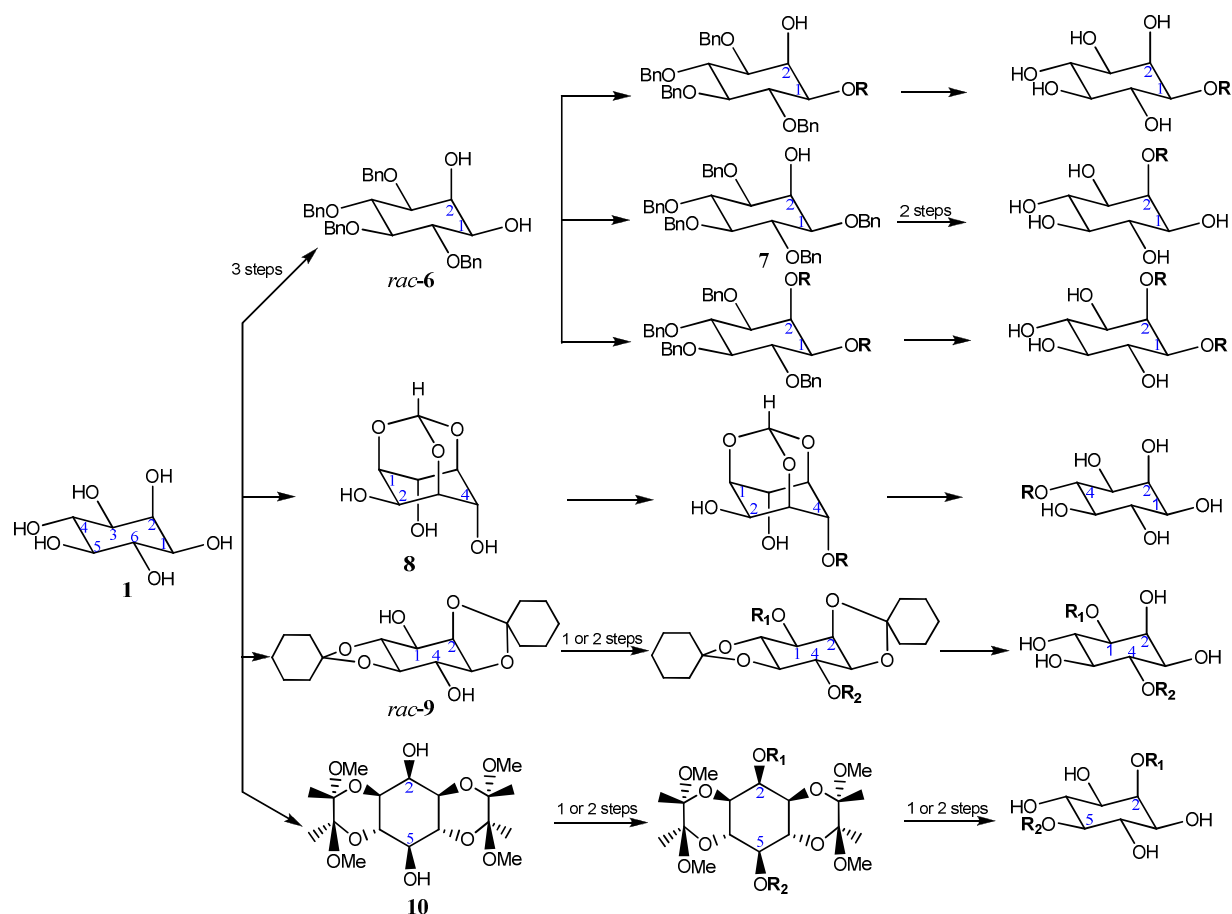
3.1. Syntheses

3.1.1. Protective group strategies with respect to *myo*-inositol

When a chemical reaction is to be carried out selectively at one reactive site in a multifunctional compound, other reactive sites must be temporarily blocked. Many protective groups have been, and are being, developed for this purpose. A protective group must fulfil a number of requirements: it must react selectively in good yield to give a protected substrate that is stable to the projected reactions; it must be selectively removed in good yield by readily available, preferably non-toxic reagents that do not attack the regenerated functional group; should form a crystalline derivative that can be easily separated from side products associated with its formation or cleavage; should have a minimum of additional functionality to avoid further sites of reaction. [50]

The well-established protecting group chemistry[51-55] of *myo*-inositol (**1**) mainly consists of selective acetalization, etherification, esterification, and the respective deprotection reactions. The main factor for the synthetic differentiation of the dissimilar ring positions in *myo*-inositol (**1**) is the axial hydroxyl function at the 2-position. On one hand, this leads to the formation of *cis*-annealed 6-ring/5-ring acetals which are energetically favoured over the respective *trans*-annealed structures and on the other hand, the axial or the equatorial hydroxyl functions can be distinguished by their accessibility and reactivity.

Subsequent application of such protecting group strategies allows specifically addressing and modifying the different ring positions in *myo*-inositol. Exemplary, Scheme 3.1 presents a number of possible strategies which are described more detailed later in the present work.

Scheme 3.1. Protective group strategies for selective substitution of the hydroxyl function in *myo*-inositol (R – any substituent).

3.1.1.1. Synthesis of 1,4,5,6- tetra-*O*-benzyl-*myo*-inositol (*rac*-6)

In order to functionalise the position 1 and/or position 2 from the inositol ring, it is necessary at first to synthesize the 1,4,5,6-tetra-*O*-benzyl-*myo*-inositol (*rac*-6). For this purpose the desired free hydroxyl groups have to be selective protected. Therefore the hydroxyl groups from C_1 and C_2 were protected by acetalisation with cyclohexanone. The four free remaining hydroxyl functions were subsequently benzylated and finally the acetal was hydrolized to give *rac*-6 (Scheme 3.2).
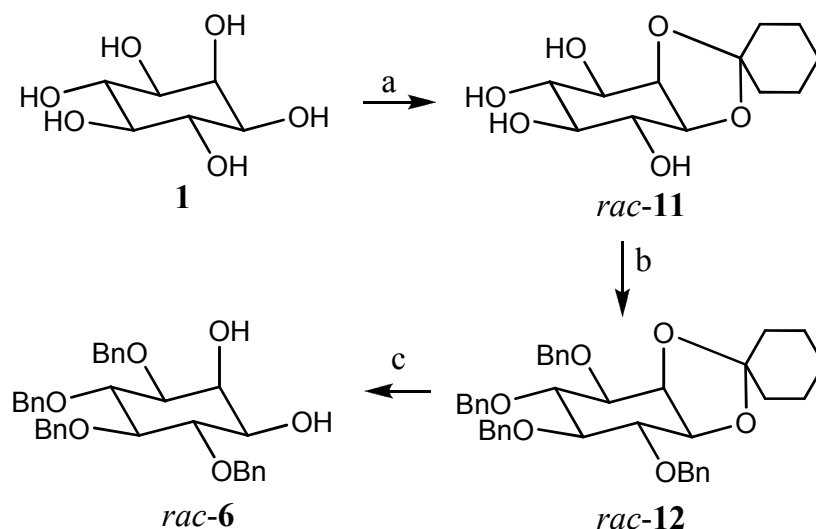
Scheme 3.2. The synthetic route towards 1,4,5,6-tetra-*O*-benzyl-*myo*-inositol (*rac*-**6**):
a) cyclohexanone, *p*-TsOH, toluene, 170 °C, 80%; b) BnCl, KOH, 100 °C, 80%;
c) acetic acid, H$_2$O, 100 °C, 98%.

For the synthesis of 1,2-*O*-cyclohexylidene-*myo*-inositol (*rac*-**11**), *myo*-inositol (**1**) was refluxed for 6 hours with cyclohexanone in toluene and *p*-toluene sulfonic acid monohydrate as catalyst with continuously separation of formed water using a Dean-Stark separator. To use only a small amount of *p*-toluene sulfonic acid as catalyst is important because in larger concentrations it promotes the self-condensation of the cyclohexanone. Using a big excess of cyclohexanone, a mixture of di- and triketals together with the desired monocyclohexylidene derivative is formed, but these by-products could mildly be hydrolyzed to the desired monoketal by addition of ethanol. The acetal *rac*-**11** was obtained by recrystallization from ethanol with a yield of 80% (lit.[56] 82%).

The next step is the protection of the remaining hydroxyl functions as benzyl ethers leading to 1,4,5,6-tetra-*O*-benzyl-2,3-*O*-cyclohexylidene-*myo*-inositol (*rac*-**12**). For this aim, the tetraol *rac*-**11** was heated with benzyl chloride and potassium hydroxide for 20 hours at 100°C. The desired *rac*-**12** was obtained after recrystallization from methanol in 80% yield (lit.[57] 74%).

The final step for achieving the 1,4,5,6-tetra-*O*-benzyl-*myo*-inositol (*rac*-**6**) resides in *rac*-**12** hydrolysis which was performed by heating with acetic acid and water at 100 °C for 2.5 hours with a yield of 98 % (lit.[57] 84%) followed by recrystallization from methanol.

3.1.1.2. Synthesis of 1,3,4,5,6-penta-*O*-benzyl-*myo*-inositol (7)

In order to selectively attach a substituent to the hydroxyl at position 2 of the *myo*-inositol ring, all the other 5 hydroxyl functions should be protected. One of the possibilities to achieve this goal is the synthesis of 1,3,4,5,6-penta-*O*-benzyl-*myo*-inositol (**7**) (Scheme 3.3).
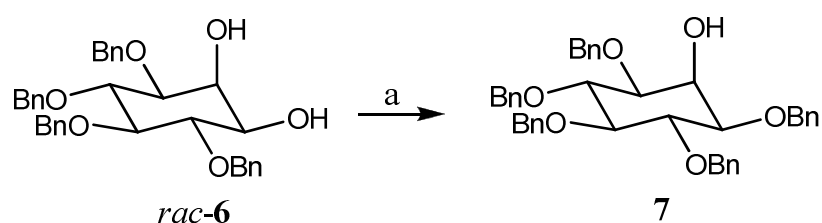
Scheme 3.3. Selective synthesis of 1,3,4,5,6-penta-*O*-benzyl-*myo*-inositol (**7**):
a)1. Bu$_2$SnO, MeOH, reflux; 2. BnBr, CsF (1.3 eq), DMF, toluene; 90%.

The regioselective manipulation of hydroxyl groups via stannylene derivatives has been already applied in carbohydrate chemistry since many years and is noteworthy because it accomplishes the regioselective activation of a specific hydroxyl function e.g. the equatorial hydroxyl of a six-membered ring *cis*-1,2-diol.[58] The origin of the activation is not yet clear but structural evidence including X-ray data point to dimeric (or oligomeric) stannylene structures in which the tin atoms are in the centre of a trigonal bi-pyramid with the butyl groups occupying the two equatorial positions (Scheme 3.4). The more electronegative of the two oxygen atoms occupies the apical position and is co-ordinated to only one tin atom whereas the less electronegative oxygen is ensconced in a Sn$_2$O$_2$ bridge and is therefore co-ordinated to two tin atoms. Thus the observed regioselectivity is a consequence of a selection of a particular pair of hydroxyl functions for stannylene formation followed by orientation of the more electronegative oxygen in the apical position, which is intrinsically more reactive.[59]
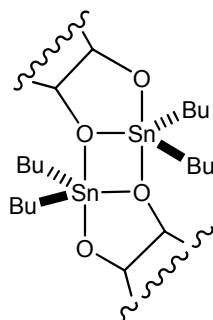
Scheme 3.4. Dimeric structure of stannylene derivatives of 1,2-diols.

To synthesize 1,3,4,5,6-penta-*O*-benzyl-*myo*-inositol (**7**), the first step consisted in refluxing 1,4,5,6-tetra-*O*-benzyl-*myo*-inositol (*rac*-**6**) with dibutyltin oxide in dry methanol for 3 hours. After evaporation of the solvent, the resulted crude mixture was dissolved into a 1:1 mixture of DMF and toluene and reacted with benzyl bromide and CsF to afford the desired 1,3,4,5,6-penta-*O*-benzyl-*myo*-inositol (**7**) with 90% (lit.[15] 96%) yield.

3.1.1.3. Synthesis of 1,3,5-*O*-*myo*-inositol orthoformate (8)

In the last decade, protection of the hydroxyl groups at positions 1, 3, and 5 of *myo*-inositol as the corresponding orthoester has frequently been used. This is mainly because orthoesters of *myo*-inositol can be easily obtained in gram scale as a single product.

The formation of the 1,3,5-orthoester of *myo*-inositol involves inversion of the inositol ring (Scheme 3.5). Consequently, this orthoester has five oxygen atoms in axial positions and an oxygen atom in the equatorial position with respect to the *myo*-inositol ring. The *myo*-inositol orthoester is in fact a highly functionalized adamantane. Three of the carbon atoms in adamantane are replaced by three oxygen atoms (C_1, C_3 and C_5 oxygen atoms of the inositol ring) and three of the methylene groups of adamantane are hydroxylated (C_2, C_4 and C_6 of the inositol ring). This results in an analogue of the adamantane molecule, which has two pairs of 1,3-*trans* hydroxyl groups and one pair of 1,3-*cis* hydroxyl groups.
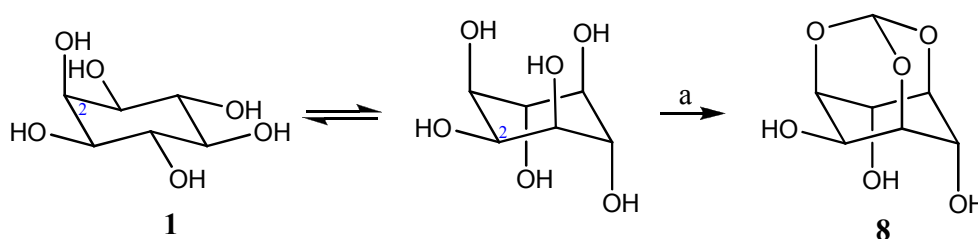
Scheme 3.5. Synthesis of 1,3,5-*O*-myo-inositol orthoformate (**8**):
a) CH(EtO)$_3$, *p*-TsOH, DMF, 100 °C, 80%.

The 1,3,5-*O*-*myo*-inositol orthoformate (**8**) was prepared by heating of *myo*-inositol (**1**) with triethyl orthoformate and *p*-toluenesulfonic acid in dry DMF at 100 °C. The desired product was isolated by column chromatography in 80% yield (lit.[60,61] 80%).

3.1.1.4. Synthesis of 1,2:4,5-di-*O*-cyclohexylidene-*myo*-inositol (*rac*-9)

To selectively functionalize the hydroxyl groups from positions 1 or/and 4 of *myo*-inositol, it would be necessary to protect the other four hydroxyl groups. This aim could be achieved by a one step synthesis of 1,2:4,5-di-*O*-cyclohexylidene-*myo*-inositol (*rac*-9) (Scheme 3.6).
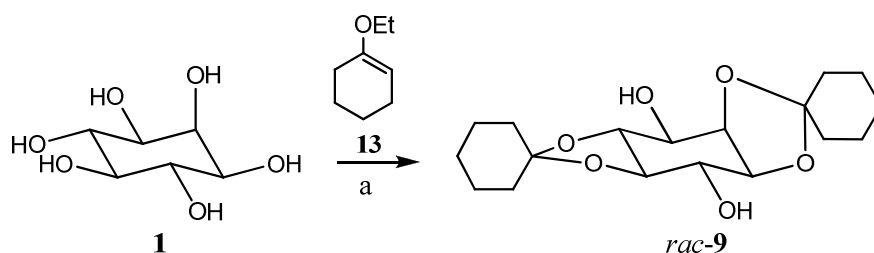

Scheme 3.6. Synthesis of 1,2:4,5-di-*O*-cyclohexylidene-*myo*-inositol (*rac*-9):
a) **13**, *p*-TsOH, DMF, 100 °C, 30%.

Treatment of *myo*-inositol (**1**) with 1-ethoxycyclohexene (**13**) and a catalytic amount of *p*-toluenesulfonic acid in dry DMF produced a mixture of three derivatives: 1,2:3,4-, 1,2:4,5-, and 1,2:5,6-di-*O*-cyclohexylidene-*myo*-inositol in yields of 20, 30 and 35%. The desired 1,2:4,5 derivative (*rac*-9) can be easily separated from the mixture by crystallization whereas column chromatography is necessary to separate the other two derivatives.[62,63]

3.1.1.5. Synthesis of 1,6:3,4-bis-*O*-(2',3'-methoxybutane-2',3'-diyl)-*myo*-inositol (10)

The application of the butane-2,3-diacetal (BDA) protecting group for the selective protection of *trans*-1,2-diols in various monosaccharide derivatives was first demonstrated by Montchamp et al.[64] These authors also reported the first synthesis of **6** on a 1 g scale by acidic-catalysed reaction of *myo*-inositol with 2,2,3,3-tetramethoxybutane (TMB) in refluxing methanol for 135 h in the presence of trimethyl orthoformate as a dehydrating agent. It was later shown[65] that the BDA group could be introduced into a variety of polyols using cheap and commercially available butane-2,3-dione instead of TMB. Potter et al[66] reported that, in addition to the symmetrical diol **10**, a second major product also results from the acid-catalysed reaction of butane-2,3-dione with *myo*-inositol: namely the asymmetrical DL-1,6:4,5-bis-*O*-(2',3'-dimethoxybutane-2',3'-diyl)-*myo*-inositol (±) **14** (Scheme 3.7).

Furthermore, it was found that long reaction times would give better yields for **10** but led to the gradual accumulation of a less polar by-product, which is difficult to remove. For large-scale production of **10** therefore it was preferable to use moderate reaction times (20-96 h).[67]
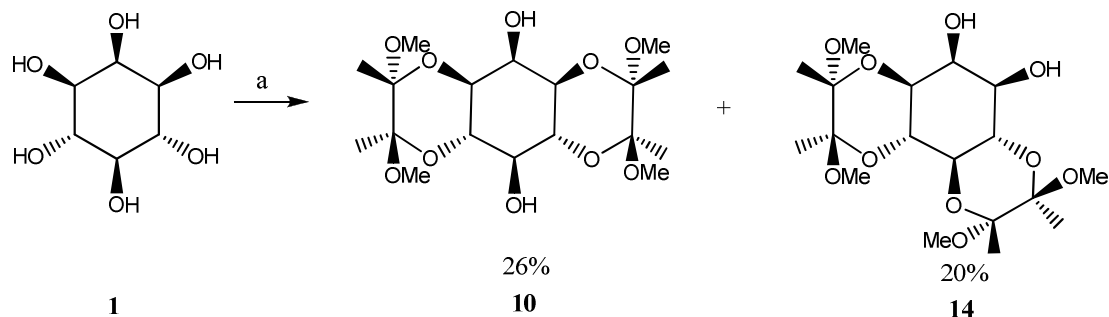
Scheme 3.7. Application of BDA protection of 1,2-diols on *myo*-inositol:
a) HC(OMe)$_3$, MeOH, CSA, butane-2,3-dione.

Refluxing *myo*-inositol (**1**) with trimethyl orthoformate, butane-2,3-dione and a catalytic amount of camphor sulphonic acid in methanol for around 40 hours, the symmetric diol **10** was obtained with 26% yield. The modest yield is acceptable considering the low cost of the starting materials, convenience of the method, and ease of isolation. Because the diol **10** has a very low solubility in methanol, while the other major product **14**, and various minor by-products at this stage are all soluble, the product is simply filtered off from the cooled reaction mixture and dried.

3.1.2. Synthetic strategies towards *myo*-inositol derivatives

3.1.2.1. Synthesis of 1-*O*-[2'-[2''-[2'''-(dodecyloxy)ethoxy]ethoxy]ethyl]-*myo*-inositol (*rac*-19)

Rac-19 is the first representative of a new class of inositol-based surfactants that combine the properties of classical sugar surfactants and oligo(ethylene oxide) alkyl surfactants.

Its synthesis starts with a Williamson etherification of triethylene oxide, analogue to lit.[68] For this purpose, triethylene oxide (15) were stirred for 1 hour at 100 °C with 50% aq NaOH followed by the dropwise addition of dodecyl bromide. The reaction was allowed to proceed for 23 hours at 100 °C. After the required work-up and purification, the triethylene oxide monododecyl ether (16) was obtained with 82 % yield and subsequently tosylated[69] with *p*-tosyl chloride and 17% aq NaOH in THF at 0 °C for four hours. The tosylated triethylene glycol monododecyl ether (17) was obtained in 85% yield (Scheme 3.8).
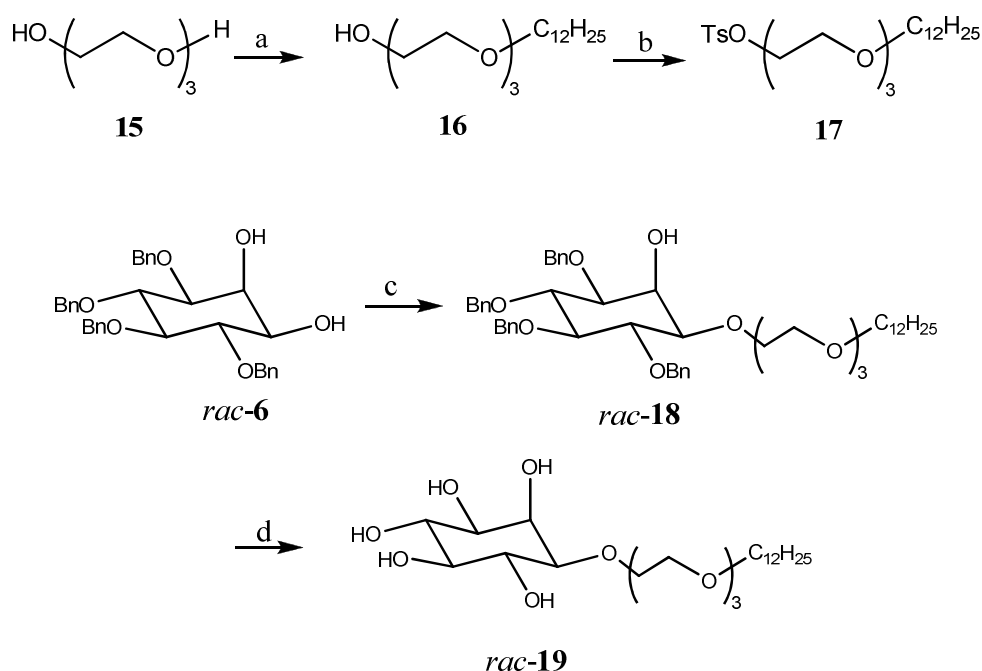
Scheme 3.8. Synthesis of *rac*-19:
a) $C_{12}H_{25}Br$, NaOH 50% aq, 100°C, 82%; b) *p*-TsCl, NaOH 17% aq, THF, 0 °C, 85%;
c) 1. Bu_2SnO, MeOH, reflux; 2. **17**, CsF, DMF, rt; 50%; d) H_2, Pd/C (10 mol%),
MeOH, EtOAc, 90%.

The next step consists of the regioselective combination of the two building blocks, *rac*-6 and **17**. This step was realized by refluxing *rac*-6 for three hours with dibutyltin oxide in methanol

followed, after evaporation of the solvent, by the addition of tosylate **17** in presence of caesium fluoride in dry DMF, and stirring at r.t. for 48 hours. After the necessary work-up and purification, the protected *rac*-**18** was obtained in 50% yield (Scheme 3.8).

The new derivative *rac*-**19** was produced after deprotection by hydrogenolysis under pressure (~ 8 bars) with 10 mol% Pd/charcoal, which gave *rac*-**19** in 90% yield (Scheme 3.8).

The desired 1-*O*-[2'-[2''-[2'''-(dodecyloxy)ethoxy]ethoxy]ethyl]-*myo*-inositol (*rac*-**19**) was obtained in seven steps starting from *myo*-inositol with an overall yield of 20%.

3.1.2.2. Synthesis of 2-*O*-[2'-[2''-[2'''-(dodecyloxy)ethoxy]ethoxy]ethyl]-*myo*-inositol (21)

In order to study the influence of regiochemical position of the attached alkyl-triethylene oxide chain to *myo*-inositol ring with regard to mesomorphism and surface activity, a further new derivative (**21**) – in which the sidechain is attached to the hydroxyl group at the 2-position (the axial) of *myo*-inositol – was synthesized in eight steps starting from *myo*-inositol in 31% overall yield.

To arrive at this compound, the 1,3,4,5,6-penta-*O*-benzylated-*myo*-inositol **7** was reacted with tosylate **17** in the presence of NaH (55-65% in mineral oil) and dry DMF to give the protected **20** in 90% yield. This intermediate was subsequently deprotected in presence of hydrogen (pressure ~ 8 bars) and Pd/charcoal to cleave the five benzyl ethers and to give the desired **21** in 88% yield (Scheme 3.9)
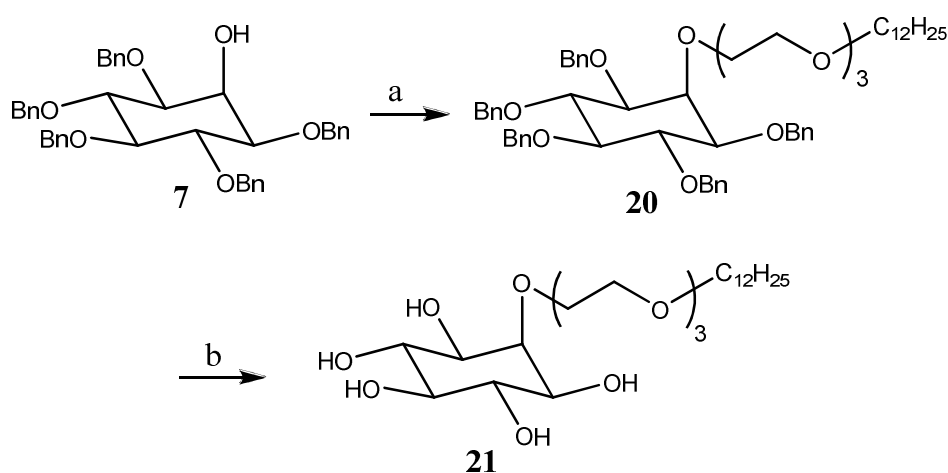
Scheme 3.9. The last two steps from the synthesis of the *meso* derivative **21**:
a) **17**, NaH, DMF, rt, 90%; b) H_2, Pd/C, MeOH, EtOAc, 88%.

3.1.2.3. Synthesis of 4-*O*-[2'-[2''-[2'''-(dodecyloxy)ethoxy]ethoxy]ethyl]-*myo*-inositol (*rac*-26)

Another possible isomer of *rac*-19 would be *rac*-26 in which the alkyl-triethylene oxide chain is attached to the hydroxyl group of position 4 of *myo*-inositol ring.

As it was previously mentioned (subchapter 3.1.1.3), the *myo*-inositol orthoester (8) is in fact a highly functionalized adamantane. The rigidity of the adamantane frame-work and the presence of six oxygen atoms in the molecule impart unusual chemical and physical properties on *myo*-inositol orthoesters and its derivatives. This orthoester has *meso* configuration and hence two of the hydroxyl groups (C_4 and C_6) are chemically equivalent. The C_4 and C_6 hydroxyl groups form a strong intramolecular hydrogen bond[61,70] (Scheme 3.10) as a result of which, one of these hydroxyl groups is more acidic than the C_2 hydroxyl group. Hence bases that can deprotonate the more acidic hydroxyl group (C_4 or C_6) result in the formation of the corresponding anion 23 which is also stabilized by intramolecular hydrogen bonding with the other axial hydroxyl group. When the metal hydrides are used as bases, the resulting alkoxide at the C_4 or the C_6 hydroxyl group is stabilized by chelation (24) with the *cis*-hydroxyl group. As the result of these intramolecular interactions, selective mono functionalization of one of the 1,3-*cis*-hydroxyl groups or the C_2 hydroxyl group can be achieved.[71]
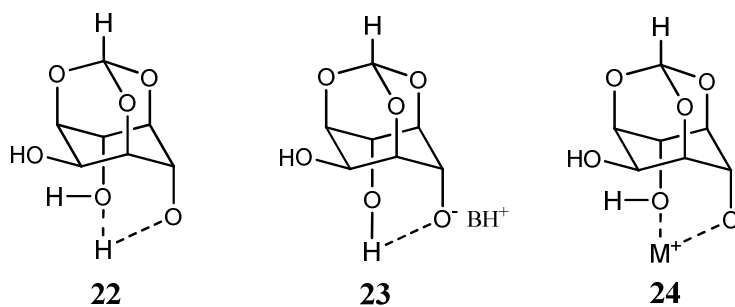
Scheme 3.10. Intramolecular interactions in *myo*-inositol orthoester

Alkylation of *myo*-inositol orthoformate 8 with the tosylate 17 in presence of NaH and dry DMF results in formation of the corresponding C_4 ether 25 in 62% yield. The final step is the hydrolysis of orthoester 25 by refluxing it with methanol and 6M HCl for four hours to achieve *rac*-26 in 83% yield after purification (Scheme 3.11).
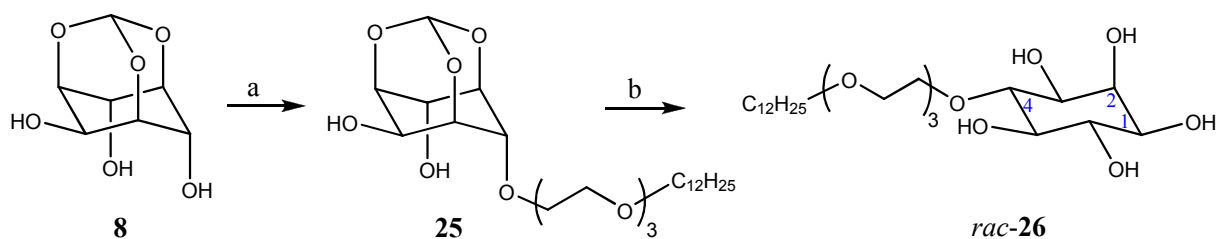
Scheme 3.11. The last steps of synthesis of *rac*-**26**:
a) **17**, NaH, DMF, rt, 62%; b) MeOH, HCl 6 M, reflux, 83%

The new isomer, *rac*-**26**, could be obtained in five steps starting from *myo*-inositol with an overall yield of 30%.

3.1.2.4. Synthesis of 1-*O*-dodecyl-4-*O*-[2'-[2''-[2'''-(hydroxy)ethoxy]ethoxy]ethyl]-*myo*-inositol (*rac*-32)

In order to study and compare the influence of the molecular arrangement of the oligo(ethylene oxide) and sugar units on mesomorphism and surface activity, a new inositol-based derivative (*rac*-**32**) was synthesized which has the alkyl chain attached to the hydroxyl group from position 1 and the triethylene oxide unit attached to hydroxyl group from position 4. The surfactant *rac*-**19** represents the sequence inositol–triethylene oxide–dodecyl chain, while *rac*-**32** represents the "inversed" sequence, triethylene oxide–inositol–dodecyl chain. This "inversion" of the building block results in interesting differences with regard to physical properties, as it will be presented in chapter 3.2.

As the synthesis of *rac*-**19**, the synthesis of *rac*-**32** begins with the corresponding preparation of the triethylene oxide building block. For this purpose, the triethylene oxide **15** was first protected at one end by etherification with benzyl chloride and 50% aq NaOH for 19 hours at 100 °C to give the monobenzyl ether **27** in 65% yield (lit.[72,73] 60%). The protected triethylene oxide **27** was next tosylated by reaction with *p*-tosyl chloride and 17% aq NaOH at 0 °C to give the desired tosylate **28** in 85% yield (Scheme 3.12).[74]
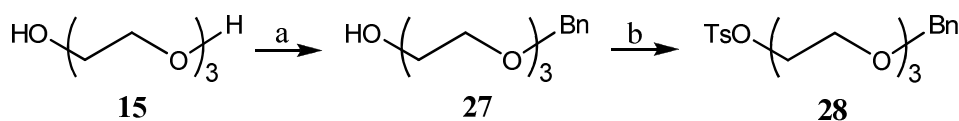
Scheme 3.12. The synthesis of tosylate **28**:
a) BnCl, NaOH 50% aq, 100°C, 65%; b) *p*-TsCl, NaOH 17% aq, THF, 0 °C, 85%;
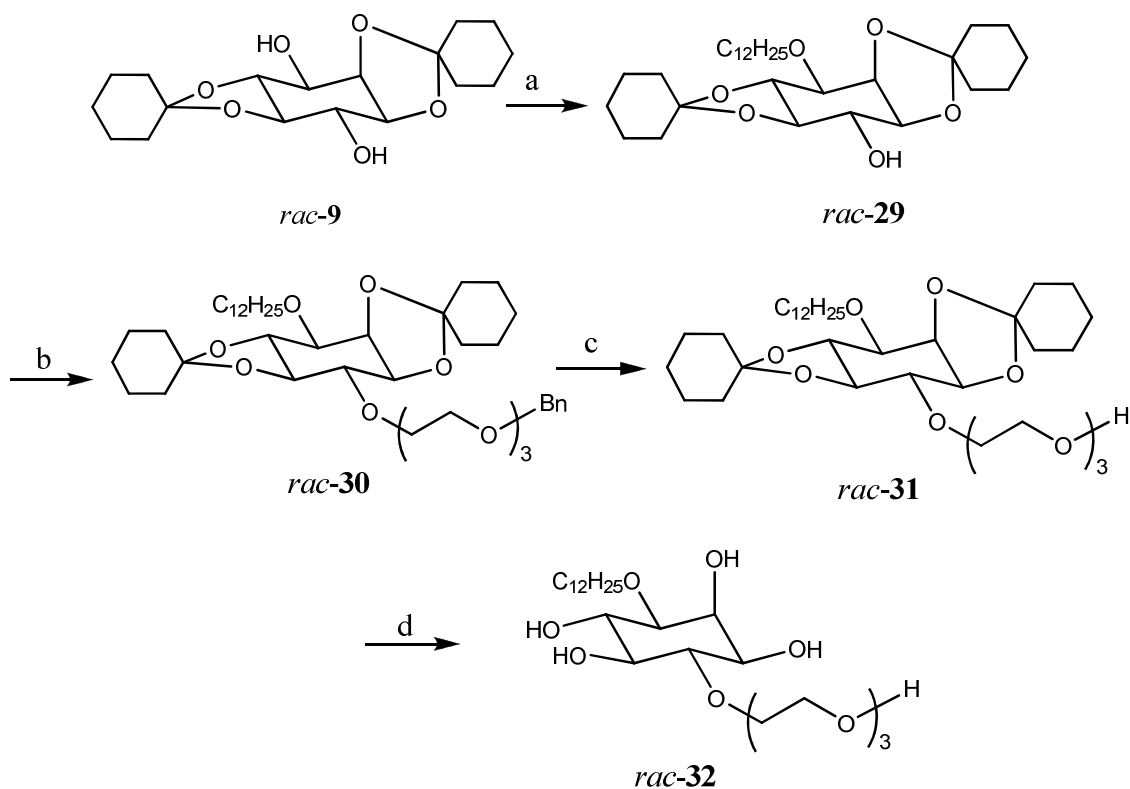
Scheme 3.13. The synthesis of the "inverse" *rac*-**32**:
a) $C_{12}H_{25}Br$, NaH, DMF, rt, 65%; b) **28**, NaH, DMF, rt, 90%;
c) H_2, Pd/C, MeOH, EtOAc, 98%; d) acetic acid, H_2O, reflux, 70%.

The synthesis continues with the attachment of the alkyl chain to the protected inositol *rac*-**9** via an alkylation with dodecyl bromide in presence of NaH suspended in dry DMF to give *rac*-**29** in 65% yield. The next step consists of an alkylation of *rac*-**29** with the monobenzyl ether **28** in presence of NaH/DMF to give *rac*-**30** with 90% yield. This compound was subsequently deprotected first by Pd/charcoal catalyzed hydrogenolysis to cleave the benzyl ether (98% yield) and secondly by hydrolysis of the cyclohexylidene acetals by refluxing with a concentrated aqueous solution of acetic acid to finally give the new inositol-based derivative *rac*-**32** in 70% yield (Scheme 3.13).

The new derivative *rac*-**32** was obtained in seven steps starting from *myo*-inositol with an overall yield of 8%.

3.1.2.5. Synthesis of 2-*O*-dodecyl-5-*O*-[2'-[2''-[2'''-(hydroxy)ethoxy]ethoxy]ethyl]-*myo*-inositol (36)

For the purpose of studying the influence of molecular symmetry on physical properties like solubility, mesomorphism or surface activity, a new inositol-based derivative (**36**) was synthesized starting from *myo*-inositol in seven steps in 7% overall yield.

The selective alkylation of the hydroxyl group at C_5 with dodecyl bromide in presence of NaH and DMF generated the desired monoalkylated intermediate with 40% yield, whereas the further alkylation with tosylate **28** and NaH in DMF afforded **34** in 70% yield (Scheme 3.14).
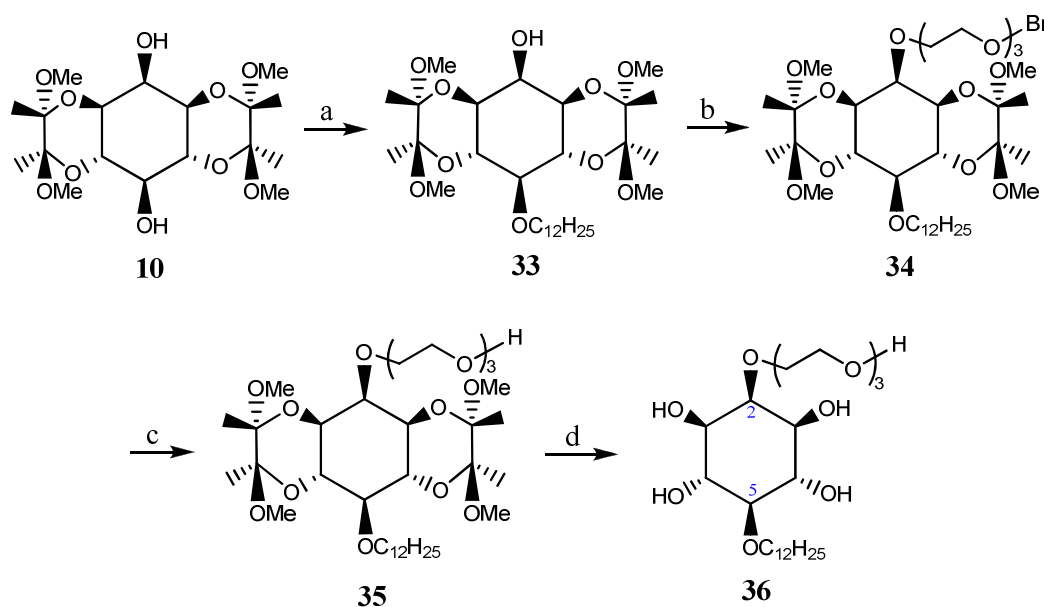
Scheme 3.14. The synthesis of the symmetric derivative **36**:
a) $C_{12}H_{25}Br$, NaH, DMF, rt, 40%; b) **28**, NaH, DMF, rt, 70%;
c) H_2, Pd/C, MeOH, EtOAc, 98%; d) TFA, H_2O, DCM, rt, 93%.

The next step is the cleavage of the benzyl ether via hydrogenolysis with Pd/charcoal catalyst to give **35** in 98% yield. The cleavage of the BDA protection groups, as the last step of this synthesis, was achieved in presence of an aqueous solution of trifluoracetic acid and DCM and gave the desired compound **36** in 93% yield (Scheme 3.14).

3.1.2.6. Synthesis of 2-*O*-[2'-[2''-[2'''-(dodecyloxy)ethoxy]ethoxy]ethyl]-5-*O*-dodecyl-*myo*-inositol (38)

In order to study the influence of the hydrophilic–hydrophobic ratio on various physical properties of inositol-based surfactants, a number of new derivatives were synthesized. In all derivatives presented up to this point (*rac*-**19**, **21**, *rac*-**32**, **36**) the hydrophilic–hydrophobic ratio was 2:1, which means two hydrophilic head groups (*myo*-inositol and triethylene oxide units) and one hydrophobic tail (the dodecyl chain).

A derivative which presents a hydrophilic–hydrophobic ratio of 2:2 is **38**, which contains two hydrophilic head groups (*myo*-inositol and triethylene oxide units) and two hydrophobic tails (dodecyl chains). The synthesis of **38** counts six steps starting from *myo*-inositol and was realised in 8% overall yield.

The last two steps of this synthesis comprise of an alkylation and a cleavage of the BDA protection groups. The alkylation of **33** with the corresponding tosylate **17** was done in the presence of NaH/DMF leading to **37** in 82% yield. The cleavage of BDA protection groups was achieved in the presence of an aqueous solution of trifluoracetic acid and DCM and gave the desired **38** in 95% yield (Scheme 3.15).
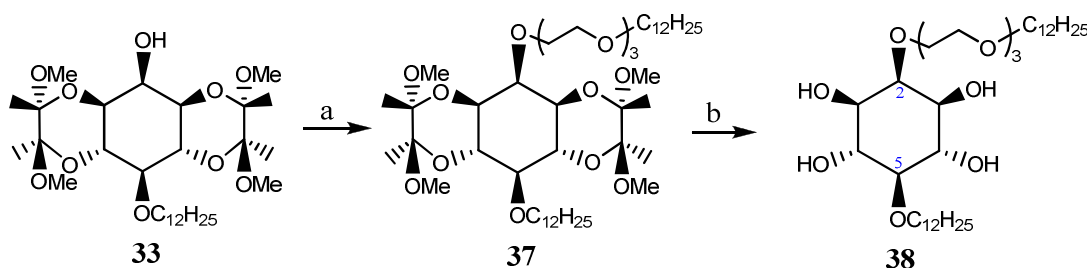
Scheme 3.15. Completion of the synthesis of compound **38**:
a) **17**, NaH, DMF, rt, 82%; b) TFA, H$_2$O, DCM, rt, 95%

3.1.2.7. Synthesis of 1,2-bis-*O*-[2'-[2''-[2'''-(dodecyloxy)ethoxy]ethoxy]ethyl]-*myo*-inositol (*rac*-40)

A hydrophilic–hydrophobic ratio 3:2 can be achieved by synthesis of *rac*-**40**, its molecule containing three hydrophilic head groups (one *myo*-inositol and two triethylene oxide units) and two hydrophobic tails (dodecyl chains). The synthesis of *rac*-**40** has seven steps starting from *myo*-inositol and was realised in 21% overall yield.
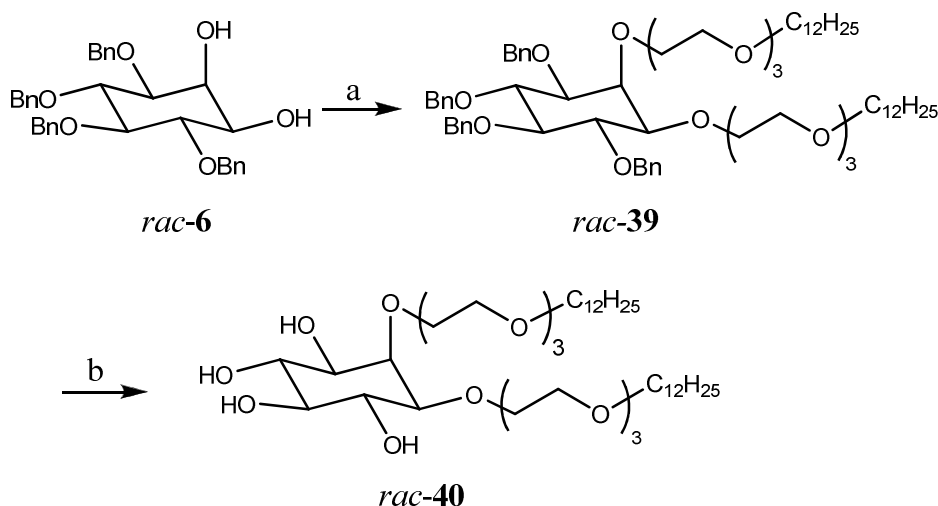
Scheme 3.16. Completion of the synthesis of *rac*-**40**:
a) **17**, NaH, DMF, rt, 51%; b) H$_2$, Pd/C, MeOH, EtOAc, 95%.

The remaining free hydroxyl groups in *rac*-**6** were alkylated with the tosylate **17** in presence of NaH/DMF leading to a mixture of mono- and di-substituted compounds from which *rac*-**39** was isolated in 51% yield. The cleavage of the benzyl ethers was realized by hydrogenolysis under pressure (~ 8 bars) with 10 mol% Pd/charcoal catalyst to give the desired derivative *rac*-**40** in 95% yield (Scheme 3.16).

3.1.2.8. Synthesis of 1,4-bis-*O*-[2'-[2''-[2'''-(dodecyloxy)ethoxy]ethoxy]ethyl]-*myo*-inositol (*rac*-42)

The position of the two *O*-attached alkyl-triethylene oxide chains at the *myo*-inositol ring could create major differences in various physical properties. In this way a new possible derivative which has the hydrophilic–hydrophobic ratio 3:2 – *rac*-**42** – can be achieved in five steps in 10% overall yield.

For this purpose, the corresponding protected *rac*-**9** was treated with the tosylate **17** and NaH/DMF to give *rac*-**41,** after work-up and purification, in 50% yield. The last step consists of the cleavage of the cyclohexylidene acetals which was realized by reflux with a concentrated aqueous solution of acetic acid to obtain *rac*-**42,** after a tedious purification, in 74% yield (Scheme 3.17).
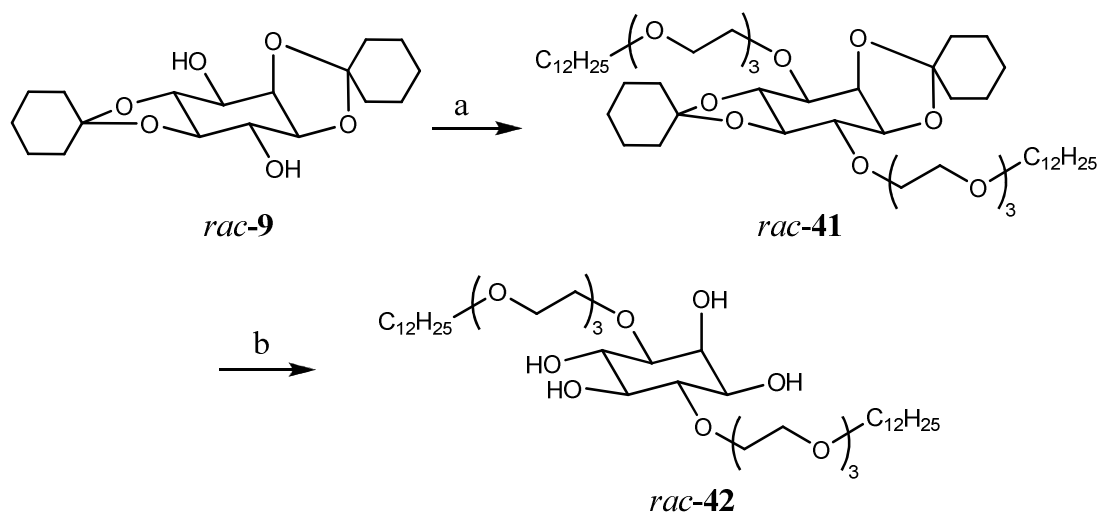
Scheme 3.17. The last two steps of the synthesis of *rac*-**42**
a) **17**, NaH/DMF, rt, 50%; b) acetic acid, H₂O, reflux, 74%.

3.1.2.9. Synthesis of 2,5-bis-*O*-[2'-[2''-[2'''-(dodecyloxy)ethoxy]ethoxy]ethyl]- *myo*-inositol (44)

The last synthesized derivative which has the hydrophilic–hydrophobic ratio 3:2 is the *meso* compound **44** which has two alkyl-triethylene oxide chains attached at the hydroxyl groups from C_2 and C_5.
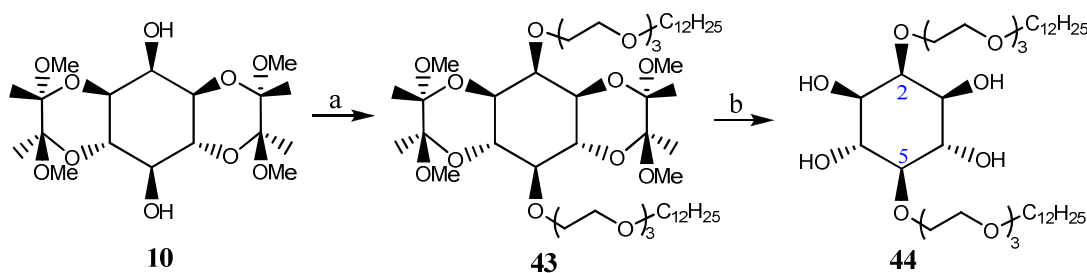
Scheme 3.18. The last two steps of the synthesis of compound **44**:
a) **17**, NaH, DMF, rt, 50%; b) TFA, H₂O, DCM, rt, 53%.

For this purpose the BDA protected inositol **10** was treated with the corresponding tosylate **17** in the presence of NaH/DMF to afford **43** in 50% yield followed by the cleavage of the BDA protection groups with aqueous trifluoracetic acid and DCM to achieve the final compound **44** in 53% yield after purification by flash chromatography and recrystallization, (Scheme 3.18). The synthesis of **44** was completed in five steps in 7% overall yield.

3.2. Physical properties

This section comprises studies regarding thermotropic and lyotropic mesomorphism displayed by the new synthesized inositol-based derivatives as well as their solution properties and surface activity in aqueous media. The assignment of different types of mesophases was achieved by polarization microscopy (PM) and differential scanning calorimetry (DSC). The solution properties were described using surface tension measurements in aqueous solutions, total internal reflection (TIR) Raman spectroscopy and self-diffusion NMR experiments (DOSY).

The surface tension measurements were performed in collaboration with the research group of Prof. Dr. Cosima Stubenrauch at University College Dublin, School of Chemistry and Bioprocess Engineering, Ireland, and were carried out by Dipl. Chem. Valeria Gärtner, Dr. Sandeep Patil and myself.

Total internal reflection (TIR) Raman spectroscopy measurements were performed in collaboration with research group of Prof. Dr. Colin Bain at University of Durham, United Kingdom, and were carried out by Dr. Eric Tyrode and Dr. Scott Shaw.

The self-diffusion NMR experiments (DOSY) were performed at Universität zu Köln, Institut für Organische Chemie.

In this chapter some abbreviations as C_{12}, E_3 or I_1 were added. This abbreviations stand for: C_{12} = dodecyl chain, E_3 = triethylene oxide unit, I_1 = one *myo*-inositol unit. In order to simplify the description of connections between the hydrophilic head group and the hydrophobic tail every compound is addressed as well using these abbreviations. For example: *rac*-**19** (**1-C$_{12}$E$_3$I$_1$**) means that dodecyl chain (**C$_{12}$**) is connected with triethylene oxide (**E$_3$**) to the hydroxyl group from position **1** of one *myo*-inositol ring (**I$_1$**).

3.2.1. Thermotropic mesomorphism

The most common thermotropic mesophase displayed by carbohydrate liquid crystals is the smectic A phase. This phase requires comparable space demands of the sugars and the alkyl chains. Nearly all monoalkylated carbohydrates exhibit this phase as a thermotropic mesophase. Moreover, sugars with two alkyl chains will give a thermotropic columnar phase, since the two alkyl chains need more space than the sugar moiety. This creates a curvature of the separation plane which is bent to a cylinder. The cylinders are "filled" with the sugars and are surrounded by the alkyl chains. The cylinders themselves are arranged in the best way of

packing, i.e. in a hexagonal lattice. If one molecular part is more dominant, a discontinuous cubic phase is formed.[75]

With few exceptions, the mesomorphic behaviour of the newly synthesized inositol-based derivatives follows these features. The phase transition data of different types of inositol-based liquid crystals are presented in the Tables 3.1, 3.2, 3.3.

**Table 3.1.** Phase transition data of the amphiphilic inositol derivatives of type $C_{12}E_3I_1$ and $C_{12}I_1$ (Fig. 3.1.)

Pentol	Cr_1		Cr_2		M		I
rac-**19** ($1\text{-}C_{12}E_3I_1$)	•	81/80.1 (43.3)	-	-	SmA	153/153.1 (0.5)	•
21 ($2\text{-}C_{12}E_3I_1$)	•	- /51.8 (23.0)	•	- /149.0 (29.6)	$\{M_1$	- /147.1 (0.7)$\}$	•
rac-**26** ($4\text{-}C_{12}E_3I_1$)	•	85/-	-	-	SmA	159/-	•
rac-**45** ($1\text{-}C_{12}I_1$)[11,12]	•	124/127.6 (32.0)	-	-	SmA	221/221.7 (1.8)	•
46 ($2\text{-}C_{12}I_1$)[11,12]	•	220/223.5 (48.8)	-	-	$\{M_1$	215/216.7 (6.6)$\}$	•
rac-**47** ($4\text{-}C_{12}I_1$)[10]	•	147/150.2 (29.1)	-	-	SmA	216/216.3 (1.8)	•

Temperatures in °C; polarizing microscopy/differential scanning calorimetry: PM/DSC; enthalpies (kJ mol^{-1}) in brackets; heating rate 5 K min^{-1}. Cr: crystalline, M: thermotropic mesophase, SmA: smectic A, M_1 a monotropic mesophase most probably of a smectic type, I: isotropic liquid.

rac-**19** ($1\text{-}C_{12}E_3I_1$)

rac-**45** ($1\text{-}C_{12}I_1$)

21 ($2\text{-}C_{12}E_3I_1$)

46 ($2\text{-}C_{12}I_1$)

rac-**26** ($4\text{-}C_{12}E_3I_1$)

rac-**47** ($4\text{-}C_{12}I_1$)
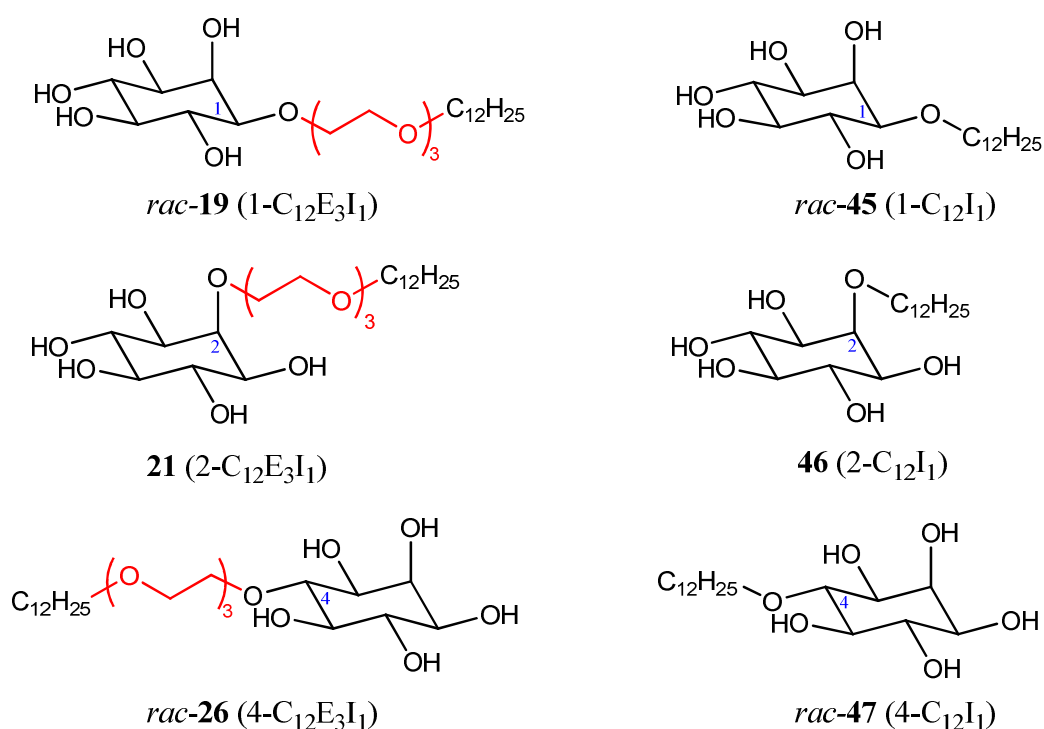
Fig.3.1. Derivatives of type $C_{12}E_3I_1$ and $C_{12}I_1$.

For the sake of comparison, the data for the ethoxylated inositol derivatives are presented together with the similar inositol derivatives in which the triethylene oxide unit is lacking (Fig. 3.1). As can be seen, the ethoxylated inositol derivatives *rac*-**19** (1-$C_{12}E_3I_1$) and *rac*-**26** (4-$C_{12}E_3I_1$) display the same thermotropic behaviour as the non-ethoxylated systems (*rac*-**45** and *rac*-**47**) presenting a smectic A (SmA) mesophase (Fig 3.2, 3.3), but the melting and clearing temperatures decrease significantly by introducing the triethylene oxide chain.
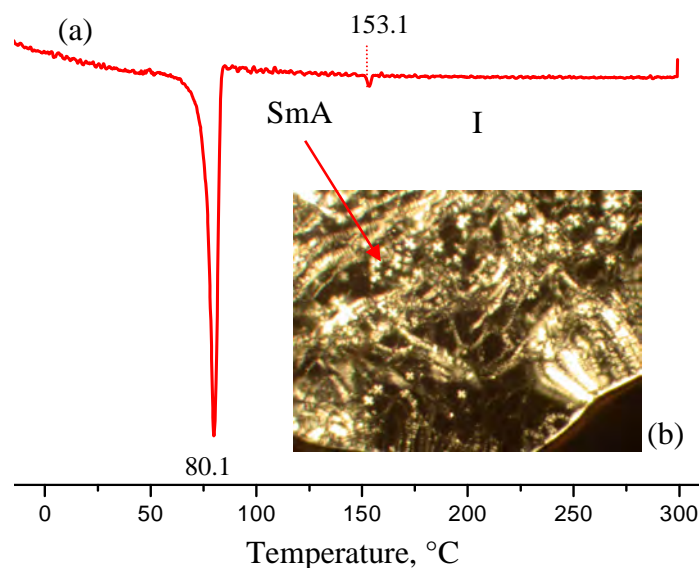
Fig. 3.2. (a) DSC curve (heating); (b) PM: the oily streak-like texture of the thermotropic SmA phase of *rac*-**19** (1-$C_{12}E_3I_1$) at 90°C.
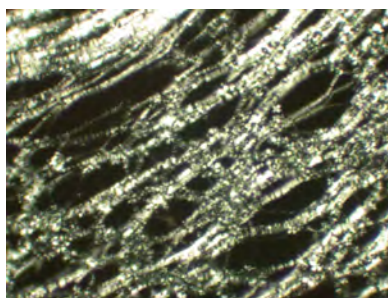
Fig. 3.3. PM: the oily streak-like texture of the thermotropic SmA phase of *rac*-**26** (4-$C_{12}E_3I_1$) at 103 °C.

In general, axial functional groups weaken the stability of the mesophase exhibited by inositol derivatives. The more symmetric such a monoether derivative with respect to its functional groups, the lower its tendency to exhibit a mesophase of the above mentioned type.[10] The axial derivative **21** (2-$C_{12}E_3I_1$) does not exhibit an enantiotropic SmA but a monotropic mesophase most probably of smectic type. Fig. 3.4 presents the DSC curves for heating (a) and cooling (b) for the axial derivative together with PM photography of the isotropic phase

at ~ 148 °C by cooling when it was possible to observe the presence of batonnets which led to idea of a monotropic phase of a smectic type.
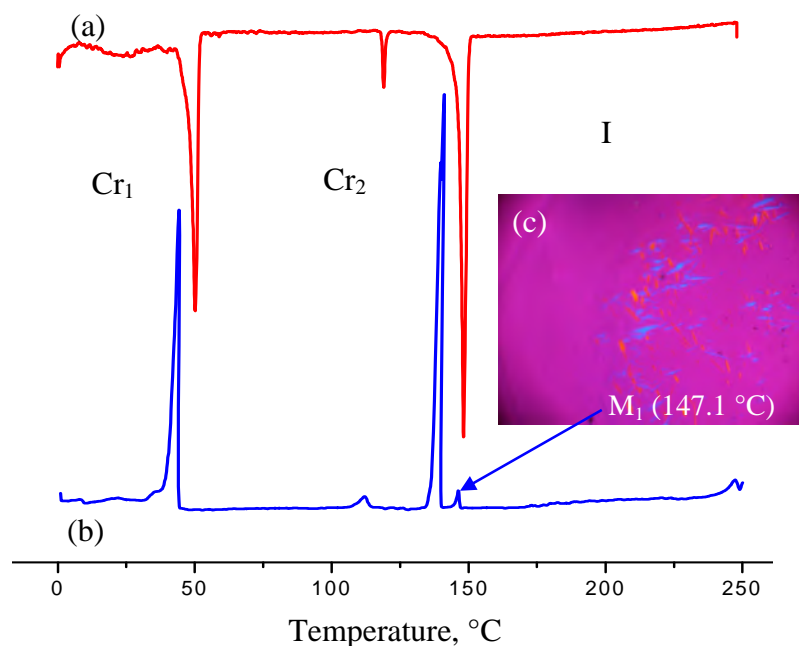
Fig. 3.4. DSC curve (a) heating, (b) cooling; (c) PM: the appearance of batonnets for **21** (2-$C_{12}E_3I_1$) at ~ 148 °C.

No thermotropic liquid crystalline properties could be detected for derivatives of type $C_{12}I_1E_3$ (Fig. 3.5) which represents the inversed situation in which the triethylene oxide is connected as the terminal hydrophilic head group having an unsubstituted hydroxyl group at the end. The phase transition data of the derivatives of this type are presented in Table 3.2.

rac-**32** (1-$C_{12}I_1E_3$)   **36** (2-$C_{12}I_1E_3$)
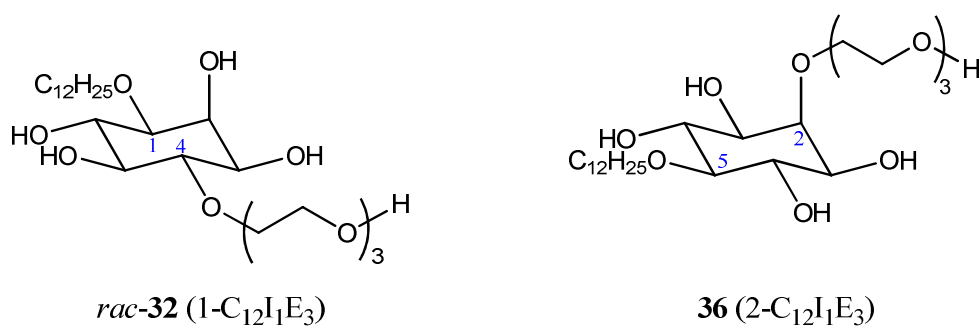
Fig. 3.5. The structures of the $C_{12}I_1E_3$ type derivatives.

Table 3.2. Phase transition data of derivatives of type $C_{12}I_1E_3$

Tetrol	Cr		I
rac-**32** (1-$C_{12}I_1E_3$)	•	80/80.6 (38.92)	•
36 (2-$C_{12}I_1E_3$)	•	174/173.7 (46.4)	•

Temperatures in °C; polarizing microscopy/differential scanning calorimetry: PM/DSC; enthalpies (kJ mol^{-1}) in brackets; heating rate 5 K min^{-1}. Cr: crystalline, I: isotropic liquid

It seems that the presence of a terminal triethylene oxide unit disturbs the hydrogen bond network in such a way that it does not allow the initiation of stable aggregates which enable the formation of thermotropic liquid crystalline phases.

By attaching an additional alkyl-triethylene oxide chain to the *myo*-inositol ring as it is realised in compounds of type $(C_{12}E_3)_2I_1$, the mesomorphic behaviour changes depending on the position of the substituents.

The phase transition data of the newly synthesized diethers are presented in Table 3.3 together with the data for the similar compounds[11] in which the triethylene oxide unit is missing (Fig. 3.6).

rac-**40** [1,2-$(C_{12}E_3)_2I_1$]   *rac*-**48** [1,2-$(C_8)_2I_1$]

rac-**42** [1,4-$(C_{12}E_3)_2I_1$]   *rac*-**49** [1,4-$(C_8)_2I_1$]

44 [2,5-$(C_{12}E_3)_2I_1$]
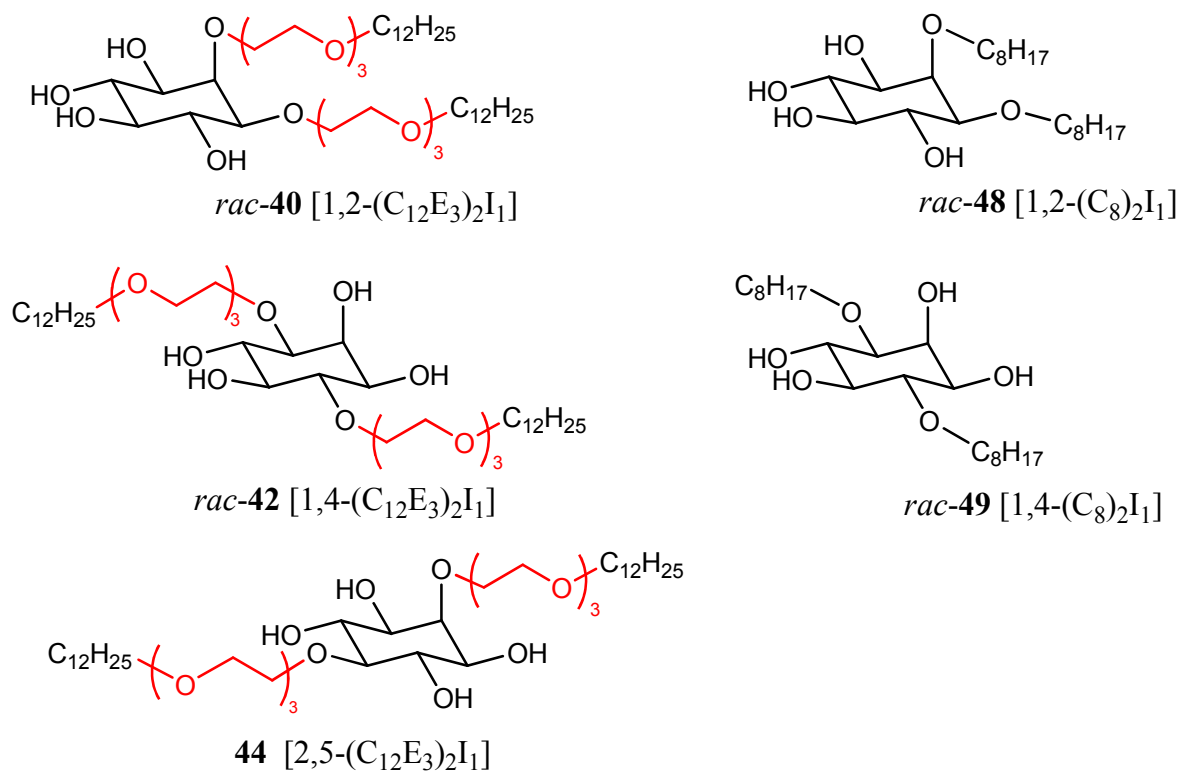
Fig. 3.6. Derivatives of type $(C_{12}E_3)_2I_1$ and $(C_8)_2I_1$.

Table 3.3. Phase transition data of derivatives of type $(C_{12}E_3)_2I_1$ and $(C_8)_2I_1$

Tetrol	Cr$_1$			Cr$_2$		M		M		I
rac-**40** 1,2(C$_{12}$E$_3$)$_2$I$_1$	•	16/14.8 (34.08)	-		-	Cub	26/24.4 (0.78)	Col$_h$	46/45.4 (0.46)	•
rac-**42** 1,4(C$_{12}$E$_3$)$_2$I$_1$	•	20/15.8 (33.1)	•	57/57.3 (70.9)		-	-	-	-	•
44 2,5(C$_{12}$E$_3$)$_2$I$_1$	•	43/42.4 (38.68)	•	110/108.8 (44.07)		-	-	-	-	•
rac-**48** 1,2(C$_8$)$_2$I$_1$[10]	•	102/101.8 (20.8)	-		-	Col$_h$	131/131.7 (1.2)	-	-	•
rac-**49** 1,4(C$_8$)$_2$I$_1$[10]	•	139/141.2 (28.8)	-		-	SmA	168/170.1 (10.5)	-	-	•

Temperatures in °C; polarizing microscopy/differential scanning calorimetry: PM/DSC; enthalpies (kJ mol^{-1}) in brackets; heating rate 5 K min^{-1}. Cr$_1$, Cr$_2$: crystalline, M: thermotropic mesophase, SmA: smectic A phase, Col$_h$: hexagonal columnar phase, Cub: cubic phase, I: isotropic liquid.

The first remarks are the dramatically decreased melting and clearing temperatures in the presence of the triethylene oxide between the alkyl chain and *myo*-inositol ring.

Most often, mesogenic molecules of the peg-shaped geometry like *rac*-**40** (1,2-(C$_{12}$E$_3$)$_2$I$_1$) and *rac*-**48** (1,2-(C$_8$)$_2$I$_1$) aggregate into columns which are arranged in a hexagonal lattice. As can be seen from Table 3.3 and Fig. 3.7, derivative *rac*-**40** (1,2-(C$_{12}$E$_3$)$_2$I$_1$) exhibits a hexagonal columnar mesophase as the similar derivative *rac*-**48** (1,2-(C$_8$)$_2$I$_1$) but additionally presents also a cubic mesophase which appears homeotropic by polarized microscopy and which could be detected by cooling down to low temperatures.
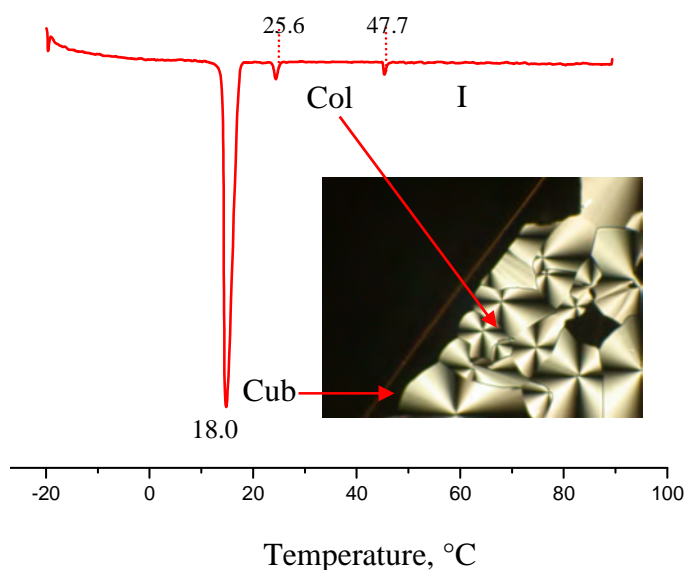
Fig. 3.7. (a) DSC curve (heating); (b) PM picture of *rac*-**40** (1,2-(C$_{12}$E$_3$)$_2$I$_1$) at 33,4°C (cooling).

An interesting feature appeared in case of the 1,4 disubstituted, ethoxylated derivative *rac*-**42** (1,4-$(C_{12}E_3)_2I_1$) which was expected to exhibit a smectic A mesophase as does the similar non-ethoxylated inositol derivative *rac*-**49** (1,4-$(C_8)_2I_1$)[10]. However, this is not the case: *rac*-**42** (1,4-$(C_{12}E_3)_2I_1$) presents crystalline polymorphism (Fig. 3.8) but no thermotropic mesomorphism.
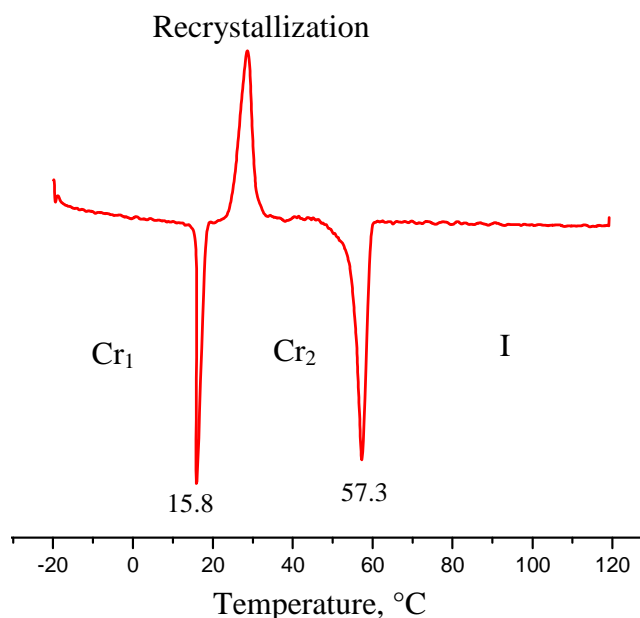
Fig 3.8. DSC curve for *rac*-**42** (1,4-$(C_{12}E_3)_2I_1$).

As previously shown, high molecular symmetry in inositol derivatives appears to be disadvantageous to the formation of mesophases. It seems that this is also the case for derivative **44** (2,5-$(C_{12}E_3)_2I_1$) which shows crystalline polymorphism but no thermotropic mesomorphism as can be also seen from the DSC curve (Fig. 3.9) as well.
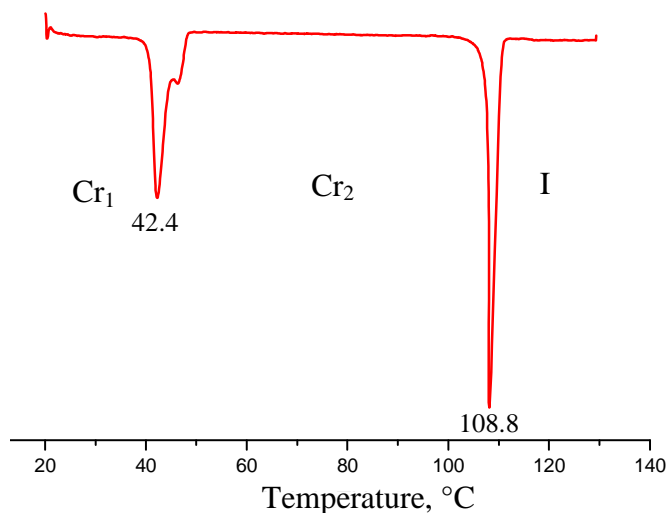
Fig. 3.9. DSC curve of derivative **44** (2,5-$(C_{12}E_3)_2I_1$).

As concluding remarks, the appearance of a mesophase on heating of each of the ethoxylated inositol derivatives seems to be determined by the relative molecular symmetry originating from the different localization of the ether groups at the inositol core. From the study of various liquid crystalline target compounds by polarizing microscopy and differential scanning calorimetry it emerges that the occurrence, type, and stability of their mesophases are clearly determined by the number, the position, and the stereochemical arrangement of both the triethylene oxide group and the alkyl chains at the inositol ring

3.2.2. Lyotropic mesomorphism

The binary systems water – inositol-based derivatives were studied by polarizing microscopy using so called penetration experiments for all new synthesized compounds. A complete phase study with known concentrations at various temperatures was completed only in case of *rac*-**19** (1-$C_{12}E_3I_1$).[76]

The samples for the penetration experiments were prepared by melting the crystalline derivative between a microscope glass slide and a microscope cover glass. The samples were cooled down to approximately 22°C. Water was then added at the edge of the smaller top glass plate. By diffusion of water, a concentration gradient was created laterally between the two glass plates and it was further studied by polarizing microscopy.

The binary system water – *rac*-**19** (1-$C_{12}E_3I_1$) was studied by polarizing microscopy and the resulting phase diagram is shown in Fig. 3.10. Measurements with samples of known concentration at various temperatures were made for concentrations less than ~60 wt % surfactant. Sample preparation at higher concentrations was not possible due to the high viscosity of the solution. To obtain additional information about the phase diagram for concentrations higher than 60 wt % we used the contact preparation technique. Thus the concentrations to which the readings belong are only rough estimates. The temperature dependent measurements revealed that the phase behavior is not temperature sensitive within the studied temperature range (23 to 70°C). Consequently it is justified to draw the vertical phase boundaries for that temperature range as seen in Fig. 3.10. The phase diagram mainly consists of an isotropic phase (L_1) up to concentrations of about 35 wt % which is followed by a hexagonal phase (H_1) from ~ 40 – 57 wt %, and a bicontinuous cubic phase (V_1) from ~ 80 – 85 wt %. The high concentration region above ~ 85 wt % shows a lamellar phase (L_α). In between these single phase regions lie two phase regions where both adjoining phases coexist.[76]

Above 35 wt.-% all studied samples formed liquid crystalline phases over the whole studied temperature range. In view of the fanlike textures seen between 40 and 57 wt % under crossed polarizers, this phase can clearly be identified as a hexagonal liquid crystal (H_1), which is followed by the optically isotropically appearing bicontinuous cubic phase (V_1). Both of these phases are much more viscous than the lamellar phase (L_α), which follows in phase diagram at higher concentrations.[76]
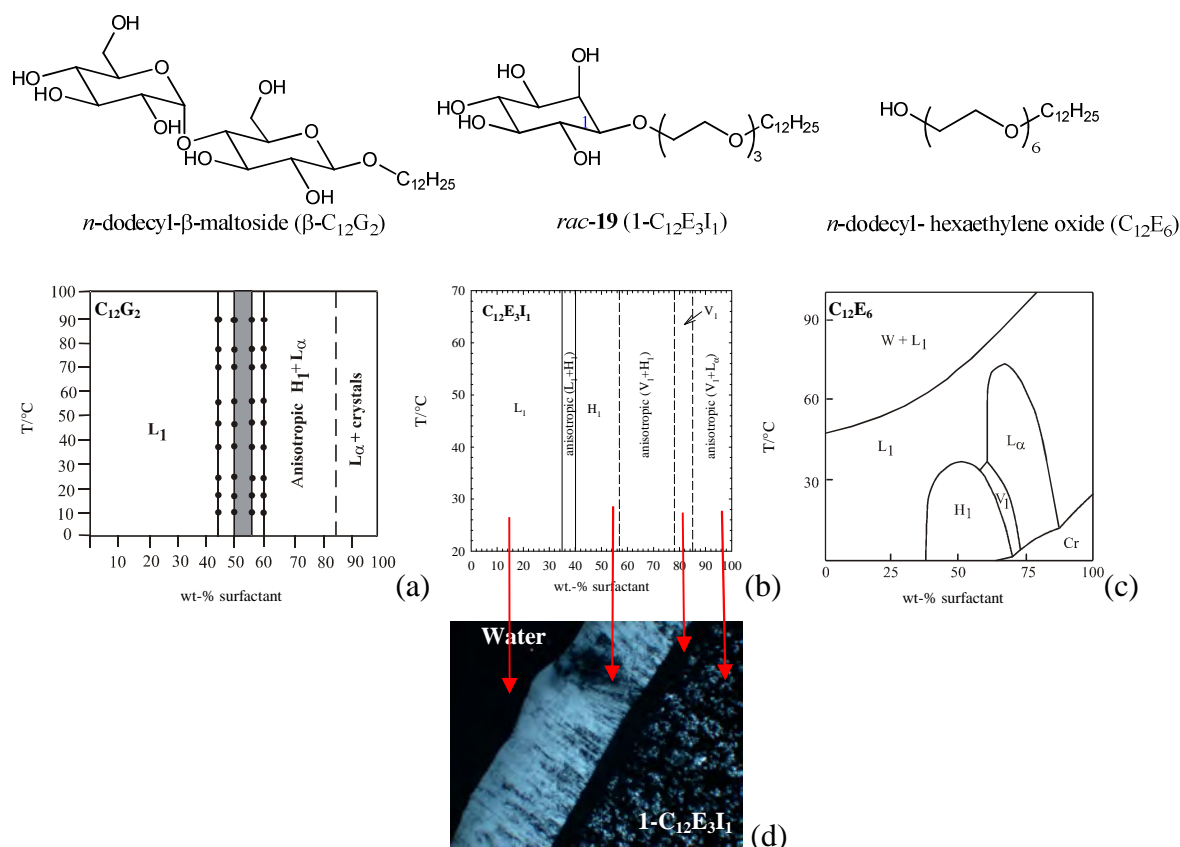
Fig. 3.10. Phase diagrams of the binary systems (a) water – *n*-dodecyl-β-maltoside ($C_{12}G_2$)[77], (b) water – *rac*-**19** (1-$C_{12}E_3I_1$), (c) water – *n*-dodecyl-hexaethylene oxide ($C_{12}E_6$)[78], and (d) the texture of the system water – *rac*-**19** (1-$C_{12}E_3I_1$) between crossed polarizers (from penetration experiment).

For the sake of comparison the phase diagrams of the binary system (a) water – *n*-dodecyl-β-maltoside (β-$C_{12}G_2$) and (c) water – *n*-dodecyl-hexaethylene oxide ($C_{12}E_6$) are presented together in Fig. 3.10. As can be seen, the phase diagram of water – *n*-dodecyl-β-maltoside (β-$C_{12}G_2$) is as temperature-insensitive as the one of water – *rac*-**19** (1-$C_{12}E_3I_1$). In the former, two liquid crystalline phases are observed, namely the hexagonal (H_1) and the lamellar (L_α) phase. In contrast to *n*-dodecyl-β-maltoside (β-$C_{12}G_2$) and *rac*-**19** (1-$C_{12}E_3I_1$), the phase behavior of the binary system water – *n*-dodecyl-hexaethylene oxide ($C_{12}E_6$) is very temperature-sensitive. Three liquid crystalline phases are observed, namely a hexagonal (H_1),

a bicontinuous cubic (V_1), and a lamellar phase (L_α). In addition, a miscibility gap is observed at higher temperatures and lower surfactant concentrations. The temperature insensitivity of aqueous solutions of the maltoside surfactant is due to the strong hydrogen bonds between the sugar units and water, which prevent a significant dehydration of the head group with increasing temperature. On the other hand, the ethylene oxide units can be easily dehydrated with increasing temperature as the interactions between water and oligo(ethylene oxide) are much weaker (mainly weak dipole-dipole interactions). Assuming that the hydration of the *myo*-inositol substructure is comparable to that of a glucoside head group, one expects an "intermediate" behavior for the new *rac*-**19** (1-$C_{12}E_3I_1$). This, however, is not the case. The presence of the three ethylene oxide units obviously does not lead to a temperature-dependent phase behavior, an observation that cannot yet be explained.

As will be explained later (subchapter 3.2.3.1) the isomer **21** (2-$C_{12}E_3I_1$) has lower solubility in water, a situation which has been met as well in other sugar-based surfactants with the hydrophobic tail attached to an axial (α) position. This is the reason why the lyotropic mesomorphsim of **21** (2-$C_{12}E_3I_1$) is compared with the glucosidic analogue *n*-octyl-α-D-glucoside (α-C_8G_1) (Fig. 3.11). The glucoside α-C_8G_1 has a Kraft boundary starting from 38 °C and increases with increasing surfactant concentration (the dashed line in Fig. 3.12 b)[39]. There are micellar, hexagonal and lamellar phases present. The penetration experiment of the binary system water – **21** (2-$C_{12}E_3I_1$) revealed no lyotropic mesophase at 25°C but on heating up to ~ 55 °C the sequence micellar – hexagonal – cubic – crystal was present. The optically isotropically appearing zone between the hexagonal and crystal phase was established to be a bicontinuous cubic phase because this phase is more viscous than an isotropic fluid.

21 (2-$C_{12}E_3I_1$)   *n*-octyl-α-glucoside (α-C_8G_1)
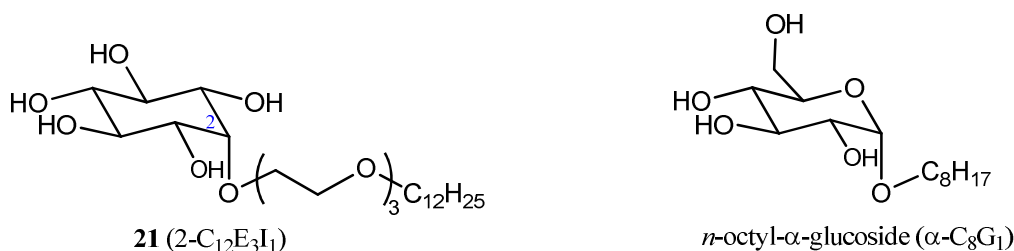
Fig. 3.11. The structure of **21** (2-$C_{12}E_3I_1$) and *n*-octyl-α-glucoside (α-C_8G_1)
in which the side chain is attached in axial position.
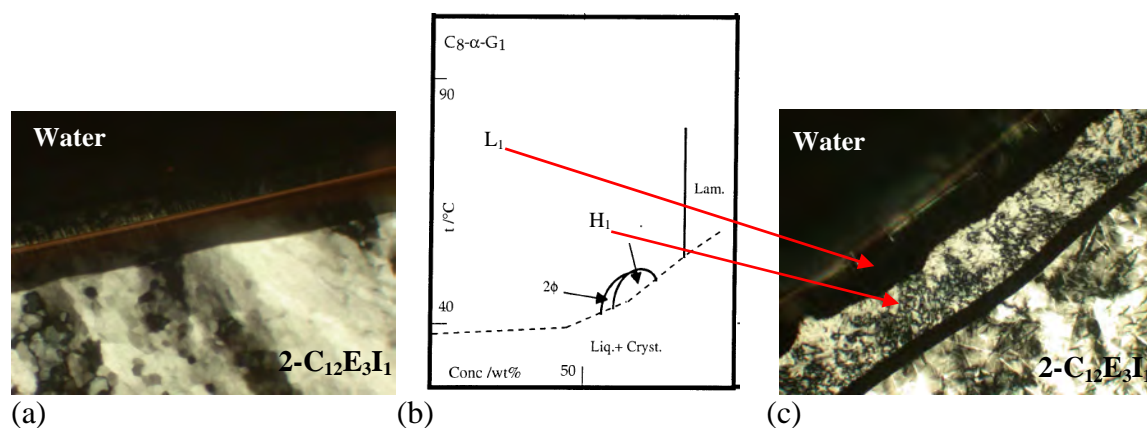
Fig. 3.12. a) The penetration experiment of binary system water – **21** (2-$C_{12}E_3I_1$) at 25 °C; b) the phase diagrams of the binary systems water – *n*-octyl-α-glucoside (α-C_8G_1)[39], c) the penetration experiment of binary system water – **21** (2-$C_{12}E_3I_1$) at 55 °C (Lam = lamellar phase, Liq+Cryst = water in equilibrium with crystalline surfactant, and 2Φ = two-phase region).

As it was mentioned above, the binary system *rac*-**19** (1-$C_{12}E_3I_1$) behaves more like the maltoside-based surfactant and is insensitive towards temperature. It seems that this is not the case for the binary system water – *rac*-**32** (1-$C_{12}I_1E_3$) for which, the preliminary penetration experiments revealed that the lyotropic mesophase sequence changes by increasing temperature. A drawback of this experimental technique is that one cannot determine boundaries of a specific phase situation. The more comprehensive study of the phase behaviour is going to be done soon.

The disubstituted derivatives of type $(C_{12}E_3)_2I_1$ (*rac*-**40**, *rac*-**42**, **44**) do not show lyotropic mesomorphism in the presence of water. Some preliminary penetration experiments with apolar solvents revealed the appearance of lyotropic mesophases but the systems need to be studied in more detail in order to assign the type of the observed mesophases.

As concluding remarks, it can be stated that from the studies of binary system solvent – inositol-based surfactants by polarizing microscopy it emerges that, as in case of thermotropism, the occurrence, type, and stability of their lyotropic mesophases are clearly determined by the number, the position, and the stereochemical arrangement of both the triethylene oxide group and the alkyl chains on the inositol ring.

3.2.3. Solution properties and surface activity

3.2.3.1. Solubility in aqueous solution

Solubility in water is a very important physical property which a compound needs to possess in order to be studied for its solution properties and surface activity. Previous work of our group revealed that only one unit of *myo*-inositol as hydrophilic head group is not enough to assure a good solubility in water and consequently the *cmc* could not be measured.[79] By increasing the head group with a triethylene oxide unit, it was hoped that the solubility issue could be solved, but it seems that there are other factors which can influence the solubility in water. Table 3.4 summarizes the characterization of all new synthesized inositol-based derivatives with respect to their aqueous solubilitiy.

Table 3.4. The solubility of new inositol-based derivatives

Compound	Solubility
rac-**19** (1-$C_{12}E_3I_1$)	+
21 (2-$C_{12}E_3I_1$)	low
rac-**26** (4-$C_{12}E_3I_1$)	+
rac-**32** (1-$C_{12}I_1E_3$)	+
36 (2-$C_{12}I_1E_3$)	low
38 (2-($C_{12}E_3$)I_1-5-C_{12})	-
rac-**40** (1,2-($C_{12}E_3$)$_2I_1$)	-
rac-**42** (1,4-($C_{12}E_3$)$_2I_1$)	-
44 (2,5-($C_{12}E_3$)$_2I_1$)	-

As can be observed from Table 3.4, the symmetric derivative **21** (2-$C_{12}E_3I_1$) has lower solubility in water compared with its non-symmetric isomers *rac*-**19** (1-$C_{12}E_3I_1$) and *rac*-**26** (4-$C_{12}E_3I_1$). It is well known that molecular symmetry has a pronounced effect on the melting properties and solubility of organic compounds. As a general rule, symmetrical molecules in crystalline form have higher melting temperatures and exhibit lower solubility compared with molecules of similar structure but with lower symmetry. Symmetry in a molecule imparts a positive amount of residual entropy in the solid phase (*i.e.*, more possible arrangements leading to the same structure). This means that the entropy of a crystal of symmetric molecules is greater than the entropy of crystal of a similar, but non-symmetric molecule. In fact, symmetrical molecules are less soluble precisely because of the higher melting temperature of their crystals.[80-83]

Coming back to the inositol-based derivatives, all symmetric inositol derivatives, which have the substituents attached to the C_2 (axial) or/and C_5 hydroxyl group (**21** (2-$C_{12}E_3I_1$), **36** (2-$C_{12}I_1E_3$), **44** (2,5-($C_{12}E_3$)$_2I_1$) have melting points higher than their similar non-symmetric

isomers *rac*-**19** (1-C$_{12}$E$_3$I$_1$), *rac*-**26** (4-C$_{12}$E$_3$I$_1$), *rac*-**32** (1-C$_{12}$I$_1$E$_3$), *rac*-**40** (1,2-(C$_{12}$E$_3$)$_2$I$_1$) and *rac*-**42** (1,4-(C$_{12}$E$_3$)$_2$I$_1$) (Tables 3.1, 3.2, 3.3, subchapter 3.2.1.) which leads to idea that the symmetric derivatives form more stable crystal lattices. This crystal stability could be the reason why this type of inositol-based surfactants is much less soluble than the non-symmetric ones. Actually, this feature is met also in sugar-based surfactants (Fig. 3.13), where the α-linkage (axial) between the hydrocarbon chain and the sugar head group promotes a more stable crystal packing than in case of β-linkage (equatorial). As a consequence, the Krafft boundary is considerably higher in the α-linkage case, as compared to the β-linkage. For example the *n*-octyl-α-glucoside has a Krafft boundary starting from 38 °C and increases with increasing surfactant concentration, whereas the *n*-octyl-β-glucoside is soluble down to the freezing point of water.[41]
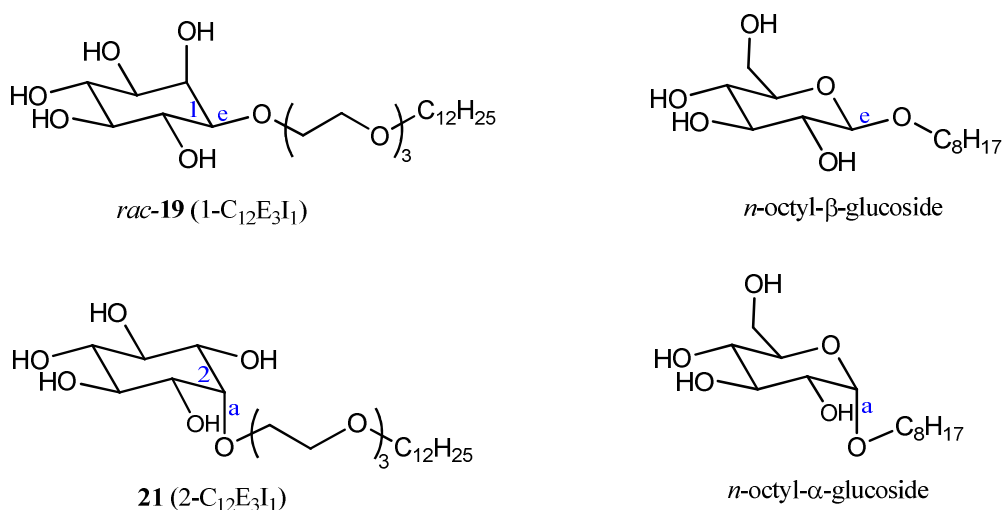
Fig. 3.13. The structures of sugar-based surfactants indicating how the hydrocarbon chain is attached to the sugar molecule: to the equatorial (e) (*rac*-**19** (1-C$_{12}$E$_3$I$_1$) and *n*-octyl-β-glucoside) or the axial (a) hydroxyl group (**21** (2-C$_{12}$E$_3$I$_1$) and *n*-octyl-α-glucoside).

In case of the double substituted inositol derivatives, **38** (2-(C$_{12}$E$_3$)I$_1$-5-C$_{12}$), *rac*-**40** (1,2-(C$_{12}$E$_3$)$_2$I$_1$), *rac*-**42** (1,4-(C$_{12}$E$_3$)$_2$I$_1$), and **44** (2,5-(C$_{12}$E$_3$)$_2$I$_1$) (Fig. 3.14) the presence of two dodecyl chains increases the hydrophobic part of the amphiphiles which can also be a reason for very low aqueous solubility.

38 (2-(C$_{12}$E$_3$)I$_1$-5-C$_{12}$)   *rac*-**40** (1,2-(C$_{12}$E$_3$)$_2$I$_1$)

44 (2,5-(C$_{12}$E$_3$)$_2$I$_1$)   *rac*-**42** (1,2-(C$_{12}$E$_3$)$_2$I$_1$)
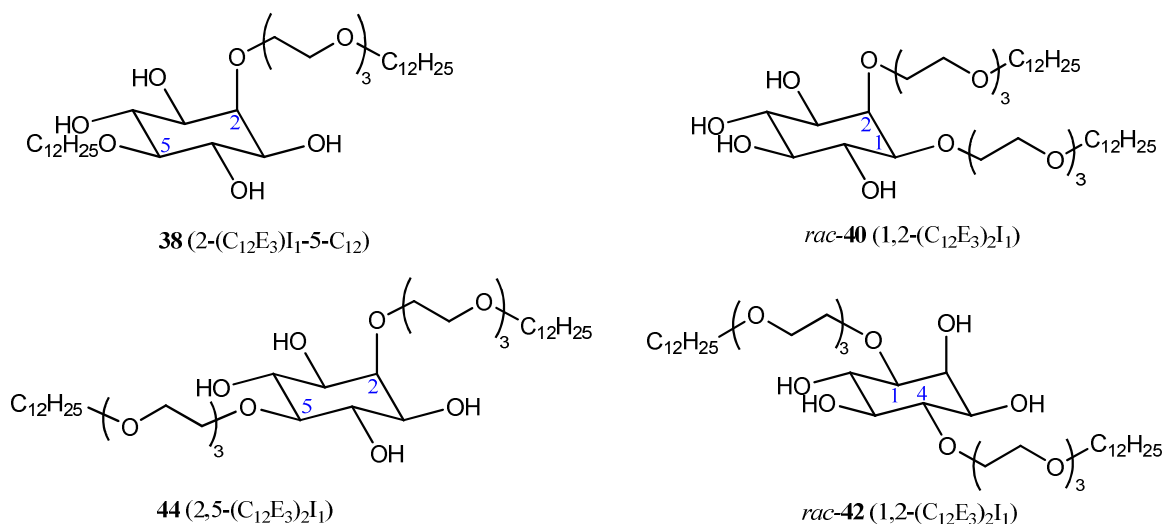
Fig. 3.14. The structures of the double substituted derivatives **38** (2-(C$_{12}$E$_3$)I$_1$-5-C$_{12}$), *rac*-**40** (1,2-(C$_{12}$E$_3$)$_2$I$_1$), *rac*-**42** (1,4-(C$_{12}$E$_3$)$_2$I$_1$), and **44** (2,5-(C$_{12}$E$_3$)$_2$I$_1$).

3.2.3.2. Surface tension

Figures 3.17 and 3.18 show the surface tension σ as a function of the concentration c of the inositol-based derivatives which were enough soluble in water in order to make possible the measurements (Fig. 3.15).

rac-**19** (1-C$_{12}$E$_3$I$_1$)   **21** (2-C$_{12}$E$_3$I$_1$)

rac-**32** (1-C$_{12}$I$_1$E$_3$)   *rac*-**26** (4-C$_{12}$E$_3$I$_1$)
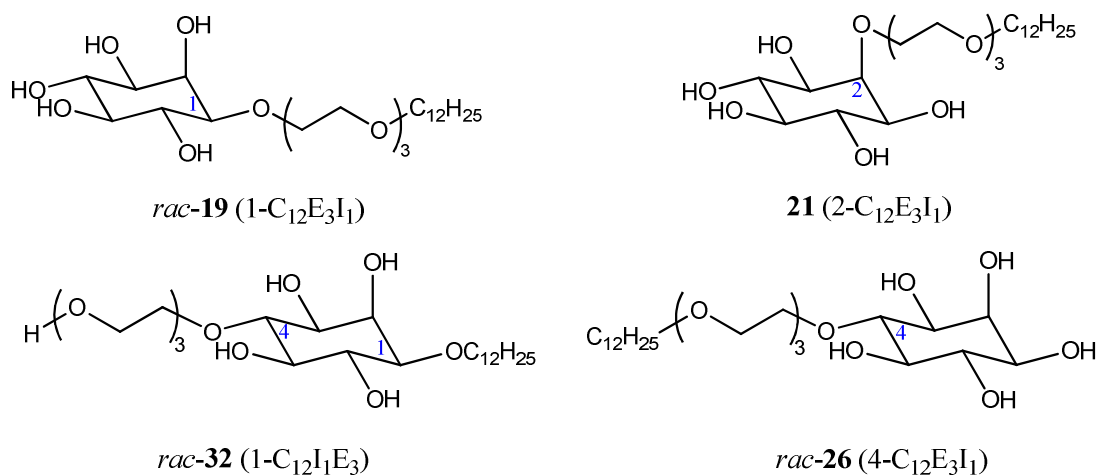
Fig. 3.15. The structures of the investigated inositol–based surfactants: *rac*-**19** (1-C$_{12}$E$_3$I$_1$), **21** (2-C$_{12}$E$_3$I$_1$), *rac*-**26** (4-C$_{12}$E$_3$I$_1$), and *rac*-**32** (1-C$_{12}$I$_1$E$_3$).

The surface tension increases with decreasing surfactant concentration until it levels off at the value of the surface tension of pure water (72.3 mN/m at 23 °C). All curves are fitted with *Frumkin* isotherm[26], model which describes the experimental data very well. Because the surface tension is very sensitive to slight impurities, which is usually reflected in a minimum or a smooth levelling off at concentrations around *cmc*, the σ–c curve serves as indicator for

the purity of a surfactant. As can be seen from Fig. 3.16 and 3.17, the surface tension curves of the newly synthesized inositol-based surfactants have a sharp bend and no minimum at *cmc*, which indicates that the analyzed compound are very pure.
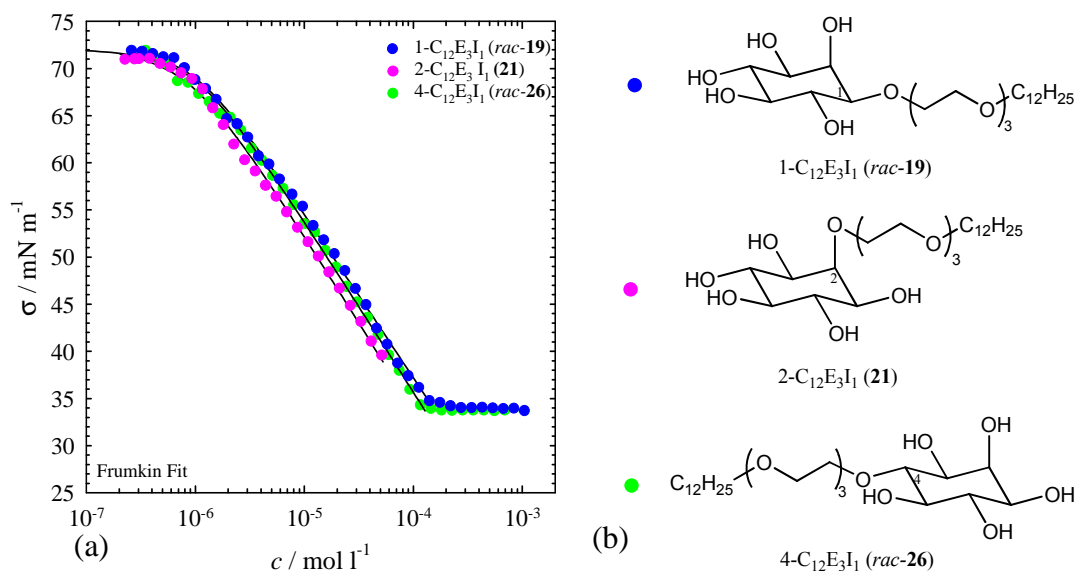
Fig. 3.16. (a) Surface tension σ as a function of the surfactant concentration c
(b) molecular structures 1-$C_{12}E_3I_1$ (*rac*-**19**), 2-$C_{12}E_3I_1$ (**21**), and 4-$C_{12}E_3I_1$ (*rac*-**26**).

Fig. 3.16 presents as well the σ–c curve of **21** (2-$C_{12}E_3I_1$), but in this case the *cmc* could not be measured because this compound is low soluble in water and the solution turned turbid at concentration ~ 5.2 x 10^{-5} M. From the same figure can be also seen that the position of the hydrophobic chain attached to the hydrophilic head group has only a minor effect on both the *cmc* and the surface concentration when the chain is attached to an equatorial position of inositol ring (Table 3.5).

Table 3.5. Physicochemical properties of β-$C_{12}G_2$, 1-$C_{12}E_3I_1$, 4-$C_{12}E_3I_1$, 1-$C_{12}I_1E_3$, and $C_{12}E_6$

Surfactant	cmc/mM	σ_{cmc}/mN m^{-1}	Γ_∞ 10^{-6}/mol m^{-2}	A_{min}/nm^2
β-$C_{12}G_2$ (*n*-dodecyl- β-maltoside)	0.16	34.7	3.8	0.44
1-$C_{12}E_3I_1$ (*rac*-**19**)	0.14	34.4	3.1	0.53
4-$C_{12}E_3I_1$ (*rac*-**26**)	0.13	33.7	3.3	0.51
1-$C_{12}I_1E_3$ (*rac*-**32**)	0.37	35.0	3.5	0.47
$C_{12}E_6$ (*n*-dodecyl hexaethylene oxide)	0.09	31.6	3.1	0.53

For the sake of comparison, in Fig. 3.17a the σ–c curves of inositol-based surfactants are plotted together with those of the corresponding sugar (n-dodecyl-β-maltoside, β-$C_{12}G_2$) and ethylene oxide (n-dodecyl hexaethylene oxide, $C_{12}E_6$) surfactants (Fig. 3.17 b).
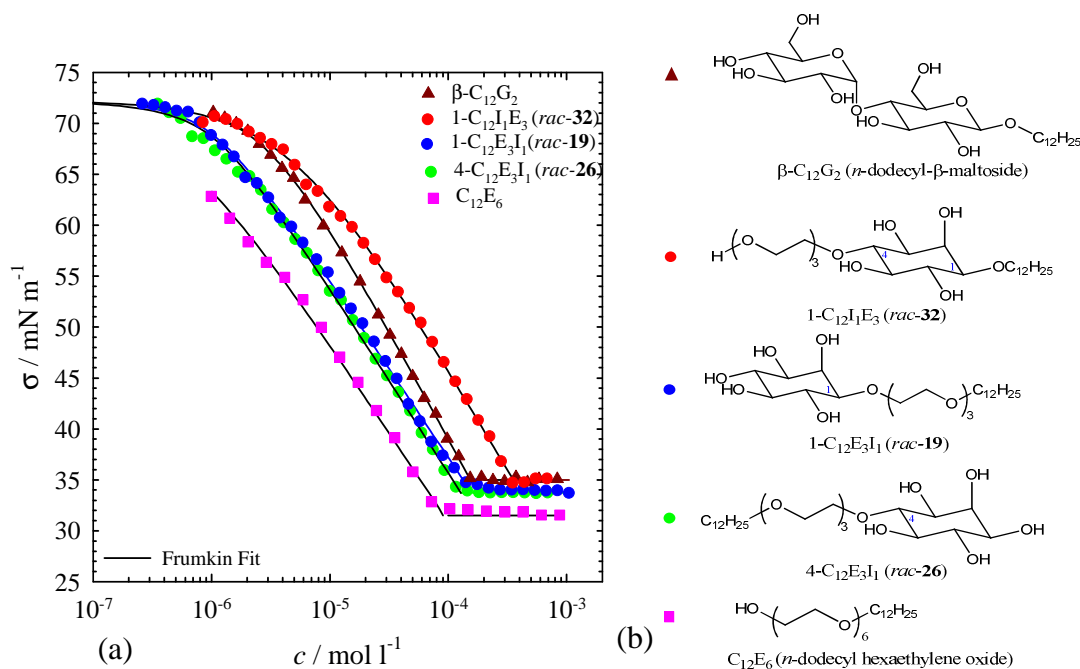
Fig. 3.17. (a) Surface tension σ as a function of the surfactant concentration c and (b) molecular structures of β-$C_{12}G_2$, 1-$C_{12}I_1E_3$, 1-$C_{12}E_3I_1$, 4-$C_{12}E_3I_1$ and $C_{12}E_6$

The *cmc* of 1-$C_{12}E_3I_1$ (*rac*-**19**) and 4-$C_{12}E_3I_1$ (*rac*-**26**) are very close to those of β-$C_{12}G_2$ and $C_{12}E_6$ which is expected for nonionic surfactants with the same hydrophobic chain length. However, the *cmc* values of 1-$C_{12}E_3I_1$ (*rac*-**19**), 4-$C_{12}E_3I_1$ (*rac*-**26**) and β-$C_{12}G_2$ are much more similar than those of the inositol derivatives and $C_{12}E_6$ which can be explained by similar monomeric solubilities. Also the plateau values of the surface tension (i.e., the surface tension at concentrations above *cmc*) of 1-$C_{12}E_3I_1$ (*rac*-**19**) and 4-$C_{12}E_3$ I_1 (*rac*-**26**) are much more similar to that of β-$C_{12}G_2$ than to the plateau value obtained for $C_{12}E_6$.[76] On the other hand, 1-$C_{12}I_1E_3$ (*rac*-**32**), as can be observed from Fig. 3.18a, is less surface active than β-$C_{12}G_2$, 1-$C_{12}E_3I_1$ (*rac*-**19**), 4-$C_{12}E_3I_1$ (*rac*-**26**) and $C_{12}E_6$, and thus has a higher *cmc* value which means that the I_1E_3 head group is more hydrophilic than G_2, E_3I_1 and E_6.
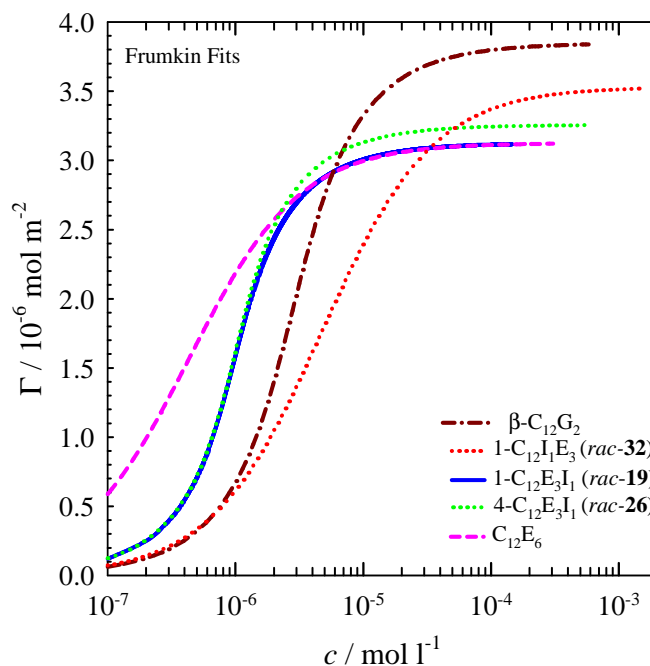
Fig. 3.18. Surface concentration Γ as a function of the surfactant concentration of β-$C_{12}G_2$, 1-$C_{12}I_1E_3$, 1-$C_{12}E_3I_1$, 4-$C_{12}E_3I_1$ and $C_{12}E_6$.

The corresponding adsorption isotherms of the five surfactants are shown in Fig. 3.18 and the adsorption parameters are listed in Table 3.5. The isotherms were derived by differentiating the Frumkin fits and using the Gibbs equation. As can be seen, the surface concentration curves of the 1-$C_{12}E_3I_1$ (*rac-**19***) and 4-$C_{12}E_3I_1$ (*rac-**26***) are very similar to that of hexaethylene oxide surfactant $C_{12}E_6$ and level off in the same or almost the same Γ_∞ value. This is rather unexpected, recalling the observation that these three surfactants have different plateau values of the surface tension (see Table 3.5). As a rule of thumb, one can say that the lower the plateau value the more densely packed is the monolayer. Thus one would expect that the maximum surface concentration Γ_∞ of $C_{12}E_6$ is larger than that of 1-$C_{12}E_3I_1$ (*rac-**19***) and 4-$C_{12}E_3 I_1$ (*rac-**26***). However, this is not the case. A possible explanation could be that the E_3I_1 head group is as flexible as the hexaethylene oxide head group thus needing as much surface area as the E_6 unit. Secondly, a monolayer consisting of E_6 units can obviously pack more densely compared to one consisting of E_3I_1 units leading to a lower surface tension at the *cmc*.

On the other hand, the minimum area per head group (= the maximum surface concentration) for 1-$C_{12}I_1E_3$ (*rac-**32***), is in between that for β-$C_{12}G_2$ and $C_{12}E_6$ which means that attaching an inositol unit directly to the hydrophobic chain reduces the surface area considerably compared to $C_{12}E_6$, while the terminating E_3 group still provides a certain amount of flexibility and thus volume. Comparing the three inositol derivatives it can be seen that the minimum area per

head group for $1\text{-}C_{12}I_1E_3$ (*rac*-**32**), is smaller than that for $1\text{-}C_{12}E_3I_1$ (*rac*-**19**) and $4\text{-}C_{12}E_3I_1$ (*rac*-**26**), therefore Γ_∞ is higher. The explanation would be most likely the conformation and orientation of the surfactants at the surface.

In order to monitor the conformation and orientation of the surfactants at the surface molecular dynamic simulations or more sophisticated surface sensitive techniques are required.

3.2.3.3. Adsorption on silica surface studied by Total Internal Reflection Raman spectroscopy (TIR Raman)

Knowledge of the adsorption behaviour of a surfactant is crucial for understanding the underlying mechanisms for applications such as wetting, detergency and lubrication. Previous studies on sugar and ethylene oxide surfactants revealed that the former hardly adsorb on silica, while the later adsorb strongly on this oxide surface. The standard explanation put forward to describe the adsorption of nonionic surfactants on hydrophilic surfaces from aqueous solutions is hydrogen bonding. The main difficulty with this hypothesis is that water is able to form very strong hydrogen bonds with both the surface and the surfactant head group and it is hard to see how replacements of such hydrogen bonds with surfactant head group – surface hydrogen bonds will result in an energy gain. Nevertheless, the enthalpy of adsorption for poly(ethylene oxide) on silica is negative. The conclusion would be that the driving force for adsorption is not yet well-understood. However, one may perceive a situation where water hydrogen bonded both to the surface and the surfactant head group mediates the surfactant – surface interactions.[2,3]

The aim of the present project was to determine the adsorption behaviour of inositol-based surfactants due to structural changes and to correlate this to similar relationships for alkyl polyglucoside ($\beta\text{-}C_{12}G_2$) and ethylene oxide ($C_{12}E_6$) surfactants.

The technique used to study the adsorption behaviour was TIR Raman spectroscopy. Raman scattering has a reputation for being a weak effect: typical Raman scattering cross-sections are ten orders of magnitude lower than infrared absorption cross-sections.[84] With the use of evanescent waves to enhance the surface signal and discriminate against bulk signals, total internal reflection Raman scattering (TIR-Raman) is in reality the most sensitive form of vibrational spectroscopy for studying adsorption on dielectric materials.[85]

In TIR-Raman experiments for the present work, an evanescent wave with a penetration depth of 100 nm is used to probe the adsorbed surfactant film at the silica-water interface.

A schematic of the experimental setup is shown in Fig. 3.19. A 532 nm CW laser was directed to the centre of a silica hemisphere at an angle of 73 degrees from the surface normal. The Raman scattered

Fig. 3.19. Diagram of the TIR

light was collected with a microscope objective placed immediately above the hemisphere, and directed towards a spectrograph and CCD camera where the spectra was recorded. Raman scattering is not intrinsically surface sensitive and TIR-Raman spectra therefore contain contributions from the silica substrate and the solution within the evanescent field as well as from the adsorbed surfactant layer. The contributions from the bulk silica are removed by subtraction of a background spectrum.

Fig. 3.20 shows representative subtracted TIR Raman spectra obtained for the adsorption of n-dodecyl-β-maltoside (β-$C_{12}G_2$), n-dodecyl hexaethylene oxide ($C_{12}E_6$), and rac-**19** (1-$C_{12}E_3I_1$) on silica. All spectra shown were collected at concentrations above the respective critical micellar concentrations (cmc). The results clearly indicate that the $C_{12}G_2$ and 1-$C_{12}E_3I_1$ do not adsorb in any measurable quantities on silica. However, as expected, the ethylene oxide surfactant does adsorb.
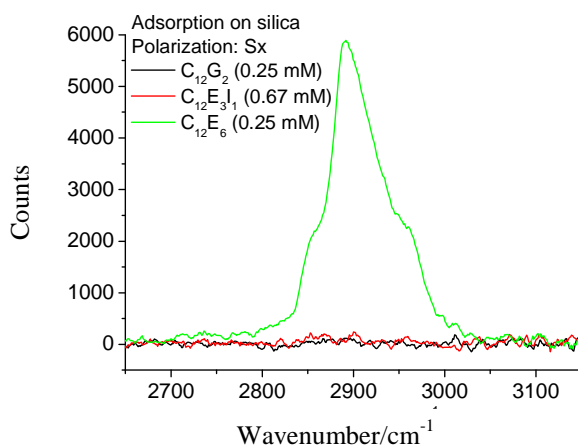
Fig. 3.20. TIR Raman subtracted spectra of silica in contact with n-dodecyl-β-maltoside (β-$C_{12}G_2$), n-dodecyl hexaethylene oxide ($C_{12}E_6$), and rac-**19** (1-$C_{12}E_3I_1$) solutions collected under the polarization combinations Sx, at concentrations above the cmc.

The measurements for the "invers" derivative *rac*-**32** (1-C$_{12}$I$_1$E$_3$) are presented in Fig. 3.21 and 3.22. The four spectra in each plot are labelled with the concentration of *rac*-**32** (1-C$_{12}$I$_1$E$_3$) in the original solution and with a temperature at which the data were recorded. The concentrations were chosen so that one would be well below the *cmc* (0.03 mM) and the other very near the *cmc* (0.3 mM). The difference between the data on each individual graph is the polarization of the incident and collected light. Each different polarization is sensitive to vibrational modes of the *rac*-**32** (1-C$_{12}$I$_1$E$_3$) orientated in a different direction with respect to the interface. For example, the Px polarization indicates that the incident beam is polarized in the 'P' direction with samples modes that are perpendicular to the interface, while the 'x' indicates that the collected light is turned 90 degrees around an axis perpendicular to the interface. The result is two sample modes perpendicular to the interface that are also in a specific orientation along another axis.

Looking at the data for the Px case, the really interesting result comes from the 0.03 mM concentration of the *rac*-**32** (1-C$_{12}$I$_1$E$_3$). At lower temperatures the molecule shows lower overall signal intensity than at higher temperatures which could mean that there is a rather dramatic reorganization of the adsorbed *rac*-**32** (1-C$_{12}$I$_1$E$_3$) as a function of temperature. In theory, the change in signal intensity could be due to the molecules being compact at lower temperatures, and then becoming increasingly solvated and elongated at higher temperatures. Understanding why this would happen for a lower concentration and not for a higher concentration would be interesting.
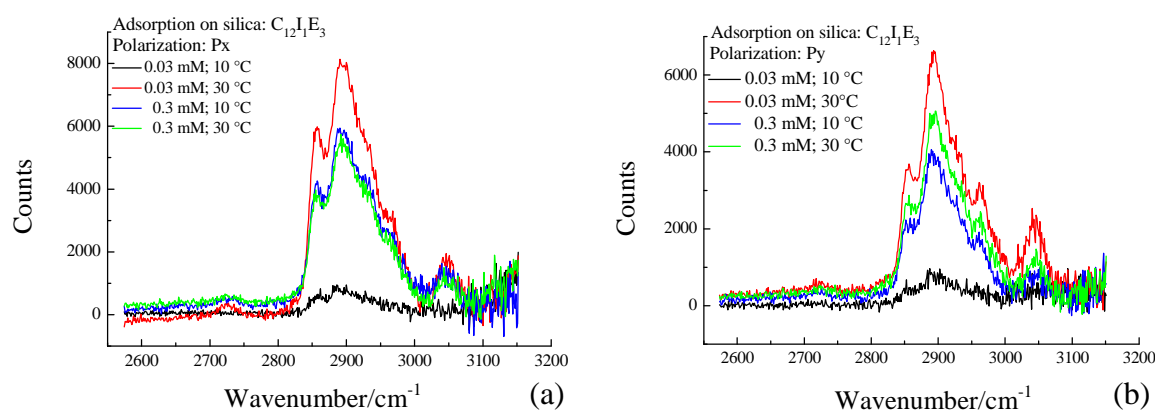
Fig. 3.21. TIR Raman subtracted spectra of silica in contact with *rac*-**32** (1-C$_{12}$I$_1$E$_3$) solutions of different concentrations (0.03 mM and 0.3 mM) and temperatures (10 °C and 30 °C) collected under the polarization combinations (a) Px and (b) Py.
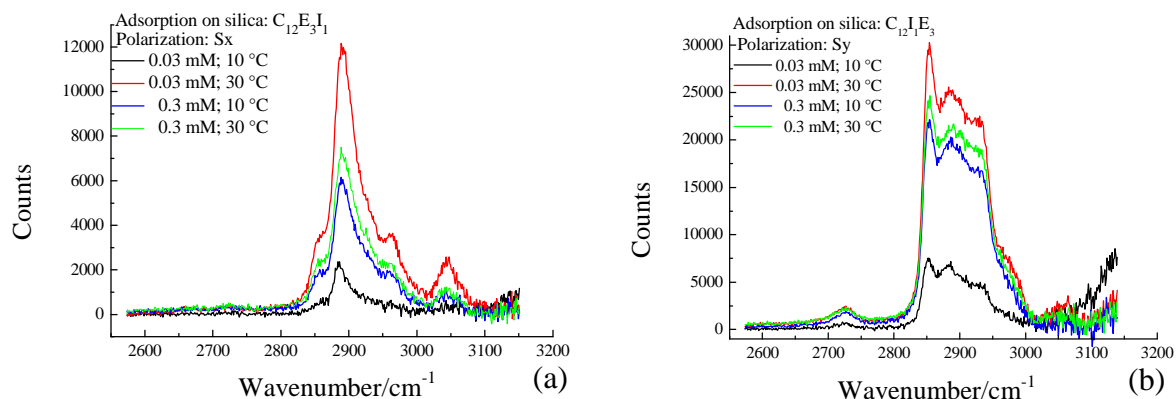
Fig. 3.22. TIR Raman subtracted spectra of silica in contact with *rac*-**32** (1-$C_{12}I_1E_3$) solutions of different concentrations (0.03 mM and 0.3 mM) and temperatures (10 °C and 30 °C) collected under the polarization combinations (a) Sx and (b) Sy.

These results may imply that adsorption behaviour is controlled by the nature of the terminal group. These are only preliminary results. The same study at a concentration above the *cmc* would be interesting as would a study at trace levels of *rac*-**32** (1-$C_{12}I_1E_3$) or acquiring data for more than two temperatures and also determining if this change in intensity with temperature is reversible.

3.2.3.4. Self-diffusion NMR (DOSY)

In order to find out more information about the hydration of the inositol-based surfactants, self-diffusion coefficients were measured using a magnetic field gradient method called **d**iffusion **o**rdered **s**pectroscop**y** (DOSY).

Because the measurements were desired to be performed in water at very low surfactant concentrations (10^{-4} M) two main problems occurred: the handling of the spectrometer (lock solvent and shimming) in absence of a deuterated solvent and the quality of spectrum because of the deleterious effects of the huge water resonance.

To solve the technical problem regarding the spectrometer handling, a special type of tubes were used, namely NMR tubes with stem coaxial inserts of type WGS-5BL from Rototec-Spintec, having the reference capacity of 60 µL and the sample capacity of 530 µL (Fig. 3.23). The deuterated solvent was introduced in the inner tube and the examination material was placed in the outer tube. As can be seen, the reference capacity is low (60 µL) and for this reason it was necessary to use a solvent with a high percentage of deuterium. After few tests with different deuterated solvents, the deuterium oxide (D_2O) has given the best results and consequently it was further used for measurements.
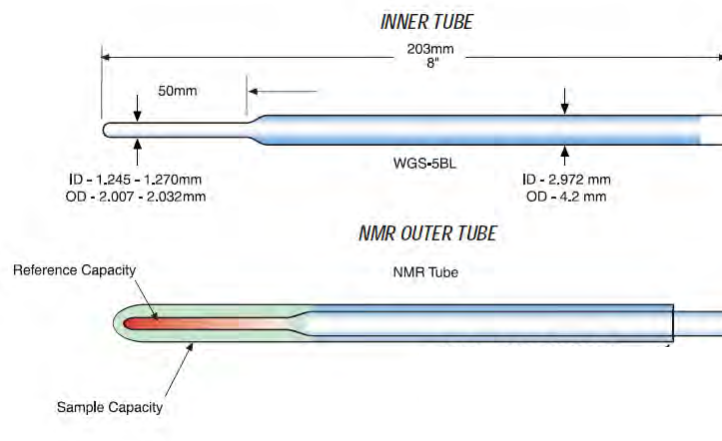
Fig. 3.23. The NMR tube used for DOSY experiments

Dealing with low concentration samples, the signals of the compound of interest were almost invisible compared with water signal in the ^{1}H NMR spectra. This is the reason why a new pulse sequence (stebpgpes1s1d.sek) was developed including the suppression of water signal by excitation sculpting using arbitrary waveforms and pulsed field gradients. In order to check the reliability of the results obtained with the new developed method (with water suppression), test experiments were done with literature known compound *n*-octyl-β-D-glucoside using both methods, with and without water suppression. The measured values for

the self-diffusion coefficient D were very similar (D = 4.424 10^{-11} m^2 s^{-1} for the sequence without water suppression and D = 4.428 10^{-11} m^2 s^{-1} for the sequence with water suppression) and comparable with the values from literature.[42] The detailed pulse program is presented in chapter 7 (Experimental part).

DOSY experiments were performed on two inositol derivatives *rac*-**19** (1-C$_{12}$E$_3$I$_1$) and *rac*-**32** (1-C$_{12}$I$_1$E$_3$) as well as on the reference systems *n*-dodecyl hexaethylene oxide (C$_{12}$E$_6$) and *n*-dodecyl-β-maltoside (β-C$_{12}$G$_2$). Figures 3.24, 3.25, 3.26, 3.27 present examples of diffusion spectra (a) 2D and (b) 1D for every compound at concentrations 6 x *cmc*.
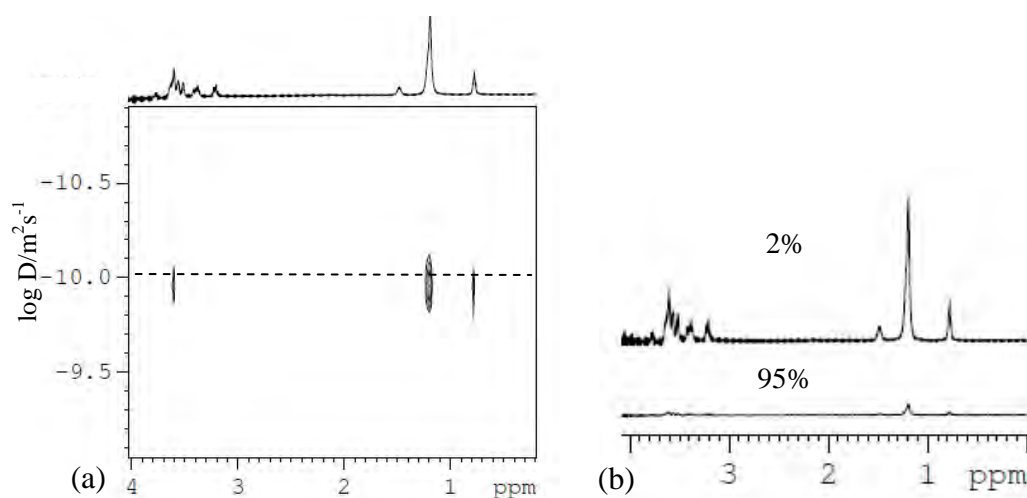
Fig. 3.24. (a) 2D DOSY spectrum and (b) ^{1}H spectrum at 2% and 95% gradient strength for *rac*-**19** (1-C$_{12}$E$_3$I$_1$) in aqueous solution.
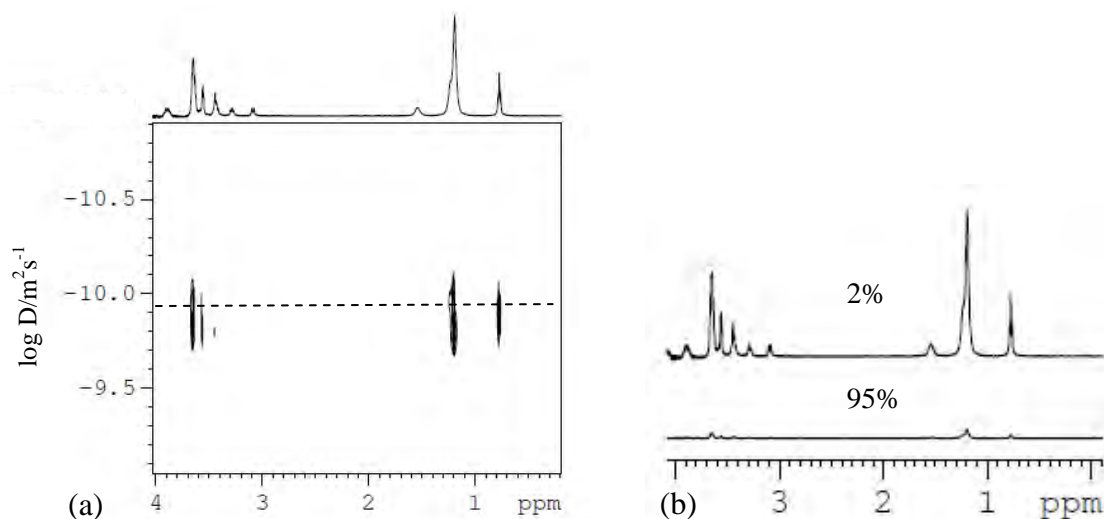
Fig. 3.25. (a) 2D DOSY spectrum and (b) ^{1}H spectrum at 2% and 95% gradient strength for *rac*-**32** (1-C$_{12}$I$_1$E$_3$) in aqueous solution.
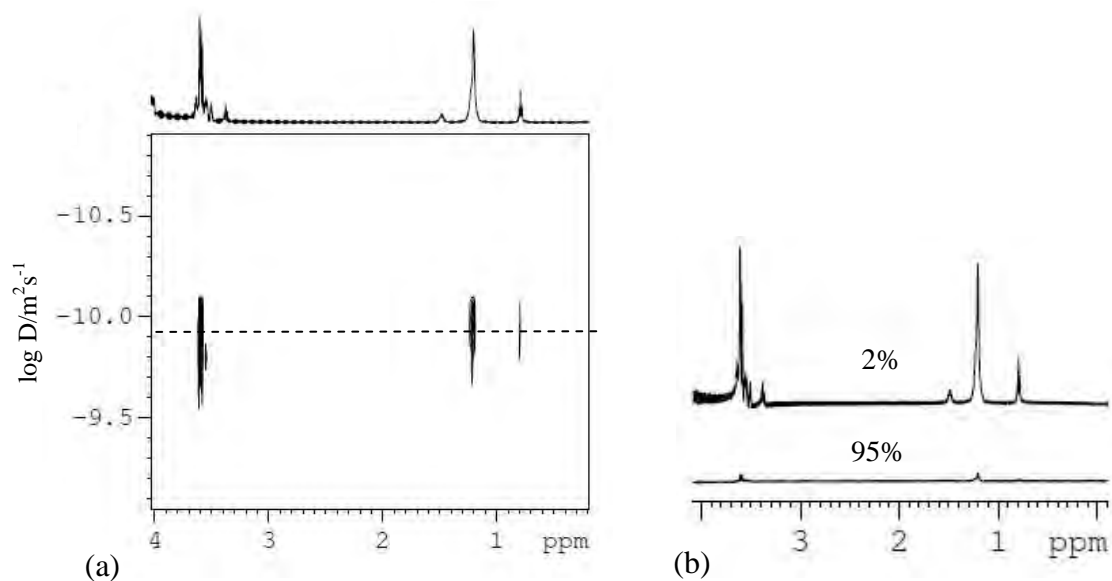
Fig. 3.26. (a) 2D DOSY spectrum and (b) ^{1}H spectrum at 2% and 95% gradient strength for *n*-dodecyl hexaethylene oxide (C$_{12}$E$_6$) in aqueous solution.
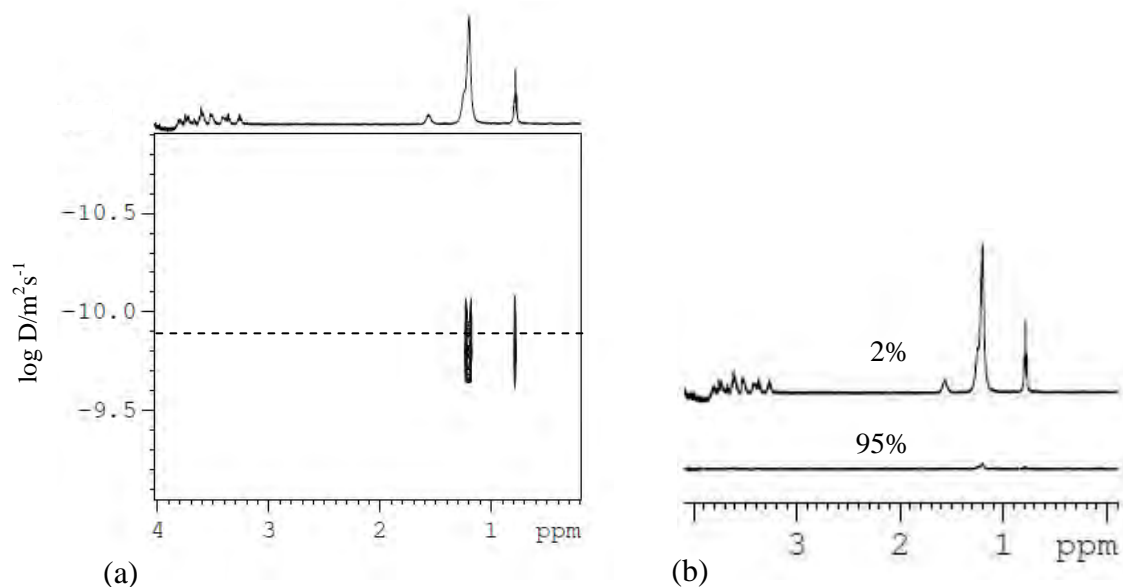
Fig. 3.27. (a) 2D DOSY spectrum and (b) ^{1}H spectrum at 2% and 95% gradient strength for *n*-dodecyl-β-maltoside (β-C$_{12}$G$_2$) in aqueous solution.

The readings of the self-diffusion coefficient belong to C$_{12}$ chain signal which is the most intense signal in the ^{1}H NMR and consequently the less influenced by the errors. The self-diffusion coefficient *D* was obtained by fitting equation 2.10 to the obtained NMR data.

$$I = I_0 \exp\left(-(\gamma \delta G)^2 D\left(\Delta - \frac{\delta}{3}\right)\right)$$

(2.10, see chapter 2.1.5.2)

where I_0 is the signal intensity at zero gradient strength, γ is the proton magnetogyric constant, G is the gradient strength, D is the diffusion coefficient, $\varDelta$ is the diffusion time and δ is the length of the gradient.

The obtained results are presented as plots of the diffusion coefficient D versus the total surfactant concentration c (Fig. 3.28) and of the diffusion coefficient D versus c/cmc ratio ($c =$ total surfactant concentration), cmc = critical micelle concentration) (Fig. 3.29).
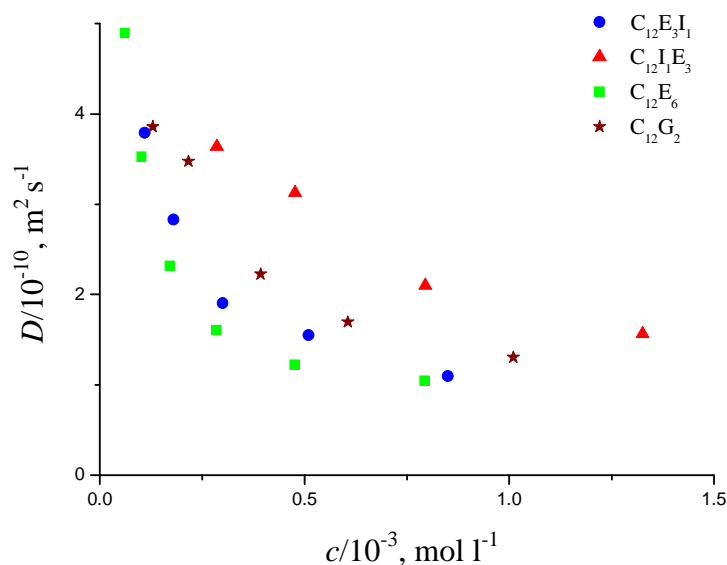
Fig. 3.28. The measured self-diffusion coefficients versus concentration in the micellar region of the four surfactants *rac*-**19** (1-$C_{12}E_3I_1$), *rac*-**32** (1-$C_{12}I_1E_3$), $C_{12}E_6$, $C_{12}G_2$; the first point from each plot represents D_{mono} (the diffusion coefficient of free monomer).
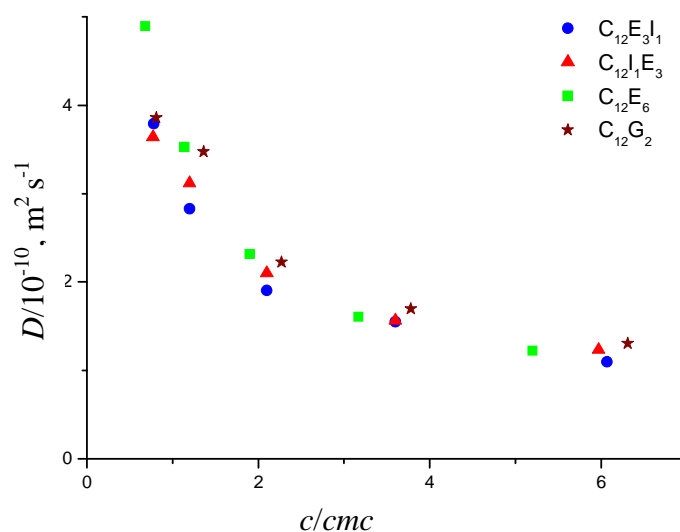
Fig. 3.29. The measured self-diffusion coefficients versus c/cmc ratio, in micellar region of the four surfactants *rac*-**19** (1-$C_{12}E_3I_1$), *rac*-**32** (1-$C_{12}I_1E_3$), $C_{12}E_6$, $C_{12}G_2$.

The rapid decrease of the diffusion coefficients with increasing concentrations at low surfactant concentrations can be attributed to the formation of aggregates and their subsequent growth but also to the decrease in fraction of surfactant present as monomer. Aggregate/aggregate obstruction effects at finite micellar concentrations also lower the surfactant diffusion coefficients.

The value of D_{mono} (the diffusion coefficient of the free monomer) was obtained performing experiments at concentrations below the *cmc*, where the diffusion coefficient is expected to have a constant value and the obtained results are presented in Table 3.6.

Table 3.6. The measured D_{mono} for the four investigated surfactants

Surfactant	$c = 0.8\ cmc/10^{-3}$, mol l^{-1}	$D_{mono}/10^{-10}$, m^2 s^{-1}
n-dodecyl-β-maltoside ($C_{12}G_2$)	0.13	3.86
rac-**19** (1-$C_{12}E_3I_1$)	0.11	3.79
rac-**32** (1-$C_{12}I_1E_3$)	0.30	3.64
n-dodecyl hexaethylene oxide ($C_{12}E_6$)	0.07	4.89

Rounding the D_{mono}-values in Table 3.6 according to the errors given in section 7.5 (3.86 ± 0.09, 3.79 ± 0.09, 3.64 ± 0.04, 4.89 ± 0.07) one clearly sees that the self-diffusion coefficients of the two inositol-based surfactants and of the sugar surfactant are the same, while that of $C_{12}E_6$ is larger. The later observation is indeed very surprising.

A possible reason for $D_{C12E6} > D_{C12G2}$ could be simply the lower total surfactant concentration. Although both systems were measured at 0.8 *cmc*, in case of $C_{12}E_6$ this corresponds to 0.06 mM, while it corresponds to 0.13 mM in case of $C_{12}G_2$. Arguing via the total surfactant concentration explains the results for $C_{12}E_6$, $C_{12}G_2$ and *rac*-**19**. However, the value obtained for *rac*-**32** should be much lower if it were only the total surfactant concentration that plays a role. One possible explanation could be the different shape of the molecules (stiff, rod-like in case of $C_{12}G_2$ and *rac*-**19**, coil-like in case $C_{12}E_6$ and *rac*-**32**). The obstruction factor of the former is larger and thus diffusion is more hindered compared to coil-like molecules at the same total surfactant concentration. In other words, *rac*-**32** has the same coefficient as *rac*-**19** at a much larger total surfactant concentration as it is coil-like rather than rod-like. Note that at the time being, this is only speculation.

Another explanation could be the contribution of pre-micellar aggregates (dimmers, trimers, tetramers, etc). The *cmc* is no "fixed" value but rather a concentration range. Depending on the technique and the model via which the data are evaluated different values are obtained. Thus choosing $c = 0.8\ cmc$ as concentration for the determination of D_{mono} could be too close

to the *cmc*, which means that in some cases pre-micellar aggregates may already be formed. These aggregates could decrease the D_{mono} value significantly compared to a solution of "real" monomers.

The self-diffusion coefficients measured for concentrations above *cmc* can be used to infer information about the possible size/structure of the micelles present. One problem that has to overcome before such an analysis can be performed is the fact that there are contributions from the surfactant present in free monomer form. This contribution can be accounted by means of a simple two-site exchange model which yields the following relation:[42]

$$D_{\text{obs}} = PD_{\text{mic}} + (1 - P)D_{\text{mono}} \qquad \text{(2.11, see chapter 2.1.5.2)}$$

where D_{obs} is the observed diffusion coefficient, D_{mic} is the micellar diffusion coefficient, D_{mono} is the monomer diffusion coefficient, and P is the fraction of micellized surfactant, which is given by equation 2.12:

$$P = \frac{c - cmc}{c} \qquad \text{(2.12, see chapter 2.1.5.2)}$$

As it was mentioned above, in presence of micelles, aggregate obstructions effects must be taken into account. In case of spherical micelles, a functional form according to the following equation 2.13 is often used:

$$D_{mic} = D_0\left(1 - k\Phi\right) \qquad \text{(2.13, see chapter 2.1.5.2)}$$

where D_{mic} is the measured micelle diffusion coefficient, D_0 is the micelle diffusion coefficient at infinite dilution, k is a constant and Φ is the volume fraction of micelles. In case of spherical aggregates, $k \approx$ 2-2.5, depending on the surfactant. Eq. 2.13 can be applied only for the case of spherical micelles, in case of other geometries (e.g. prolates, oblates or hemisphere capped rods) this expression will be different.[41,86]

Using the equations 2.8, 2.11 and the relevant expressions for the different geometries together with the acquired experimental data, a number of new information about the formed aggregates can be achieved. These calculations are to be done therefore they are not included in the present work.

4. RESULTS AND DISCUSSION II

4.1. Phosphine oxides metal complexes

n-Dodecyldimethyl phospine oxide (C_{12}DMPO) was synthesized and purified for an ongoing project at University College Dublin (UCD) under the supervision of Prof. Dr. Cosima Stubenrauch. This project aims to study the correlation between single foam films and foams by varying the surfactant mixing ratio, thus providing new insights into how to tune the properties of foams. Foams are widely used in industrial applications and everyday products such as cleaning agents, beverages, fire-fighting and flotation. However, the reason for their stability - or instability - is not yet understood in sufficient detail so that the development of new products is mostly based on "trial and error". Studying surfactant mixtures is indispensable in order to understand and to optimize technical products and processes where foam films and foams are involved. Phosphine oxide surfactants are an ideal candidate for this project as they are chemically quite resistant, pH- and temperature stable.[87,88] A hydrophobic chain length of C_{12} was chosen to allow for optimum foaming condition.

Phosphine oxide groups can bind various metal cations such as alkaline, alkaline earth, transition and lanthanide metal ions through ion dipolar interactions. This property allows phosphine oxide-based derivatives to be used in various fields of large social and economical impacts, such as environmental sciences, medical diagnostics, cell biology, etc.[89-91] Lipophilic phosphine oxides like the respective trioctyl derivative (TOPO) or more specialized derivatives with additional complexation sites have been used also as extraction agent for precious metals from aqueous solutions.[92,93] This property inspired the question if it would be possible to induce supramolecular order like e.g. thermotropic or lyotropic liquid crystallinity in phosphine oxides metal complexes amphiphiles. The results of respective investigations will be presented in this chapter. However, it has to be mentioned that parallel to present studies on such (calamitic) amphiphilic phosphine oxides, a report on a columnar liquid crystal based on discotic triphenylphosphine oxide and on its interaction with alkaline metal ions was published by Kato et al.[94]

4.1.1. Syntheses

The synthesis of *n*-dodecyldimethyl phospine oxide (C$_{12}$DMPO, **52**) is well known[95-98] and straightforward as can be seen from Scheme 4.1:
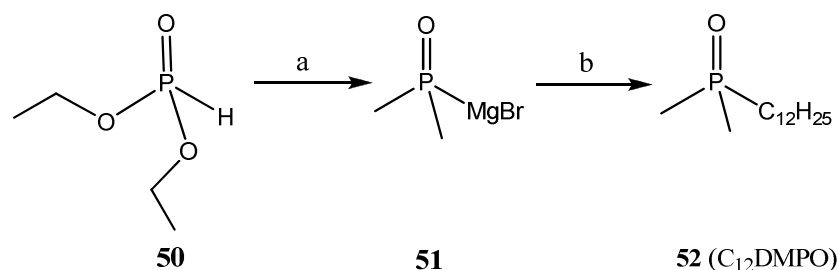
Scheme 4.1. Synthetic steps towards the *n*-dodecyldimethyl phospine oxide **52** (C$_{12}$DMPO): a) MeMgBr, THF, rt; b) C$_{12}$H$_{25}$Br, reflux; 80% after two steps.

The synthesis starts from commercially available diethyl phosphite which was added dropwise into a solution of methyl magnesium bromide (1 M in THF) under argon atmosphere in such a way that the inner temperature did not rise 25 °C. After stirring for 1 h at ambient temperature, dodecyl bromide was added and the reaction was refluxed for 10 additional hours. After the required work-up, the crude product was thoroughly purified by bulb-to-bulb distillation and few recrystallizations from n-hexane.

The preparation of C$_{12}$DMPO metal complexes consisted in mixing the phosphine oxide with various metal salts (Scheme 4.2) for ~ 1.5 h at room temperature in presence of a proper solvent (methanol or water), followed by the concentration to dryness. In a number of cases homogeneous products were obtained showing sharp transition temperatures indicating a defined complexation (Table 4.1).
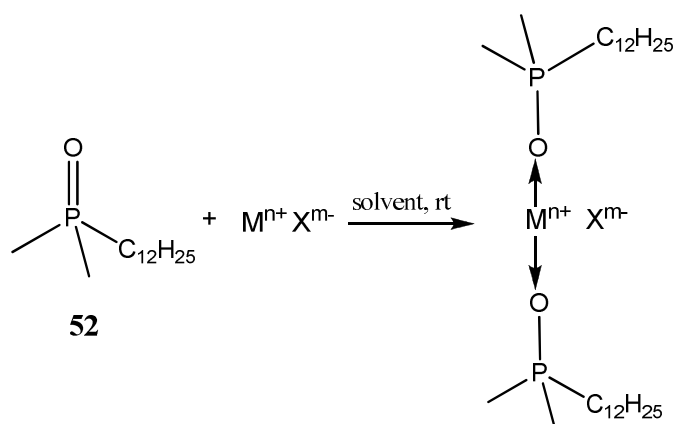
Scheme 4.2. Synthetic step towards the *n*-dodecyldimethyl phospine oxide (C$_{12}$DMPO) metal complexes.

Table 4.1. Composition and transition temperatures of $C_{12}DMPO$: salt mixtures

M^{n+}	X^m	Hmg	Cr_1		Cr_2		Cr_3	I
Cu^{2+}	Cl^-	+	•	55/53,4 (28,0)				•
Cu^{2+}	SO_4^{2-}	-	•	-/51.1 (1.65)	•	83/79,1 (11,9)		•
Cu^{2+}	Br^-	+	•	48/48,9 (25,4)				•
Cu^{2+}	BF_4^-	+	•	-/34.5 (1.3)	•	55/54,5 (0,5)	•	[b]
Cu^{2+}	$C_5H_7O_2^-$	-	•	83/81,4 (34,3)				•
Cu^{2+}	CH_3COO^-	-	•	83/82,3 (27,3)				•
Li^+	Cl^-	+	•	92/93,5 (0,3)	•	116,0/115,9 (3,5)		•
Li^+	Br^-	+	•	72/69,9 (17,5)				•
Na^+	Cl^-	-	•	85/81,0 (27,7)				•

[a]Temperatures given in °C: PM / DSC (ΔH_{rel} in kJ/mol); $\Delta H_{rel} = \Delta H_{abs}(x_1 M_{C12DMPO} + x_2 M_{salt})$; x_1, x_2 = molar fractions; ΔH_{abs} measured by DSC; Hmg = Homogeneity;
[b] Complex thermal behavior upon repeated heating/cooling cycles, the clearing point is not visible in DSC and in PM is between 70 – 90°C. PM = polarized microscopy; Cr = crystalline; Iso = isotropic.

The first analytical method which was used to confirm the complexation of $C_{12}DMPO$ (**52**) with various salts is infrared spectroscopy (IR). As can be seen from Fig. 4.1, the IR spectra of resulting compounds are almost identical to the IR spectra of pure $C_{12}DMPO$, with the exception that the P – O band is shifted and/or deformed which is indicative for complexation at the oxygen atom of phosphine oxide group.

The IR spectra are presented as following: Fig. 4.1a – spectra belong to $C_{12}DMPO$ complexes which have the same cation (Cu^{2+}) but different inorganic anions (Cl^-, SO_4^{2-}, Br^-, BF_4^-); Fig. 4.1b – spectra belong to $C_{12}DMPO$ complexes which have the same cation (Cu^{2+}) but different organic anions ($C_5H_7O_2^-$, CH_3COO^-); Fig. 4.2a – spectra belong to $C_{12}DMPO$ complexes which have the same anion (Cl^-) but different cations (Cu^{2+}, Li^+, Na^+); Fig. 4.2b – spectra belong to $C_{12}DMPO$ complexes which have the same anion (Br^-) but different cations (Cu^{2+}, Li^+).
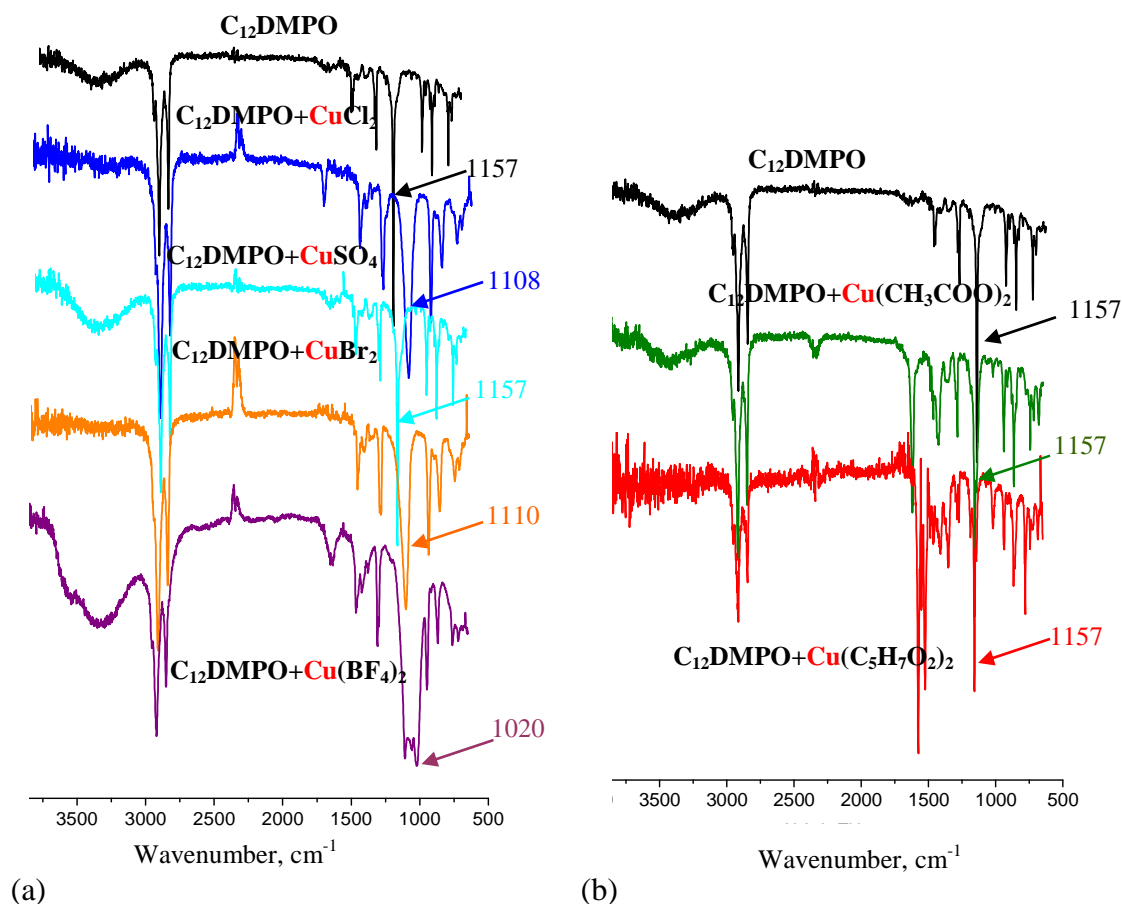
Fig. 4.1. The IR spectra of C_{12}DMPO : salt mixtures having the same cation (Cu^{2+}) but different (a) inorganic anion and (b) organic anion.

In Fig. 4.1a and b can be observed that the P – O band is shifted and/or deformed for those mixtures C_{12}DMPO : salt which are homogeneous (see Table 4.1), but not for those ones which are inhomogeneous, like C_{12}DMPO + $CuSO_4$, $Cu(CH_3COO)_2$ or $Cu(C_5H_7O_2)_2$. This fact means that the P – O band was not affected by the presence of the salt consequently the complexation was not achieved.

The same situation can be observed in Fig. 4.2a for C_{12}DMPO + NaCl which again forms an inhomogeneous mixture and the P – O band from 1157 cm^{-1} was not affected.

The conclusion which rises from figures 4.1 and 4.2 is that C_{12}DMPO is able to form complexes with metal salts but the complexation depends on both the cation and the anion of the respective salt.
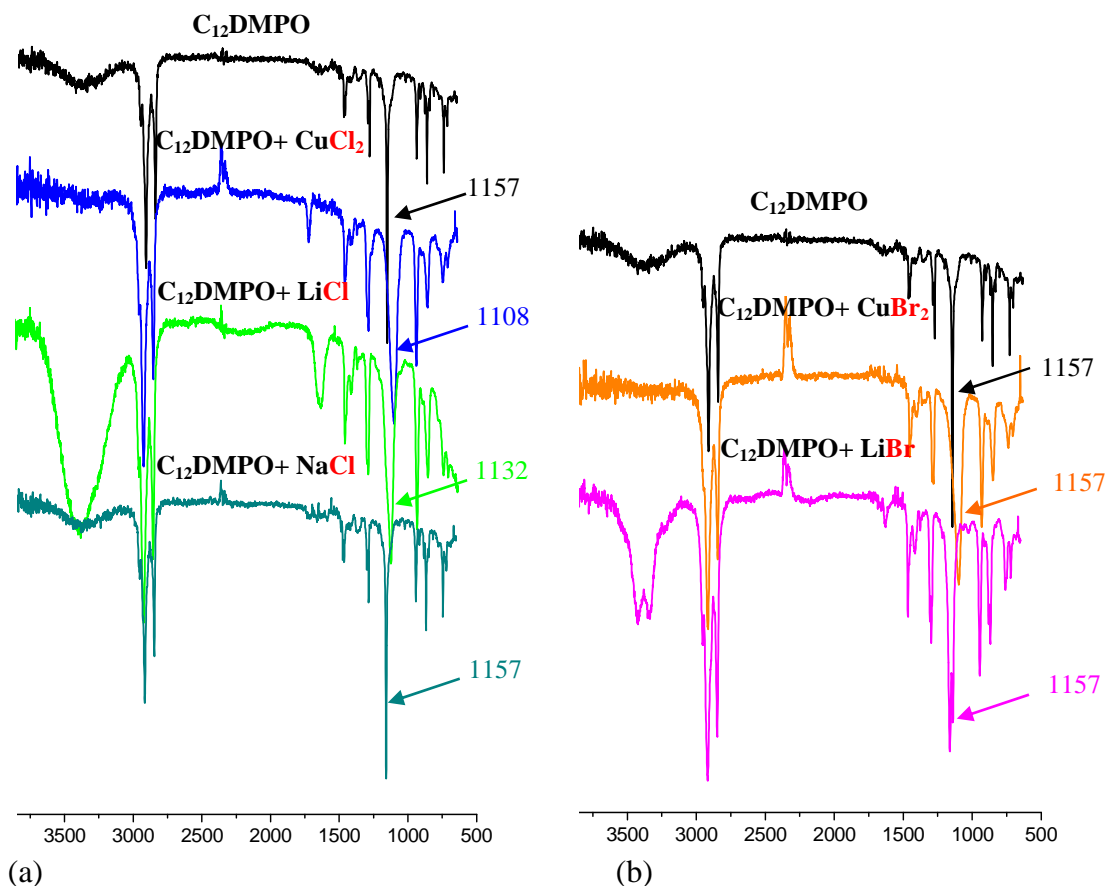
Fig. 4.2. The IR spectra of C_{12}DMPO : salt mixtures having the same anion (a: Cl^-; b: Br^-) but different anion (a: Cu^{2+}, Li^+, Na^+; b: Cu^{2+}, Li^+).

The ability of C_{12}DMPO to form complexes was proven by X-ray investigations. As can be seen in Table 4.1., the melting points of the C_{12}DMPO : salt complexes are low, hence a normal recrystallization from solvents was not successful. For this reason it has been tried to obtain proper crystals from melt by cooling very slow (0,1 °C/10min). The crystal structure of C_{12}DMPO : $CuCl_2$ complex is presented in Fig. 4.3.
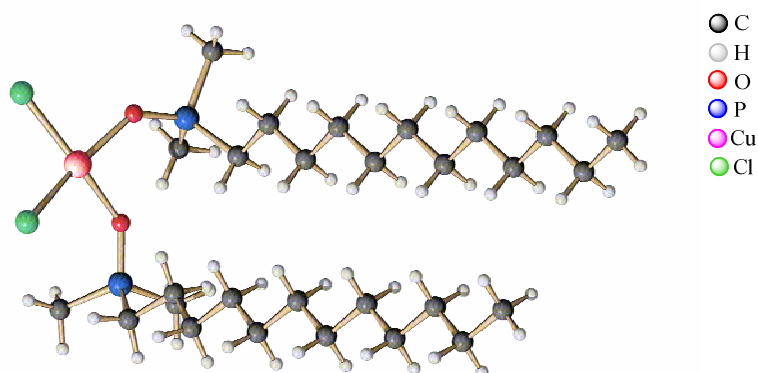
Fig. 4.3. Crystal structure of C_{12}DMPO : $CuCl_2$ complex.

4.1.2. Physical properties

4.1.2.1. Thermotropic mesomorphism

Thermotropic behaviour of $C_{12}DMPO$: salt complexes was investigated by polarizing microscopy (PM) and differential scanning calorimetry (DSC). Their phase transition data are summarized in Table 4.1. Three of the studied mixtures exhibit crystalline polymorphism but none of the observed phases were liquid crystalline.

4.1.2.2. Lyotropic mesomorphism

As can be seen from the phase diagram (Fig. 4.4a) already the pure $C_{12}DMPO$ displays lyotropic mesophases. Most of $C_{12}DMPO$: salt mixtures show also lyotropic phase behavior, but from preliminary PM investigations they partly differ in phase types, stabilities and sequence (Fig. 4.5, 4.6) from pure $C_{12}DMPO$ (Fig. 4.4b).

(a)   (b)
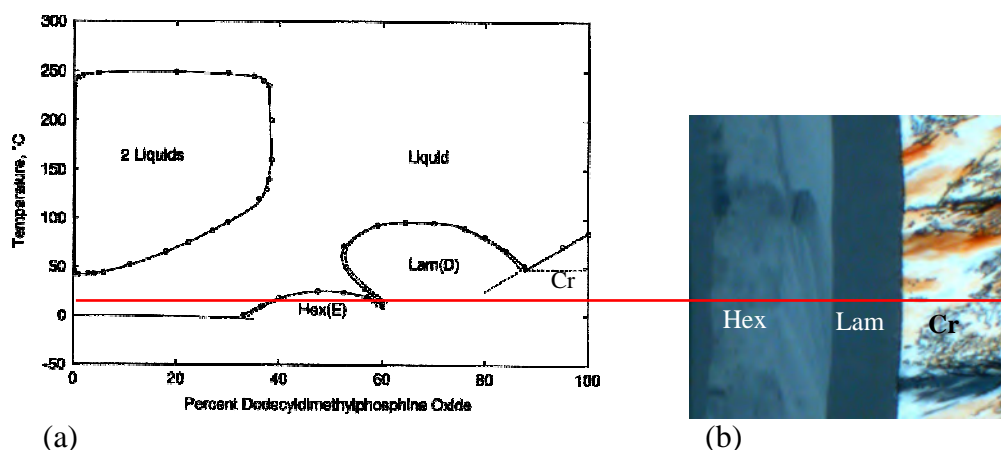
Fig. 4.4. (a) Phase diagram of binary system water – $C_{12}DMPO$[28], (b) Penetration experiment of binary system water – $C_{12}DMPO$ showing the phase sequence Cr, Lam, Hex at 12,1°C (Cr = crystalline, Lam = lamellar, Hex = hexagonal).
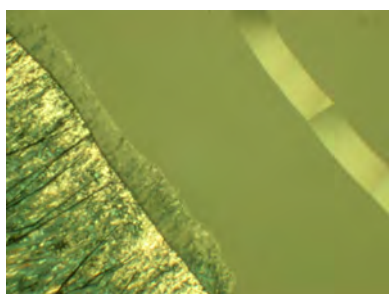
Fig. 4.5. Penetration experiment of binary system water – $C_{12}DMPO$+LiCl at 23 °C.
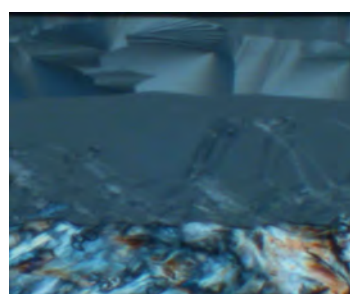
Fig. 4.6. Penetration experiment of binary system water – $C_{12}DMPO$+LiBr at 25°C.

The pentration experiment of binary system water – $C_{12}DMPO+LiCl$ revealed the sequence micellar – hexagonal – cubic V_1 – lamellar – crystalline, while the binary system water – $C_{12}DMPO+LiBr$ presents the sequence micellar – hexagonal – lamellar – crystalline.

The concluding remarks regarding this topic are that $C_{12}DMPO$ is able to form complexes with metal salts depending both on cation and anion, and the newly formed complexes present lyotropic but not thermotropic mesomorphism.

5. SUMMARY AND OUTLOOK I

This chapter is going to present a summary of studies towards the syntheses and characterization of novel inositol-based amphitropic liquid crystals and surfactants together with a short outlook.

5.1. Syntheses

The aim of the present work from synthetically point of view consists on synthesis of novel inositol-based derivatives as amphitropic liquid crystals and surfactants. Previous work in this field showed that one inositol unit is not enough to induce a good solubility in aqueous media of this type of sugar-based amphiphiles. In order to improve the inositol derivatives with respect to this property, the hydrophilic head group was increased by addition of a triethylene oxide unit leading to a new class of inositol-based amphiphiles.

The first representative of this new class of inositol derivatives is *rac*-**19** (1-$C_{12}E_3I_1$) which has the ethoxylated chain and the hydrophobic tail attached to the hydroxyl group from position 1 of *myo*-inositol ring. Its synthesis was achieved in seven steps with an overall yield of 20% (Scheme 5.1).

In order to functionalise the hydroxyl group from C_1, it was necessary to protect the other four positions, which was realized in three steps with an overall yield of 62%. In parallel, the dodecyl chain was attached via a Williamson etherification to the triethylene oxide, which was subsequently tosylated to give **17** with 70% yield after two steps. Next step consisted in regioselective unification of the two building blocks, *rac*-**6** and **17**, which was achieved via a stannylene intermediate. The last step of this synthesis was the cleavage of benzyl protecting groups by palladium/charcoal catalyzed hydrogenolysis under pressure (~ 8 bars) (Scheme 5.1).
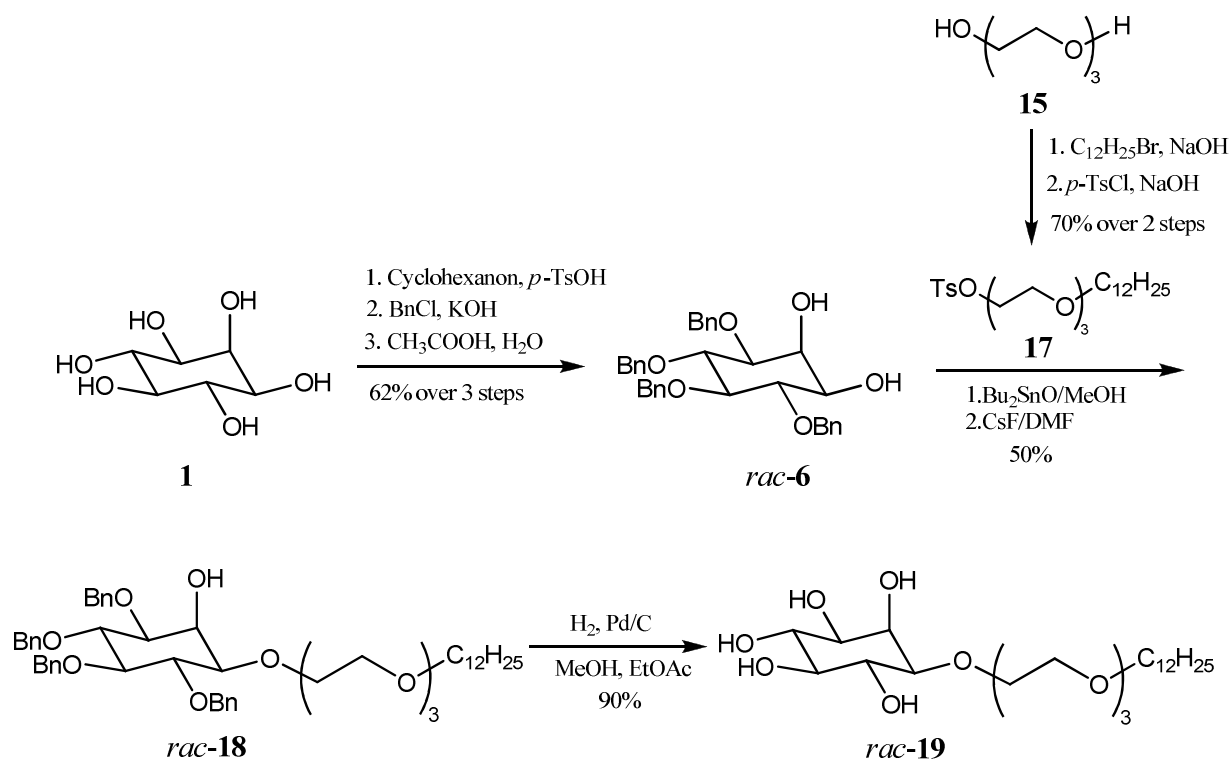
Scheme 5.1. Total synthesis of *rac*-**19** (1-$C_{12}E_3I_1$).

To study the influence of position of the alkyl-triethylene oxide on *myo*-inositol ring with regard to mesomorphsim and surface activity, a new derivative, **21** (2-$C_{12}E_3I_1$), was synthesized in eight steps starting from *myo*-inositol (**1**) and triethylene oxide (**15**), in 31% overall yield. To arrive to **21**, the hydroxyl groups from positions 1, 3, 4, 5, and 6 were protected over four steps with an overall yield of 56%. The addition of alkyl-triethylene oxide chain was achieved by reaction with the corresponding tosylate **17** in the presence of NaH and DMF with 90% yield. The final step, the cleavage of benzyl ethers, was realized by palladium/charcoal catalysed hydrogenolysis in 88% yield (Scheme 5.2).
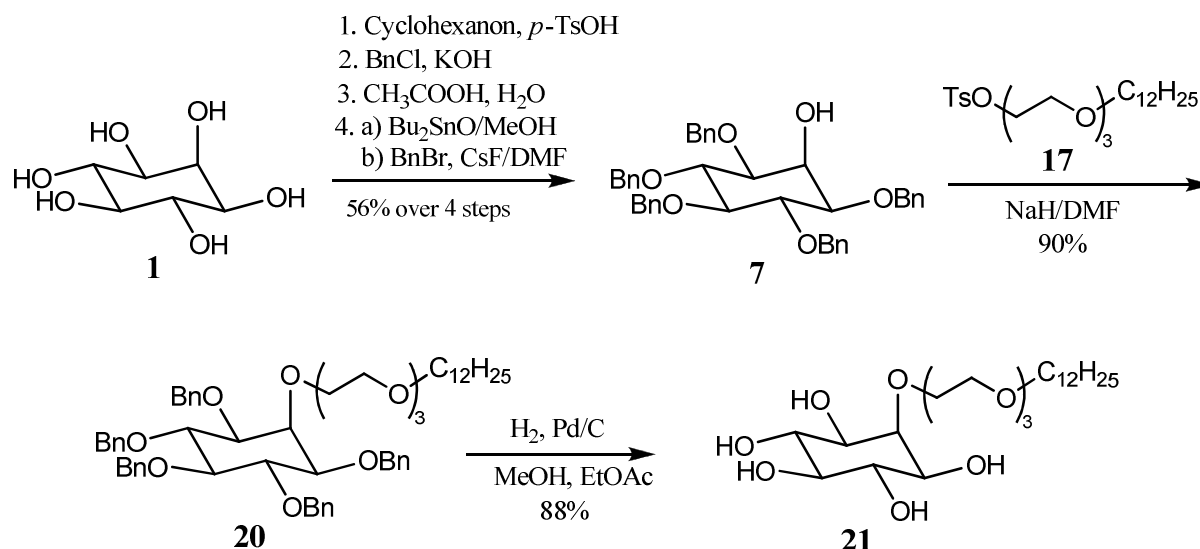
Scheme 5.2. Total synthesis of derivative **21** (2-$C_{12}E_3I_1$).

In order to attach the alkyl-triethylene oxide chain to hydroxyl group from position 4, another protective group strategy was applied, respectively the formation of *myo*-inositol orthofomate, **8**. Addition of tosylate **17** to orthoformate **8** in the presence of NaH/DMF resulted in formation of corresponding C_4 ether **25** in 62% yield. After the hydrolysis of orthoester **25** with methanol/HCl, *rac*-**26** (4-$C_{12}E_3I_1$) was obtained with 83% yield (Scheme 5.3).
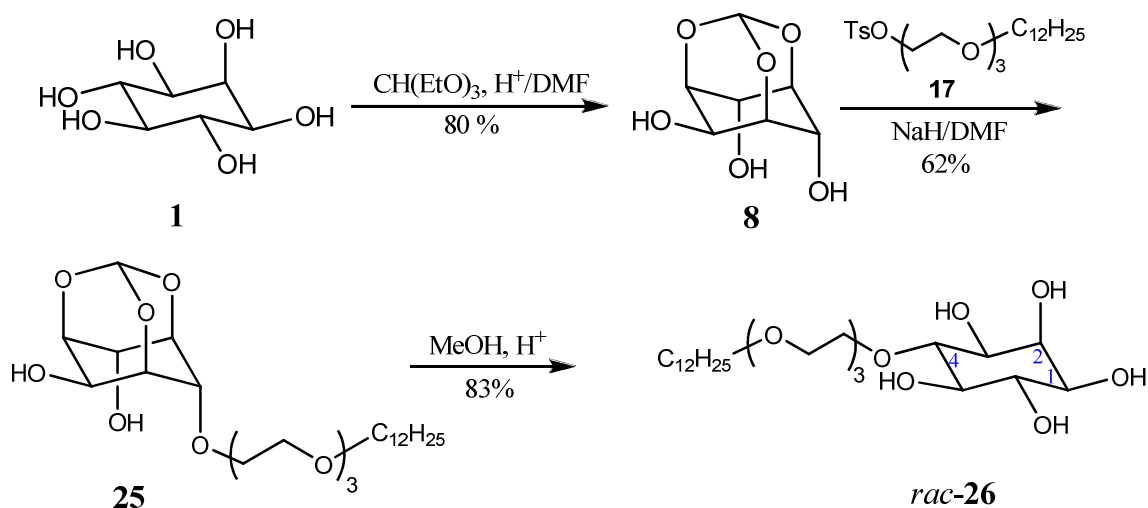
Scheme 5.3. Total synthesis of *rac*-**26** (4-$C_{12}E_3I_1$).

To study and compare the influence of molecular arrangement of oligo(ethylene oxide) and sugar units, a new inositol-based derivative, *rac*-**32** (1-$C_{12}I_1E_3$) was synthesized. This derivative represents the "inversed" sequence triethylene oxide – inositol – dodecyl chain, which induced interesting differences with regard to physical properties.

Synthesis of *rac*-**32** was realised in seven steps with 8% overall yield. The first step is represented by protection of hydroxyl groups from positions 1, 2, 4, and 5 by acetalization with cyclohexanone, followed by alkylation with dodecyl bromide and the attachment of tosylate **28** to the hydroxyl group from C_6. The last step, the cleavage of acetals, was done in acidic conditions (Scheme 5.4).
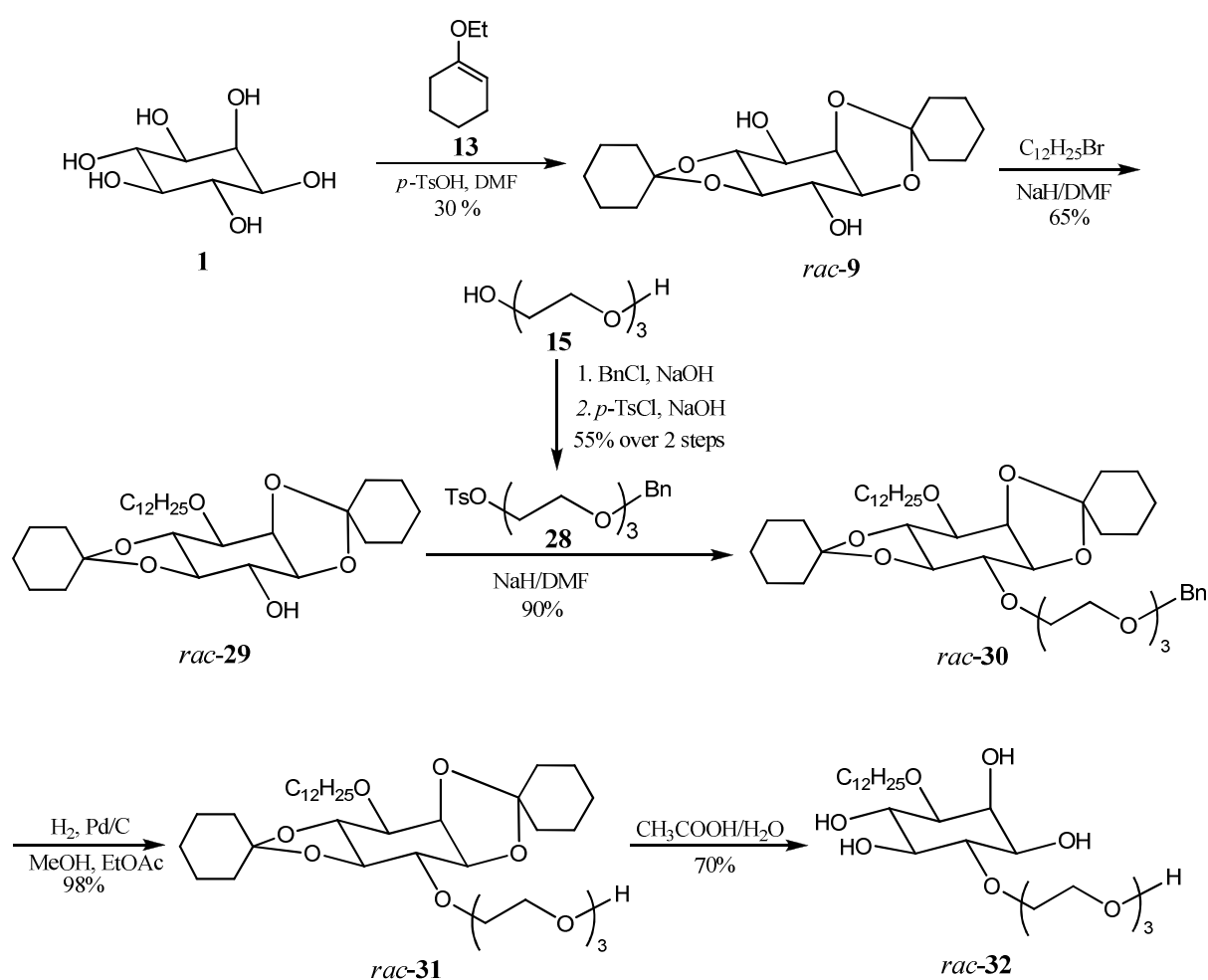
Scheme 5.4. Total synthesis of *rac*-**32** (1-$C_{12}I_1E_3$).

The *meso* compound **36** (2-$C_{12}I_1E_3$) was synthesized in seven steps (overall yield 7%) for the purpose of studying the influence of symmetry on physical properties. Its synthesis resemble the one for *rac*-**32**, but in this case the acetalization was realised selectively for *trans* hydroxyl functions using butane-2,3-dione. After alkylation of free positions 2 and 5 with the desired

side chains (alkyl and triethylene oxide, respectively), the last two steps consisted in deprotection reactions in order to cleave the benzyl ether and the acetals (Scheme 5.5).
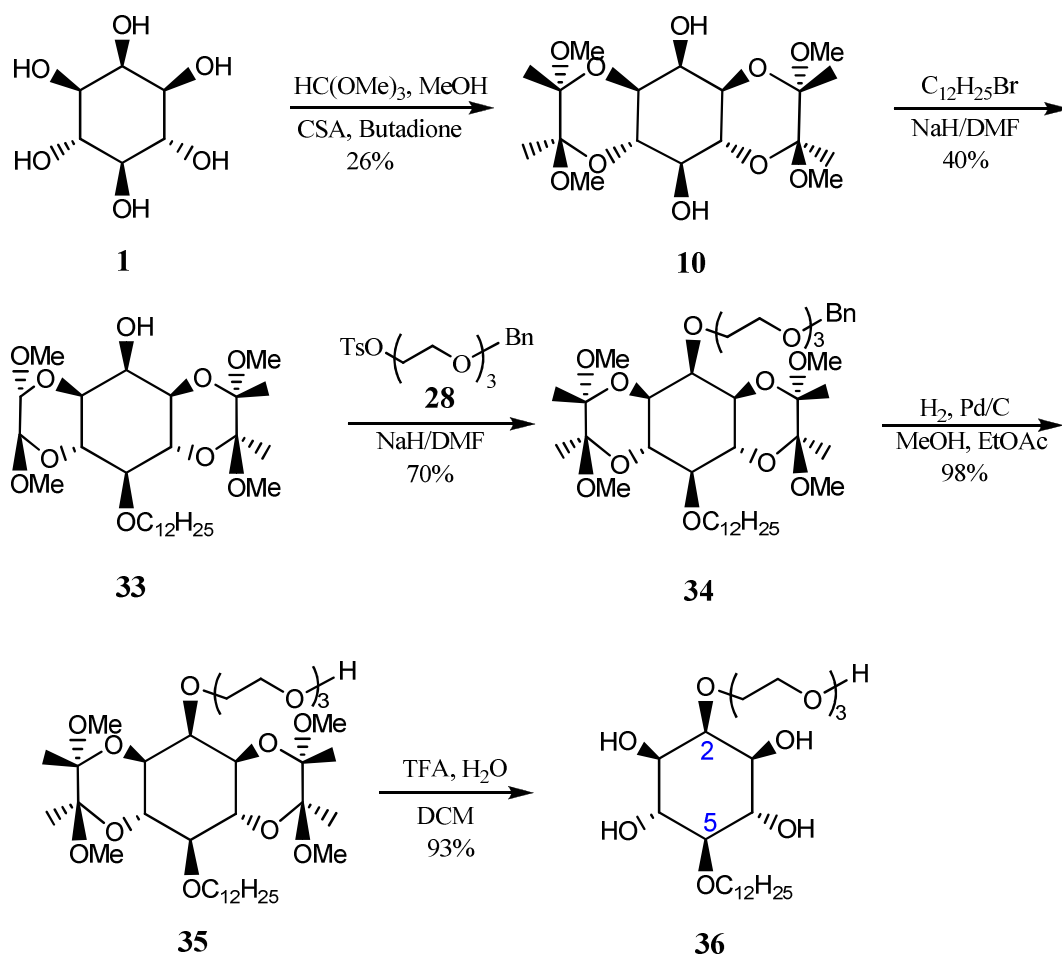
Scheme 5.5. Total synthesis of derivative **36** (2-C$_{12}$I$_1$E$_3$).

The hydrophilic–hydrophobic ratio could have a considerable influence on various physical properties, therefore new derivatives were synthesized. In all derivatives presented up to this point (*rac*-**19**, **21**, *rac*-**26**, *rac*-**32**, **36**) the hydrophilic–hydrophobic ratio was 2:1, which means two hydrophilic head groups (*myo*-inositol and triethylene oxide unit) and one hydrophobic tail (dodecyl chain). A derivative which presents the ratio 2:2 is **38**, whose synthesis counts six steps starting from *myo*-inositol and was realised in 8% overall yield, using similar procedures as for **36** (Scheme 5.6).
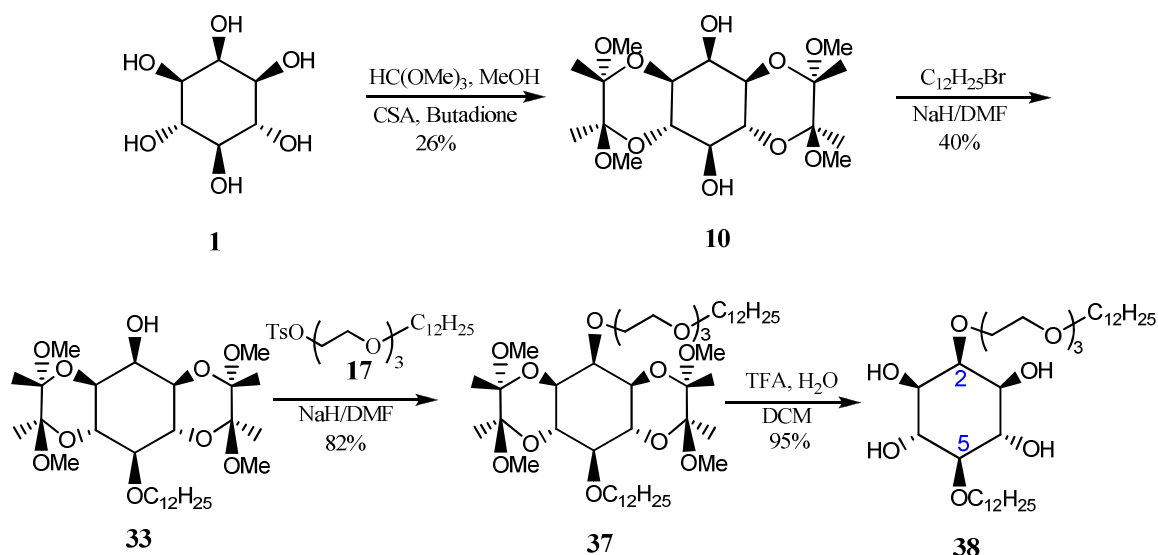
Scheme 5.6. Total synthesis of compound **38**.

The hydrophilic–hydrophobic ratio 3:2 can be achieved by synthesis of *rac*-**40** (1,2-$(C_{12}E_3)_2I_1$). Its molecule contains three hydrophilic head groups (one *myo*-inositol and two triethylene oxide units) and two hydrophobic tails (dodecyl chains). Synthesis of *rac*-**40** has seven steps starting from *myo*-inositol and triethylene oxide, and was realised in 21% overall yield (Scheme 5.7).
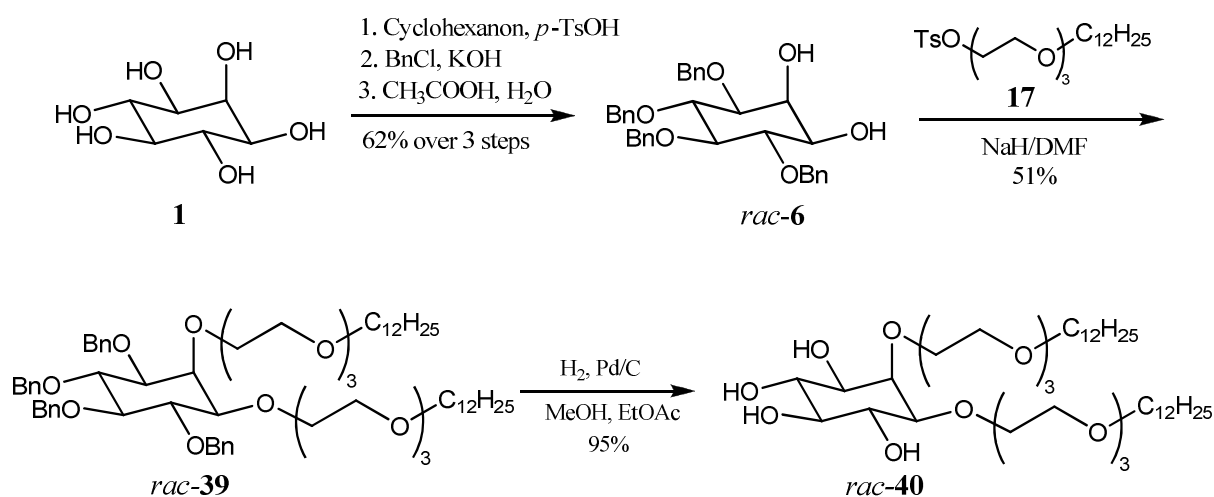
Scheme 5.7. Total synthesis of *rac*-**40** (1,2-$(C_{12}E_3)_2I_1$).

A similar compound which has hydrophilic–hydrophobic ratio 3:2 is *rac*-**42** (1,4-$(C_{12}E_3)_2I_1$) in which the alkyl-triethylene oxide chains are attached to the hydroxyl groups from position 1 and 4. This derivative can be achieved in five steps with 10% overall yield (Scheme 5.8).
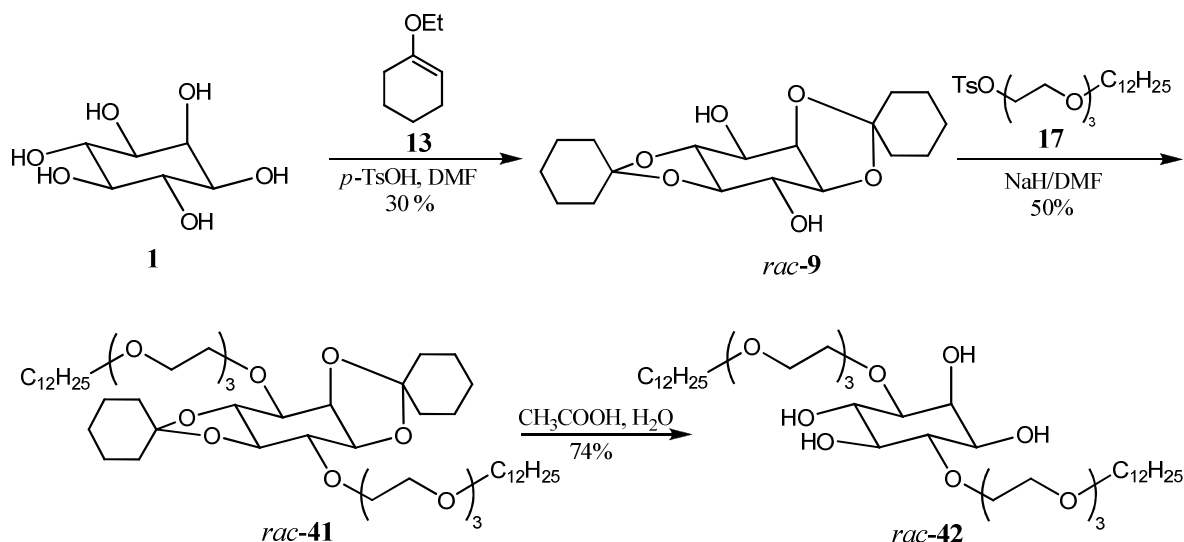
Scheme 5.8. Total synthesis of *rac*-**42** (1,4-$(C_{12}E_3)_2I_1$).

The last synthesized derivative which has hydrophilic–hydrophobic ratio 3:2 is represented by the *meso* compound **44** (2,5-$(C_{12}E_3)_2I_1$) which has two alkyl-triethylene oxide chains attached at the hydroxyl groups from C_2 and C_5. Its synthesis was completed in five steps in 7% overall yield (Scheme 5.9).
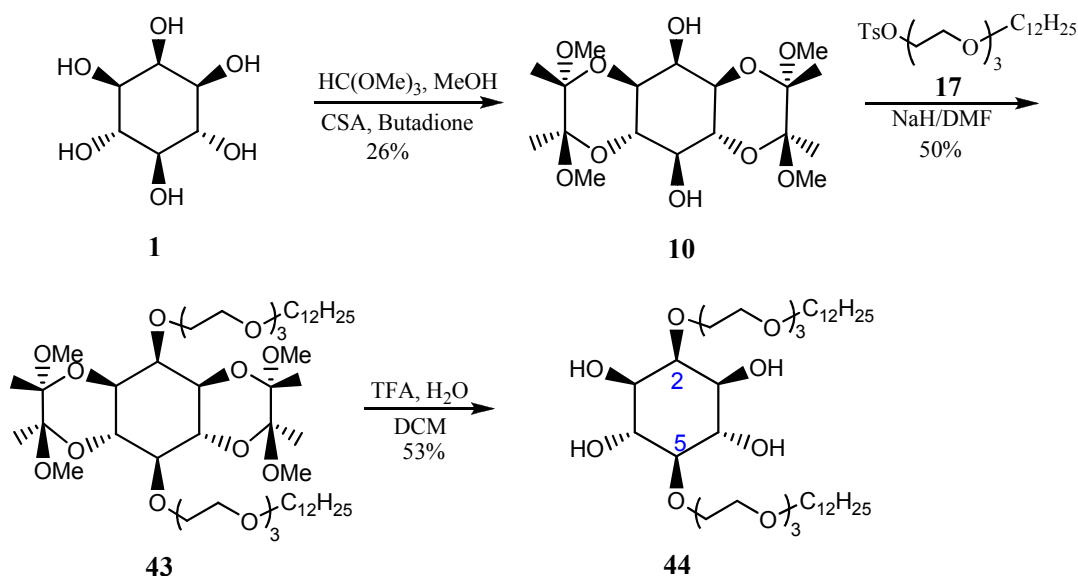
Scheme 5.9. Total synthesis of derivative **44** (2,5-$(C_{12}E_3)_2I_1$).

Consequently, by present work was possible to synthesize a number of nine representatives of a new class of inositol-based amphiphiles.

What else can be done in this field? There are a number of new ideas which could be approached. As it could be seen, excepting the *meso* compounds, all the other synthesized

derivatives are racemic mixtures. It would be interesting to study the influence of the chirality on the mesomorphism and solution properties of the enantiomerically pure inositol-based amphiphiles. Actually, this is an ongoing project in our group and the final results will be presented somewhere else.

Other possible projects which could be approached would be the synthesis of so-called bola amphiphiles of type **53** or maltose-like diinositol derivatives of type **54** or glycolipid-like amphiphiles of type **55** where R_1, R_2 (identical or different) could both be alkyl chains or combination of an alkyl chain, ethylene oxide units or another sugar unit.

53

54

55
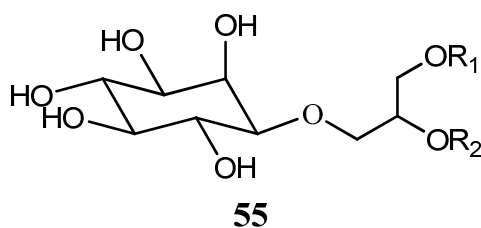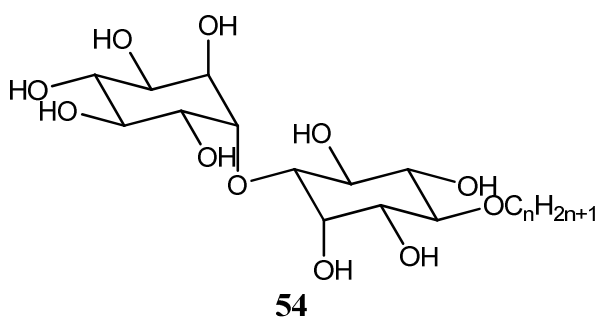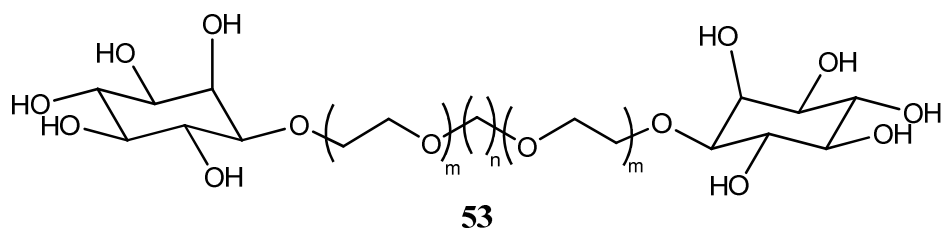
5.2. Physical properties

The novel inositol derivatives were characterized with respect of their thermotropic and lyotropic mesomorphism, as well as their solution properties and surface activity in aqueous media. The assignment of different types of mesophases was achieved using polarization microscopy (PM) and differential scanning calorimetry (DSC). Solution properties were described using surface tension measurements in aqueous solutions, total internal reflection (TIR) Raman spectroscopy and self-diffusion NMR experiments (DOSY).

5.2.1 Thermotropic mesomorphism

The appearance of mesophases on heating for each of the ethoxylated inositol derivatives seems to be determined by the relative molecular symmetry originating from different localization of the ether groups at inositol core. From study of various liquid crystalline target compounds by polarizing microscopy and differential scanning calorimetry it emerges that the occurrence, type, and stability of their mesophases are clearly determined by number, position, and stereochemical arrangement of the triethylene oxide group or/and the alkyl chains at inositol ring. The phase transition data of newly synthesized inositol derivatives are summarized in table 5.1.

Tabel 5.1. The summarized phase transition data of novel inositol derivatives

Compound	Cr_1		Cr_2		M		M		I
rac-**19** ($1\text{-}C_{12}E_3I_1$)	•	81/80.1 (43.3)	-	-	SmA	153/153.1 (0.5)	-	-	•
21 ($2\text{-}C_{12}E_3I_1$)	•	- /51.8 (23.0)	•	- /149.0 (29.6)	{M_1	- /147.1 (0.7)}	-	-	•
rac-**26** ($4\text{-}C_{12}E_3I_1$)	•	85/-	-	-	SmA	159/-	-	-	•
rac-**32** ($1\text{-}C_{12}I_1E_3$)	•	80/80.6 (38.92)	-	-	-	-	-	-	•
36 ($2\text{-}C_{12}I_1E_3$)	•	174/173.7 (46.4)	-	-	-	-	-	-	•
rac-**40** $1,2(C_{12}E_3)_2I_1$	•	16/14.8 (34.08)	-	-	Cub	26/24.4 (0.78)	Col_H	46/45.4 (0.46)	•
rac-**42** $1,4(C_{12}E_3)_2I_1$	•	20/15.8 (33.1)	•	57/57.3 (70.9)	-	-	-	-	•
44 $2,5(C_{12}E_3)_2I_1$	•	43/42.4 (38.68)	•	110/108.8 (44.07)	-	-	-	-	•

Temperatures in °C; polarizing microscopy/differential scanning calorimetry: PM/DSC; enthalpies (kJ mol^{-1}) in brackets; heating rate 5 K min^{-1}. Cr_1, Cr_2: crystalline, M: thermotropic mesophase, SmA: smectic A phase, M_1: monotropic mesophase most probably of a smectic type, Col_H: hexagonal columnar phase, Cub: cubic phase, I: isotropic liquid.

5.2.2. Lyotropic mesomorphism

Binary systems solvent–inositol-based derivative were studied by polarizing microscopy using so called penetration experiments for all novel compounds. A phase study with known concentrations at various temperatures was completed in case of *rac*-**19** (1-$C_{12}E_3I_1$). Water was the solvent used to study binary systems for all compounds. Preliminary studies were also done with some other apolar solvents but these systems need to be studied more comprehensive.

The phase diagram of *rac*-**19** (1-$C_{12}E_3I_1$) consists of an isotropic micellar (L_1), a hexagonal phase (H_1), a bicontinuous cubic phase (V_1), and a lamellar phase (L_α) with vertical phase boundaries within the studied temperature range (23 to 70 °C). In between these single phase regions lie two phase regions where both adjoining phases coexist. The presence of the vertical phase boundaries means that the phase behaviour is not temperature sensitive.

Penetration experiment of binary system water–**21** (2-$C_{12}E_3I_1$) revealed no lyotropic mesophase at 25 °C but by heating up to ~ 55 °C the sequence micellar–hexagonal–cubic–lamellar was present. The optically isotropically appearing zone between hexagonal and lamellar phase was established to be bicontinuous cubic phase because it appears to be more viscous than an isotropic fluid. This type of behaviour was compared with the glucosidic analogue *n*-octyl-α-glucoside (C_8G_1) which has as well the hydrophobic tail attached to the axial position. The Kraft boundary in case of *n*-octyl-α-glucoside starts from 38 °C and increases with increasing surfactant concentration. There are micellar, hexagonal and lamellar phases present.

As it was mentioned above, the binary system water–*rac*-**19** (1-$C_{12}E_3I_1$) is insensitive toward the temperature. It seems that this is not the case anymore for the binary system water–*rac*-**32** (1-$C_{12}I_1E_3$) for which seems to be temperature-sensitive.

Disubstituted derivatives of type $(C_{12}E_3)_2I_1$ (*rac*-**40**, *rac*-**42**, **44**) do not present lyotropic mesomorphism in mixtures with water. Some preliminary penetration experiments with apolar solvents revealed the appearance of lyotropic mesophases but the systems need to be studied in more detail in order to assign the type of the observed mesophases.

The main conclusion which results from these analyses is that the aqueous phase behaviour of the inositol-based amphiphiles is very much influenced by the end-capping group of the molecules. When the end of the hydrophilic head group is inositol (*rac*-**19**, 1-$C_{12}E_3I_1$), the aqueous phase behaviour is temperature-insensitive as in case of the reference system $C_{12}G_2$, despite its three ethylene oxide units. It seems that this is not the case for the "inverse"

derivative *rac*-**32** (1-$C_{12}I_1E_3$), where the end of the hydrophilic head group is represented by the three ethylene oxide units. Preliminary studies using the penetration experiments showed that the binary system water–*rac*-**32** (1-$C_{12}I_1E_3$) is temperature-sensitive. A complete phase study with known concentrations at various temperatures is going to be done soon and the obtained phase diagram could be then compared with the one from the binary system water–*rac*-**19** (1-$C_{12}E_3I_1$).

5.2.3. Solution properties and surface activity

One of the aims of the present work was to design new inositol-based surfactants with a good aqueous solubility. In order to achieve this aim, the head group was increase with three units of ethylene oxide. In general, the solubility issue was solved but the studies regarding the solution properties of novel inositol derivatives proved that the size of the hydrophilic head group is not the only feature which has to be taken into account to assure a good solubility in water. Table 5.2 summarize the characterization of all newly synthesized inositol-based derivatives with respect to their aqueous solubility.

Table 5.2. The solubility of new inositol-based derivatives

Compound	Solubility
rac-**19** (1-$C_{12}E_3I_1$)	+
21 (2-$C_{12}E_3I_1$)	low
rac-**26** (4-$C_{12}E_3I_1$)	+
rac-**32** (1-$C_{12}I_1E_3$)	+
36 (2-$C_{12}I_1E_3$)	low
38 (2-($C_{12}E_3)I_1$-5-C_{12})	-
rac-**40** (1,2-($C_{12}E_3)_2I_1$)	-
rac-**42** (1,4-($C_{12}E_3)_2I_1$)	-
44 (2,5-($C_{12}E_3)_2I_1$)	-

As can be noticed from Table 5.2, the symmetric derivatives **21** (2-$C_{12}E_3I_1$) and **36** (2-$C_{12}I_1E_3$) present lower solubility in water compared with their non-symmetric isomers *rac*-**19** (1-$C_{12}E_3I_1$), *rac*-**26** (4-$C_{12}E_3I_1$) and *rac*-**32** (1-$C_{12}I_1E_3$). This phenomenon reminds about the glucosidic analogues where the hydrophobic tail is attached to the axial (α) position (*n*-octyl-α-glucoside) compared with the ones where is attached to the equatorial (β) (*n*-octyl-β-glucoside). It seems that axial/α–linkage promotes a more stable crystal packing than in case of equatorial/β–linkage and consequently, the Krafft boundary is considerably higher and the solubility is lower.

In case of double substituted inositol derivatives **38** (2-($C_{12}E_3$)I_1-5-C_{12}), *rac*-**40** (1,2-($C_{12}E_3$)$_2$$I_1$), *rac*-**42** (1,4-($C_{12}E_3$)$_2$$I_1$) and **44** (2,5-($C_{12}E_3$)$_2$$I_1$), the presence of two alkyl chains increases the hydrophobic part of amphiphiles which led to a very low aqueous solubility.

Surface tension measurements were carried out for *rac*-**19** (1-$C_{12}E_3I_1$), **21** (2-$C_{12}E_3I_1$), *rac*-**26** (4-$C_{12}E_3I_1$) and *rac*-**32** (1-$C_{12}I_1E_3$). The *cmc* values could not be measured for derivative **21** (2-$C_{12}E_3I_1$), since the solutions turned turbid because of low aqueous solubility of this derivative. For the sake of comparison, the results are presented together with reference systems *n*-dodecyl-β-maltoside (β-$C_{12}G_2$) and *n*-dodecyl hexaethylene oxide ($C_{12}E_6$).

Table 5.3. Physicochemical properties of β-$C_{12}G_2$, 1-$C_{12}E_3I_1$, 4-$C_{12}E_3I_1$, 1-$C_{12}I_1E_3$, and $C_{12}E_6$

Surfactant	cmc/mM	σ_{cmc}/mN m^{-1}	Γ_∞ 10^{-6}/mol m^{-2}	A_{min}/nm^2
β-$C_{12}G_2$	0.16	34.7	3.80	0.44
rac-**19** (1-$C_{12}E_3I_1$)	0.14	34.4	3.10	0.53
rac-**26** (4-$C_{12}E_3I_1$)	0.13	33.7	3.25	0.51
rac-**32** (1-$C_{12}I_1E_3$)	0.37	35.0	3.52	0.47
$C_{12}E_6$	0.09	31.6	3.10	0.53

From these measurements can be concluded that the analyzed compounds are pure because the surface tension curves have a sharp bend and no minimum at *cmc*. The position of alkyl-triethylene oxide chain attached to the inositol ring has only a minor effect on both the *cmc* and the surface concentration when the chain is attached to an equatorial position.

The *cmc* values of *rac*-**19** (1-$C_{12}E_3I_1$) and *rac*-**26** (4-$C_{12}E_3I_1$) are between those of β-$C_{12}G_2$ and $C_{12}E_6$ as it was expected but this is not the case for *rac*-**32** (1-$C_{12}I_1E_3$) whose *cmc* is almost three times higher than its isomers. The "inverse" derivative *rac*-**32** (1-$C_{12}I_1E_3$) seems to be less surface active than β-$C_{12}G_2$, *rac*-**19** (1-$C_{12}E_3I_1$), *rac*-**26** (4-$C_{12}E_3I_1$) and $C_{12}E_6$ and thus has a higher *cmc* value which means that the I_1E_3 head group is more hydrophilic than G_2, E_3I_1 and E_6.

The corresponding adsorption isotherms of the three surfactants, *rac*-**19** (1-$C_{12}E_3I_1$), *rac*-**26** (4-$C_{12}E_3I_1$) and *rac*-**32** (1-$C_{12}I_1E_3$), are also presented. From these studies, one could say that the "inverse" derivative *rac*-**32** (1-$C_{12}I_1E_3$) pack more densely than its isomers thus its minimum area per head group is smaller than that for 1-$C_{12}E_3I_1$ and 4-$C_{12}E_3I_1$, therefore Γ_∞ is higher. The explanation would be most likely the conformation and orientation of the surfactants at the surface.

In order to monitor the conformation and orientation of the surfactants at the surface molecular dynamic simulations or more sophisticated surface sensitive techniques are required.

The adsorption behaviour of inositol-based surfactants on silica surface was studied using TIR Raman spectroscopy. The experiments were done for *rac*-**19** (1-$C_{12}E_3I_1$) and *rac*-**32** (1-$C_{12}I_1E_3$) using solution below and above the *cmc* and were compared with the reference systems *n*-dodecyl-β-maltoside (β-$C_{12}G_2$) and *n*-dodecyl hexaethylene oxide ($C_{12}E_6$).

The results of these studies revealed that adsorption behaviour is controlled by the nature of the terminal group. The *rac*-**19** (1-$C_{12}E_3I_1$) has a maltoside-like behaviour since it does not adsorb in any measurable quantities on silica whilst the "inverse" isomer *rac*-**32** (1-$C_{12}I_1E_3$) it adsorbs on silica surface. However, in case of later, at lower temperatures the molecule shows lower overall signal intensity than at higher temperatures which could mean that there is a rather dramatic reorganization of the adsorbed surfactant as a function of temperature. In theory, the change in signal intensity could be due to the molecules being compact at lower temperatures, and then becoming increasingly solvated and elongated at higher temperatures. These were only preliminary results. The same study at concentrations above the *cmc* would be interesting as would a study at trace levels of *rac*-**32** (1-$C_{12}I_1E_3$) or acquiring data for more than two temperatures and also determining if this change in intensity with temperature is reversible.

In order to find out more information about the hydration of the inositol-based surfactants, self-diffusion coefficients were measured using a magnetic field gradient method called DOSY (**D**iffusion **O**rdered **S**pectroscop**Y**).

Because the measurements were desired to be performed in water at very low concentrations (10^{-4} M), there were some problems which were solved by developing a new pulse sequence (stebpgpes1s1d.sek) including the suppression of water signal, and using a special type of NMR tubes with stem coaxial inserts of type WGS-5BL from Rototec-Spintec.

The experiments were done using aqueous solution of *rac*-**19** (1-$C_{12}E_3I_1$), *rac*-**32** (1-$C_{12}I_1E_3$), *n*-dodecyl hexaethylene oxide ($C_{12}E_6$) and *n*-dodecyl-β-maltoside (β-$C_{12}G_2$) for concentrations from 0.8 *cmc* to 6 *cmc*.

The results for the diffusion coefficient of free monomer (D_{mono}), which were obtained performing experiments at concentrations below the *cmc*, are presented in Table 5.4.

Studying these values, one could say that the molecules of novel inositol-based derivatives, *rac*-**19** (1-$C_{12}E_3I_1$) and *rac*-**32** (1-$C_{12}I_1E_3$), are moving slower than the reference systems which can lead to the conclusion that the hydrodynamic radius (R_H) of the inositol derivatives has a higher value than the hydrodynamic radius (R_H) of the reference systems, and consequently, inositol-based surfactants molecules are more hydrated.

Table 5.4. The *cmc* measured D_{mono} for the four surfactants

Surfactant	$c = 0.8\ cmc/10^{-3}$, mol l^{-1}	$D_{mono}/10^{-10}$, m^2 s^{-1}
n-dodecyl-β-maltoside (β-$C_{12}G_2$)	0.13	3.86
rac-**19** (1-$C_{12}E_3I_1$)	0.11	3.79
rac-**32** (1-$C_{12}I_1E_3$)	0.30	3.64
n-dodecyl hexaethylene oxide ($C_{12}E_6$)	0.07	4.894

Rounding the D_{mono}-values in Table 3.6 according to the errors given in section 7.5 (3.86 ± 0.09, 3.79 ± 0.09, 3.64 ± 0.04, 4.89 ± 0.07) one clearly sees that the self-diffusion coefficients of the two inositol-based surfactants and of the sugar surfactant are the same, while that of $C_{12}E_6$ is larger.

A possible reason for $D_{C12E6} > D_{C12G2}$ could be simply the lower total surfactant concentration. Arguing via the total surfactant concentration explains the results for $C_{12}E_6$, $C_{12}G_2$ and *rac*-**19**. However, the value obtained for *rac*-**32** should be much lower if it were only the total surfactant concentration that plays a role. One possible explanation could be the different shape of the molecules (stiff, rod-like in case of $C_{12}G_2$ and *rac*-**19**, coil-like in case $C_{12}E_6$ and *rac*-**32**). In other words, *rac*-**32** has the same coefficient as *rac*-**19** at a much larger total surfactant concentration as it is coil-like rather than rod-like. Another explanation could be the contribution of pre-micellar aggregates (dimmers, trimers, tetramers, etc). These aggregates could decrease the D_{mono} value significantly compared to a solution of "real" monomers. At the time being, these are only speculations.

Self-diffusion coefficients measured for concentrations above the *cmc* can be used to infer information about the possible size/structure of micelles present, but for the time being, these studies were not finished, therefore they are not included in the present work.

6. SUMMARY AND OUTLOOK II

n-Dodecyldimethyl phospine oxide (C$_{12}$DMPO) was synthesized and purified for an ongoing project at University College Dublin (UCD) under the supervision of Prof. Dr. Cosima Stubenrauch. This project aims to study the correlation between single foam films and foams by varying the surfactant mixing ratio, thus providing new insights into how to tune the properties of foams.

The special property of phosphine oxides to bind various metal cations through ion dipolar interactions inspired the question if it would be possible to induce supramolecular order like e.g. thermotropic or lyotropic liquid crystallinity in phosphine oxides amphiphiles.

The preparation of C$_{12}$DMPO metal complexes consisted in mixing the phosphine oxide with various metal salts for ~ 1.5 h at room temperature in presence of a proper solvent (methanol or water), followed by the concentration to dryness (Scheme 6.1).
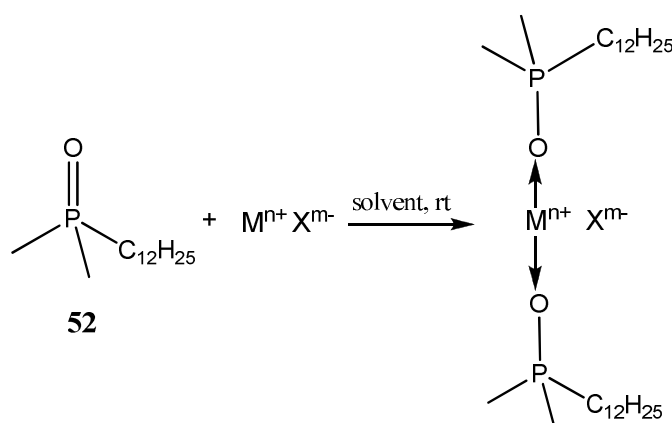
Scheme 6.1. Synthetic step towards the *n*-dodecyldimethyl phospine oxide (C$_{12}$DMPO) metal complexes

A number of homogeneous products were obtained showing sharp transition temperatures indicating a defined complexation (Table 6.1).

The analytical methods used to confirm the complexation of C$_{12}$DMPO were X-ray analysis and infrared spectroscopy (IR). The crystalline structure of the complex C$_{12}$DMPO : CuCl$_2$ is presented in Fig. 6.1. As can be seen from Table 6.1 the melting points of these complexes are relatively low, hence a proper recrystallization was not successful. The crystalline structure which is presented in Fig. 6.1 was obtained from the melt of respectively compound.
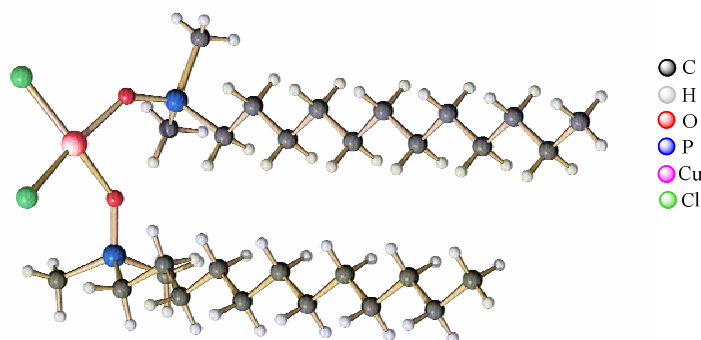
Fig. 6.1. Crystal structure of $C_{12}DMPO : CuCl_2$ complex.

The infrared analysis of the phosphine oxide metal complexes showed that $C_{12}DMPO$ is able to form complexes with metal salts depending both on cation and anion.

The thermotropic and lyotropic mesomorphism were investigated by polarizing microscopy (PM) and differential scanning calorimetry (DSC). Their thermotropic phase transition data are summarized in Table 6.1. Three of studied mixtures exhibit crystalline polymorphism but none of the observed phases were thermotropic liquid crystalline.

Table 6.1. Composition and transition temperatures of the $C_{12}DMPO : salt$ mixtures

M^{n+}	X^m	Hmg	Cr_1		Cr_2		Cr_3	I
Cu^{2+}	Cl^-	+	•	55/53,4 (28,0)				•
Cu^{2+}	SO_4^{2-}	-	•	-/51.1 (1.65)	•	83/79,1 (11,9)		•
Cu^{2+}	Br^-	+	•	48/48,9 (25,4)				•
Cu^{2+}	BF_4^-	+	•	-/34.5 (1.3)	•	55/54,5 (0,5)	•	[b]
Cu^{2+}	$C_5H_7O_2^-$	-	•	83/81,4 (34,3)				•
Cu^{2+}	CH_3COO^-	-	•	83/82,3 (27,3)				•
Li^+	Cl^-	+	•	92/93,5 (0,3)	•	116,0/115,9 (3,5)		•
Li^+	Br^-	+	•	72/69,9 (17,5)				•
Na^+	Cl^-	-	•	85/81,0 (27,7)				•

[a]Temperatures given in °C: PM / DSC (ΔH_{rel} in kJ/mol); $\Delta H_{rel} = \Delta H_{abs}(x_1 M_{C12DMPO}+x_2 M_{salt})$; x_1, x_2 = molar fraction; ΔH_{abs} measured by DSC; Hmg = Homogeneity;
[b] Complex thermal behavior upon repeated heating/cooling cycles, the clearing point is not visible in DSC and in PM is between 70 – 90°C. PM = polarized microscopy; Cr = crystalline; Iso = isotropic.

Most of the $C_{12}DMPO$ metal complexes show lyotropic mesomorphism, their penetration experiments presenting various types of mesophases.

Being easy to synthesize and non-toxic, $C_{12}DMPO$ could be a good solution for metal extractions, therefore should be further investigated, especially for other valuable metals like Hg, Pt, Pd, etc.

7. EXPERIMENTAL PART

7.1. General

Water or air sensitive reactions were carried out under an argon atmosphere using Schlenk techniques. The glassware was flame-dried in high vacuum (0.5-1 mbar) and allowed to cool down under an argon atmosphere. The syringes, needles and transfer cannulas were dried in an oven at 70°C and were flushed with argon directly before use.

Solvents and reagents

Reagents and solvents were purchased from *Merck, Aldrich, Fluka, Strem, Lancaster, Acros, Glycon* or *Deutero* (deuterated solvents for NMR Spectroscopy) and were used without further purification except the following cases:

Pyridine was dried by distillation from CaH_2 and stored over molecular sieve (4 Å) under argon.

CH₂Cl₂ was dried by distillation from CaH_2 under argon atmosphere prior to use.

THF and toluene were dried by distillation from sodium/benzophenone under argon atmosphere prior to use.

DMF was dried by distillation from $MgSO_4$ at reduce pressure and stored over molecular sieve (3 Å) under argon.

MeOH was dried by distillation from magnesium and stored over molecular sieve (3 Å) under argon.

Distillations

The solvent evaporation from reaction mixtures was done using a rotary evaporator *R-114* from *Büchi* (pressure 10-1013 mbar, water bath temperature: 40 °C). The advanced drying was performed at room temperature by applying an oil-pump vacuum.

Molecular sieves

Molecular sieves (3 Å or 4 Å, from *Roth*) were dried under vacuum at 300 °C and stored under argon atmosphere.

Pressure reactor

Reactions under pressure were carried out using an autoclave *Miniclave 35624 DN50*, *10 bar* from *Büchi.*

Flash-chromatography

Chromatographic purification and separation was done using silica 60 (230-400 mesh) supplied by *Merck*.

Thin layer chromatography (TLC)

Qualitative analysis of reaction mixtures via TLC was done using *Merck*-TLC-aluminium sheets coated with silica 60 F 254. The staining reagent used was a solution of potassium permanganate. The corresponding R_f values were determined as the distance travelled by the compound (the middle of spot) divided by the distance travelled by the solvent. The $KMnO_4$ solution was prepared from 3 g $KMnO_4$ mixed with 20 g K_2CO_3, 5 ml NaOH 5% aq, and 300 ml water.

Melting points (m.p.)

Melting points were measured by PM (Polarized Microscopy) or DSC (Differential Scanning Calorimetry) (see below).

Differential Scanning Calorimetry (DSC)

The differential scanning calorimetry analyses were carried out using a *Mettler* TA 3000/DSC 30-S instrument with TA 72.5 software.

Polarized Microscopy (PM)

The polarized microscopy (**PM**) analyses were carried out using a *Leitz* Laborlux 12 Pol microscope equipped with a *Linkam* THMS 600 hot stage and a *Linkam* THM 91 control unit.

Nuclear magnetic resonance (NMR)

The **^{1}H-NMR**-spectra were recorded on Bruker Avance II 600 (600 MHz) or Bruker Avance DRX 500 (500 MHz) apparatus. Chemical shifts (δ) are given in ppm relative to the solvent reference as the internal standard ($CDCl_3$: $\delta = 7.26$ ppm, DMSO-d_6: $\delta = 2.50$ ppm). Data are reported as follows: chemical shift (multiplicity: s for singlet, d for doublet, t for triplet, and m for multiplet, coupling constant [Hz], integration, atom number).

The ^{13}**C-NMR** spectra were recorded on Bruker Avance II 600 (150 MHz) or Bruker Avance DRX 500 (125 MHz) apparatus. Chemical shifts (δ) are given in ppm relative to the solvent reference as the internal standard (CDCl$_3$: δ = 77.00 ppm, DMSO-d$_6$: δ = 39.43 ppm). Data are reported as follows: chemical shift (multiplicity: s for quaternary carbon, d for tertiary carbon, t for secondary carbon, q for primary carbon, atom number). Multiplicities were assigned based on the APT (Attached Proton Test) spectra.

Numbering of the atoms was done based on the priority of the atom-containing subunit on the name of compound. Numbers stand for both, carbon and hydrogen atoms. Spectra processing was done using the programs *Mestre-C* and *Topspin*.

DOSY experiments were performed on a Bruker Avance II 600 spectrometer, equipped with a 600 MHz (14.1 Tesla) Narrow bore magnet and a 5 mm TBI probe head. The system is equipped with a field gradient probe, capable of generating field gradients strength of 1.0 T/m. The measurements were performed at 25 °C.

Fourier transform infrared spectroscopy (FT-IR)

IR-spectra were recorded on a *Perkin Elmer* FT-IR Paragon 1000 spectrometer as ATR (Attenuated Total Reflectance) using a ZnSe-crystal. Absorption bands are given in wave numbers ($\tilde{\upsilon}$, cm^{-1}). Intensities of the bands are given as follows: 's' for strong bands, 'm' for bands with medium intensity and 'w' for weak signals. Broad bands are marked with supplement 'br'.

Mass spectrometry

Mass spectra (**MS**) were recorded on a *Finnigan* Incos 50 Galaxy System, and high resolution mass spectra (**HR-MS**) were recorded on a *Finnigan* MAT 900S. The method of ionization is given individually at each spectrum in parentheses.

Elemental analyses (**EA**)

Elemental analyses were carried out using an Elementart Vario El instrument.

X-ray

The crystal data were recorded on a *Nonius-Kappa* CCD-diffractometer.

Surface tension measurements

The surface tensions were measured as a function of the surfactant concentration by Du Noüy ring method, using a STA1 Tensiometer from Sinterface Technologies. All samples were prepared with Milli-Q water.

7.2. Studies towards the synthesis of alkyl-oligoethoxylated *myo*-inositol derivatives

7.2.1 Synthesis of 1-*O*-[2'-[2''-[2'''-(dodecyloxy)ethoxy]ethoxy]ethyl]-3,4,5,6-tetra-*O*-benzyl-*myo*-inositol (*rac*-18)

rac-6   *rac*-18
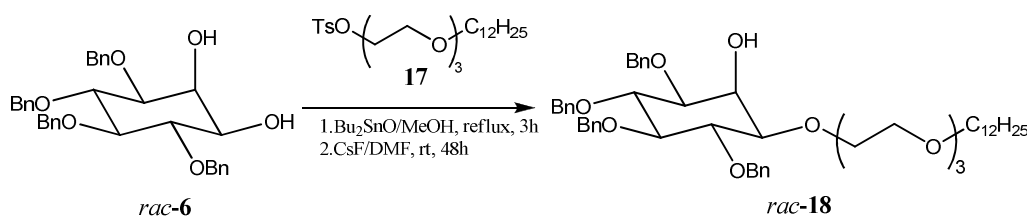
2.5 g (4.63 mmol) of 3,4,5,6-tetra-*O*-benzyl-*myo*-inositol (*rac*-6) and 1.17 g (4.30 mmol) of di-*n*-butyltin oxide were dissolved in 100 ml dry methanol and refluxed for 3 hours under argon. The crude mixture was cooled to r.t. and the solvent was evaporated. To the residual syrup 1.4 g (9.21 mmol) of caesium fluoride were added and the mixture was kept under high vacuum for 1 hour, when a solution of 4.37 g (9.25 mmol) of tosylate **17** in 100 ml dry DMF was added and the reaction was allowed to proceed at r.t. for 48 h. 70 ml MTBE were added and the resulting mixture was washed with 50 ml water, 40 ml Na_2CO_3 and again 50 ml water. The combined organic fractions were dried over $MgSO_4$ and solvents were evaporated. The crude product was purified by flash chromatography (silica, DCM:EtOAc = 4:1 → 3:2). The benzylated *rac*-18 was obtained as a yellow oil (1.9 g, 2.26 mmol, 50 %).

rac-18
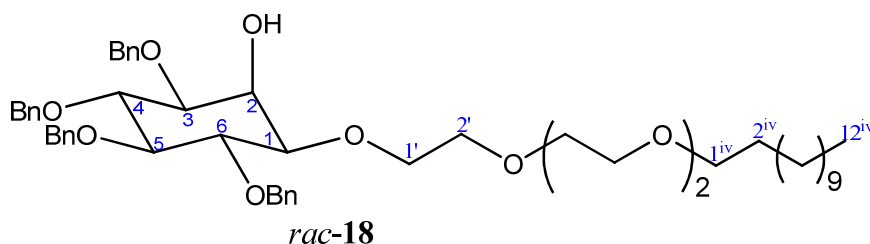
M ($C_{52}H_{72}O_9$) = 841.1227 g/mol;

TLC (SiO_2, CyHex:AcOEt = 7:3): R_f = 0.17;

^{1}H-NMR (500 MHz, $CDCl_3$): δ [ppm] = 7.27 – 7.38 (m, 20H; 20 Aryl-H), 4.71 – 4.93 (m, 8H; 4 OCH_2 from Bn), 4.32 (t, ^3J = 2.5 Hz, 1H; 2-H), 4.03 (t, ^3J = 9.5 Hz, 1H; 4-H), 3.93 (t, ^3J = 9.5 Hz, 1H; 6-H), 3.76 – 3.82 (m, 2H; 1'-H), 3.53 – 3.67 (m, 10H; 5 OCH_2 of triethylene oxide chain), 3.39 – 3.46 (m, 4H; 3-H, 5-H and 1^{iv}-H), 3.28 (dd, ^3J = 2.5 Hz, ^3J = 9.5 Hz, 1H;

1-H), 2.95 (s, 1H; OH), 1.58 (m, 2H; 2^{iv}-H), 1.21 – 1.35 (m, 18H; 9 CH_2 of dodecyl chain), 0.88 (t, ^3J = 6.9 Hz, 3H; 12^{iv}-H);

^{13}C-NMR (125 MHz, CDCl$_3$): δ [ppm] = 138.89, 138.71, 138.68, 138.08 (4s; 4 C from Aryl), 128.34, 128.28, 128.25, 128.03, 127.92, 127.81, 127.76, 127.66, 127.50, 127.46 (10d; 10 CH of Bn), 83.03 (d; C-5), 81.18 (d; C-4 or C-6), 81.14 (d; C-4 or C-6), 81.11 (d; C-1), 79.63 (d; C-3), 75.92, 75.86, 75.74 (3t; 4 OCH$_2$ of Bn), 72.41 (t; C-1'), 71.51 (t; C-1^{iv}), 70.72, 70.55, 70.46, 69.94, 69.64 (5t; 5 OCH$_2$ of triethylene oxide chain), 66.84 (d; C-2), 31.87, 29.63, 29.60, 29.58, 29.52, 29.46, 22.31, 26.02, 22.65 (9 t; 10 CH$_2$ of dodecyl chain), 14.10 (q; C-12^{iv});

FT-IR (ATR) $\tilde{v}$ [cm^{-1}] = 3446 (br, m), 2921 (s), 2852 (s), 1723 (w), 1495 (w), 1452 (m), 1357 (m), 1275 (w), 1209 (w), 1087 (s), 1069 (s), 1027 (m), 731 (s), 695 (s), 614 (w);

MS (positive ESI) m/z (%): 836.61 (100) [M+Na]$^+$, 773.40 (6), 319.22 (4);

HR-MS (ESI) calc. for C$_{52}$H$_{72}$O$_9$Na [M+Na]$^+$: 863.507, found: 863.507.

7.2.2. Synthesis of 1-*O*-[2'-[2''-[2'''-(dodecyloxy)ethoxy]ethoxy]ethyl]-*myo*-inositol (*rac*-19)
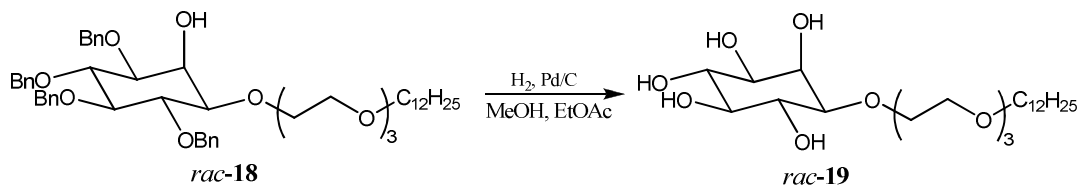
A solution of 0.640 g (0.76 mmol) *rac*-18 in 10 ml of a MeOH:EtOAc = 3:1 mixture was degassed with argon for 30 min. To this solution, 0.080 g (0.076 mmol) Pd (10% supported on charcoal) were added and the reaction was proceeded under hydrogen atmosphere (pressure ~ 8 bar) for 3 days. The resulting mixture was filtrated over celite and concentrated to dryness. The crude product was purified by flash chromatography (silica, DCM:MeOH = 4:1). The pentol *rac*-19 was obtained as a white waxy solid (0.328 g, 0.68 mmol, 90 %).

rac-19
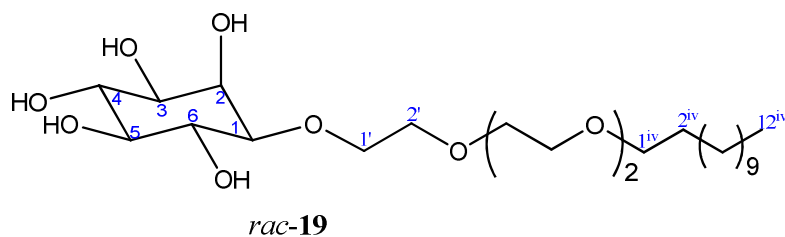
M (C$_{24}$H$_{48}$O$_9$) = 480.6325 g/mol;

TLC (SiO$_2$, DCM:MeOH = 4:1): R$_f$ = 0.34;

Melting point: liquid crystal (see Table 3.1, chapter 3.2.1. Thermotropic mesomorphism);

^{1}H-NMR (600 MHz, DMSO-d$_6$): δ [ppm] = 4.58 (d, ^3J = 3.4 Hz, 1H; OH), 4.50 (d, ^3J = 3.1 Hz, 1H; OH), 4.44 (d, ^3J = 4.3 Hz, 1H; OH), 4.37 (m, 2H; 2 OH), 3.88 (m, 1H; 2-H), 3.58 – 3.69 (m, 2H; 1'-H), 3.48 – 3.55 (m, 8H; 4 OCH$_2$ of triethylene oxide chain), 3.40 – 3.47 (m, 3H; 6-H and OCH$_2$ of triethylene oxide chain), 3.37 – 3.31 (m, 3H; 4-H and 1^{iv}-H), 3.09 (d, ^3J= 8.3 Hz, 1H; 3-H), 2.98 (dd, ^3J = 2.3 Hz, ^3J = 9.7 Hz, 1H; 1-H), 2.91 (ddd, ^3J = 2.6 Hz, ^3J = 8.9 Hz, ^3J = 9.0 Hz, 1H; 5-H), 1.44 – 1.48 (m, 2H; 2^{iv}-H), 1.17 – 1.30 (m, 18H; 9 CH$_2$ of dodecyl chain), 0.85 (t, ^3J = 6.5 Hz, 3H; 12^{iv}-H);

^{13}C-NMR (150 MHz, DMSO-d$_6$): δ [ppm] = 80.48 (d; C-1), 75.19 (d; C-5), 72.37 (d, C-3), 71.73 (d; C-4 or C-6), 71.60 (d; C-4 or C-6), 70.21 (t; C-1^{iv}), 69.94, 69.68, 68.36, 68.33 (4 t; 5 OCH$_2$ of triethylene oxide chain), 68.32 (d; C-2), 68.33 (t; OCH$_2$ of triethylene oxide chain), 31.20, 29.10, 28.92, 28.77, 28.61, 25.55, 21.99 (7t; 10 CH$_2$ of dodecyl chain), 13.85 (q; C-12^{iv});

FT-IR (ATR) $\tilde{\nu}$ [cm^{-1}] = 3357 (br, m), 2919 (s), 2851 (s), 1456 (m), 1351 (m) 1113 (br, s), 859 (m), 720 (m);

MS (positive ESI) m/z (%): 503.22 (100) [M+Na]$^+$, 481.26 (8);

HR-MS (ESI) calc. for C$_{24}$H$_{48}$O$_9$Na [M+Na]$^+$: 503.319, found: 503.320.

7.2.3. Synthesis of 1,3,4,5,6-penta-*O*-benzyl-2-*O*-[2'-[2''-[2'''-(dodecyloxy)ethoxy] ethoxy] ethyl]-*myo*-inositol (20)
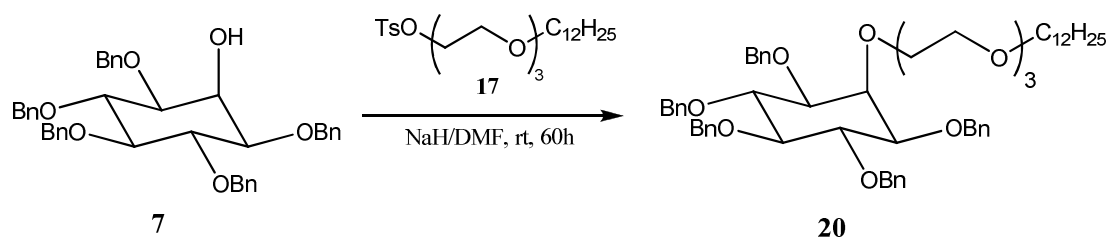
To a solution of 0.133 g (3.33 mmol) NaH (55-65% in mineral oil) in 50 ml dry DMF were added 1.5 g (2.38 mmol) of compound **7** under argon atmosphere and the mix was stirred at 0°C for 15 min when 1.57 g (3.33 mmol) of tosylate **17** were introduced and the reaction proceeded under argon for 60 h at r.t. The resulting mixture was poured onto 100 ml ice-water and 70 ml brine were added. After extraction with EtOAc (3 x 80 ml) the combined organic layers were dried over MgSO$_4$, filtrated and dried under vacuum. The crude product was purified by flash chromatography (silica, CyHex:EtOAc = 4:1).

The benzylated derivative **20** was obtained as a colourless oil (1.991 g, 2.14 mmol, 90%).

20
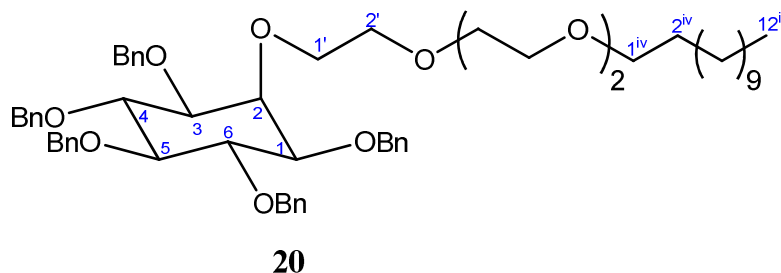
M ($C_{59}H_{78}O_9$) = 931.2452 g/mol;

TLC (SiO_2, CyHex:EtOAc = 4:1): R_f = 0.37;

¹H-NMR (500 MHz, $CDCl_3$): δ [ppm] = 7.26 – 7.34 (m, 25H; 5 Aryl-H), 4.67 – 4.89 (m, 10H; 5 CH_2 of Bn), 3.95 – 4.01 (m, 5H; 2-H, 4-H, 6-H and 1'-H), 3.53 – 3.67 (m, 10H; 5 OCH_2 of triethylene oxide chain), 3.44 (dd, ^3J = 6.65 Hz, ^3J = 11.72 Hz, 1H; 5-H), 3.40 (t, ^3J = 6.86 Hz, 2H; 1^{iv}-H), 3.32 (dd, ^3J = 2.02 Hz, ^3J = 9.84 Hz, 2H; 1-H and 3-H), 1.51 – 1.57 (m, 2H; 2^{iv}-H), 1.24 – 1.31 (m, 18H; 9 CH_2 of dodecyl chain), 0.88 (t, ^3J = 6.91 Hz, 3H; 12^{iv}-H);

¹³C-NMR (125 MHz, $CDCl_3$): δ [ppm] = 138.78, 138.75, 138.30 (3s; 5 C of Bn), 128.37, 128.33, 128.29, 128.02, 127.84, 127.64, 127.61, 127.50 (8d; 25 CH of Bn), 83.58 (d; C-5), 81.56 (d; C-4 and C-6), 80.64 (d; C-1 and C-3), 75.95, 75.83, 72.65 (3t; 5 CH_2 of Bn), 75.68 (d; C-2), 72.42 (t; C-1'), 71.53 (t; C-1^{iv}), 70.87, 70.64, 70.60, 70.57, 70.00 (5t; 5 OCH_2 of triethylene oxide chain), 31.90, 29.65, 29.63, 29.61, 29.59, 29.48, 29.34, 26.06, 22.68 (9t; 10 CH_2 of dodecyl chain), 14.12 (q; C-12^{iv});

FT-IR (ATR) $\tilde{v}$ [cm⁻¹] = 3023 (w), 2921 (m), 2851 (m), 1495 (w), 1453 (m), 1358 (m), 1304 (w), 1208 (w), 1085 (br, s), 1067 (s), 1038 (m), 1027 (m), 731 (s), 694 (s);

MS (positive ESI) m/z (%): 953.54 (100) [M+Na]⁺, 181.5 (4), 91.06 (4);

HR-MS (ESI) calc. for $C_{59}H_{78}O_9Na$ [M+Na]⁺: 953.554; found: 953.554;

EA: calc: 76.10 % C; 8.44 % H; found: 75.98% C; 8.59% H.

7.2.4. Synthesis of 2-*O*-[2'-[2''-[2'''-(dodecyloxy)ethoxy]ethoxy]ethyl]-*myo*-inositol (21)

20   **21**
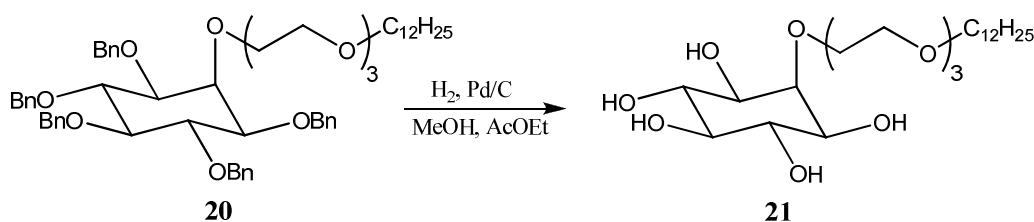
A solution of 1.60 g (1.76 mmol) compound **20** in 30 ml of a MeOH:EtOAc = 3:1 mixture was degassed with argon for 30 min. To this solution, 0,187 g (0.17 mmol) Pd (10% supported on charcoal) were added and the reaction proceeded under hydrogen atmosphere (pressure ~ 8 bar) for 5 days. The resulting mixture was filtrated over celite and concentrated to dryness. The crude product was purified by flash chromatography (silica, DCM:MeOH = 9:1). The pentol **21** was obtained as a white solid (0.74 g, 1.54 mmol, 88%).

21
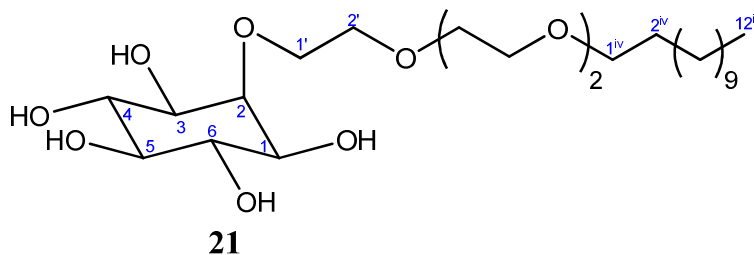
M ($C_{24}H_{48}O_9$) = 480.6325 g/mol;

TLC (SiO_2, DCM:MeOH = 4:1): R_f = 0.38;

Melting point: liquid crystal, (see Table 3.1, chapter 3.2.1. Thermotropic mesomorphism);

^{1}H-NMR (500 MHz, DMSO-d_6): δ [ppm] = 4.59 (dd, ^3J = 4.39 Hz, ^3J = 8.06 Hz, 3H; 3 OH), 4.39 (d, ^3J = 5.72 Hz, 2H; 2 OH), 3.76 (t, ^3J = 5.16 Hz, 2H; 1'-H), 3.44 – 3.52 (m, 11H; 2-H and 5 OCH$_2$ of triethylene oxide chain), 3.35 (t, ^3J = 6.62 Hz, 2H; 1^{iv}-H), 3.29 (dt, ^3J = 4.50 Hz, ^3J = 9.37 Hz, ^3J = 9.30 Hz, 2H; 4-H and 6-H), 3.15 – 3.18 (m, 2H; 1-H and 3-H), 2.87 (ddd, ^3J = 4.26 Hz, ^3J = 8.99 Hz, ^3J = 9.01 Hz, 1H; 5-H), 1.48 – 1.43 (m, 2H; 2^{iv}-H), 1.24 – 1.31 (m, 18H; 9 CH$_2$ of dodecyl chain), 0.85 (t, ^3J = 6.81 Hz, 3H; 12^{iv}-H);

^{13}C-NMR (125 MHz, DMSO-d_6): δ [ppm] = 82.54 (d; C-2), 75.06 (d; C-5), 73.02 (d; C-4 and C-6), 72.17 (t; C-1'), 71.85 (d; C-1 and C-3), 70.30 (t; C-1^{iv}), 69.99, 69.77, 69.73, 69.67, 69.44 (5t; 5 OCH$_2$ of triethylene oxide chain), 31.30, 29.19, 29.02, 28.88, 28.72, 25.64, 22.10 (7t; 10 CH$_2$ of dodecyl chain), 13.96 (q; C-12^{iv});

FT-IR (ATR) $\tilde{v}$ [cm^{-1}] = 3254 (br, s), 2916 (s), 2846 (s), 1660 (br, w), 1468 (m), 1361 (m), 1232 (w), 1118 (s), 1082 (w), 1040 (s), 1014 (m), 960 (w), 861 (w), 715 (m);

MS (positive ESI) m/z (%): 503.24 (100) [M+Na]$^+$, 481.28 (8);

HR-MS (ESI) calc. for $C_{24}H_{48}O_9Na$ [M+Na]$^+$: 503.319; found: 503.319.

7.2.5. Synthesis of 4-*O*-[2'-[2''-[2'''-(dodecyloxy)ethoxy]ethoxy]ethyl]-*myo*-inositol orthoformate (25)
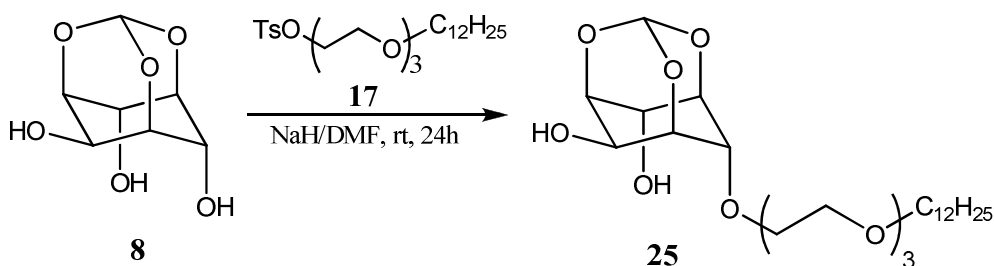
0.5 g (2.63 mmol) of *myo*-inositol orthoformate **8** were dissolved into a suspension of 0.12 g (2.5 mmol) NaH (55-65% mineral oil) in 40 ml dry DMF under argon atmosphere and the mix was stirred for 15 min at 0°C. 1.24 g (2.63 mmol) of tosylate **17** were added dropwise and the reaction mixture was stirred under argon for additional 24 h at r.t. The crude mix was poured onto 50 ml ice-water and 25 ml brine were added. After extraction with EtOAc (3 x 50 ml) the combined organic fractions were dried over MgSO$_4$, filtrated and concentrated under vacuum. The crude product was purified by flash chromatography (silica, DCM:EtOAc = 4:1). The compound **25** was obtained as colourless oil (0.795 g, 1.62 mmol, 62%).

25
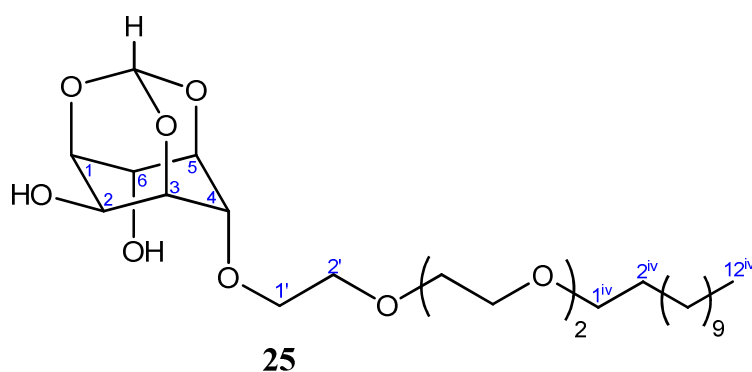
M (C$_{25}$H$_{46}$O$_9$) = 490.6273 g/mol;

TLC (SiO$_2$, DCM:EtOAc = 1:1): R$_f$ = 0.21;

^{1}H-NMR (500 MHz, DMSO-d$_6$): δ [ppm] = 5.46 (d, ^3J = 0.86 Hz, 1H; CH of orthoformate), 5.29 (d, ^3J = 6.09 Hz, 1H; 2-OH), 4.86 (d, ^3J = 6.24 Hz, 1H; 6-OH), 4.26– 4.29 (m, 1H; 5-H), 4.21 – 4.25 (m, 1H; 6-H), 4.15 (m, 1H; 4-H); 4.03 – 4.06 (m, 1H; 3-H), 3.93 (t, ^3J = 5.06 Hz, 1H; 2-H), 3.87 – 3.90 (m, 1H; 1-H), 3.59 – 3.72 (m, 2H; 1'-H), 3.42 – 3.54 (m, 10H; 5 OCH$_2$ of triethylene oxide chain), 3.35 (t, ^3J = 6.59 Hz, 2H; 1^{iv}-H), 1.42 – 1.50 (m, 2H; 2^{iv}-H), 1.31 – 1.18 (m, 18H; 9 CH$_2$ of dodecyl chain), 0.85 (t, ^3J = 6.79 Hz, 3H; 12^{iv}-H);

^{13}C-NMR (125 MHz, DMSO-d$_6$): δ [ppm] = 102.06 (d; CH of orthoformate), 74.49 (d; C-1 or C-4), 74.38 (d; C-1 or C-4), 72.35 (d; C-3), 70.24 (t; C-1^{iv}), 69.72, 69.69, 69.60, 69.39, 68.06 (5t; 6 OCH$_2$ of triethylene oxide chain), 68.25 (d; C-5), 67.18 (d; C-6), 58.70 (d; C-2), 31.25, 29.14, 29.00, 28.99, 28.96, 28.82, 28.67, 25.59, 22.05 (9t; 10 CH$_2$ of dodecyl chain), 13.91 (q; C-12^{iv});

FT-IR (ATR) $\tilde{v}$ [cm^{-1}] = 3467 (br, m), 2920 (s), 2846 (s), 1459 (m), 1415 (w), 1350 (w), 1296 (m), 1242 (m), 1161 (s), 1092 (br, s), 990 (s), 955 (s), 876 (m), 804 (m), 769 (m), 722 (w), 694 (m);

MS (positive ESI) m/z (%): 513.20 (100) [M+Na]$^+$, 427.22 (4), 341.21 (10), 301.22 (6);

HR-MS (ESI) calc. for C$_{25}$H$_{46}$O$_9$Na [M+Na]$^+$: 513.304; found: 513.304;

EA: calc: 61.20% C; 9.45% H; found: 61.36% C; 9.56% H.

7.2.6. Synthesis of 4-*O*-[2'-[2''-[2'''-(dodecyloxy)ethoxy]ethoxy]ethyl]-*myo*-inositol (*rac*-26)
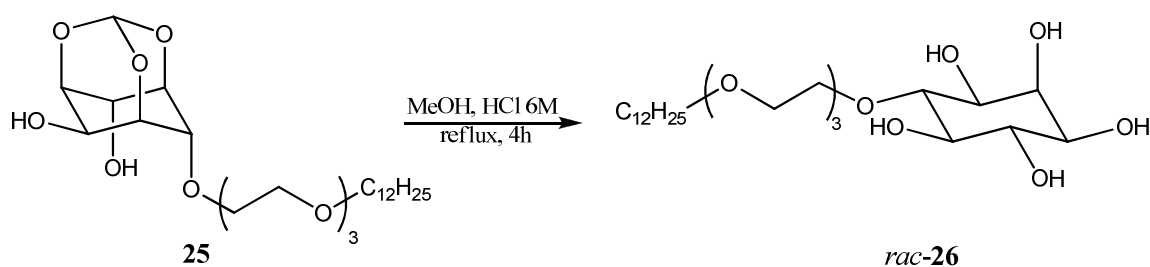
A solution of 0.625 g (1.27 mmol) compound **25** in 60 ml methanol and 11 ml HCl 6M was heated to reflux for 4 hours. After cooling down, the mix was neutralized with NaOH 50%, filtrated, dried over MgSO$_4$, concentrated and dried under vacuum. The crude product was purified by flash chromatography (silica, DCM:MeOH = 9:1).

The pentol *rac*-26 was obtained as a white waxy solid (0.503 g, 1.05 mmol, 83%).

rac-26
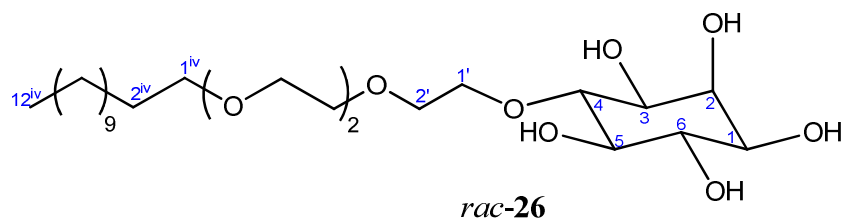
M (C$_{24}$H$_{48}$O$_9$) = 480.6325 g/mol;

TLC (SiO$_2$, DCM:MeOH = 4:1): R$_f$ = 0.37;

Melting point: liquid crystal, (see Table 3.1, chapter 3.2.1. Thermotropic mesomorphism);

^{1}H-NMR (500 MHz, DMSO-d_6): δ [ppm] = 4.61 (d, ^3J = 3.47 Hz, 1H; OH), 4.56 (dd, ^3J = 4.46 Hz, ^3J = 9.54 Hz; 2H; 2 OH), 4.41 (d, ^3J = 5.55 Hz, 1H; OH), 4.38 (d, ^3J = 5.15 Hz, 1H; OH), 3.71 – 3.80 (m, 2H; 1'-H), 3.68 (m, 1H; 2-H), 3.44 – 3.52 (m, 10H; 5 OCH$_2$ of triethylene oxide chain), 3.33 – 3.37 (m, 3H; 6-H and 1^{iv}-H), 3.19 – 3.23 (m, 2H; 3-H and 4-H), 3.06 -3.10 (m, 1H; 1-H), 2.99 (dt, ^3J = 4.39 Hz, ^3J = 4.39 Hz, ^3J = 13.38 Hz, 1H; 5-H), 1.43 – 1.49 (m, 2H; 2^{iv}-H), 1.17 – 1.30 (m, 18H; 9 CH$_2$ of dodecyl chain), 0.85 (t, ^3J = 6.83 Hz, 3H; 12''-H);

^{13}C-NMR (125 MHz, DMSO-d_6): δ [ppm] = 82.65 (d; C-4), 74.58 (d; C-5), 72.75 (d; C-6), 72.60 (d; C-2), 71.52 (d; C-1), 71.17 (d; C-3), 70.82, 70.25, 68.70, 69.66, 69.54, 69.38 (6t; 6 OCH$_2$ of triethylene oxide chain), 70.02, 31.24, 29.14, 28.99, 28.98, 28.96, 28.82, 28.66, 25.59, 22.05 (10t; 11 CH$_2$ of dodecyl chain), 13.91 (q; C-12^{iv});

FT-IR (ATR) $\tilde{v}$ [cm^{-1}] = 3358 (br, s), 2920 (s), 2851 (s), 1656 (br, w), 1456 (w), 1347 (w), 1293 (w), 1245 (w), 1113 (br, s), 1058 (s), 1000 (m), 936 (w), 882 (w), 718 (m);

MS (positive ESI) m/z (%): 503.22 (100) [M+Na]$^+$, 481.26 (6), 440.67 (4);

HR-MS (ESI) calc. for C$_{24}$H$_{48}$O$_9$Na [M+Na]$^+$: 503.319; found: 503.319;

7.2.7. Synthesis of 1,2:4,5-di-*O*-cyclohexylidene-3-*O*-dodecyl–*myo*-inositol (*rac*-29)
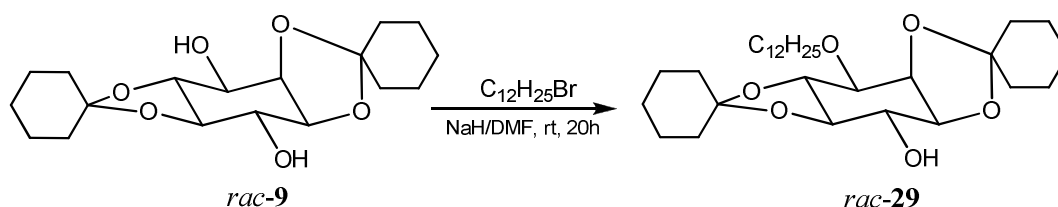
To a solution of 0.141 g (2.94 mmol) NaH (55-65% in mineral oil) in 30 ml dry DMF were added 0.500 g (1.47 mmol) of *rac*-**9** under argon atmosphere and the suspension was stirred at 0°C for 15 min. After the addition of 0.35 ml (0.366 g, 1.47 mmol) of *n*-dodecyl bromide the reaction proceeded under argon for 20 h at r.t. The resulting mixture was poured onto 100 ml ice-water and 50 ml brine were added. After extraction with DCM (3 x 80 ml) the combined organic fractions were dried over MgSO$_4$, filtrated and dried under vacuum. The crude product was purified by flash chromatography (silica, CyHex:EtOAc = 7:3).

The desired *rac*-**29** was obtained as a colourless oil (0.485 g, 0.955 mmol, 65%).

rac-**29**
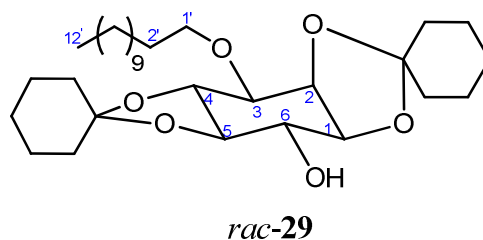
M (C$_{30}$H$_{52}$O$_6$) = 508.7303 g/mol;

TLC (SiO$_2$, CyHex:AcOEt = 7:3): R$_f$ = 0.36;

^{1}H-NMR (500 MHz, CDCl$_3$): δ [ppm] = 4.49 (m, 1H; 2-H), 4.00 (dd, ^3J = 5.10 Hz, ^3J = 6.44 Hz, 1H; 1-H), 3.94 (t, ^3J = 9.74 Hz, 1H; 4-H), 3.86 (dd, ^3J = 6.71 Hz, ^3J = 10.66 Hz, 1H;6-H), 3.71 (dd, ^3J = 3.48 Hz, ^3J = 4.43 Hz, 1H; 3-H), 3.65 (t, ^3J = 6.98 Hz, 2H; 1'-H), 3.29 (dd, ^3J=9.60 Hz, ^3J = 10.48 Hz, 1H; 5-H), 2.76 (s, 1H; OH), 1.58 – 1.76 (m, 18H; 2'-H and 8 CH$_2$ of cyclohexylidene rings), 1.24 – 1.38 (m, 22H; 9 CH$_2$ of dodecyl chain and 2 CH$_2$ of cyclohexylidene rings), 0.87 (t, ^3J = 6.91 Hz, 3H; 12'-H);

^{13}C-NMR (125 MHz, CDCl$_3$): δ [ppm] = 112.87, 110.66 (2s; 2 C of cyclohexylidene rings), 81.25 (d; C-1), 78.14 (d; C-5), 76.43 (d; C-4), 76.30 (d; C-3), 75.62 (d; C-2), 75.01 (d; C-6), 70.22 (t; C-1'), 37.74, 36.44, 36.28, 35.076 (4t; 5 CH$_2$ of cyclohexylidene ring), 31.88, 29.68, 29.65, 29.61, 29.52, 29.42, 29.32, 25.98, 22.65 (9t; 10 CH$_2$ of dodecyl chain), 23.90, 23.70, 23.67, 25.58 (4t; 5 CH$_2$ of cyclohexylidene ring), 14.10 (q; 12'-C);

FT-IR (ATR) $\tilde{v}$ [cm^{-1}] = 3453 (br, w), 2922 (s), 2850 (s), 1447 (m), 1364 (m) 1332 (w), 1275 (m), 1250 (w), 1229 (w), 1162 (s), 1113 (s), 1060 (s), 1004 (m), 933 (s); 907 (s), 847 (m), 777 (m), 730 (m);

MS (positive ESI) m/z (%): 1039.74 (42) [2(M+Na)]$^+$, 963.72 (6), 663.42 (10), 547.31 (10), 531.31 (100) [M+Na]$^+$, 411,25 (4), 127.02 (4), 99.06 (6);

**HR-MS** (ESI) calc. for C$_{30}$H$_{52}$O$_6$Na [M+Na]$^+$: 531.366, found: 531.366;

EA: calc: 70.83% C; 10.30% H; found: 70.82% C; 10.31% H.

7.2.8. Synthesis of 6-*O*-[2'-[2''-[2'''-(benzyloxy)ethoxy]ethoxy]ethyl]-1,2:4,5–di–*O*-cyclohexylidene-3-*O*-dodecyl-*myo*-inositol (*rac*-**30**)

rac-**29**   *rac*-**30**
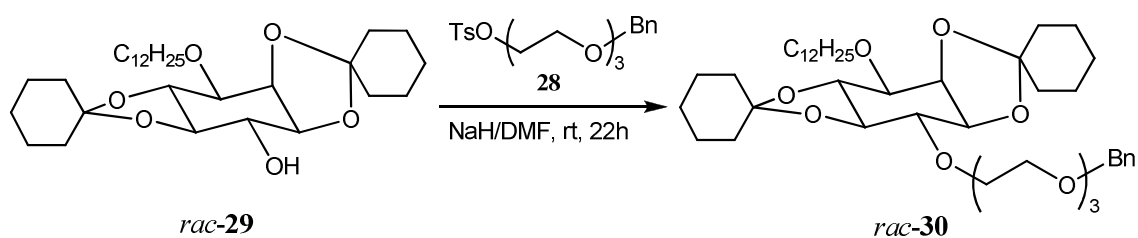
To a solution of 0.104 g (2.4 mmol) NaH (55-65% in mineral oil) in 15 ml dry DMF were added 0.610 g (1.2 mmol) of *rac*-**29** under argon and the suspension was stirred at 0°C for 15 min. 0.520 g (1.32 mmol) of tosylate **28** were then introduced and the reaction proceeded under argon for 22 h at r.t. The resulting mixture was poured onto 100 ml ice-water and 50 ml brine were added. After extraction with DCM (3 x 80 ml) the combined organic fractions were dried over $MgSO_4$, filtrated and dried under vacuum. The crude product was purified by flash chromatography (silica, CyHex:EtOAc = 7:3).

The pure *rac*-**30** was obtained as colourless oil (0.788 g, 1.08 mmol, 90%).

rac-**30**
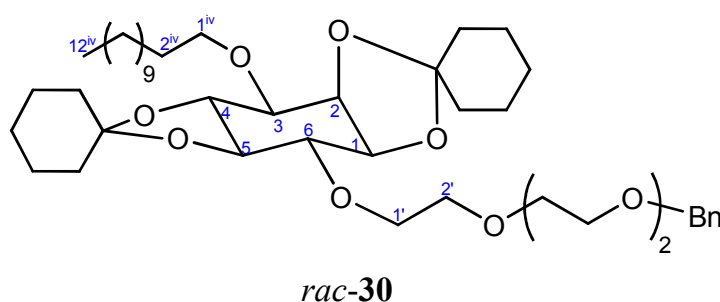
M ($C_{43}H_{70}O_9$) = 731.0105 g/mol;

TLC (SiO_2, CyHex: EtOAC = 7:3): R_f = 0.36;

^{1}H-NMR (500 MHz, $CDCl_3$): δ [ppm] = 7.26 – 7.34 (m, 5H; 5 Aryl-H), 4.58 (s, 2H; CH_2 of Bn), 4.45 (t, ^3J = 4.56 Hz, 1H; 2-H), 4.05 (dd, ^3J = 5.06 Hz, ^3J = 6.35 Hz, 1H; 1-H), 3.90 – 3.96 (m, 3H; 4-H and 1'-H), 3.65 – 3.71 (m, 10H; 5 OCH_2 of triethylene oxide chain), 3.60 – 3.64 (m, 3H; H-3 and 1^{iv}-H), 3.57 (dd, ^3J = 6.61 Hz, ^3J = 10.27 Hz, 1H; 6-H), 3.30 (dd, 1H, ^3J = 9.42 Hz, ^3J = 10.51; H-5), 1.58 – 1.76 (m, 18H; 2^{iv}-H and 8 CH_2 of cyclohexylidene ring), 1.24 – 1.38 (m, 22H; 9 CH_2 of dodecyl chain and 2 CH_2 of cyclohexylidene ring), 0.87 (t, ^3J = 6.92 Hz, 3H; 12^{iv}-H);

^{13}C-NMR (125 MHz, $CDCl_3$): δ [ppm] = 138.24 (s; C from Aryl), 128.32, 127.72, 127.54 (3d; 5 CH of Aryl), 112.43, 110.45 (2s; 2 C of cyclohexylidene rings), 82.40 (d; C-6), 80.71 (d; C-1), 78.23 (d; C-5), 76.24 (d; C-4), 76.17 (d; C-3), 75.64 (d; C-2), 73.20 (t; CH_2 of Bn), 70.63, 70.48, 70.39, 70.33, 70.19, 70.07 (6t; 6 OCH_2 of triethylene oxide chain), 69.40 (t; C-1^{iv}), 37.96, 37.72, 36.42, 36.38, 35,13 (5t; 5 CH_2 of cyclohexylidene ring), 31.89, 29.86, 29.71, 29.66, 29.61, 29.44, 29.33, 25.99, 22.67 (9t; 10 CH_2 of dodecyl chain), 25.03, 24.97, 23.93, 23.75, 23.58 (5t; 5 CH_2 of cyclohexylidene ring), 14.11 (s, C-12^{iv});
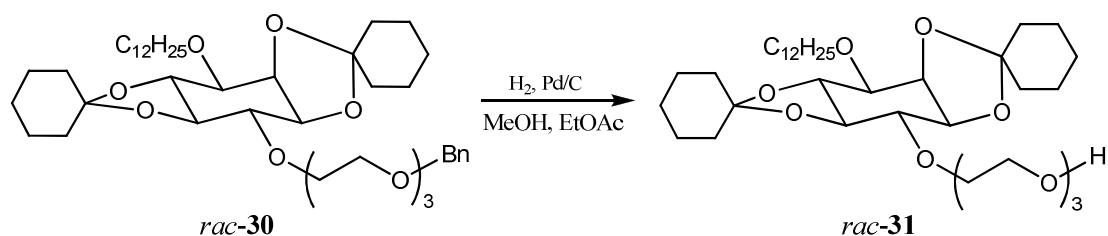
FT-IR (ATR) $\tilde{v}$ [cm^{-1}] = 2923 (s), 2851 (s), 1448 (m), 1363 (m), 1331 (w), 1276 (m), 1250 (w), 1229 (w), 1162 (m), 1096 (br, s), 1030 (m), 934 (s), 907 (s), 847 (m), 777 (m), 732 (m), 696 (m);

MS (positive ESI) m/z (%): 753.44 (100) [M+Na]$^+$;

**HR-MS** (ESI) calc. for C$_{43}$H$_{70}$O$_9$Na [M+Na]$^+$: 753.491, found: 753.491;

EA: calc: 70.65% C; 9.65% H; found: 70.26%C; 9.58% H.

7.2.9. Synthesis of 1,2:4,5-di-*O*-cyclohexylidene-3-*O*-dodecyl-6-*O*-[2'-[2''-[2'''-(hydroxy)ethoxy]ethoxy]ethoxy]ethyl]-*myo*-inositol (*rac*-31)

rac-30   *rac*-31

A solution of 0.586 g (0.803 mmol) *rac*-**30** in 38 ml of a MeOH:EtOAc = 3:1 mixture was degassed with argon for 30 min. To this solution, 0,085 g (0.080 mmol) Pd (10% supported on charcoal) were added and the reaction mixture was stirred at r.t. under hydrogen atmosphere (pressure ~ 1.5 bar) for two days. The resulting mix was filtrated over celite and concentrated to dryness. The crude product was purified by flash chromatography (silica, DCM: EtOAc = 3:2 → 1:1). The desired *rac*-**31** was obtained as a white solid (0.503 g, 0.786 mmol, 98%).

rac-**31**
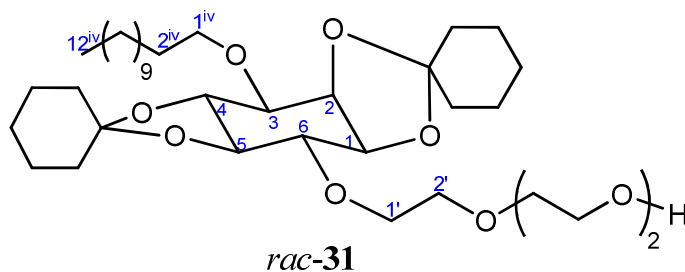
M (C$_{36}$H$_{64}$O$_9$) = 640.4550 g/mol;

TLC (SiO$_2$, DCM:EtOAC = 2:3): R$_f$ = 0.34;

^{1}H-NMR (500 MHz, CDCl$_3$): δ [ppm] = 4.47 (t, ^3J = 4.47 Hz, 1H; 2-H), 4.07 (t, ^3J = 5.6 Hz, 1H; 1-H), 3.88 – 3.96 (m, 3H; 4-H and 1'-H), 3.64 – 3.72 (m, 11H; 3-H and 5 OCH$_2$ of

triethylene oxide chain), 3.60 – 3.64 (m, 2H; 1^{iv}-H), 3.57 (dd, $^3J = 4.0$ Hz, $^3J = 6.4$ Hz, 1H; 6-H), 3.32 (m, 1H; 5-H), 2.98 (s, 1H; OH), 1.58 – 1.76 (m, 18H; 2^{iv}-H and 8 CH_2 of cyclohexylidene rings), 1.24 – 1.38 (m, 22H; 9 CH_2 of dodecyl chain and 2 CH_2 of cyclohexylidene rings), 0.87 (t, $^3J = 6.83$ Hz, 3H; 12^{iv}-H);

^{13}C-NMR (125 MHz, CDCl$_3$): δ [ppm] = 112.59, 110.44 (2s; 2 C of cyclohexylidene rings), 82.35 (d; C-6), 80.69 (d; C-1), 78.10 (d; C-5), 76.27 (d; C-4), 76.12 (d; C-3), 75.69 (d; C-2), 72.61 (t; C-1^{iv}), 70.57, 70.54, 70.23, 70.00, 61.70 (5t; 6 OCH$_2$ of triethylene oxide chain), 37.73, 36.43, 36.34, 35.11 (4t; 4 CH$_2$ of cyclohexylidene ring), 31.91, 29.72, 29.68, 29.63, 29.45, 29.35, 26.00, 22.68 (8t; 10 CH$_2$ of dodecyl chain), 25.01, 24.96, 23.94, 23.81, 23.75, 23.60 (6t; 6 CH$_2$ of cyclohexylidene ring), 14.13 (q; C-12^{iv});

FT-IR (ATR) $\tilde{v}$ [cm^{-1}] = 3447 (br, w), 2921 (s), 2850 (s), 1456 (m), 1448(m), 1364 (m), 1277 (m), 1249 (w), 1229 (w), 1162 (m), 1108 (br, s), 1067 (s), 1035 (m), 1011 (m), 964 (w), 936 (m), 908 (m), 849 (w), 833 (w), 778 (w), 729 (w);

MS (positive ESI) m/z (%): 663.43 (100) [M+Na]$^+$, 241.10 (4);

HR-MS (ESI) calc. for C$_{36}$H$_{64}$O$_9$Na [M+Na]$^+$: 663.444, found: 663.445.

7.2.10 Synthesis of 1-*O*-dodecyl-4-*O*-[2'-[2''-[2'''-(hydroxy)ethoxy]ethoxy]ethyl]-*myo*-inositol (*rac*-32)
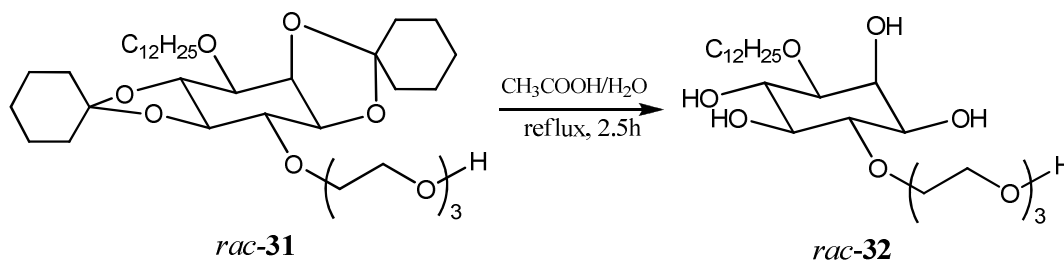
0.197 g (0.307 mmol) of *rac*-31 with a mixture of 0.73 ml (0.76 mg, 12.7 mmol) glacial acetic acid and 0.18 ml water were heated to reflux for 2.5 hours. The resulting mixture was evaporated under reduced pressure to dryness. In order to remove the remaining traces of acetic acid the mix was dissolved in methanol (2 x 20 ml) and toluene (2 x 30 ml) and subsequently concentrated. The crude solid product was purified by flash chromatography (silica, DCM:MeOH = 9:1).The tetrol *rac*-32 was obtained as a white waxy solid (0.103 g, 0.214 mmol, 70%).

rac-**32**
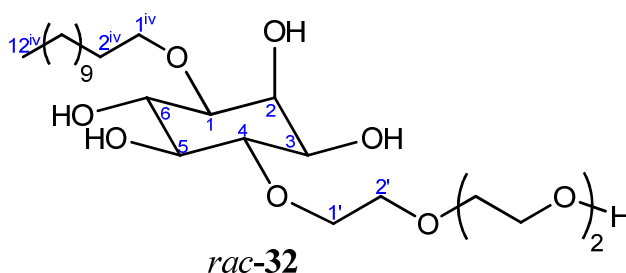
M ($C_{24}H_{48}O_9$) = 480.6325 g/mol;

TLC (SiO_2, DCM:MeOH = 8:1): R_f = 0.36;

Melting point (DSC): 80.6 °C;

^{1}H-NMR (500 MHz, DMSO-d_6): δ [ppm] = 4.56 – 4.58 (m, 2H; OH of triethylene oxide chain and 5-OH), 4.49 – 4.48 (m, 2H; 2-OH and 6-OH), 4.42 (d, ^3J = 4.88 Hz, 1H; 3-OH), 3.85 (m, 1H; 2-H), 3.72 – 3.81 (m, 2H; 1'-H), 3.35 – 3.52 (m, 13H; 5 OCH_2 of triethylene oxide chain, 6-H and 1^{iv}-H), 3.23 – 3.20 (m, 2H; 3-H and 4-H), 3.01 (dd, ^3J = 6.54 Hz, ^3J = 13.03 Hz, 1H,; 5-H), 2.88 (dd, ^3J = 2.08 Hz, ^3J = 9.69 Hz, 1H; 1-H), 1.47 (m, 2H; 2^{iv}-H), 1.28 – 1.24 (m, 18H; 9 CH_2 of dodecyl chain), 0.85 (t, ^3J = 6.80 Hz, 3H; 12^{iv}-H);

^{13}C-NMR (125 MHz, CDCl$_3$): δ [ppm] = 82.37 (d; C-4), 79.81 (d; C-1), 74.63 (d; C-5), 71.78 (d; C-6), 71.03 (d; C-3), 69.12 (d; C-2), 69.04 (t; C-1^{iv}), 72.24, 69.98, 69.57, 69.54, 60.11 (5t; 6 OCH_2 of triethylene oxide chain), 31.19, 29.50, 28.97, 28.91, 28.60, 25.48, 21.98 (7t; 10 CH_2 of dodecyl chain), 13.85 (q, C-12^{iv});

FT-IR (ATR) $\tilde{v}$ [cm^{-1}] = 3398 (br, s), 2919 (s), 2850 (s), 1660 (w), 1463 (w), 1347 (w), 1296 (w), 1245 (w), 1119 (w), 1081 (br, s), 1021 (m), 933 (w), 885 (w), 708 (w);

**MS** (positive ESI) m/z (%): 503.27 (100) [M+Na]$^+$, 481.29 (4);

HR-MS (ESI) calc. for $C_{24}H_{48}O_9Na$ [M+Na]$^+$: 503.319, found: 503.320;

EA: calc: 59.97% C; 10.07% H; found: 59.70% C; 9.99% H.

7.2.11. Synthesis of 5-*O*-dodecyl-1,6:3,4-bis-*O*-(2',3'-methoxybutane-2',3'-diyl)-*myo*-inositol (33)
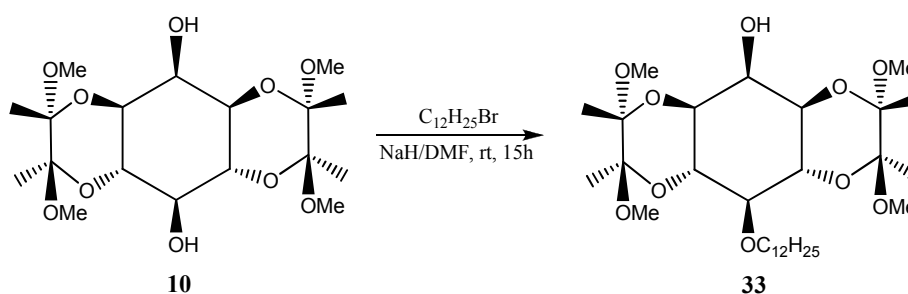
0.5 g (1.22 mmol) compound **10** was dissolved into a suspension of 0.03 g (1.47 mmol) NaH (in 55-65% mineral oil) in 40 ml dry DMF and the mix was stirred for 1h at 70°C under argon. After cooling down, 0.87 ml (0.90 g, 3.6 mmol) of *n*-dodecyl bromide were added and the mixture was stirred under inert atmosphere for 15h at r.t. The crude mixture was poured onto 80 ml ice-water and extracted with EtOAc (3 x 50 ml). The combined organic fractions were dried over MgSO$_4$, filtrated, concentrated and dried under vacuum. The crude product was purified by flash chromatography (silica, DCM:EtOAc = 4:1). Compound **30** was obtained as a white powder (0.277g, 0.480 mmol, 40%).

33
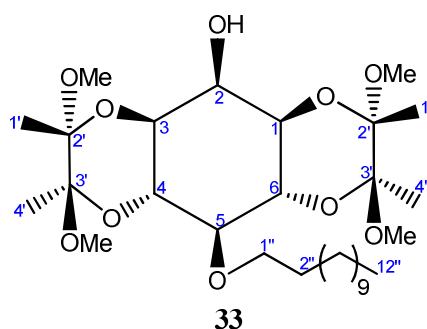
M (C$_{30}$H$_{56}$O$_{10}$) = 576.7596 g/mol;

TLC (SiO$_2$, CyHex:EtOAc = 1:1): R$_f$ = 0.41;

Melting point (DSC): 110 °C;

^{1}H-NMR (500 MHz, CDCl$_3$): δ [ppm] = 3.98 (t, ^3J = 9.84 Hz, 2H; 4-H and 6-H), 3.70 (t, ^3J = 6.45 Hz, 2H; 1''-H), 3.61 – 3.65 (m, 2H; 2-H and 5-H), 3.46 (dd, ^3J = 2.26 Hz, ^3J = 10.28 Hz, 2H; 1-H and 3-H), 3.22, 3.26 (2s, 12H; 2 2'-OCH$_3$ and 2 3'-OCH$_3$), 2.42 (s, 1H; OH), 1.54 – 1.60 (m, 2H; 1''-H), 1.25 – 1.35 (m, 30H; 9 CH$_2$ of dodecyl chain, 2 1'-H and 2 4'-H), 0.87 (t, ^3J = 6.91 Hz, 3H; 12''-H);

^{13}C-NMR (125 MHz, CDCl$_3$): δ [ppm] = 99.51, 99.01 (2s; 2 C-2' and 2 C-3'), 76.58 (d; C-5), 72.57 (t; C-1''), 70.75 (d; C-2), 69.27 (d; C-4 and C-6), 69.03 (d; C-1 and C-3), 47.90, 47.81 (2q; 2 2'-OCH$_3$ and 2 3'-OCH$_3$), 31.92, 30.09, 29.74, 29.69, 29.65, 29.60, 29.36, 26.00, 22.68 (9t; 10 CH$_2$ of dodecyl chain), 17.77, 17.64 (2q; 2 C-1' and 2 C-4'), 14.12 (q; C-12'');
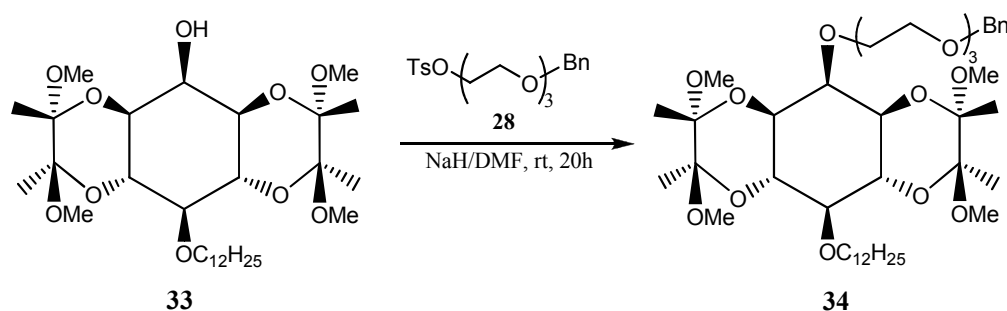
FT-IR (ATR) $\tilde{v}$ [cm^{-1}] = 3502 (br, m), 2921 (s), 2851 (s), 1457 (m), 1373 (s), 1112 (br, s), 1034 (s), 950 (m), 917 (m), 882 (m), 845 (m), 781 (m), 728 (m), 672 (m), 629 (m);

MS (positive ESI) m/z (%): 599.36 (100) [M+Na]$^+$;

**HR-MS** (ESI) calc. for C$_{30}$H$_{56}$O$_{10}$Na [M+Na]$^+$: 599.377; found: 599.377;

EA: 62.47% C; 9.79% H; found: 62.49% C; 9.77% H.

7.2.12. Synthesis of 2-*O*-[2'-[2''-[2'''-(benzyloxy)ethoxy]ethoxy]ethyl]-5-*O*-dodecyl-1,6:3,4-bis-*O*-(2,3-methoxybutane-2,3-diyl)-*myo*-inositol (34)

33   **34**

0.5 g (0.86 mmol) of **33** were dissolved into a suspension of 0.05 g (1.04 mmol) NaH (55-65% mineral oil) in 30 ml dry DMF and the mix was stirred for 15 min at 0°C under argon. 0.41 g (1.04 mmol) of tosylate **28** were added dropwise and the reaction mixture was stirred under inert atmosphere for additional 20 h at r.t. The crude mix was poured onto 70 ml ice-water and 25 ml brine were added. After extraction with DCM (3 x 50 ml) the combined organic fractions were dried over MgSO₄, filtrated, concentrated and dried under vacuum. The crude product was purified by flash chromatography (silicagel, CyHex:EtOAc = 6:1).

The benzylated **34** was obtained as colourless oil (0.479 g, 0.60 mmol, 70%).

30
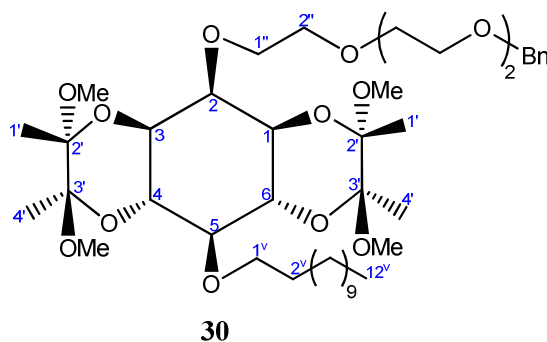
M ($C_{43}H_{74}O_{13}$) = 799.0399 g/mol;

TLC (SiO₂, CyHex:EtOAc = 7:3): R_f = 0.24;

¹H-NMR (500 MHz, DMSO-d₆): δ [ppm] = 7.33 – 7.33 (m, 5H; 5 Aryl-H), 4.55 (s, 2H; CH₂ of Bn), 4.03 – 4.00 (m, 2H; 4-H and 6-H), 3.93 (dd, ³*J* = 4.79 Hz, ³*J* = 5.15 Hz, 2H; 1''-H), 3.60 – 3.69 (m, 12H; 5 OCH₂ of triethylene oxide chain and 1ᵛ-H), 3.58 (m, 1H; 2-H), 3.43 – 3.45 (m, 2H; 1-H and 3-H), 3.29 (dd, ³*J* = 6.52 Hz, ³*J* = 15.82 Hz, 1H; 5-H), 3.22, 3.24 (2s,

12H; 2 2'-OCH$_3$ and 2 3'-OCH$_3$), 1.54 – 1.60 (m, 2H; 2^v-H), 1.25 – 1.35 (m, 30H; 9 CH$_2$ of dodecyl chain, 2 1'-H and 2 4'-H), 0.88 (t, ^3J = 6.87 Hz, 3H; 12^v-H);

^{13}C-NMR (125 MHz, CDCl$_3$): δ [ppm] = 138.23 (s; C of Aryl), 128.33, 127.73, 127.55 (3d; 5 CH of Aryl), 99.45, 98.87 (2s; 2 C-2' and 2 C-3'), 79.23 (d; C-5), 76.50 (d; C-2), 73.22 (t; CH$_2$ of Bn), 72.53 (t; C-1^v), 72.42, 70.87, 70.69, 70.65 (4t; 6 OCH$_2$ of triethylene oxide chain), 69.64 (d; C-4 and C-6), 69.27 (d; C-1 and C-3), 47.84, 47.70 (2q; 2 2'-OCH$_3$ and 2 3'-OCH$_3$), 31.92, 30.13, 29.73, 29.69, 29.66, 29.59, 29.36, 25.98, 22.69 (9t; 10 CH$_2$ of dodecyl chain), 17.88, 17.60 (2q; 2 C-1' and 2 C-4'), 14.12 (q; C-12^v);

FT-IR (ATR) $\tilde{\upsilon}$ [cm^{-1}] = 2921 (s), 2851 (s), 1680 (w), 1453 (m), 1373 (s), 1211 (w), 1181 (w), 1112 (br, s), 1035 (s), 950 (m), 916 (m), 882 (m), 846 (m), 732 (m), 697 (m), 671 (w), 633 (w);

MS (positive ESI) m/z (%): 821.49 (100) [M+Na]$^+$, 671.38 (4), 91.06 (4);

HR-MS (ESI) calc. for C$_{43}$H$_{74}$O$_{13}$Na [M+Na]$^+$: 821.502; found: 821.503;

EA: calc: 64.64% C; 9.33% H; found: 64.74% C; 9.38% H.

7.2.13. Synthesis of 2-*O*-[2'-[2''-[2'''-(hydroxy)ethoxy]ethoxy]ethyl]-5-*O*-dodecyl-1,6:3,4-bis-*O*-(2',3'-methoxybutane-2',3'-diyl)-*myo*-inositol (35)
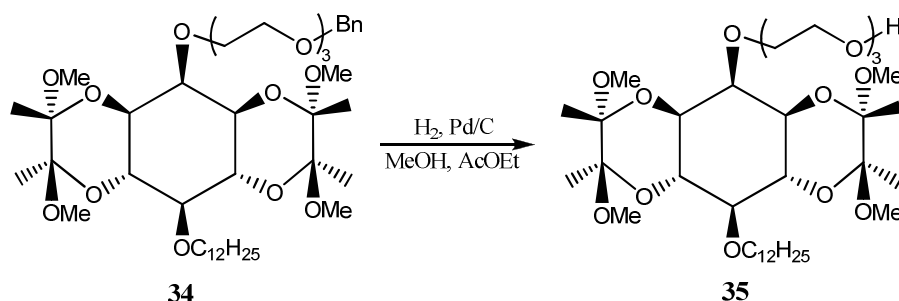
A solution of 0.3 g (0.376 mmol) **34** in 12 ml of a MeOH:EtOAc = 3:1 mixture was degassed with argon for 30 min. To this solution, 4 mg (0.037 mmol) Pd (10% supported on charcoal) were added and the reaction mixture was stirred at r.t. under hydrogen atmosphere (pressure ~ 1.5 bar) for 3 days. The resulting mix was filtrated over celite and concentrated to dryness. The crude product was purified by flash chromatography (silica, CyHex:EtOAc = 3:2 → 1:1). The deprotected derivative **35** was obtained as a colourless oil (0.26 g, 0.367 mmol, 98%).

35
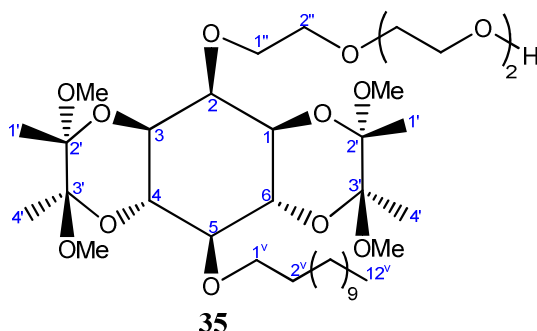
M ($C_{36}H_{68}O_{13}$) = 708.9173 g/mol;

TLC (SiO_2, DCM:EtOAc = 1:1): R_f = 0.16;

^{1}H-NMR (500 MHz, DMSO-d_6): δ [ppm] = 4.58 (t, ^3J = 5.48 Hz, 1H; OH), 3.72 -3.78 (m, 4H; 1''-H, 4-H and 6-H), 3.58 (t, ^3J = 6.08 Hz, 3H; 1^v-H and 2-H), 3.44 – 3.53 (m, 10H; 4 OCH_2 of triethylene oxide chain, 1-H and 3-H), 3.38 (t, ^3J = 5.31 Hz, 2H; OCH_2 of triethylene oxide chain), 3.17 (t, ^3J = 9.24 Hz, 1H; 5-H), 3.13, 3.14 (2s, 12H; 2 2'-OCH_3 and 2 3'-OCH_3), 1.43 – 1.48 (m, 2H; CH_2 of dodecyl chain), 1.20 – 1.36 (m, 18H; 9 CH_2 of dodecyl chain), 1.17 (d, ^3J = 1.27 Hz, 12H; 2 1'-H and 2 4'-H), 0.85 (t, ^3J = 6.84 Hz, 3H; 12^v-H);

^{13}C-NMR (125 MHz, DMSO-d_6): δ [ppm] = 98.72, 98.33 (2s; 2 C-2' and 2 C-3'), 77.93 (d; C-5), 76.09 (d; C-2), 72.31 (t; C-1''), 71.63 (t; C-1^v), 71.55, 70.03, 69.78, 69.69 (4t; 4 OCH_2 of triethylene oxide chain), 69.27 (d; C-4 and C-6), 68.22 (d; C-1 and C-3), 60.12 (t; OCH_2 of triethylene oxide chain), 47.43, 47.05 (2q; 2 2'-OCH_3 and 2 3'-OCH_3), 31.25, 29.64, 29.05, 28.94, 28.85, 28.65, 25.49, 22.05 (8t; 10 CH_2 of dodecyl chain), 17.57, 17.43 (2q; 2 C-1' and 2 C-4'), 13.92 (q, C-12^v);
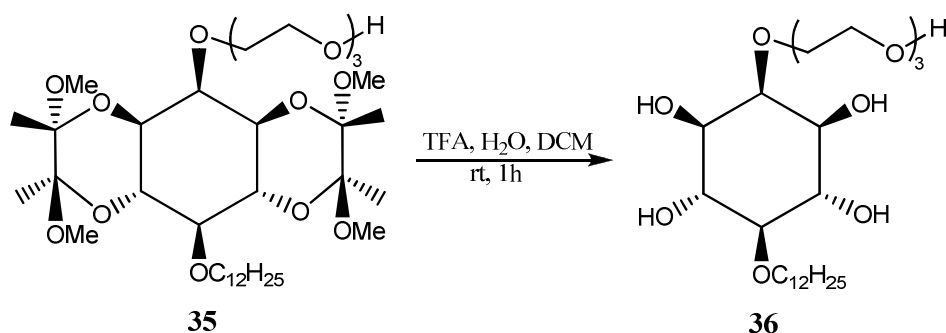
FT-IR (ATR) $\tilde{v}$ [cm^{-1}] = 3467 (br, w), 2921 (s), 2846 (s), 1455 (m), 1373 (m), 1215 (w), 1184 (w), 1113 (br, s), 1035 (s), 950 (m), 918 (m), 882 (m), 846 (m), 781 (w), 761 (w), 730 (w), 673 (w), 647 (w);

MS (positive ESI) m/z (%): 731.43 (100) [M+Na]$^+$, 581.34 (6);

**HR-MS** (ESI) calc. for $C_{36}H_{68}O_{13}Na$ [M+Na]$^+$: 731.455; found: 731.455;

EA: calc: 60.99% C; 9.67% H; found: 60.72% C; 9.72% H.

7.2.14. Synthesis of 2-*O*-dodecyl-5-*O*-[2'-[2''-[2'''-(hydroxy)ethoxy]ethoxy] ethyl] - *myo*-inositol (36)

35 → **36**

To a solution of 0.20 g (0.25 mmol) **35** in 6 ml DCM was added a solution of 1 ml (1.48 g, 12.98 mmol) trifluoroacetic acid (TFA) in 0.2 ml water and the obtained mixture was stirred at r.t. for 1 h. After evaporation of solvents, 3 x 30 ml of CHCl$_3$ were added and subsequently evaporated. The crude product was purified by flash chromatography (silica, DCM:MeOH = 15:1) and recrystallization from MeOH.

The tetrol **36** was obtained as a white solid (0.112 g, 0.233 mmol, 93%).

36   or
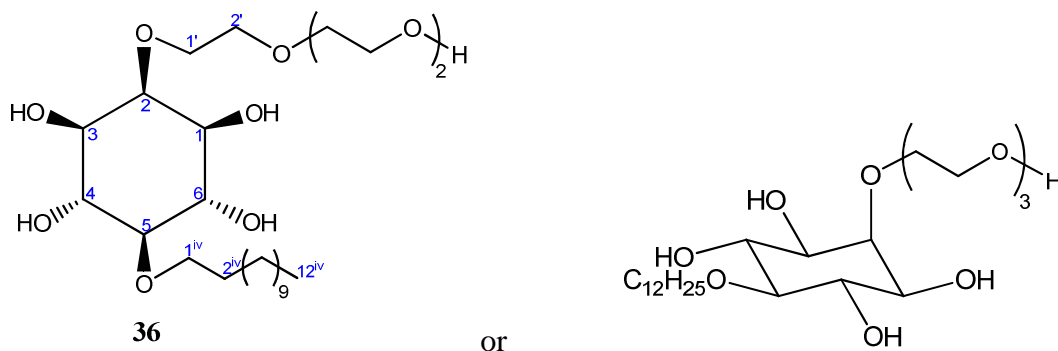
M (C$_{24}$H$_{48}$O$_9$) = 480.6325 g/mol;

TLC (SiO$_2$, DCM:MeOH = 11:1): R$_f$ = 0.16;

Melting point (DSC): 173.7 °C;

^{1}H-NMR (500 MHz, DMSO-d$_6$): δ [ppm] = 4.62 (t, ^3J = 5.38 Hz 1H; OH of triethylene oxide chain), 4.55 – 4.57 (m, 2H; 2 OH), 4.49 – 4.50 (m, 2H; 2 OH); 3.77 (t, ^3J = 4.91 Hz, 2H; 1'-H), 3.61 (t, 2H, ^3J = 6.42 Hz; 1^{iv}-H), 3.46 – 3.51 (m, 8H; 4 OCH$_2$ of triethylene oxide chain), 3.44 (m, 1H; 2-H), 3.37 – 3.41 (m, 4H; 4-H, 6-H and OCH$_2$ of triethylene oxide chain), 3.16 – 3.20 (m, 2H; 1-H and 3-H), 2.79 (t, ^3J = 9.03 Hz, 1H; 5-H), 1.45 – 1.43 (m, 2H; 2^{iv}-H), 1.28 – 1.23 (m, 18H; 9 CH$_2$ of dodecyl chain), 0.85 (t, ^3J = 6.44 Hz, 3H; 12^{iv}-H);

^{13}C-NMR (125 MHz, DMSO-d$_6$): δ [ppm] = 85.29 (d; C-5), 82.07 (d; C-2), 73.14 (t; C-1^{iv}), 72.95 (d; C-4 and C-6), 72.35 (d; C-1 and C-3), 72.82, 71.37, 70.55, 70.16, 70.14, 60.66 (6t; 6 OCH$_2$ of triethylene oxide chain), 31.79, 30.41, 29.59, 29.53, 29.22, 26.13, 22.58 (7t; 10 CH$_2$ of dodecyl chain), 14.45 (q, C-12^{iv});

FT-IR (ATR) $\tilde{v}$ [cm^{-1}] = 3336 (br, s), 2917 (s), 2848 (m), 1650 (br, w), 1466 (w), 1354 (w), 1235 (w), 1136 (br, m), 1068 (m), 1038 (s), 929 (w), 718 (m);

MS (positive ESI) m/z (%): 503.25 (100) [M+Na]$^+$, 481.29 (10);

HR-MS (ESI) calc. for C$_{24}$H$_{48}$O$_9$Na [M+Na]$^+$: 503.319; found: 503.319.

7.2.15. Synthesis of 2-*O*-[2'-[2''-[2'''-(dodecyloxy)ethoxy]ethoxy]ethyl]-5-*O*-dodecyl-1,6:3,4-bis-*O*-(2,3-methoxybutane-2,3-diyl)-*myo*-inositol (37)
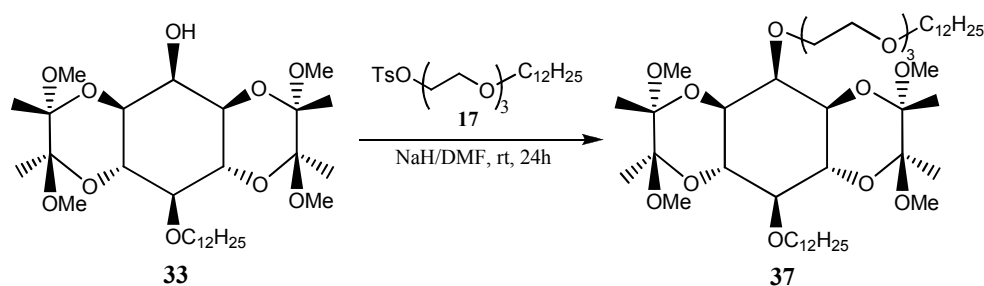
0.5 g (0.87 mmol) of alkylated **33** were dissolved into a suspension of 0.09 g (1.87 mmol) NaH (in 55-65% mineral oil) in 25 ml dry DMF and the mix was stirred for 15 min at 0°C under argon. 0.6 g (1.52 mmol) of tosylate **17** were added dropwise, and the reaction mixture was stirred under inert atmosphere for additional 24 h at r.t. The crude mix was poured onto 100 ml ice-water and 25 ml brine were added. After extraction with EtOAc (3 x 50 ml) the combined organic layers were dried over MgSO$_4$, filtrated, concentrated and dried under vacuum. The crude product was purified by flash chromatography (silica, DCM: EtOAc = 4:1). The protected derivative **37** was obtained as yellow oil (0.62 g, 0.706 mmol, 82%).

37
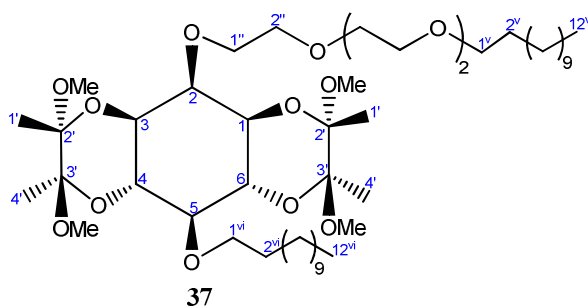
M ($C_{48}H_{92}O_{13}$) = 877.2363 g/mol;

TLC (SiO_2, Cyhex: EtOAc = 7:3): R_f = 0.38;

^{1}H-NMR (500 MHz, $CDCl_3$): δ [ppm] = 4.02 (t, ^3J = 9.80 Hz, 2H; 4-H and 6-H), 3.93 (t, ^3J = 4.92 Hz, 2H; 1''-H), 3.65 – 3.68 (m, 4H, 1^{vi}-H and 2''-H), 3.61 – 3.64 (m, 6H; 3 OCH_2 of triethylene oxide chain), 3.57 – 3.59 (m, 1H; 2-H), 3.55 – 3.56 (m, 2H; OCH_2 of triethylene oxide chain), 3.45 (dd, ^3J = 8.61 Hz, ^3J = 4.14 Hz, 2H; 1-H and 3-H), 3.43 (t, ^3J = 6.80 Hz, 2H; 1^v-H), 3.29 (t, ^3J = 9.29 Hz, 1H; 5-H), 3.22, 3.24 (2s, 12H; 2 2'-OCH_3 and 2 3'-OCH_3), 1.51 – 1.59 (m, 4H; 2^v-H and 2^{vi}-H), 1.23 – 1.34 (m, 48H; 18 CH_2 of dodecyl chains, 2 1'-H and 2 4'-H), 0.88 (t, ^3J = 6.74 Hz, 6H; 12^v-H and 12^{vi}-H);

^{13}C-NMR (125 MHz, $CDCl_3$): δ [ppm] = 99.43, 98.85 (2s; 2 C-2' and 2 C-3'), 79.22 (d; C-5), 76.48 (d; C-2), 72.52, 72.42 (2t; 2 OCH_2 of triethylene oxide chain), 71.55 (t; C-1^{vi}), 70.85, 70.63, 70.34, 70.03 (4t; 4 OCH_2 of triethylene oxide chain and C-1^v), 69.63 (d; C-4 and C-6), 69.26 (d; C-1 and C-3), 47.85, 47.70 (2q; 2 2'-OCH_3 and 2 3'-OCH_3), 31.92, 31.91, 30.13, 29.73, 29.69, 29.66, 29.61, 29.49, 29.37, 29.35, 26.07, 25.98, 22.69 (13t; 20 CH_2 of dodecyl chains), 17.88, 17.60 (2q; 2 C-1' and 2 C-4'), 14.13 (q; C-12^v and C-12^{vi});
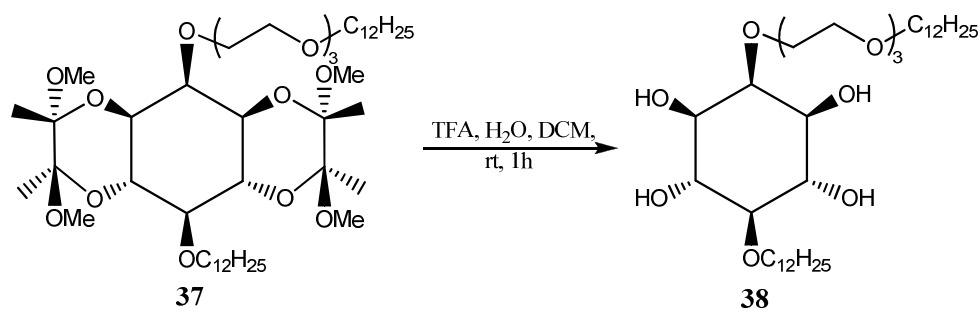
FT-IR (ATR) $\tilde{v}$ [cm^{-1}] = 2920 (s), 2851 (s), 1462 (m), 1373 (m), 1211 (w), 1184 (w), 1113 (br, s), 1036 (s), 950 (m), 916 (m), 882 (m), 846 (m), 780 (w), 759 (w), 722 (w), 671 (w);

MS (positive ESI) m/z (%): 899.68 (100) [M+Na]$^+$, 749.48 (4), 597.47 (9);

**HR-MS** (ESI) calc. for $C_{48}H_{92}O_{13}Na$ [M+Na]$^+$: 899.643; found: 899.644;

EA: calc: 65.72% C; 10.57% H; found: 65.67% C; 10.54% H.

7.2.16. Synthesis of 2-*O*-[2'-[2''-[2'''-(dodecyloxy)ethoxy]ethoxy]ethyl]-5-*O*-dodecyl-*myo*-inositol (38)

To a solution of 0.5 g (0.57 mmol) derivative **37** in 6 ml DCM was added a solution of 1.9 ml (2.85 g, 25 mmol) trifluoroacetic acid (TFA) in 0.3 ml water and the obtained mixture was stirred at r.t. for 1 h. After evaporation of solvents, 3 x 30 ml of CHCl$_3$ were added and again evaporated. The crude product was purified by recrystallization from MeOH.

The final compound **38** was obtained as a white solid (0.35 g, 0.54 mmol, 95%).

38   or
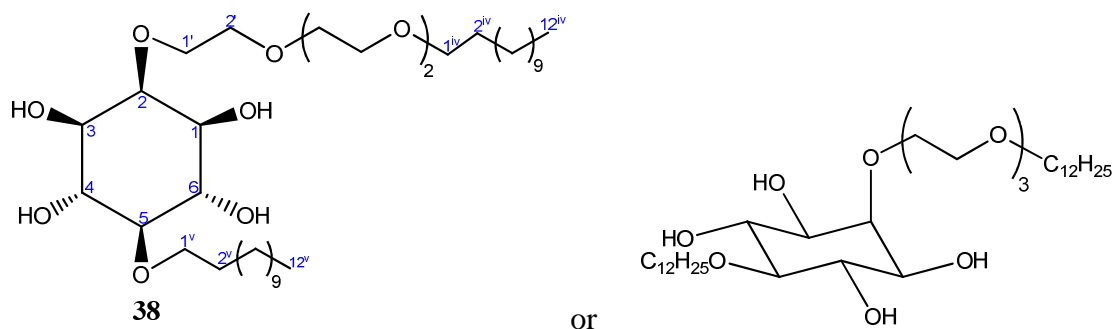
M (C$_{36}$H$_{72}$O$_9$) = 648.9515 g/mol;

TLC (SiO$_2$, DCM: MeOH = 10:1): R$_f$ = 0.37;

Melting point (DSC): 155.1 °C;

^{1}H-NMR (500 MHz, DMSO-d$_6$): δ [ppm] = 4.54 (d, ^3J = 4.52 Hz, 2H; 2 OH), 4.47 (d, ^3J = 4.96 Hz, 2H; 2 OH), 3.76 (t, ^3J = 5.16 Hz, 2H; 1'-H), 3.61 (t, ^3J = 6.52 Hz, 2H; 1^v-H), 3.49 – 3.52 (m, 8H; 4 OCH$_2$ of triethylene oxide chain), 3.44 – 3.46 (m, 3H; 2-H and OCH$_2$ of triethylene oxide chain), 3.40 (ddd, ^3J = 4.59 Hz, ^3J = 9.42 Hz, ^3J = 9.47 Hz, 2H; 4-H and 6-H), 3.35 (t, ^3J = 6.61 Hz, 2H; 1^{iv}-H), 3.16 – 3.19 (m, 2H; 1-H and 3-H), 2.78 (t, ^3J = 9.05 Hz, 1H; 5-H), 1.41 – 1.49 (m, 4H; 1^{iv}-H and 1^v-H), 1.19 – 1.31 (m, 36H; 18 CH$_2$ of dodecyl chains), 0.85 (t, ^3J = 6.77 Hz, 6H; 12^{iv}-H and 12^v-H);

^{13}**C-NMR** (125 MHz, DMSO-d$_6$): δ [ppm] = 84.79 (d; C-5), 81.52 (d; C-2), 72.56 (t; C-1^v), 72.41 (d; C-4 and C-6), 71.82 (d; C-1 and C-3), 72.85 (t; C-1'), 70.24 (t; C-1^{iv}) 70.03, 69.70, 69.67, 69.57, 69.39 (5t; 5 OCH$_2$ of triethylene oxide chain), 31.24, 29.89, 29.13, 29.05, 28.99, 28.82, 28.68, 25.61, 25.59, 22.04 (10t; 20 CH$_2$ of dodecyl chains), 13.90 (q; C-12^{iv} and C-12^v);
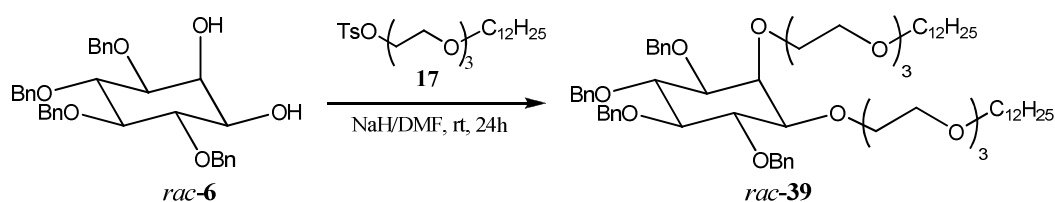
FT-IR (ATR) $\tilde{v}$ [cm^{-1}] = 3324 (br, m), 2917 (s), 2846 (s), 1660 (br, w), 1466 (m), 1373 (w), 1311 (w), 1132 (s), 1074 (w), 1037 (s), 983 (w), 966 (w), 861 (w), 718 (m);

MS (positive ESI) m/z (%): 671.47 (100) [M+Na]$^+$, 649.51 (16), 319.21 (6), 257.24 (4);

HR-MS (ESI) calc. for C$_{36}$H$_{72}$O$_9$Na [M+Na]$^+$: 671.507; found: 671.508;

EA: calc: 66.63% C; 11.18% H; found: 66.46% C; 11.12% H.

7.2.17. Synthesis of 1,2-bis-*O*-[2'-[2''-[2'''-(dodecyloxy)ethoxy]ethoxy]ethyl]-3,4,5,6-tetra-*O*-benzyl-*myo*-inositol (*rac*-39)

1.71 g (3.17 mmol) of *rac*-6 were dissolved into a suspension of 0.33 g (6.98 mmol) NaH (in 55-65% mineral oil) in 50 ml dry DMF and the mix was stirred under argon for 15 min at 0°C. 3 g (6.35 mmol) of tosylate **17** were added dropwise, and the reaction mixture was stirred under inert atmosphere for additional 24 h at r.t. The crude mix was poured onto 100 ml ice-water and 20 ml brine were added. After extraction with EtOAc (3 x 50 ml) the combined organic fractions were dried over MgSO$_4$, filtrated, concentrated and dried under vacuum. The crude product was purified by flash chromatography (silica, CyHex: EtOAc = 4:1 → 3:2).

The benzylated *rac*-39 was obtained as yellow oil (1.842 g, 1.61 mmol, 51%).

rac-**39**
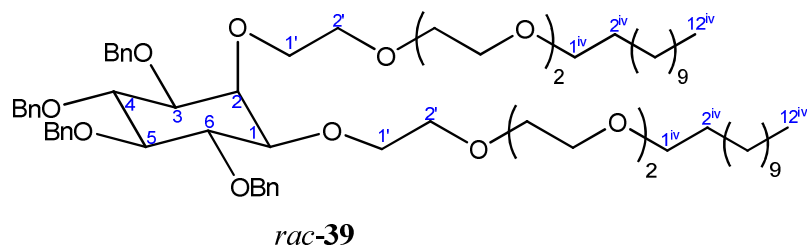
M ($C_{70}H_{108}O_{12}$) = 1141.5993 g/mol;

TLC (SiO_2, CyHex:EtOAc = 7:3): R_f = 0.28;

^{1}H-NMR (500 MHz, $CDCl_3$): δ [ppm] = 7.26 – 7.36 (m, 20H; 20 Aryl-H), 4.67 – 4.90 (m, 8H; 4 OCH_2 of Bn), 4.00 – 4.03 (m, 1H; 2-H), 3.92 – 3.99 (m, 3H; 4-H and 1'-H), 3.90 (t, ^3J = 7.06 Hz, 1H; 6-H), 3.71 – 3.79 (m, 2H; 1'-H), 3.66 – 3.69 (m, 4H; OCH_2 of triethylene oxide chain), 3.58 – 3.64 (m, 12H; OCH_2 of triethylene oxide chain), 3.53 – 3.55 (m, 4H; OCH_2 of triethylene oxide chain), 3.39 – 3.53 (m, 5H; 5-H and 2 1^{iv}-H), 3.34 (dd, ^3J = 2.09 Hz, ^3J = 9.84 Hz, 1H; 3-H), 3.23 (dd, ^3J = 2.06 Hz, ^3J = 9.82 Hz, 1H; 1-H), 1.52 – 1.58 (m, 4H; 2 2^{iv}-H), 1.19 – 1.36 (m, 36H; 18 CH_2 of dodecyl chains), 0.88 (t, 6H, ^3J = 6.93 Hz; 2 12^{iv}-H);

^{13}C-NMR (125 MHz, $CDCl_3$): δ [ppm] = 138.99, 138.78, 138.77, 138.37 (4s; 4 C of Aryl), 128.35, 128.31, 128.29, 128.27, 128.04, 127.94, 127.86, 127.57, 127.49, 127.47 (10d; 10 CH of Aryl), 83.48 (d; C-5), 81.79 (d; C-1), 81.54 (d; C-4), 81.47 (d; C-6), 80.63 (d; C-3), 75.93, 75.83 (2t; 2 OCH_2 of Bn), 75.69 (d; C-2), 75.62, 72.61 (2t; 2 OCH_2 of Bn), 71.54 (t; 2 C-1^{iv}), 72.43, 70.93, 70.80, 70.65, 70.60, 70.59, 70.58, 70.57, 70.54, 70.10, 70.00, 69.98 (12t; 12 OCH_2 of triethylene oxide chains), 31.90, 29.66, 29.63, 29.61, 29.49, 29.34, 26.07, 22.68 (8 t; 20 CH_2 of dodecyl chains), 14.13 (q; 2 C-12^{iv});
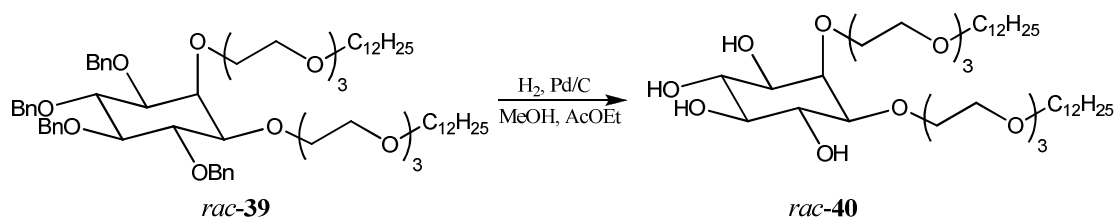
FT-IR (ATR) $\tilde{v}$ [cm^{-1}] = 2920 (s), 2846 (s), 1493 (w), 1452 (m), 1356 (m), 1300 (w), 1245 (w), 1208 (w), 1085 (br, s), 1067 (s), 1024 (w), 943 (w), 8756 (w), 731 (s), 694 (s);

MS (positive ESI) m/z (%): 1163.77 (100) [M+Na]$^+$, 598.30 (8), 301.23 (4);

**HR-MS** (ESI) calc. for $C_{70}H_{108}O_{12}Na$ [M+Na]$^+$: 1163.774; found: 1163.775;

EA: 73.65% C; 9.54% H; found: 73.66% C; 9.54% H.

7.2.18. Synthesis of 1,2-bis-*O*-[2'-[2''-[2'''-(dodecyloxy)ethoxy]ethoxy]ethyl]-*myo*-inositol (*rac*-40)

rac-39 → *rac*-40

A solution of 0.80 g (0.70 mmol) *rac*-39 in 20 ml of a MeOH:EtOAc = 3:1 mixture was degassed with argon for 30 min. To this solution, 0,074 g (0.070 mmol) Pd (10% supported on charcoal) were added and the reaction mixture was stirred at r.t. under hydrogen atmosphere (pressure ~ 8 bar) for 3 days. The resulting mix was filtrated over celite and concentrated to dryness.

The tetrol *rac*-40 was obtained as a white solid (0.523 g, 0.67 mmol, 95%).

rac-40
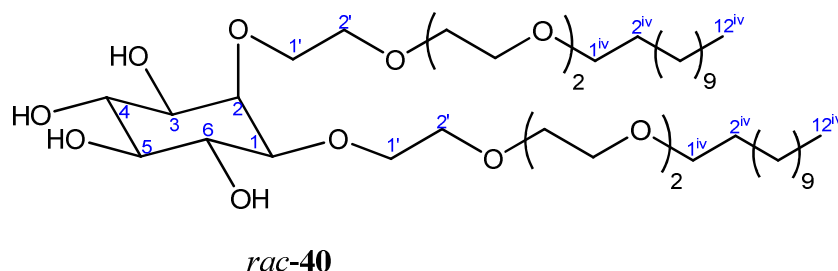
M ($C_{42}H_{84}O_{12}$) = 781.1092 g/mol;

TLC (SiO_2, DCM: MeOH = 9:1): R_f = 0.38;

Melting point: liquid crystal, (see Table 3.3, chapter 3.2.1. Thermotropic mesomorphism);

^{1}H-NMR (500 MHz, DMSO-d_6): δ [ppm] = 4.57 – 4.64 (m, 3H; OH); 4.37 (s, 1H; OH), 3.59 – 3.80 (m, 5H; 2-H and 2 1'-H), 3.50 – 3.45 (m, 20H; 10 OCH$_2$ of triethylene oxide chains), 3.33 – 3.40 (m, 5H; 6-H and 2 1^{iv}-H), 3.28 (t, ^3J = 9.08 Hz, 1H; 4-H), 3.15 (dd, ^3J = 1.92 Hz, ^3J = 9.63 Hz, 1H; 3-H), 3.02 (dd, ^3J =1.77 Hz, ^3J = 9.84 Hz, 1H; 1-H), 2.89 (ddd, ^3J = 4.21 Hz, ^3J = 8.90 Hz, ^3J = 8.95 Hz, 1H; 5-H), 1.46 (m, 4H; 2 2^{iv}-H), 1.23 – 1.26 (m, 36H; 18 CH$_2$ of dodecyl chains), 0.85 (t, ^3J = 6.35 Hz, 6H; 2 12^{iv}-H);

^{13}C-NMR (125 MHz, DMSO-d_6): δ [ppm] = 80.81 (d; C-1), 79.25 (d, C-2), 75.11 (d; C-5), 72.77 (d; C-4), 72.01 (d; C-6), 71.88 (t; 2 C-1'), 71.62 (d, C-3), 70.30, 70.09 (2t, 2 C-1^{iv}), 70.06, 69.79, 69.69, 69.46, 69.18 (5t; 10 OCH$_2$ of triethylene oxide chains), 31.31, 29.20, 29.05, 29.03, 28.89, 28.73, 25.65, 22.10 (8t; 20 CH$_2$ of dodecyl chains), 13.94 (q; 2 C-12^{iv});
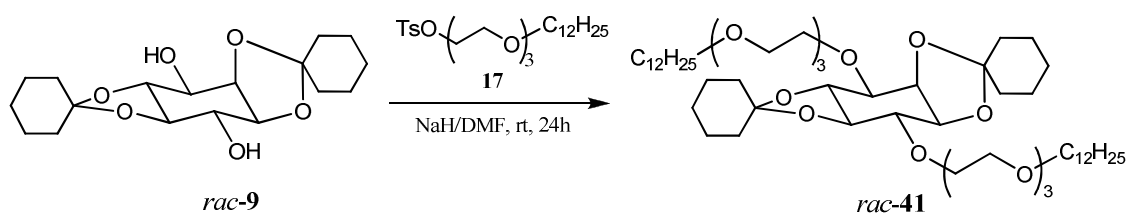
FT-IR (ATR) $\tilde{v}$ [cm^{-1}] = 3399 (br, m), 2918 (s), 2850 (s), 1463 (m), 1347 (w), 1293 (w), 1242 (w), 1110 (br, s), 1034 (w), 1000 (w), 933 (w), 878 (w), 715 (m);

**MS** (positive ESI) m/z (%): 803.54 (100) [M+Na]$^+$, 781.55 (6), 319.23 (4);

HR-MS (ESI) calc. for C$_{42}$H$_{84}$O$_{12}$Na [M+Na]$^+$: 803.586; found: 803.586;

EA: calc: 64.58% C; 10.84% H; found: 64.52% C; 10.85% H.

7.2.19. Synthesis of 1,2:4,5-di-*O*-cyclohexylidene-3,6-bis-*O*-[2'-[2''-[2'''-(dodecyloxy) ethoxy]ethoxy]ethyl]-*myo*-inositol (*rac*-41)

0.3 g (0.88 mmol) of *rac*-9 were dissolved into a suspension of 0.09 g (1.93 mmol) NaH (in 55-65% mineral oil) in 40 ml dry DMF and the mix was stirred for 15 min at 0°C under argon. 0.95 g (2.01 mmol) of tosylate **17** were added dropwise, and the reaction mixture was stirred under argon atmosphere for additional 20 h at r.t. The crude mix was poured onto 70 ml ice-water and 25 ml brine were added. After extraction with DCM (3 x 50 ml) the combined organic layers were dried over MgSO$_4$, filtrated, concentrated and dried under vacuum. The crude product was purified by flash chromatography (silica, CyHex:EtOAc = 3:1). The protected derivative *rac*-41 was obtained as a yellow oil (0.4 g, 0.43 mmol, 50%).
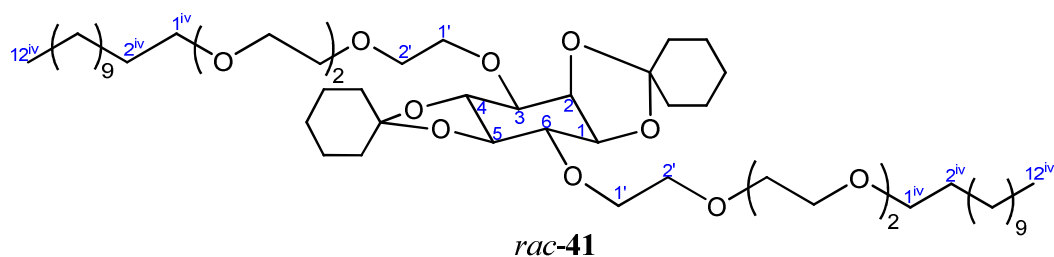
M (C$_{54}$H$_{100}$O$_{12}$) = 941.3646 g/mol;

TLC (SiO$_2$, CyHex:EtOAc = 1:1): R$_f$ = 0.30;

^{1}H-NMR (500 MHz, CDCl$_3$): δ [ppm] = 4.49 (t, ^3J = 4.46 Hz, 1H; 2-H), 4.05 (t, ^3J = 5.65 Hz, 1H; 3-H), 3.84 – 3.95 (m, 5H; 6-H and 2 1'-H), 3.79 (dd, ^3J = 3.99 Hz, ^3J = 10.19 Hz, 1H; 1-H), 3.62 – 3.73 (m, 16H; 8 OCH$_2$ of triethylene oxide chains), 3.56 – 3.58 (m, 5H; 4-H and 2

OCH$_2$ of triethylene oxide chains), 3.44 (t, ^3J = 6.82 Hz, 4H; 2 1^{iv}-H), 3.30 (t, ^3J = 9.95 Hz, 1H; 5-H), 1.53 – 1.75 (m, 20H; 2 2^{iv}-H and 8 CH$_2$ of cyclohexylidene rings), 1.19 – 1.37 (m, 40H; 18 CH$_2$ of dodecyl chains and 2 CH$_2$ of cyclohexylidene rings), 0.87 (t, ^3J = 6.85 Hz, 6H; 2 12^{iv}-H);

^{13}**C-NMR** (125 MHz, CDCl$_3$): δ [ppm] = 112.51, 110.39 (2s; 2 C of cyclohexylidene rings), 82.37 (d; C-4), 80.75 (d; C-3), 78.22 (d; C-5), 76.64 (d; C-1), 76.32 (d; C-6), 75.84 (d; C-2), 71.54 (t; 2 C-1^{iv}), 70.74, 70.61, 70.57, 70.48, 70.07, 70.03, 69.25 (7t; 12 OCH$_2$ of triethylene oxide chains), 37.70, 36.43, 36.38, 35.22 (4t; 4 CH$_2$ of cyclohexylidene rings), 31.90, 29.65, 29.61, 29.49, 29.34, 26.07, 22.67 (7t; 20 CH$_2$ of dodecyl chains), 25.01, 24.97, 23.93, 23.81, 23.77, 23.57 (6t; 6 CH$_2$ of cyclohexylidene rings), 14.12 (q, 2 C-12^{iv});

FT-IR (ATR) $\tilde{v}$ [cm^{-1}] = 2920 (s), 2850 (s), 2354 (w), 1461 (w), 1448 (m), 1364 (m), 1276 (m), 1250 (w), 1230 (w), 1103 (br, s), 1031 (w), 960 (w), 934 (m), 907 (w), 847 (m), 830 (w), 776 (m), 718 (w);

MS (positive ESI) m/z (%): 963.72 (100) [M+Na]$^+$, 727.75 (14), 641.52 (36), 427.24 (6), 319.25 (6), 109.00 (3);

**HR-MS** (ESI) calc. for C$_{54}$H$_{100}$O$_{12}$Na [M+Na]$^+$: 963.711; found: 963.712.

7.2.20. Synthesis of 1,4-bis-*O*-[2'-[2''-[2'''-(dodecyloxy)ethoxy]ethoxy]ethyl]-*myo*-inositol (42)

rac-**41**   *rac*-**42**
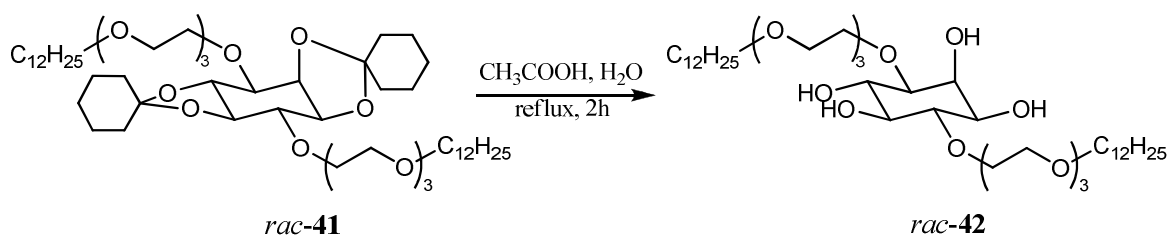
A mixture of 0.28 g (0.36 mmol) *rac*-**41**, 1.6 ml (1.68 g, 28 mmol) glacial acetic acid and 0.4 ml water was stirred for 2 h at 95°C. To the resulting crude mix 3 x 50 ml methanol were added and subsequently evaporated. In order to remove the traces of acetic acid, the obtained solid was dissolved in 3 x 50 ml toluene, subsequently evaporated and dried under vacuum. The crude product was purified by flash chromatography (silica, DCM:EtOAc = 3:2, and DCM: MeOH = 10:1).

The tetrol *rac*-**42** was obtained as a white waxy solid (0.206 g, 0.26 mmol, 74% yield).

rac-**42**
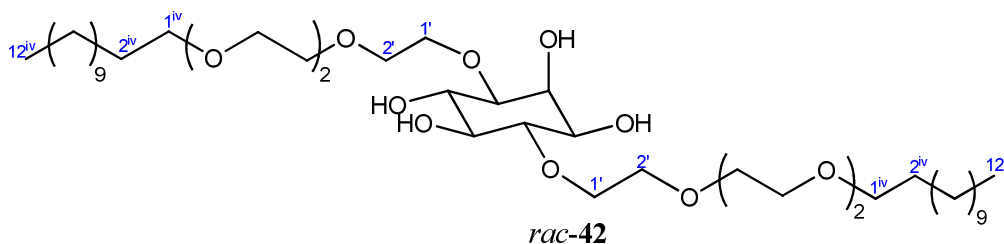
M ($C_{42}H_{84}O_{12}$) = 781.1092 g/mol;

TLC (SiO_2, DCM:MeOH = 9.5:0.5): R_f =0.22;

Melting point (DSC): 57.3 °C;

^{1}H-NMR (500 MHz, CDCl$_3$): δ [ppm] = 4.61 (d, ^3J = 4.36 Hz, 1H; 5-OH), 4.52 – 4.57 (m, 2H; 2-OH and 6-OH), 4.42 (d, ^3J = 4.71 Hz, 1H; 2-OH), 3.86 (m, 1H; 2-H), 3.71 – 3.80 (m, 2H; 1'-H), 3.55 – 3.67 (m, 2H; 1'-H), 3.42 – 3.54 (m, 21H; 6-H and 10 OCH$_2$ of triethylene oxide chains), 3.33 – 3.36 (m, 4H; 2 1^{iv}-H), 3.16 – 3.22 (m, 2H; 3-H and 4-H), 2.98 – 3.03 (m, 1H; 5-H), 2.96 (t, 1H, ^3J = 9.66 Hz; 1-H), 1.42 – 1.51 (m, 4H; 2 2^{iv}-H), 1.17 – 1.31 (m, 36H; 18 CH$_2$ of dodecyl chains), 0.85 (t, ^3J = 6.75 Hz, 6H; 2 12^{iv}-H);

^{13}C-NMR (125 MHz, CDCl$_3$): δ [ppm] = 82.39 (d; C-4), 80.26 (d; C-1), 74.62 (d; C-5), 71.87 (d; C-6), 71.00 (d; C-3), 70.02 (t; 2 C-1^{iv}), 70.87, 70.25, 69.98, 69.71, 69.55, 69.39, 68.42 (7t; 12 OCH$_2$ of triethylene oxide chains), 69.34 (d; C-2), 31.25, 29.14, 28.97, 28.83, 28.67, 25.59, 22.05 (7t; 20 CH$_2$ of dodecyl chains), 13.91 (q, 2 C-12^{iv});

FT-IR (ATR) $\tilde{v}$ [cm^{-1}] = 3428 (br, m), 2919 (s), 2851 (s), 1734 (w), 1663 (w), 1465 (m), 1350 (w), 1297 (w), 1112 (br, s), 1033 (w), 942 (w), 887 (w), 720 (m);

MS (positive ESI) m/z (%): 803.58 (100) [M+Na]$^+$, 781.58 (20);

HR-MS (ESI) calc. for $C_{42}H_{84}O_{12}Na$ [M+Na]$^+$: 803.586; found: 803.586.

7.2.21. Synthesis of 2,5-bis-*O*-[2'-[2''-[2'''-(dodecyloxy)ethoxy]ethoxy]ethyl]-1,6:3,4-bis-*O*-(2',3'-methoxybutane-2',3'-diyl)-*myo*-inositol (43)
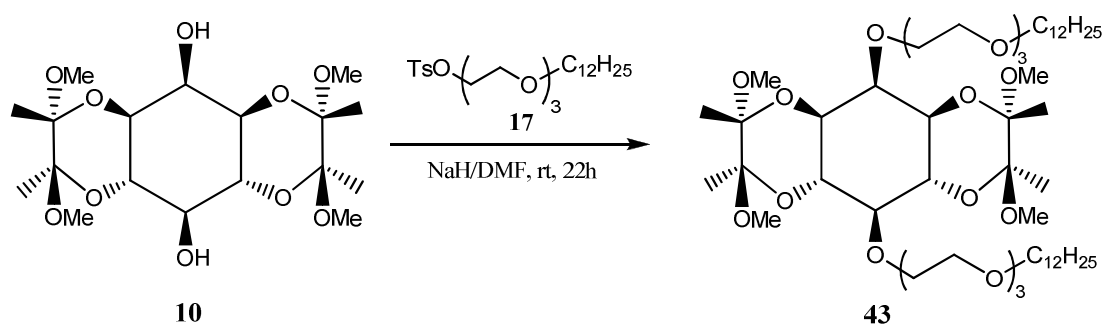
1 g (2.45 mmol) of derivative **10** were dissolved into a suspension of 0.24 g (4.90 mmol) NaH (in 55-65% mineral oil) in 50 ml dry DMF and the mix was stirred for 15 min at 0°C under argon atmosphere. 1.8 g (3.81 mmol) of tosylate **17** were added dropwise, and the reaction mixture was stirred under argon for additional 22 h at r.t. The crude mix was poured onto 100 ml ice-water and 25 ml brine were added. After extraction with EtOAc (3 x 50 ml) the combined organic fractions were dried over MgSO₄, filtrated, concentrated and dried under vacuum. The crude product was purified by flash chromatography (silica, CyHex:EtOAc = 3:1). Compound **43** was obtained as a yellow oil (1.234 g, 1.22 mmol, 50%).

43
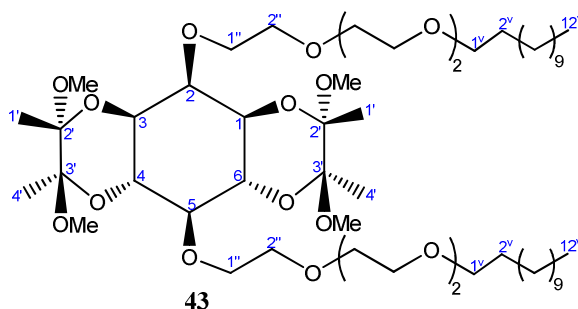
M ($C_{54}H_{104}O_{16}$) = 1009.3940 g/mol;

^{1}H-NMR (500 MHz, CDCl₃): δ [ppm] = 3.96 – 4.01 (m, 2H; 4-H and 6-H), 3.90 – 3.94 (m, 2H; 1''-H), 3.87 (t, ^3J = 5.18 Hz, 2H; 1''-H), 3.76 – 3.80 (m, 2H; 2''-H), 3.55 – 3.71 (m, 19H; 2-H and 9 OCH₂ of triethylene oxide chains), 3.41 – 3.49 (m, 6H; 1-H, 3-H and 2 1^v-H), 3.30 (t, ^3J = 9.32 Hz, 1H; 5-H), 3.22 – 3.26 (m, 12H; 2 2'-OCH₃ and 2 3'-OCH₃), 1.52 – 1.61 (m, 4H; 2 2^v-H), 1.19 – 1.34 (m, 48H; 2 1'-H , 2 4'-H and 18 CH₂ of dodecyl chains), 0.88 (t, ^3J = 6.92 Hz, 6H; 2 12^v-H);

^{13}C-NMR (125 MHz, CDCl₃): δ [ppm] = 99.48, 98.90 (2s; 2 C-2' and 2 C-3'), 79.02 (d; C-5), 77.15 (d; C-2), 72.69, 72.45 (2t; 2 OCH₂ of triethylene oxide chain), 71.55, 71.54 (2t; C-1^v), 70.90, 70.83, 70.70, 70.64, 70.57, 70.56, 70.51, 70.46, 70.34, 70.02 (10t; 10 OCH₂ of triethylene oxide chain), 69.56 (d; C-4 and C-6), 69.07 (d; C-1 and C-3), 47.88, 47.75 (2q; 2 2'-OCH₃ and 2 3'-OCH₃), 31.91, 29.66, 29.64, 29.63, 29.61, 29.51, 29.49, 29.35, 28.08, 22.68 (10t; 20 CH₂ of dodecyl chains), 17.85, 17.62 (2q; 2 C-1' and 2 C-4'), 14.13 (q; 2 C-12^v);
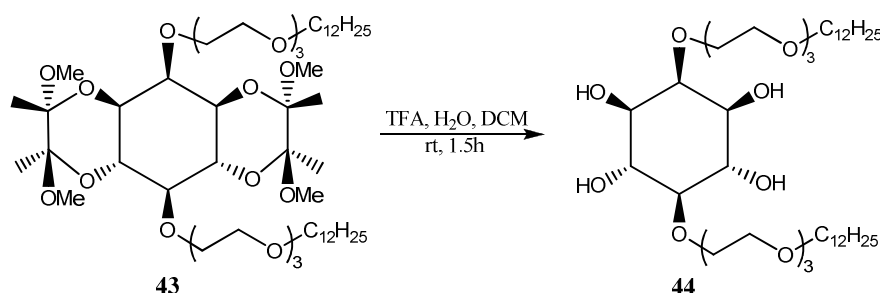
FT-IR (ATR) $\tilde{v}$ [cm^{-1}] = 2920 (s), 2851 (s), 1457 (m), 1373 (m), 1296 (w), 1247 (w), 1212 (w), 1182 (w), 1111 (br s), 1035 (s), 950 (m), 917 (m), 882 (m), 846 (m), 781 (w), 755 (w), 731 (w), 673 (w), 641 (w);

MS (positive ESI) m/z (%): 1031.70 (100) [M+Na]$^+$, 881.72 (10), 731.43 (12), 641.49 (38), 373.14 (3);

**HR-MS** (ESI) calc. for $C_{54}H_{104}O_{16}Na$ $[M+Na]^+$: 1031.722; found: 1031.725;

EA: calc: 64.25% C; 10.39% H; found:64.37% C; 10.44% H.

7.2.21. Synthesis of 2,5-bis-*O*-[2'-[2''-[2'''-(dodecyloxy)ethoxy]ethoxy]ethyl]-*myo*-inositol (44)

To a solution of 1.2 g (1.2 mmol) **43** in 10 ml DCM was added a solution of 5 ml (7.4 g, 64.9 mmol) trifluoroacetic acid (TFA) in 1 ml water and the mixture was stirred at r.t. for 1.5 h. After evaporation of solvents, 3 x 30 ml of CHCl₃ were added and again evaporated. The crude product was purified by recrystallization from MeOH.

The tetrol **44** was obtained as a white solid (0.490 g, 0.63 mmol, 53%).
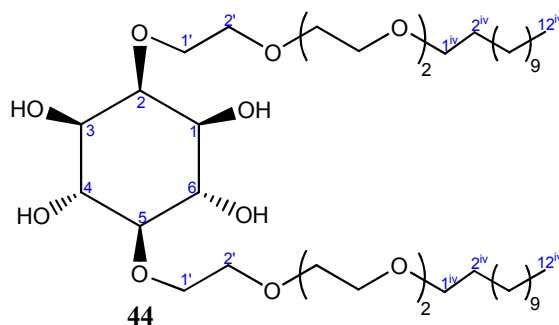
M ($C_{42}H_{84}O_{12}$) = 781.1092 g/mol;

TLC (SiO_2, DCM: MeOH = 15:1): R_f =0.24;

Melting point (DSC): 108.8 °C;

¹H-NMR (500 MHz, DMSO-d₆): δ [ppm] = 4.56 (d, ^3J = 4.47 Hz, 2H; 4-OH and 6-OH), 4.46 (d, ^3J = 5.69 Hz, 2H; 1-OH and 3-OH), 3.76 (dd, ^3J = 5.73 Hz, ^3J = 11.16 Hz, 4H; 2 1'-H), 3.44 – 3.52 (m, 21 H; 10 OCH₂ of triethylene oxide chain and 2-H), 3.34 – 3.40 (m, 6H; 4-H, 6-H and 2 1ⁱᵛ-H), 3.17 – 3.20 (m, 2H; 1-H and 3-H), 2.78 (t, 1H, ^3J = 9.10 Hz; 5-H), 1.42 –

1.50 (m, 4H; 2 2^{iv}-H), 1.18 – 1.30 (m, 36 H; 18 CH_2 of dodecyl chains), 0.85 (t, ^3J = 6.75 Hz, 6H; 2 12^{iv}-H);

^{13}C-NMR (125 MHz, DMSO-d_6): δ [ppm] = 84.60 (d; C-5), 82.34 (d; C-2), 72.48 (d; C-4 and C-6), 72.14 (t; C-1'), 71.73 (d; C-1 and C-3), 70.91 (t; C-1'), 70.25 (t; 2 C-1^{iv}), 70.02, 69.95, 69.71, 69.69, 69.64, 69.58, 69.39 (7t; 10 OCH_2 of triethylene oxide chains), 31.25, 29.15, 28.98, 28.84, 28.68, 25.60, 22.06 (7t; 20 CH_2 of dodecyl chains), 13.92 (q; 2 C-12^{iv});
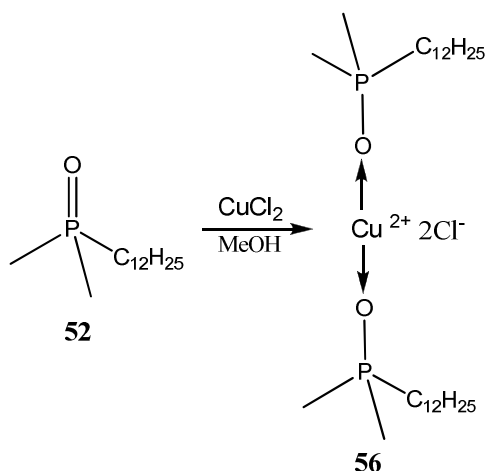
FT-IR (ATR) $\tilde{v}$ [cm^{-1}] = 3338 (br s), 2916 (s), 2849 (s), 1466 (m), 1369 (m), 1310 (w), 1290 (w), 1246 (w), 1126 (br s), 1033 (s), 960 (w), 926 (w), 880 (w), 719 (s);

MS (positive ESI) m/z (%): 803.41 (100) [M+Na]$^+$, 781.43 (18), 319.25 (10);

HR-MS (ESI) calc. for $C_{42}H_{84}O_{12}Na$ [M+Na]$^+$: 803.586; found: 803.586.

## 7.3. Studies towards the synthesis of phosphine oxide metal complexes

7.3.1. Synthesis of complex $C_{12}DMPO$: copper (II) chloride (56)

A solution of 0.264 g (1.073 mmol) $C_{12}DMPO$ (**52**) in 4 ml methanol was mixed with a solution of 0.072 g (0.54 mmol) $CuCl_2$ in 2 ml methanol when a green mixture formed. After stirring for 30 min at r. t., the solvent was evaporated to dryness. Resulting green crystalline solid was used for investigations without further purification.

Melting point (DSC): 53.4 °C;

FT-IR (ATR) $\tilde{v}$ [cm^{-1}] = 2920 (s), 2851 (s), 1464 (m), 1293 (m), 1108 (br s), 946 (s), 865 (m).
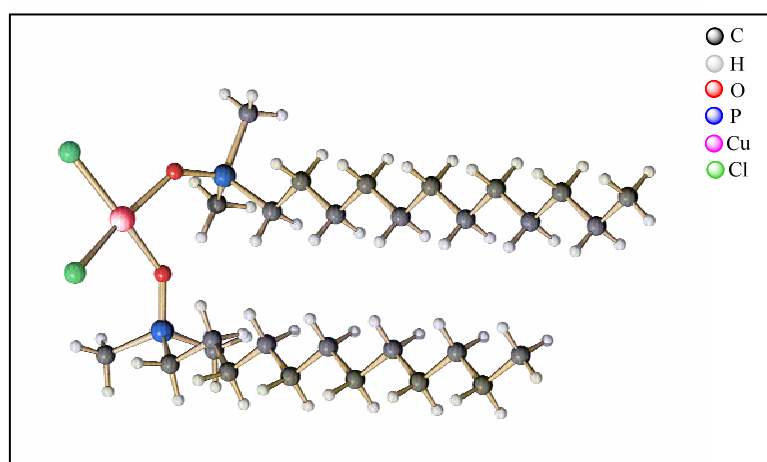

Fig. 7.1. Crystal structure of **56**

Table 7.1. Crystal data for complex $C_{12}DMPO:CuCl_2$ (**56**)

Identification code	gc43
Empirical formula	$C_{28}H_{62}O_2P_2Cl_2Cu$
Formula weight	627.16
Temperature	100(2) K
Wavelength	0.71073Å
Crystal system, space group	triclinic, P-1
Unit cell dimensions	a = 8.314(2) Å α = 80.897(7)°
	b = 9.337(2) Å β= 85.101(9)°
	c = 23.665(6) Å γ = 72.388(7)°
Volume	1727.4(7) A^3
Z, Calculated density	2, 1.206 Mg/m^3
Absorption coefficient	0.901 mm^{-1}
F(000)	678
Crystal size	0.3 x 0.2 x 0.06 mm
Crystal Colour	green
Crystals from	Melt
Theta range for data collection	0.87 to 26.99°
Limiting indices	-10<=h<=10, -11<=k<=11, -28<=l<=30
Reflections collected / unique	7705 / 6144 [R(int) = 0.0726]
Reflection observed [I>2sigma(I)]	3266
Completeness to theta = 26.99	81.50%
Absorption correction	None
Refinement method	Full-matrix least-squares on F^2
Data / restraints / parameters	6144 / 0 / 322
Goodness-of-fit on F^2	0.967
Final R indices [I>2sigma(I)]	R1 = 0.0669, wR2 = 0.1489
R indices (all data)	R1 = 0.1453, wR2 = 0.1847
Largest diff. peak and hole	0.538 and -1.010 e. $Å^{-3}$

7.3.2. Synthesis of complex C₁₂DMPO : copper (II) sulphate (57)


52   **57**
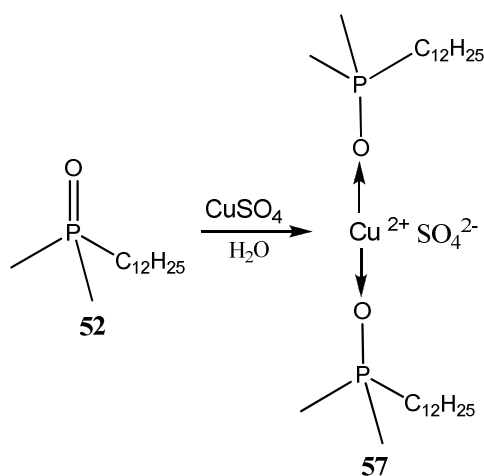
A solution of 0.246 g (1.00 mmol) C$_{12}$DMPO (**52**) in 7 ml water was mixed with a solution of 0.079 g (0.5 mmol) CuSO$_4$ in 3 ml water when a blue mixture formed. After stirring for 1 hour at r. t., the solvent was evaporated to dryness. Resulting light blue crystalline solid was used for investigations without further purification.

Melting point (DSC): 51.1 °C;

FT-IR (ATR) $\tilde{v}$ [cm^{-1}] = 3377 (br m), 2914 (s), 2846 (s), 1658 (w), 1285 (m), 1157 (s), 942 (m), 867 (m), 745 (m).

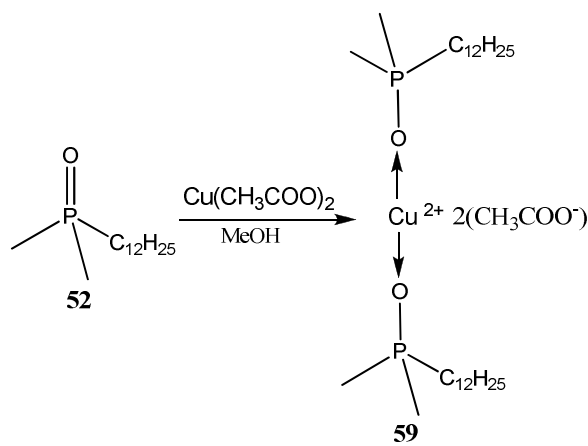### 7.3.3. Synthesis of complex C₁₂DMPO : copper (II) bromide (58)

52   **58**
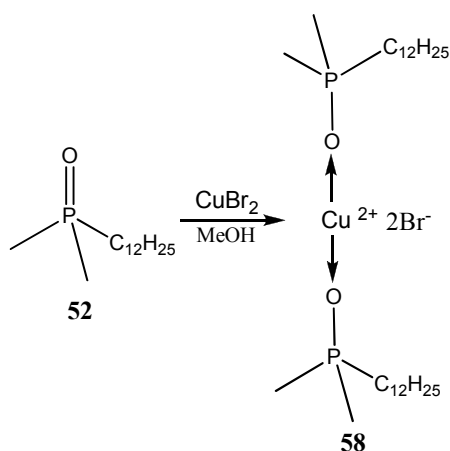
A solution of 0.123 g (0.50 mmol) C$_{12}$DMPO (**52**) in 4 ml methanol was mixed with a solution of 0,079 g (0.25 mmol) CuBr$_2$ in 3 ml methanol when a brown mixture formed. After

stirring for 1 hour at r. t., the solvent was evaporated to dryness. Resulting brown crystalline solid was used for investigations without further purification.

Melting point (DSC): 48.9 °C;

FT-IR (ATR) $\tilde{\upsilon}$ [cm^{-1}] = 2918 (s), 2850 (s), 1465 (w), 1292 (m), 1110 (br s), 946 (m), 866 (m), 753 (w).

7.3.4. Synthesis of complex C$_{12}$DMPO : copper (II) acetate (59)

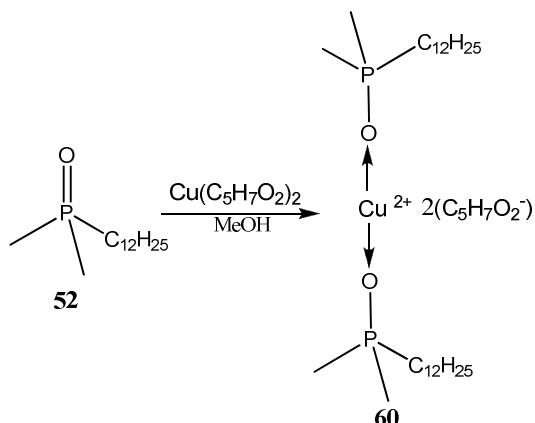A solution of 0.123 g (0.50 mmol) C$_{12}$DMPO (**52**) in 3 ml methanol was mixed with a solution of 0.045 g (0.25 mmol) Cu(CH$_3$COO)$_2$ in 10 ml methanol when a blue-green mixture formed. After stirring for 1 hour at r. t., the solvent was evaporated to dryness. Resulting blue-green crystalline solid was used for investigations without further purification.

Melting point (DSC): 82.3 °C;

FT-IR (ATR) $\tilde{\upsilon}$ [cm^{-1}] = 3416 (br w), 2915 (s), 2846 (s), 1619 (s), 1426 (m), 1285 (m), 1157 (s), 942 (m), 867 (m), 745 (w), 681 (w).

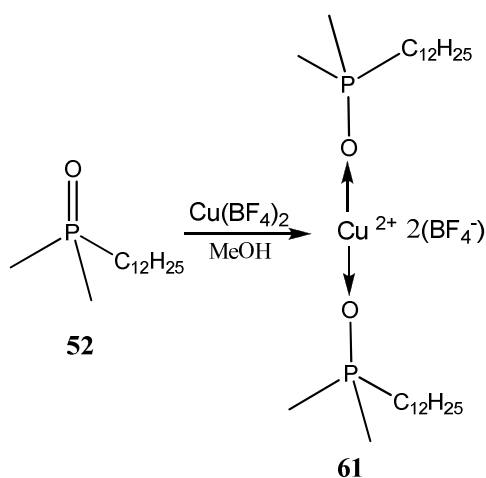### 7.3.5. Synthesis of complex C$_{12}$DMPO : copper (II) acetylacetonate (60)

A solution of 0.123 g (0.50 mmol) C$_{12}$DMPO (**52**) in 3 ml methanol was mixed with a solution of 0.065 g (0.25 mmol) Cu(C$_5$H$_7$O$_2$)$_2$ in 12 ml methanol when a grey mixture formed. After stirring for 2 hours at r. t., the solvent was evaporated to dryness. Resulting blue-grey crystalline solid was used for investigations without further purification.

Melting point (DSC): 81.4 °C;

FT-IR (ATR) $\tilde{\nu}$ [cm^{-1}] = 2913 (m), 2846 (m), 1575 (s), 1552 (m), 1524 (s), 1465 (w), 1411 (w), 1353 (w), 1285(w), 1274 (w), 1158 (s), 1021 (w), 936 (w), 867 (m), 779 (m), 745 (w), 686 (w).

7.3.6. Synthesis of complex C$_{12}$DMPO : copper (II) borofluorate (61)
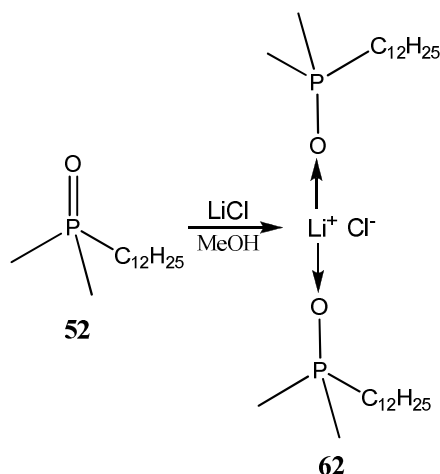
A solution of 0.123 g (0.50 mmol) C_{12}DMPO (**52**) in 3 ml methanol was mixed with a solution of 0.060 g (0.25 mmol) Cu(BF$_4$)$_2$ in 5 ml methanol when a blue mixture formed. After stirring for 1 hour at r. t., the solvent was evaporated to dryness. Resulting light blue crystalline solid was used for investigations without further purification.

Melting point (DSC): see Table 4.1, chapter 4: Results and discussion II;

FT-IR (ATR) $\tilde{v}$ [cm^{-1}] = 3300 (br m), 2920 (s), 2851 (m), 1636 (w), 1464 (m), 1309 (m), 1020 (br s), 948 (m), 868 (m), 761 (w).

7.3.7. Synthesis of complex C_{12}DMPO : lithium chloride (62)

A solution of 0.123 g (0.50 mmol) C_{12}DMPO (**52**) in 3 ml methanol was mixed with a solution of 0.010 g (0.25 mmol) LiCl in 3 ml methanol. After stirring for 1 hour at r. t., the solvent was evaporated to dryness under high vacuum. Resulting colourless solid was used for investigations without further purification.

Melting point (DSC): 115.9°C;

FT-IR (ATR) $\tilde{v}$ [cm^{-1}] = 3373 (br s), 2919 (s), 1850 (s), 1638 (br m), 1465 (m), 1296 (m), 1132 (br s), 944 (s), 865 (m).
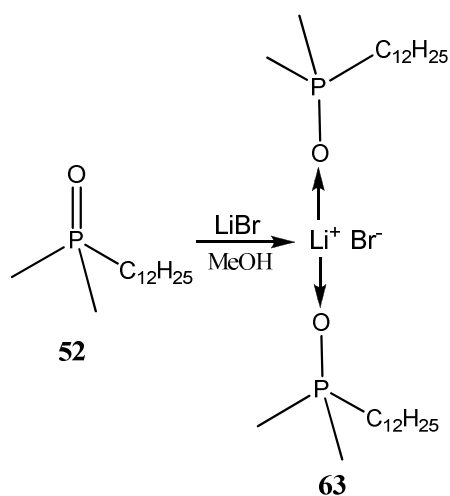
7.3.8. Synthesis of complex C₁₂DMPO : lithium bromide (63)

A solution of 0.123 g (0.50 mmol) C$_{12}$DMPO (**52**) in 3 ml methanol was mixed with a solution of 0.022 g (0.25 mmol) LiBr in 3 ml methanol. After stirring for 2 hours at r. t., the solvent was evaporated to dryness. Resulting colourless solid was used for investigations without further purification.

Melting point (DSC): 69.9 °C;

FT-IR (ATR) $\tilde{v}$ [cm^{-1}] = 3421 (m), 3336 (m), 2917 (s), 2848 (s), 1627 (w), 1466 (m), 1296 (m), 1161 (s), 1140 (s), 945 (m), 868 (m), 729 (w), 720 (w).

7.3.9. Synthesis of complex C₁₂DMPO : sodium choride (64)

A solution of 0.123 g (0.50 mmol) C_{12}DMPO (**52**) in 3 ml water was mixed with a solution of 0.146 g NaCl (0.25 mmol) in 4 ml water. After stirring for 2 hours at r. t., the solvent was evaporated to dryness. Resulting colourless solid was used for investigations without further purification.

Melting point (DSC): 81.0 °C;

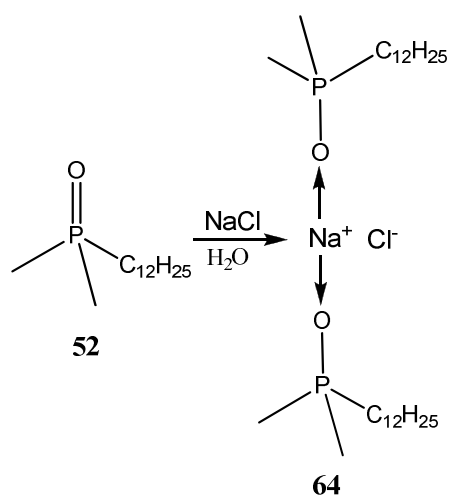**FT-IR** (ATR) $\tilde{\nu}$ [cm^{-1}] = 2915 (s), 2846 (s), 1464 (m), 1285 (m), 1157 (s), 942 (m), 868 (m), 745 (m).

7.4. Surface tension measurements

7.4.1. Surface tension measurements for *rac*-26 (4-C$_{12}$E$_3$I$_1$)

A 100 ml stock solution of 6.958×10^{-4} M was prepared from 33.6 mg of *rac*-26 (4-C$_{12}$E$_3$I$_1$) and water. For each measurement 20 ml of solution were taken out and the volumetric flask was refilled with Milli-Q water, therefore every new solution had a dilution factor of 0.8. From the 20 ml solution, 5 ml were used to rinse the measurements vessel and 15 ml were used for experiment. Necessary glassware was previously cleaned with Deconex (surfactant free solution) and was rinsed thoroughly with Milli-Q water. The same type of water was used for solutions and its purity was checked by measuring the surface tension σ over a long period of time ($\sigma = 72.8$ mN m^{-1} at 20 °C). All measurements were carried out at an ambient temperature of 20 ± 1 °C.

Experimental data are presented in table 7.2.

Table 7.2. Experimental data for surface tension measurements of *rac*-26 (4-C$_{12}$E$_3$I$_1$)

Sample	c/mol l^{-1}	σ/mN m^{-1}	Sample	c/mol l^{-1}	σ/mN m^{-1}
1	6.958×10^{-4}	33.72	18	1.566×10^{-5}	50.66
2	5.566×10^{-4}	33.65	19	1.253×10^{-5}	52.63
3	4.453×10^{-4}	33.72	20	1.003×10^{-5}	53.51
4	3.562×10^{-4}	33.73	21	8.022×10^{-6}	55.52
5	2.850×10^{-4}	33.73	22	6.417×10^{-6}	57.25
6	2.280×10^{-4}	33.70	23	5.134×10^{-6}	58.60
7	1.824×10^{-4}	33.75	24	4.107×10^{-6}	60.23
8	1.459×10^{-4}	33.91	25	3.286×10^{-6}	61.53
9	1.167×10^{-4}	34.29	26	2.628×10^{-6}	63.44
10	9.339×10^{-5}	35.93	27	2.103×10^{-6}	64.79
11	7.471×10^{-5}	37.96	28	1.682×10^{-6}	65.21
12	5.977×10^{-5}	39.60	29	1.346×10^{-6}	66.47
13	4.781×10^{-5}	41.75	30	1.076×10^{-6}	67.31
14	3.825×10^{-5}	43.57	31	8.613×10^{-7}	68.50
15	3.060×10^{-5}	45.20	32	6.891×10^{-7}	68.67
16	2.448×10^{-5}	46.85	33	5.512×10^{-7}	70.47
17	1.956×10^{-5}	48.89	34	4.409×10^{-7}	71.05
			35	3.527×10^{-7}	71.88

7.4.2. Surface tension measurements for *rac*-32 (1-C$_{12}$I$_1$E$_3$)

A 100 ml stock solution of 6.875 x 10^{-4} M was prepared from 33.0 mg of *rac*-32 (1-C$_{12}$I$_1$E$_3$) and Milli-Q water. For each measurement 20 ml of solution were taken out and the volumetric flask was refilled with Milli-Q water, therefore every new solution had a dilution factor of 0.8. From the 20 ml solution, 5 ml were used to rinse the measurements vessel and 15 ml were used for experiment. Necessary glassware was previously cleaned with Deconex (surfactant free solution) and was rinsed thoroughly with Milli-Q water. The same type of water was used for solutions and its purity was checked by measuring the surface tension σ over a long period of time (σ = 72.8 mN m^{-1} at 20 °C). All measurements were carried out at an ambient temperature of 20 ± 1 °C.

Experimental data are presented in table 7.3.

Table 7.3. Experimental data for surface tension measurements of *rac*-32 (1-C$_{12}$I$_1$E$_3$)

Sample	c/mol l^{-1}	σ/mN m^{-1}	Sample	c/mol l^{-1}	σ/mN m^{-1}
1	6.875 x 10^{-4}	35.10	16	2.418 x 10^{-5}	56.63
2	5.500 x 10^{-4}	35.10	17	1.935 x 10^{-5}	58.23
3	4.400 x 10^{-4}	34.75	18	1.548 x 10^{-5}	59.79
4	3.520 x 10^{-4}	34.68	19	1.238 x 10^{-5}	60.86
5	2.816 x 10^{-4}	36.80	20	9.908 x 10^{-6}	61.78
6	2.253 x 10^{-4}	39.25	21	7.926 x 10^{-6}	63.31
7	1.802 x 10^{-4}	40.83	22	6.341 x 10^{-6}	63.96
8	1.422 x 10^{-4}	42.90	23	5.072 x 10^{-6}	65.90
9	1.153 x 10^{-4}	44.63	24	4.058 x 10^{-6}	67.41
10	9.228 x 10^{-5}	46.53	25	3.246 x 10^{-6}	67.92
11	7.382 x 10^{-5}	48.52	26	2.597 x 10^{-6}	68.54
12	5.905 x 10^{-5}	50.43	27	2.077 x 10^{-6}	69.15
13	4.724 x 10^{-5}	51.84	28	1.662 x 10^{-6}	69.91
14	3.780 x 10^{-5}	53.58	29	1.329 x 10^{-6}	70.37
15	3.023 x 10^{-5}	54.82	30	1.063 x 10^{-6}	70.67
			31	8.510 x 10^{-7}	70.07

7.5. DOSY measurements

7.5.1. DOSY measurements for *rac*-19 (1-C$_{12}$E$_3$I$_1$)

A 10 ml stock solution of 0.85 10^{-3} M was prepared from 4.08 mg of *rac*-19 (1-C$_{12}$E$_3$I$_1$) and pure water. For each measurement 4 ml of solution were taken out and the volumetric flask was refilled with water therefore every new solution had a dilution factor of 0.6.

For experiment, 1 ml of solution was used for rinsing the NMR tube and 0.5 ml were used for measurements. The stem coaxial insert of the NMR tube was filled with 0.1 ml D$_2$O and it was used for all measurements. Samples were sealed with parafilm and allowed to equilibrate for at least 12 hours before measurement. For every sample were recorded first a standard ^{1}H-NMR, afterwards two 1D ^{1}H-NMR experiments with water suppression using the pulse sequence: stebpgpes1s1d.sek (with 2% and 95% gradient strength) and one 2D DOSY experiment with the pulse sequence stebpges1s.sek. All measurements were carried out at 25°C. Details about concentration, results and experimental parameters are presented in Table 7.4.

Table 7.4. Experimental data for *rac*-19 (1-C$_{12}$E$_3$I$_1$); TD (F$_1$) = 8k, TD (F$_2$) = 32, NS = 256

c/mM	c/cmc	$D/10^{-10}$ m^{2}s^{-1}	Δ/ms	δ/ms
0.85	6.0	1.098	100	1.5
0.51	3.6	1.551	100	1.5
0.3	2.1	1.904	50	2.0
0.18	1.2	2.828	50	1.5
0.11	0.8	3.793	50	1.3

$\Delta D = \pm 0.008 \div \pm 0.09$ (the error increases with decreases of c)

7.5.2. DOSY measurements for *rac*-32 (1-C$_{12}$I$_1$E$_3$)

A 10 ml stock solution of 2.21 10^{-3} M was prepared from 10.61 mg of *rac*-32 (1-C$_{12}$I$_1$E$_3$) and pure water. For each measurement 4 ml of solution were taken out and the volumetric flask was refilled with water, therefore every new solution had a dilution factor of 0.6.

For experiment, 1 ml of solution was used for rinsing the NMR tube and 0.5 ml were used for measurements. The stem coaxial insert of the NMR tube was filled with 0.1 ml D$_2$O and it was used for all measurements. Samples were sealed with parafilm and allowed to equilibrate for at least 12 hours before measurement. For every sample were recorded first a standard ^{1}H-NMR, afterwards two 1D ^{1}H-NMR experiments with water suppression using the pulse sequence: stebpgpes1s1d.sek (with 2% and 95% gradient strength) and one 2D DOSY

experiment with the pulse sequence stebpges1s.sek. All measurements were carried out at 25°C. Details about concentration, results and experimental parameters are presented in Table 7.5.

Table 7.5. Experimental data for *rac* **28** (1-C$_{12}$I$_1$E$_3$); TD (F$_1$) = 8k, TD (F$_2$) = 32, NS = 256

c/mM	c/cmc	$D/10^{-10}$ m^{2}s^{-1}	Δ/ms	δ/ms
2.21	5.9	1.235	100	1.5
1.32	3.6	1.565	100	1.5
0.80	2.1	2.101	50	1.7
0.47	1.2	3.118	50	1.5
0.28	0.8	3.639	50	1.3

$\Delta D = \pm 0.007 \div \pm 0.04$ (the error increases with decreases of c)

7.5.3. DOSY measurements for *n*-dodecyl hexaethylene oxide (C$_{12}$E$_6$)

A 10 ml stock solution of 0.79 10^{-3} M was prepared from 3.57 mg of *n*-dodecyl hexaethylene oxide (C$_{12}$E$_6$) and pure water. For each measurement 4 ml of solution were taken out and the volumetric flask was refilled with water therefore every new solution had a dilution factor of 0.6.

For experiment, 1 ml of solution was used for rinsing the NMR tube and 0.5 ml were used for measurements. The stem coaxial insert of the NMR tube was filled with 0.1 ml D$_2$O and it was used for all measurements. Samples were sealed with parafilm and allowed to equilibrate for at least 12 hours before measurement. For every sample were recorded a standard ^{1}H-NMR, two 1D ^{1}H-NMR experiments with water suppression using the pulse sequence stebpgpes1s1d.sek (with 2% and 95% gradient strength) and one 2D DOSY experiment with the pulse sequence stebpges1s.sek. All measurements were carried out at 25 °C. Details about concentration, results and experimental parameters are presented in Table 7.6.

Table 7.6. Experimental data for *n*-dodecyl hexaethylene oxide (C$_{12}$E$_6$); TD (F$_1$) = 8k, TD (F$_2$) = 32, NS = 256

c/mM	c/cmc	$D/10^{-10}$ m^{2}s^{-1}	Δ/ms	δ/ms
0.79	8.8	1.048	100	1.7
0.47	5.2	1.224	100	1.5
0.28	3.1	1.606	100	1.5
0.17	1.9	2.316	60	1.5
0.10	1.1	3.527	50	1.4
0.06	0.7	4.894	50	1.1

$\Delta D = \pm 0.004 \div \pm 0.07$ (the error increases with decreases of c)

7.5.4. DOSY measurements for *n*-dodecyl-β-maltoside (β-$C_{12}G_2$)

A 10 ml stock solution of 1.01 10^{-3} M was prepared from 5.15 mg of *n*-dodecyl-β-maltoside (β-$C_{12}G_2$) and pure water. For each measurement 4 ml of solution were taken out and the volumetric flask was refilled with water, therefore every new solution had a dilution factor of 0.6.

For experiment, 1 ml of solution was used for rinsing the NMR tube and 0.5 ml were used for measurements. The stem coaxial insert of the NMR tube was filled with 0.1 ml D_2O and it was used for all measurements. Samples were sealed with parafilm and allowed to equilibrate for at least 12 hours before measurement. For every sample were recorded a standard ^{1}H-NMR, two 1D ^{1}H-NMR experiments with water suppression using the pulse sequence: stebpgpes1s1d.sek (with 2% and 95% gradient strength) and one 2D DOSY experiment with the pulse sequence: stebpges1s.sek. All measurements were carried auto at 25 °C. Details about concentration, results and experimental parameters are presented in Table 7.7.

Table 7.7. Experimental data for *n*-dodecyl-β-maltoside (β-$C_{12}G_2$); TD (F_1) = 8k, TD (F_2) = 32, NS = 256

c/mM	c/cmc	D/10^{-10} m^2s^{-1}	Δ/ms	δ/ms
1.01	6.3	1.306	100	1.6
0.6	3.8	1.698	50	1.9
0.36	2.2	2.225	50	1.6
0.21	1.3	3.476	50	1.5
0.13	0.8	3.858	50	1.3

$\Delta D = \pm 0.006 \div \pm 0.09$ (the error increases with decreases of *c*)

The pulse sequence **stebpgpes1s1d.sek**:
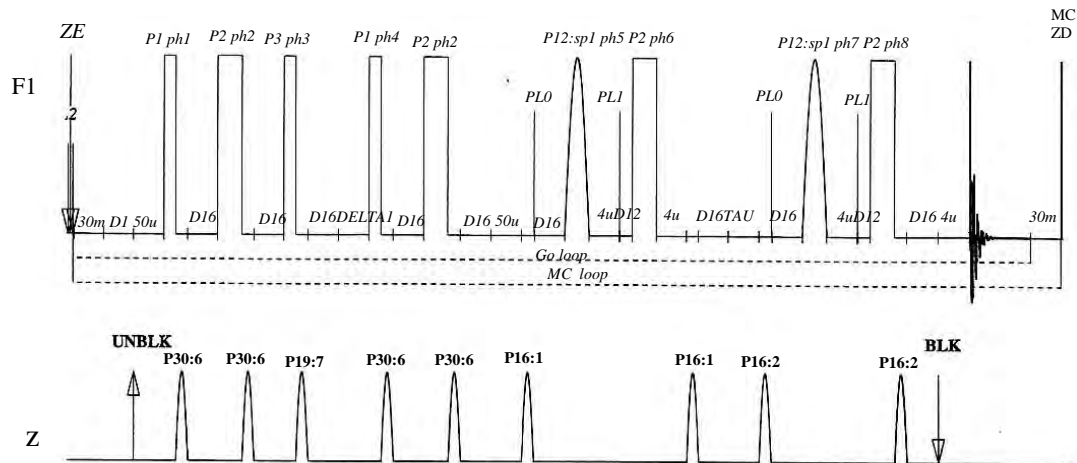
The pulse program used for diffusion experiments with water suppression is following:

;stebpgpes1s1d
;avance-version (07/05/08)
;1D sequence for diffusion measurement using stimulated echo
;using bipolar gradient pulses for diffusion
;using 1 spoil gradient
;water suppression using excitation sculpting with gradients
;T.-L. Hwang & A.J. Shaka, J. Magn. Reson., Series A 112 275-279 (1995)
;$CLASS=HighRes
;$DIM=1D
;$TYPE=
;$SUBTYPE=
;$COMMENT=
prosol relations=<triple>
#include <avance.incl>
#include <Grad.incl>
#include <Delay.incl>
"p2=p1*2"
"d12=20u"
"TAU=de+p1*2/3.1416+50u"
"DELTA1=d20-p1*2-p2-p30*2-d16*3-p19"
1 ze
2 30m
 d1
 50u UNBLKGRAD
 p1 ph1
 p30:gp6
 d16
 p2 ph2
 p30:gp6*-1
 d16

```
 p1 ph3
 p19:gp7
 d16
 DELTA1
 p1 ph4
 p30:gp6
 d16
 p2 ph2
 p30:gp6*-1
 d16
 50u
 p16:gp1
 d16 pl0:f1
 (p12:sp1 ph5:r):f1
 4u
 d12 pl1:f1
 p2 ph6
 4u
 p16:gp1
 d16
 TAU
 p16:gp2
 d16 pl0:f1
 (p12:sp1 ph7:r):f1
 4u
 d12 pl1:f1
 p2 ph8
 p16:gp2
 d16
 4u BLKGRAD
 go=2 ph31
 30m mc #0 to 2 F0(zd)
exit
ph1= 0
ph2= 0 0 0 0  2 2 2 2
ph3= 0 0 0 0  0 0 0 0  2 2 2 2  2 2 2 2
ph4= 0 1 2 3
ph5= 0 0 0 0  1 1 1 1
ph6= 2 2 2 2  3 3 3 3
ph7= 0 0 0 0  0 0 0 0 1 1 1 1 1 1 1 1
ph8= 2 2 2 2  2 2 2 2 3 3 3 3 3 3 3 3
ph31=0 3 2 1  2 1 0 3
;pl0 : 120dB
;pl1: f1 channel - power level for pulse (default)
;p1 : f1 channel -  90 degree high power pulse
;p2 : f1 channel - 180 degree high power pulse
;sp1 : f1 channel - shaped pulse 180 degree
;p12: f1 channel - 180 degree shaped pulse (Squa100.1000) [2 msec]
;p16: homospoil/gradient pulse
;p19: gradient pulse 2 (spoil gradient)
;p30: gradient pulse (little DELTA * 0.5)
```
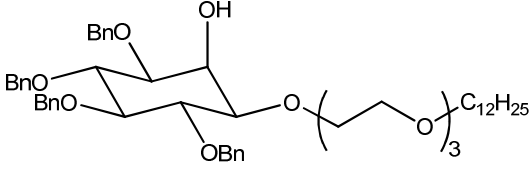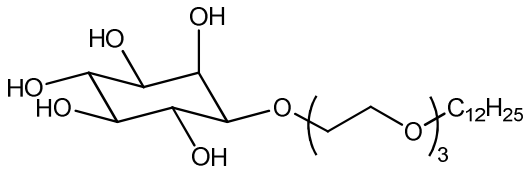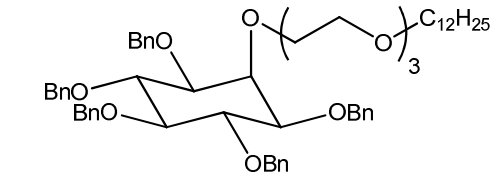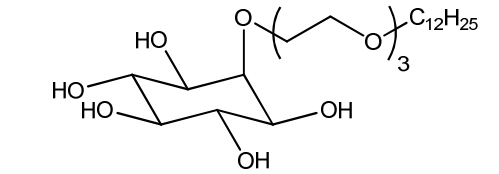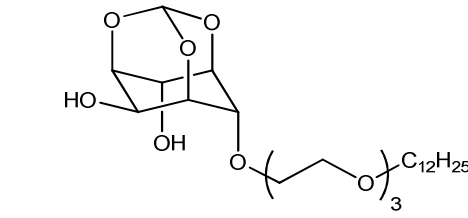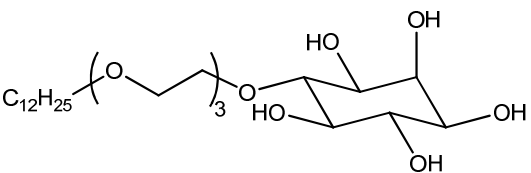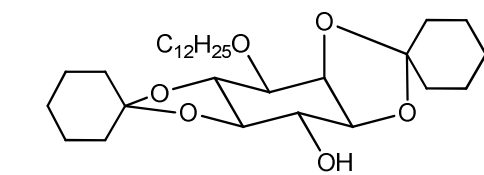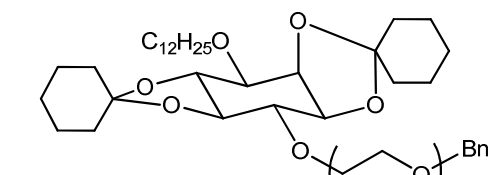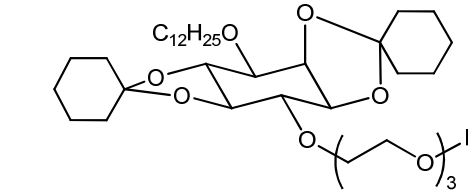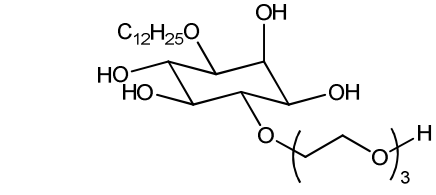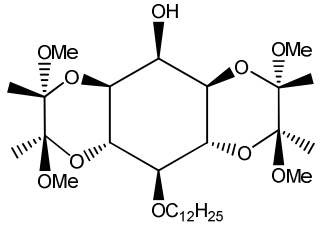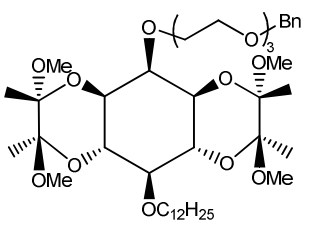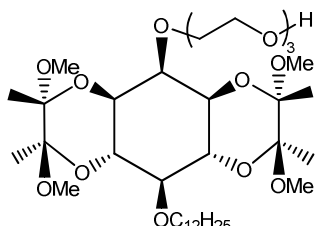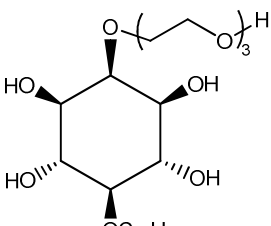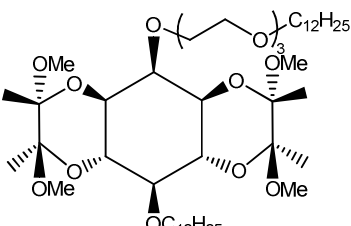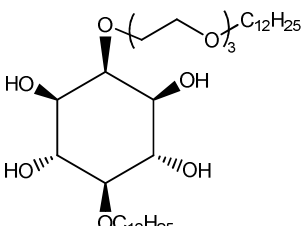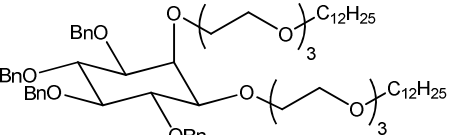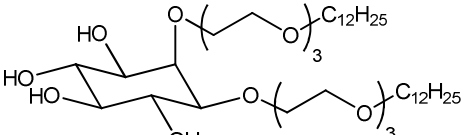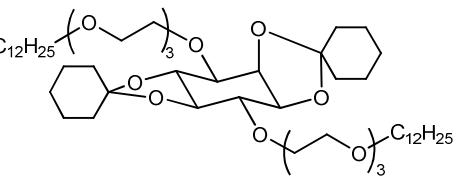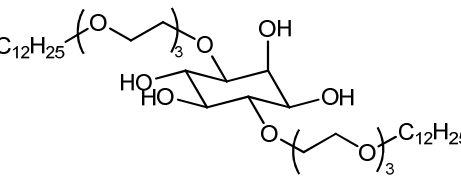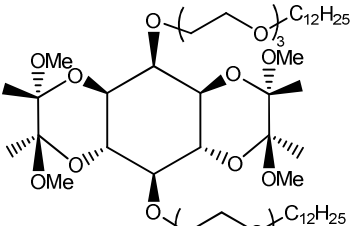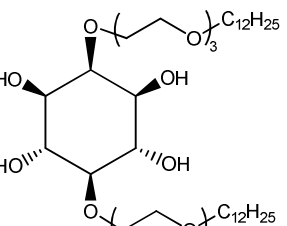
```
;d1 : relaxation delay; 1-5 * T1
;d12: delay for power switching                  [20 usec]
;d16: delay for gradient recovery
;d20: diffusion time (big DELTA)
;NS : 8 * n, total number of scans: NS * TD0
;DS : 4 * m
;use gradient ratio:    gp 6 : gp 7
;                  var  : -17.13
;use gradient ratio:    gp 1 : gp 2
;                   31 :   11
;for z-only gradients:
;gpz1: 31%
;gpz2: 11%
;gpz6: 1-100%
;gpz7: -17.13% (spoil)
;use gradient files:
;gpnam1: SINE.100
;gpnam2: SINE.100
;gpnam6: SINE.100
;gpnam7: SINE.100
;$Id: stebpgpes1s1d,v 1.0 2009/02/10 09:36:59 ber Exp $
```

8. APPENDIX
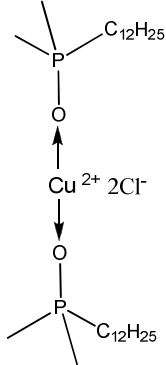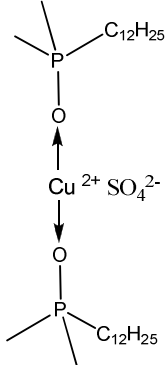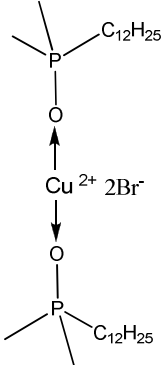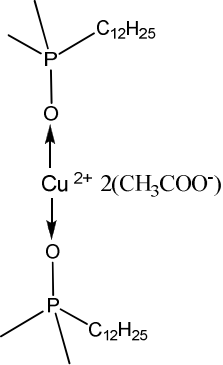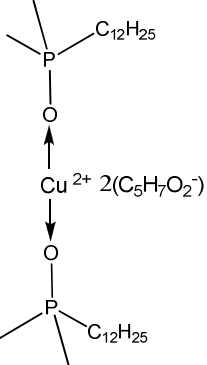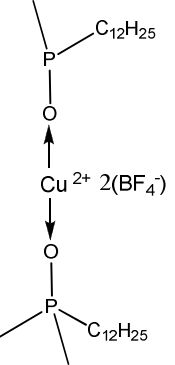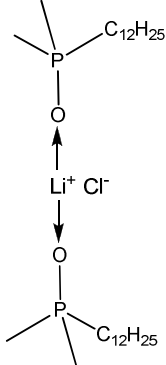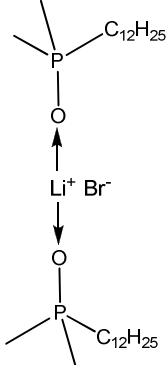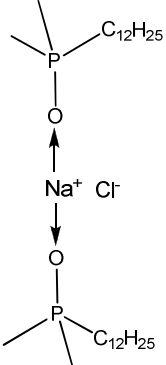
8.1. Overview over all newly synthesized compounds

8.1.1. Alkyl-ethoxylated *myo*-inositol derivatives

rac-**18**, page 111	*rac*-**19**, page 112
20, page 113	**21**, page 114
25, page 116	*rac*-**26**, page 117
rac-**29**, page 118	*rac*-**30**, page 119
rac-**31**, page 121	*rac*-**32**, page 122

33, page 123

34, page 125

35, page 126

36, page 128

37, page 129

38, page 131

rac-**39**, page 132

rac-**40**, page 134

rac-**41**, page 135

rac-**42**, page 136

43, page 137

44, page 139

8.1.2. Complexes C$_{12}$DMPO : salts

Cu^{2+} 2Cl$^-$ **56**, page 141	Cu^{2+} SO$_4^{2-}$ **57**, page 143	Cu^{2+} 2Br$^-$ **58**, page 143
Cu^{2+} 2(CH$_3$COO$^-$) **59**, page 144	Cu^{2+} 2(C$_5$H$_7$O$_2^-$) **60**, page 145	Cu^{2+} 2(BF$_4^-$) **61**, page 145
Li$^+$ Cl$^-$ **62**, page 146	Li$^+$ Br$^-$ **63**, page 147	Na$^+$ Cl$^-$ **64**, page 147

8.2. Abrevations

ATR	attenuated total reflection
APT	attached proton test
BDA	butane-2,3-diacetal
Bn	benzyl
br	broad
$C_{12}DMPO$	*n*-dodecyldimethyl phosphine oxide
calc.	calculated
Col_H	columnar hexagonal mesophase
CSA	camphor sulfonic acid
Cub	cubic mesophase
CyHex	cyclohexan
DCM	dichlormethane
DMF	*N,N*-dimethylformamide
DOSY	diffusion ordered spectroscopy
DSC	differential scanning calorimetry
EA	elemental analysis
eq	equivalent(s)
EtOAc	ethyl acetate
FT-IR	Fourier transform infrared spectroscopy
h	hour
HR-MS	high-resolution mass spectroscopy
KOH	potassium hydroxide
LC	liquid crystal
LCD	liquid crystal display
M	molar
Me	methyl
MeOH	methanol
min	minute(s)
mp	melting point
MS	mass spectroscopy
MTBE	methyl-*tert*-butylether
NaH	sodium hydride
NaOH	sodium hydroxide
NMR	nuclear magnetic resonance
Pd/C	palladium supported on charcoal
PFG	Pulsed field gradient
PM	polarization microscopy
ppm	parts per million
p-TsOH	*p*-toluene sulfonic acid
r.t.	room temperature
R_f	ratio of fronts
SmA	Smectic A mesophase
TFA	trifluoracetic acid
THF	tetrahydrofuran
TIR	total internal reflection
TLC	thin liquid chromatography
Ts	tosyl

9. REFERENCES

[1] http://www.mcrtn-socon.org.

[2] M.K. Matsson, B. Kronberg, P. Claesson, *Langmuir* **2004**, *20*, 4051-4058.

[3] M.K. Matsson, B. Kronberg, P. Claesson, *Langmuir* **2005**, *21*, 2766-2772.

[4] K. Kluge, T. Sottmann, C. Stubenrauch, R. Strey, *Tenside Surf. Det.,* **2001**, *38*, 30-40.

[5] P.M. Claesson, M. Kjellin, O. Rojas, C. Stubenrauch, *PCCP* **2006**, *8*, 5501-5514.

[6] C.M. Persson, M. Kjellin, J.C. Eriksson, *Langmuir* **2003**, *19*, 8152-8160.

[7] C. Stubenrauch, R. Cohen, D. Exerowa, *Langmuir* **2006**, *23*, 1684-1693.

[8] J. Angarska, C. Stubenrauch, E. Manev, *Colloids and Surfaces A: Physicochem. Eng. Aspects* **2007**, *309*, 189–197.

[9] H. Prade, R. Miethchen, V. Vill, *J. Prakt. Chem.* **1995**, *337*, 427-440.

[10] K. Praefcke, D. Blunk, J. Hempel, *Mol. Cryst. Liq. Cryst. Sci. Technol. Sect. A.* **1994**, *243*, 323-352.

[11] K. Praefcke, D. Blunk, *Liquid Crystals* **1993**, *14*, 1181-1187.

[12] K. Praefcke, P. Marquardt, B. Kohne, W. Stephan, *J. Carbohydr. Chem.* **1991**, *10*, 539.

[13] P. Marquardt, K. Praefcke, B. Kohne, W. Stephan, *Chem. Ber.* **1991**, *124*, 2265-2277.

[14] B. Kohne, K. Praefcke, W. Stephan, P. Nürnberg, *Z. Naturforsch., B: Chem.Sci.* **1985**, *40B*, 981-986.

[15] N. Bongartz, *Diplomarbeit,* Universität zu Köln, **2004**; *Inaugural-Dissertation*, Universität zu Köln, **2008.**

[16] M.J. Rosen, *Surfactants and interfacial phenomena*, John Wiley & Sons, Inc., Hoboken, New Jersey, **2004**, ISBN 0471478180.

[17] J.W. Goodby, *Chem. Soc. Rev.* **2007**, *36*, 1855-1856.

[18] M. Vieira de Almeida, M. Le Hyaric, *Mini-Reviews in Org. Chem.,* **2005**, *2*, 283-297.

[19] D. Balzer, H. Lüders, *Nonionic Surfactants: Alkyl Polyglucosides*, CRC Press, **2000**, ISBN 9780824793906.

[20] E. Fischer, *Ber. Dtsch. Chem. Ges.* **1893**, *26*, 2400-2412.

[21] H. Th. Böhme AG, DRP 593422, **1931**.

[22] C.C. Ruiz, *Sugar-Based Surfactants: Fundamentals and Applications*, CRC Press, **2008**, ISBN 9781420051667.

[23] N. M. van Os, *Nonionic Surfactants: Organic Chemistry*, CRC Press, **1997**, ISBN 9780824799977.

[24] I. Langmuir, *J. Am. Chem. Soc.* **1917**, *39*, 1848-1906.

[25] B. von Szyszkowski, *Z. Phys. Chem.* **1908**, *64*, 385-398.

[26] A.N., Frumkin, *Z. Phys. Chem.* **1925**, *116*, 466-484.

[27] V. Gärtner, *Diploma Thesis*, Universität zu Köln, School of Chemical and Bioprocess Engineering, University College Dublin, **2007**.

[28] R.G., Laughlin, *The Aqueous Phase Behavior of Surfactants*, Academic Press Inc., London, New York, **1996,** ISBN 0124377602.

[29] P. Joos, *Dynamic Surface Phenomena*, Editors: V.B. Fainerman, G. Loglio, E.H. Lucassen-Reynders, R. Miller and P. Petro, VSP, Utrecht, The Nederlands, **1999**, ISBN 9789067643009

[30] S.S. Dukhin, G. Kretzschmar, R. Miller, *Dynamics of Adsorption at the Liquid Interfaces: Theory, Experiment, Application*, Elsevier, Amsterdam, **1995**, ISBN 0444881174.

[31] L. du Noüy, *J. General Physiol.* **1919**, *1*, 521-524.

[32] J.W. McBain, C.S. Salmon, *J. Am. Chem. Soc.* **1920**, 42, 426-436.

[33] O. Södermann, P. Stilbs, *Progress in NMR Spectroscopy* **1994**, *26*, 445-482.

[34] Y. Cohen, L. Avram., L. Frish, *Angew. Chem. Int. Ed.* **2005**, *44*, 520-554.

[35] E.L. Hahn, *Phys. Rev.* **1950**, *80*, 580-594.

[36] O.E. Stejskal, J.E. Tanner, *J. Chem. Phys.* **1965**, *42*, 288-292.

[37] T.D.W. Claridge, *High Resolution NMR Technique in Organic Chemistry*, Elsevier, Oxford, Amsterdam, **1999**, ISBN 0080427987.

[38] M. Gueron, P. Plateau, M. Decorps, *Prog. Nucl. Magn. Reson. Spectrosc.* **1991**, *23*, 135.

[39] T.L. Hwang, A.J. Shaka, *J. Magn. Reson. Series A* **1995**, *112*, 275-279.

[40] K. Scott, J. Stonehouse, J. Keeler, T.L. Hwang, A.J. Shaka, *J. Am. Chem. Soc.* **1995**, *117*, 4199-4200.

[41] F. Nilsson , O. Söderman, I. Hohansson, *J. Coll. Interface Sci.***1998**, *203*, 131-139.

[42] F. Nilsson , O. Söderman, I. Hohansson, *Langmuir* **1996**, *12*, 902-908.

[43] B. Jönsson, H. Wennerström, P.G. Nilsson, P. Linse, *Colloid Polym. Sci*. **1986**, *264*, 77.

[44] S. Kumar, *Liquid Crystals: experimental study of physical properties and phase transitions*, Cambridge University Press, **2001**, ISBN 9780521461320.

[45] D. Demus, J. Goodby, G.W. Gray, H.-W. Spiess, V. Vill, *Handbook of Liquid Crystals, Vol. 3*, Wiley-VCH, Weinheim, New York, **1998**, ISBN 3527292721.

[46] IUPAC, *Pure and Applied Chem.*, **2001**, *73*, 845-89.

[47] D. Blunk, *Dissertation*, Technische Universität Berlin **1999**, ISBN 3934495004.

[48] P.J. Collings, M. Hird, *Introduction to liquid crystals chemistry and physics*, CRC Press, **1997**, ISBN 9780748404834.

[49] G. Höhne, W. Hemminger, H.-J. Flammersheim, *Differential Scanning Calorimetry*, Springer, **2003**, ISBN 9783540004677.

[50] T.W. Greene, *Protective groups in organic synthesis*, John Wiley&Sons, Inc., **1981**, ISBN 0471057649.

[51] S.J. Conway, G.J. Miller, *Nat. Prod. Rep.* **2007**, *24*, 687-707.

[52] B.V.L. Potter, D. Lampe, *Angew. Chem.* **1995**, *107*, 2085-2125.

[53] D.C. Billington, *Chem. Soc. Rev.* **1989**, *18*, 83-122.

[54] B.V.L. Potter, *Nat. Prod. Rep.* **1990**, *7*, 1-24.

[55] K.M. Sureshan, M.S. Shashidhar, T. Praveen, T. Das, *Chem. Rev.* **2003**, *103*, 4477-4503.

[56] S.J. Angyal, G.C. Irving, D. Rutherford, M.E. Tate, *J. Chem. Soc.* **1965,** 6662-6664.

[57] S.J. Angyal, M.E. Tate, *J. Chem. Soc.* **1965**, 6949-6955.

[58] S. David, S. Hanessian, *Tetrahedron* **1985**, *41*, 643-663.

[59] P.G.M. Wuts, T.W. Greene, *Greene's protective groups in organic synthesis*, John Wiley&Sons, **2006**, ISBN 9780471697541.

[60] H.W. Lee, Y. Kishi, *J. Org. Chem.*, **1985**, *50*, 4402-4404.

[61] C. Baudin, B.I. Glänzer, K.S. Swaminathan, A. Vassela, *Helv. Chim. Acta*, **1988**, *71*, 1367-1378.

[62] P.J. Garegg, T. Iversen, R. Johansson, B. Lindberg, *Carbohydr. Res.* **1984**, *130*, 322-326.

[63] J.P. Vacca, S. J. deSolms, J.R. Huff, D.C. Billington, R. Baker, J.J. Kulakowski, I.M. Mawer, *Tetrahedron* **1989**, *45*, 5679-5702.

[64] J.-L. Montchamp, F. Tian, M.E. Hart, J.W. Frost, *J. Org. Chem.* **1996**, *61*, 3897-3899.

[65] A. Hense, S.V. Ley, H.M.I. Osborn, D.R. Owen, J.-F. Poisson, S.L. Warriner, K.E. Wesson, *J. Chem. Soc. Perkin Trans. 1*, **1997**, 2023-2031.

[66] S.J. Mills, A.M. Riley, C. Liu, M.F. Mahon, B.V.L. Potter, *Chem. Eur. J.*, **2003**, *9*, 6207.

[67] A.M. Riley, D.J. Jenkins, B.V.L. Potter, *Carbohydr. Res.* **1998**, *314*, 277-281.

[68] T. Gibson, *J. Org. Chem.* **1980**, *45*, 1095-1098.

[69] M. Ouchi, Y. Inoue, T. Kanzaki, T. Hakushi, *J. Org. Chem.* **1984**, *49*, 1408-1412.

[70] P. Uhlmann, A. Vassela, *Helv. Chim. Acta* **1992**, *75*, 1979-1994.

[71] D.C. Billington, R. Baker, J.J. Kulakowski, I.M. Mawer, J.P. Vacca, S. J. deSolms, J.R. Huff, *J. Chem. Soc. Perkin Trans. 1* **1989**, 1423-1429.

[72] C.B. Allan, L.O. Spreer, *J. Org. Chem.* **1994**, *59*, 7695-7700.

[73] A. Zada, Y. Avny, A. Zilkha, *J. Surf. Det.* **2001**, *4*, 163-166.

[74] A. Bouzide, N. LeBerre, G. Sauvé, *Tetrahedron Letters*, **2001**, *42*, 8781-8783.

[75] V. Vill, R. Hashim, *Current Opinion in Colloid and interface science* **2002**, *7*, 395-409.

[76] G. Catanoiu, V. Gärtner, C. Stubenrauch, D. Blunk, *Langmuir* **2007**, *23*, 12802-12805.

[77] B.J. Boyd, C.J. Drummond, I. Krodkiewska, F. Gieser, *Langmuir* **2000**, *16*, 7359-7367.

[78] D.J. Mitchell, G.J.T. Tiddy, L. Waring, T. Bostock, M.P. McDonald, *J. Chem. Soc. Faraday Trans. 1* **1983**, *79*, 975-1000.

[79] D. Blunk, P. Bierganns, N. Bongartz, R. Tessendorf, C. Stubenrauch, *New J. Chem.* **2006**, *30*, 1705-1717.

[80] A. Gavezzotti, *J. Chem. Soc., Perkin Trans. 2* **1995**, 1399-1404.

[81] R.J.C. Brown, R.F.C. Brown, *J. Chem. Educ.* **2000**, *77*, 724–731.

[82] S.H. Yalkowsky, S.C. Valvani, *J. Pharm. Sci.* **1980**, *69*, 912–922.

[83] R. Pinal, *Org. Biomol.Chem.* **2004**, *2*, 2692-2699.

[84] D.A. Long, *Raman Spectroscopy*, McGraw-Hill, New York, **1977**, ISBN 0070386757.

[85] P.A. Greene, C.D. Bain, *Spectroscopy Europe* **2004,** *16*, 8-15.

[86] T. Yoshizaki, H. Yamakawa, *J. Chem. Phys.* **1980**, *72*, 57-69.

[87] D. Blunk, R. Tessendorf, N. Buchavzov, R. Strey, C. Stubenrauch, *J. Surf. Det.* **2007**, *10*, 155-165.

[88] R. Tessendorf, R. Strey, C. Stubenrauch, *Langmuir* **2008**, *24*, 11390-11398.

[89] L.J. Charbonniere, R. Ziessel, M. Montalti, L. Prodi, N. Zacherroni, C. Boehme, G. Wipff, *J. Am. Chem. Soc.* **2002**, *124*, 7779-7788.

[90] M. Baaden, G. Wipff, M.R. Yaftian, M. Burgard, D. Matt, *J. Chem. Soc., Perkin Trans. 2* **2000**, 1315-1321.

[91] H. Boerrigter, W. Verboom, D.N. Reinhoudt, *J. Org. Chem.* **1997**, *62*, 7148-7155.

[92] H. Saisho, *Bull. Chem. Soc. Japan* **1962**, *35*, 514-515.

[93] M. M. Reinoso-García, D. Jańczewski, D. N. Reinhoudt, W. Verboom, E. Malinowska, M. Pietrzak, C. Hill, B. Grüner, P. Selucky, C. Grüttner, *New J. Chem.* **2006**, *30*, 1480-1492.

[94] T. Hatano, T. Kato, *Chem. Comm.* **2006**, 1277-1279.

[95] H.R. Hays, *J. Org. Chem.* **1968**, *33*, 3690-3694.

[96] J.J. Richard, C.V. Banks, *J. Org. Chem.* **1963**, *28*, 123-125.

[97] I.M. Downie, G. Morris, *J. Chem. Soc.* **1965**, 5771.

[98] R.G. Laughlin, *J. Org., Chem.* **1965**, *30*, 1322-1324.

Erklärung

Ich versichere,

dass ich die von mir vorgelegte Dissertation selbständig angefertigt, die benutzten Quellen und Hilfsmittel vollständig angegeben und die Stellen der Arbeit – einschließlich Tabellen, Karten und Abbildungen –, die anderen Werken im Wortlaut oder dem Sinn nach entnommen sind, in jedem Einzelfall als Entlehnung kenntlich gemacht habe;

dass sie – abgesehen von unten angegebenen Teilpublikationen – noch nicht veröffentlicht worden ist sowie;

dass ich eine solche Veröffentlichung vor Abschluss des Promotionsverfahrens nicht vornehmen werde.

Die Bestimmungen der Promotionsordnung sind mir bekannt.

Die von mir vorgelegte Dissertation ist von Prof. Dr. H.-G. Schmalz betreut worden.

Köln, 12.05.2009

…………………

(Gabriela Cătănoiu)

Teilpublikationen dieser Dissertation

Publikationen:

- *„ New ethoxylated inositol surfactant"*, **G. Catanoiu**, V. Gärtner, C. Stubenrauch, D. Blunk, *Langmuir* **2007**, 23, 12802-12805.
- *"Liquid Crystalline Amphiphilic Phosphine Oxide Metal Complexes"*, **G. Catanoiu,** C. Stubenrauch, D. Blunk, *"35th Arbeitstagung Flüssigkristalle"*, März **2007,** Bayreuth, Deutschland – Extended Abstract.

Tagungsbeitrage:

1) *"34th Arbeitstagung Flüssigkristalle"*, 29-31 März **2006**, Freiburg, Deutschland, Partizipation;
2) *"Midterm Review SOCON"*, 14-17 Sept. **2006**, Budapest, Ungarn – Vortrag, *"New Inositol Surfatants: Synthesis and Perspectives"*, **G. Catanoiu;**
3) *"20th Conference of the European Colloid and Interface Society"* jointly organized with *"18th European Chemistry at Interfaces Conference"*, 17-22 Sept. **2006**, Budapest, Ungarn – Abstract und Poster, *"Self-Organization and Surface Activity of Inositol Surfactants"*, N. Bongartz, **G. Catanoiu**, N. Buchavzov, R. Strey, C. Stubenrauch, D. Blunk;
4) *"35th Arbeitstagung Flüssigkristalle"*, 21-23 März **2007**, Bayreuth, Deutschland – Extended Abstract und Poster, *"Liquid Crystalline Amphiphilic Phosphine Oxide Metal Complexes"*, **G. Catanoiu,** C. Stubenrauch, D. Blunk;
5) *"European Symposium on Organic Chemistry, ESOC 2007"*, 08-13 Juli **2007**, Dublin, Irland – Abstract and Poster, *"New Ethoxylated Inositol Surfactans"*, **G. Catanoiu,** V. Gärtner, C. Stubenrauch, D. Blunk;
6) "3rd Annual Meeting of SOCON", 06-07 Sept. **2007**, Stockholm, Schweden – Vortrag, *"Synthesis and Supramolecular Properties of New Inositol Derivatives and Phosphine Oxide Metal Complexes"*, **G. Catanoiu;**
7) *"GDCh Wissenschaftsforum Chemie"*, 16-19 Sept. **2007**, Ulm, Deutschland – Abstract und Poster, *"New Inositol Surfactants"* **G. Catanoiu,** V. Gärtner, C. Stubenrauch, D. Blunk;
8) *"36th Arbeitstagung Flüssigkristalle"*, 12-14 März **2008**, Magdeburg, Deutschland – Abstract, *"Amphotropic Inositol Liquid Crystals"*, D. Blunk, **G. Catanoiu,** V. Gärtner, C. Stubenrauch;
9) *"22nd Conference of the European Colloid and Interface Society"*, 31 Aug-05 Sept. **2008,** Krakow, Polen – Abstract und Poster, *"Synthesis and Characterization of New Inositol-based Surfactants"*, **G. Catanoiu,** V. Gärtner, C. Stubenrauch D. Blunk;
10) *"Orchem 2008"*, 01-03 Sept. **2008**, Weimar, Deutschland – Abstract and Poster, *"Synthesis and Characterization of New Inositol Derivatives"*, D. Blunk, **G. Catanoiu,** N. Bongarz, C. Stubenrauch;
11) *"4th Annual Meeting of SOCON"*, 22-23 Sept. **2008**, Durham, Großbritannien – Vortrag, *"Synthesis and Characterization of New Ethoxylated Inositol Surfactants"*, **G. Catanoiu** und Poster, *"Studies of New Surfactans and Amphotropic Materials"*, M. Guiteras Capdevila, **G. Catanoiu,** D. Blunk;

GABRIELA CĂTĂNOIU - LEBENSLAUF

Persönliche Daten:

Geburtsdatum:	11. Februar 1976
Geburtsort:	Hunedoara, Rumänien
Familienstand:	ledig
Staatsangehörigkeit	Rumänisch

Schulbildung:

09/1982 – 06/1990	Grundschule in Hunedoara, Rumänien
09/1990 – 06/1994	Gymnasium in Hunedoara, Rumänien

Studium

09/1994 – 09/1997	Nursing College, Hunedoara, Rumänien
10/1997 – 06/2002	Diplom Ingenieur - Universität "POLITEHNICA" aus Timisoara, Fakultät für Industrielle Chemie und Umweltingineurie, Rumänien Fachrichtung: Organische Chemie
09/2002 – 06/2003	Master Abschluss - Universität "POLITEHNICA" aus Timisoara, Fakultät für Industrielle Chemie und Umweltingineurie, Rumänien Fachrichtung: Organische Synthese von Feinchemikalien und Naturstoffe
seit 03/2006	Doktorarbeit - Universität zu Köln, Institut für Organische Chemie unter Anleitung von Prof. H.-G. Schmalz und Dr. D. Blunk Arbeitsthema: „Novel phosphine oxides complexes and inositol derivatives as amphitropic liquid crystals and surfactants"

Beruflicher Werdegang:

10/1994 – 09/1997	Krankenschwester im städtisches Krankenhaus, Hunedoara, Rumänien
10/2002 – 03/2006	Wissenschaftliche Mitarbeiterin an der Universität "POLITEHNICA" Timişoara, Fakultät für Industrielle Chemie und Umweltingineurie, Rumänien
03/2004 – 12/2004	Wissenschaftliche Mitarbeiterin an der Université d'Artois, I.U.T. de Bethune, Frankreich im Rahmen des EU-Programms Socrates-Erasmus
03/2006 – 12/2008	Wissenschaftliche Mitarbeiterin an der Universität zu Köln, Institut für Organische Chemie im Rahmen des EU-Programms FP6 - Marie Curie Research Training Network *"Self-Organization under Confinement (SOCON)"*

Köln, 12.05.2009

…………………..
(Gabriela Cătănoiu)